

# **Bio-Inspired Robotic Control in Underactuation: Principles for Energy Efficacy, Dynamic Compliance Interactions and Adaptability**



**Pengcheng Liu**

Faculty of Science and Technology

Bournemouth University

This dissertation is submitted for the degree of

*Doctor of Philosophy*

March 2017

©This copy of the thesis has been supplied on condition that anyone who consults it is understood to recognise that its copyright rests with its author and due acknowledgement must always be made of the use of any material contained in, or derived from this thesis.

I would like to dedicate this thesis to my wife and my entire family.

# **Declaration**

I hereby declare that except where specific reference is made to the work of others, the contents of this thesis are original work of the author.

Pengcheng Liu

2017



# Acknowledgements

The completion of this work has been made possible with the guidance, support and encouragement of many individuals to whom I owe a lot. First of all, I'm deeply indebted to my supervisory team, Prof. Hongnian Yu and Dr. Shuang Cang without the advice of whom I would never have completed this project. I would like to thank them for driving to success which has motivated me to work hard and aim high, for providing constructive feedbacks during every discussion, and above all, for their kindness and tremendous support.

Secondly, I would also like to thank my entire family for their confidence on me, for motivating me to pursue my endeavours, for their love, support, patience and encouragement throughout my life. I would like to extend my eternal thanks to my wife Qian Zhang and our beloved daughter Yinuo Liu, for their unconditional love and support at all times, for always being there for me, even when my work takes me to places I never thought I'd go. Their constant support has always been a beacon to sanity and happiness in my life.

Finally, I wish to thank all my friends in China and Bournemouth for their support, discussions and encouragement. I would like to thank Dr Emili Balaguer-Ballester, Dr. Feng Tian, Dr. Md Nazmul Huda, Pree Thiengburanatham, Yan Wang, and Rui Wang who provide kind advice during my difficult times and ensured my well-being and maintained a homely environment during my stay in UK.

# Abstract

Biological systems achieve energy efficient and adaptive behaviours through extensive autologous and exogenous compliant interactions. Active dynamic compliances are created and enhanced from musculoskeletal system (joint-space) to external environment (task-space) amongst the underactuated motions. Underactuated systems with viscoelastic property are similar to these biological systems, in that their self-organisation and overall tasks must be achieved by coordinating the subsystems and dynamically interacting with the environment. One important question to raise is: How can we design control systems to achieve efficient locomotion, while adapt to dynamic conditions as the living systems do?

In this thesis, a trajectory planning algorithm is developed for underactuated microrobotic systems with bio-inspired self-propulsion and viscoelastic property to achieve synchronized motion in an energy efficient, adaptive and analysable manner. The geometry of the state space of the systems is explicitly utilized, such that a synchronization of the generalized coordinates is achieved in terms of geometric relations along the desired motion trajectory. As a result, the internal dynamics complexity is sufficiently reduced, the dynamic couplings are explicitly characterised, and then the underactuated dynamics are projected onto a hyper-manifold. Following such a reduction and characterization, we arrive at mappings of system compliance and integrable second-order dynamics with the passive degrees of freedom. As such, the issue of trajectory planning is converted into convenient nonlinear geometric analysis and optimal trajectory parameterization.

Solutions of the reduced dynamics and the geometric relations can be obtained through an optimal motion trajectory generator. Theoretical background of the proposed approach is presented with rigorous analysis and developed in detail for a particular example. Experimental studies are conducted to verify the effectiveness of the proposed method.

Towards compliance interactions with the environment, accurate modelling or prediction of nonlinear friction forces is a nontrivial whilst challenging task. Frictional instabilities are typically required to be eliminated or compensated through efficiently designed controllers. In this work, a prediction and analysis framework is designed for the self-propelled vibro-driven system, whose locomotion greatly relies on the dynamic interactions with the nonlinear frictions. This thesis proposes a combined physics-based and analytical-based approach, in a manner that non-reversible characteristic for static friction, presliding as well as pure sliding regimes are revealed, and the frictional limit boundaries are identified. Nonlinear dynamic analysis and simulation results demonstrate good captions of experimentally observed frictional characteristics, quenching of friction-induced vibrations and satisfaction of energy requirements.

The thesis also performs elaborative studies on trajectory tracking. Control schemes are designed and extended for a class of underactuated systems with concrete considerations on uncertainties and disturbances. They include a collocated partial feedback control scheme, and an adaptive variable structure control scheme with an elaborately designed auxiliary control variable. Generically, adaptive control schemes using neural networks are designed to ensure trajectory tracking. Theoretical background of these methods is presented with rigorous analysis and developed in detail for particular examples. The schemes promote the utilization of linear filters in the control input to improve the system robustness. Asymptotic stability and convergence of time-varying reference trajectories for the system dynamics are shown by means of Lyapunov synthesis.

# Contents

Contents .....	xi
List of Figures .....	xv
List of Tables .....	xix
Nomenclature .....	xx
Abbreviations .....	xxiii
Chapter 1 Introduction .....	1
1.1 Background and Research Motivation .....	1
1.2 Aims and Objectives .....	6
1.2.1 Research Aims .....	6
1.2.2 Research Objectives .....	6
1.3 Research Contributions .....	7
1.4 Structure of the Thesis .....	9
1.5 List of Publications .....	12
Chapter 2 Literature Review .....	14
2.1 Introduction .....	14
2.2 Modelling of UMSs .....	17
2.3 Bio-Inspired Design and Bio-Inspired Control .....	20
2.3.1 UMSs with Bio-Inspired Viscoelastic Property .....	20
2.3.2 Bio-Inspired Behaviour/Motor Control .....	24

2.3.3 Undulatory Locomotion and Serpentine Robotic Systems .....	29
2.4 Periodic Trajectory Planning.....	34
2.5 Nonlinear Control Systems Design .....	40
2.5.1 Classification .....	40
2.5.2 Control Algorithms.....	43
2.6 Challenges and Future Trends.....	51
2.6.1 Theoretical Challenges and Common Difficulties .....	51
2.6.2 Trends and Future Directions.....	53
2.7 Conclusion .....	55
Chapter 3 Control Systems for 2-DOF UMSs with Underactuation Degree One .....	57
3.1 Introduction.....	57
3.2 Coordinate Transformations of 2-DOF UMSs.....	59
3.2.1 Transformation with PFL .....	59
3.2.2 Transformation with PFL-Free Approach .....	61
3.3 Control Problem Formulation .....	65
3.3.1 2-DOF UMSs Control System Design with PFL.....	65
3.3.2 2-DOF UMSs Control with PFL-Free Design.....	66
3.3.3 Control Problem Formulation.....	68
3.4 Control Properties of UMSs with 2-DOF.....	71
3.4.1 Constraint Integrability.....	71
3.5 Conclusion .....	77
Chapter 4 Geometric Analysis-Based Trajectory Planning and Tracking Control.....	78
4.1 Introduction.....	78
4.2 System Description and Mathematical Modelling .....	83
4.2.1 Bio-Inspired Self-Propelled Robotic Model with Viscoelastic Property ....	83
4.2.2 Vibro-Driven Cart System and Mathematical Modelling.....	85
4.3 Problem Formulation and Trajectory Planning .....	90
4.3.1 Problem Formulation.....	90

4.3.2 Periodic Trajectory Synthesis and Construction.....	93
4.4 Nonlinear Geometric Analysis-based Trajectory Planning.....	96
4.4.1 Coupling Characterization and Viscoelastic Parameter Identification.....	97
4.4.2 Dynamic Constraints Characterization.....	102
4.4.3 Trajectory Boundaries Computation .....	105
4.4.4 Trajectory Optimization and Parameterization .....	106
4.5 Trajectory Tracking Control System Design.....	109
4.5.1 Closed-Loop Feedback Control Scheme .....	109
4.5.2 Adaptive Robust Control Scheme with an Auxiliary Variable .....	110
4.6 Simulation Results.....	114
4.7 Robot Design and Experimental Results .....	118
4.7.1 3D Robotic System Design.....	118
4.7.2 Experiment Setup.....	121
4.7.3 Motor Controller PID Tuning .....	124
4.7.4 Experiment Results .....	126
4.8 Conclusion .....	130
Chapter 5 Analysis and Characterization of Dynamic Frictional Interactions.....	133
5.1 Introduction.....	133
5.2 Mathematical Modelling.....	138
5.2.1 System Description .....	138
5.2.2 Dynamic Model .....	139
5.2.3 Modelling and Characterization of the Frictional Interaction Dynamics..	140
5.3 Analysis of Frictional Interaction Dynamics .....	148
5.3.1 The Responses of Friction-Induced Vibrations.....	149
5.3.2 Influence of the Control Parameters .....	154
5.4 Conclusions.....	161
Chapter 6 Adaptive Control Systems for a Class of UMSs .....	162
6.1 Introduction.....	162

---

6.2 Theoretical Preliminaries .....	167
6.2.1 Dynamic Model and Properties .....	167
6.2.2 Radial Basis Function NN .....	170
6.3 Controller Design and Stability Analysis .....	172
6.4 Simulation Studies.....	183
6.4.1 2-DOF Underactuated Manipulator .....	183
6.4.2 2-DOF Underactuated VDC System.....	188
6.5 Conclusions.....	191
Chapter 7 Conclusions and Future Works.....	193
7.1 Conclusions.....	193
7.2 Aims and Objectives Revisited .....	195
7.3 Future Works.....	199
Appendix A .....	201
A.1 Underactuated Mechanical Systems.....	201
A.1.1 Lagrangian Mechanical Systems.....	201
A.1.2 Underactuated Mechanical Systems.....	203
References .....	204

## List of Figures

Figure 2.1	Block diagram of trajectory planning and control of underactuated robotic systems .....	16
Figure 2.2	Friction models for locomotive systems: (a) the Coulomb model; (b) the Coulomb viscous damping model; (c) Stiction plus Coulomb and viscous friction; (d) seven-parameter model (Olsson et al., 1998).....	19
Figure 2.3	The DLR hand arm system (Greibenstein et al., 2011).....	21
Figure 2.4	Physical model of the vibro-impact capsule system (Liu et al., 2013b) .	23
Figure 2.5	Bipedal robots based on passive-dynamic walkers (Collins et al., 2005)	26
Figure 2.6	Unpowered exoskeleton design (Collins et al., 2015) .....	27
Figure 2.7	Springactive Walk-Run ankle (Grimmer et al., 2016).....	28
Figure 2.8	Arm reaching experiment setup and force fields (Huang et al., 2012) ...	29
Figure 2.9	Worm-inspired robot (Boyle et al., 2013) .....	31
Figure 2.10	Block diagram for planning and control of overhead crane .....	35
Figure 2.11	Overall block diagram for trajectory planning in the $k$ th iteration (Ning Sun et al., 2012).....	36

---

Figure 2.12 A visualization of Poincaré surfaces and transverse linearization of a periodic orbit (red) and a trajectory converging to it (black) (Manchester et al., 2011) .....	38
Figure 2.13 The 3-DOF WIP model scheme (Yang et al., 2013).....	41
Figure 2.14 The VTOL aircraft (Hua et al., 2013).....	42
Figure 2.15 Soft computing techniques .....	47
Figure 2.16 Structure of the RBF neural network.....	48
Figure 2.17 The mobile underactuated manipulator (Li et al., 2014).....	49
Figure 3.1 The coordination transformation and decoupling of a class of 2-DOF UMSs with PFL approach.....	66
Figure 3.2 The coordination transformation and decoupling of a class of 2-DOF UMSs with PFL-free approach .....	67
Figure 4.1 The biological inspiration: (a) a four-segment <i>C. elegans</i> nematode (“Nematode,” 2017); (b) the proposed two-segment bio-inspired self-propelled model with viscoelastic property.....	84
Figure 4.2 Schematic of the vibro-driven cart system.....	86
Figure 4.3 Time histories of typical steady-state system performance .....	91
Figure 4.4 Schematic profile for the synthesized velocity trajectory.....	93
Figure 4.5 Qualitative variation laws of $\rho$ obtained for $h = 0.8, \omega = 1.7, \nu = 0.8$ and $\lambda = 3.6$ .....	99
Figure 4.6 Time histories of the cart displacements.....	100
Figure 4.7 Qualitative variation laws of $\nu$ obtained for $h = 0.8, \omega = 1.7, \rho = 0.9$ and $\lambda = 3.6$ .....	101
Figure 4.8 Time histories of the cart displacements.....	102

Figure 4.9 Simulation results of the proposed method (red solid line) and conventional method in EPC (blue dashed line) ..... 117

Figure 4.10 Simulation results of control scheme (4.57) under parametric uncertainty 118

Figure 4.11 The 3D prototype of the vibro-driven system ..... 121

Figure 4.12 Experimental components of the vibro-driven system ..... 123

Figure 4.13 Experimental rig of the vibro-driven system..... 123

Figure 4.14 Motor no-load response curve ..... 124

Figure 4.15 Motor position response curves under certain parameter conditions. ... 126

Figure 4.16 Comparison of experiment (blue solid line) and simulation (black dashed line) results of the vibro-driven cart system..... 128

Figure 5.1 Schematic of the vibro-driven underactuated encapsulated system ..... 138

Figure 5.2 Schematic of the capsule motion with interface deformation ..... 142

Figure 5.3 Schematic of the reversible (black solid line) and non-reversible (blue dashed line) characteristics of the friction forces ..... 143

Figure 5.4 Schematic of the microscopic elastic limit for sticking, presliding and pure sliding phases..... 146

Figure 5.5 Friction-induced dynamic response with LM (red solid lines) and EM (blue dashed lines): (a) angular displacements  $\theta$ , (b) angular velocities  $\theta'$ , (c) capsule displacements  $X$  and (d) capsule velocity  $X'$ , obtained for  $\lambda = 2.5$ ,  $\rho = 2.0$  and  $v = 1.0$  ..... 150

Figure 5.6 Friction-induced dynamic responses with LM (red solid lines) and EM (blue dashed lines): (a) internal state variable  $\xi$  and (b) friction forces  $f$ , obtained for  $\lambda = 2.5$ ,  $\rho = 2.0$  and  $v = 1.0$ ..... 151

---

Figure 5.7 Phase portraits for capsule systems with EM (blue dashed lines) and LM (red solid lines): (a) the pendulum subsystem and (b) the capsule subsystem, obtained for $\lambda = 2.5$ , $\rho = 2.0$ and $v = 1.0$ .....	152
Figure 5.8 Friction forces for capsule systems with EM (blue dashed lines) and LM (red solid lines) obtained for $\lambda = 2.5$ , $\rho = 2.0$ and $v = 1.0$ .....	154
Figure 5.9 Transient responses under the variation of amplitude and frequency of excitation with LM (red solid lines) and EM (blue dashed lines): (a) $h = 1.5$ , $\omega = 1.0$ , (b) $h = 2.5$ , $\omega = 1.0$ and (c) $h = 1.5$ , $\omega = 2.0$ , obtained for $\lambda = 2.5$ , $\rho = 2.0$ and $v = 1.0$ .....	156
Figure 5.10 Bifurcation diagrams for capsule systems with LM (red dotted) and EM (blue dotted) constructed under variation of mass ratio $\lambda$ , obtained for $h = 1.8$ , $\omega = 1.0$ , $\rho = 4.0$ and $v = 1.2$ .....	157
Figure 5.11 Trajectories on phase plane for the pendulum subsystem ( $y_1$ and $y_2$ ) and on time coordinate for the capsule subsystem (progressive velocity $y_4$ ), with LM (red solid lines) and EM (blue dashed lines): (a) $\lambda = 0.5$ , (b) $\lambda = 2.5$ , (c) $\lambda = 4.0$ and (d) $\lambda = 6.0$ , obtained for $h = 1.8$ , $\omega = 1.0$ , $\rho = 4.0$ and $v = 1.2$ .....	159
Figure 5.12 Time histories of capsule displacements under varying mass ratio ( $\lambda = 0.8, 2.0$ and $4.0$ ): (a) with LM and (b) with EM, obtained for $h = 1.8$ , $\omega = 1.0$ , $\rho = 4.0$ and $v = 1.2$ .....	160
Figure 6.1 Structure of the RBF neural network.....	171
Figure 6.2 The planar underactuated manipulator with two revolute joints.....	184
Figure 6.3 Trajectory tracking performance of joint 1.....	186
Figure 6.4 Trajectory tracking performance of joint 2.....	186
Figure 6.5 Trajectory tracking error of joint 1.....	187
Figure 6.6 Control torque.....	187
Figure 6.7 $\chi_z$ and $\dot{\chi}_z$ .....	187

## LIST OF FIGURES

---

Figure 6.8 NN approximation error.....	188
Figure 6.9 Trajectory tracking performance .....	190
Figure 6.10 Trajectory tracking error .....	190
Figure 6.11 Performance of the VDC system .....	191
Figure 6.12 Control torque.....	191

## List of Tables

Table 2.1 Undulation-based bio-inspired robots using vertical waves.....	32
Table 2.2 Undulation-based bio-inspired robots using linear expansion.....	33
Table 2.3 Comparison among trajectory planning algorithms for UMSs based on key features.....	39
Table 2.4 Comparison among nonlinear control algorithms for UMSs based on key features.....	50
Table 4.1 Trajectory parameters for numerical simulation (s).....	115

# Nomenclature

## Commonly used Mathematical Symbols

$\mathcal{R}$	Field of real numbers.
$\mathcal{R}^n$	Linear space of real vectors of dimension $n$ .
$\mathcal{R}^{n \times m}$	Ring of matrices with $n$ row and $m$ columns and elements in $\mathcal{R}$ .
$I_n$	The identity matrix of dimension $n$ .
$\ x\ $	The Euclidean norm of $x \in R^n$ .
$\ x\ _p$	The $p$ -norm of $x \in R^n$ .
$\frac{dz}{d\xi}$	Derivative of $z = f(\xi)$ .
$\frac{dz}{d\bar{\xi}}$	Derivative of $z = f(\bar{\xi})$ .
$\frac{\partial z}{\partial \xi}$	Differentiation operator with respect to $\xi$ .
$\rightarrow$	Mapping from a domain into a range. Also “tends to”.

$\mapsto$	Mapping of two elements into their image.
$\triangleq$	“Defined as”.
$p \triangleq \frac{d}{dt}$	Differentiation operator.
$\text{diag}\{ \}$	Diagonal operator: transform a vector into a diagonal matrix.
$\bar{\Delta}$	The closure of distribution $\Delta$ .
$\hat{\alpha}$	The estimate of a parameter (or vector of parameters) $\alpha$ .
$\tilde{\alpha}$	The estimation error.
$\lambda_{\min}(K)$	The smallest eigenvalue of $K$ .
$\lambda_{\max}(K)$	The largest eigenvalue of $K$ .
$\text{Tr}(K)$	The trace operator.
$(\cdot)^T$	The transport operator.
$(\cdot)^{-1}$	The inverse operator.
$A_{ij}$	$ij$ -th element of the matrix $A$ .

### Capital Roman Letters

$G$	Gravity terms.
$D$	Inertia matrix.
$L$	System Lagrangian.
$R$	Dissipation function.
$T$	Kinetic energy.
$V$	Potential energy.

$B$	Non-square matrix of external forces with full column rank.
$C$	Vector of Coriolis and centrifugal terms.
$I_n$	The identify matrix of dimension $n$ .
$X$	A $n \times 1$ arbitrary vector.
$X^T$	The transpose of $X$ .
$H$	The total energy.
$A$	Amplitude of the harmonic excitation.
$M$	Mass of the platform.
$X$	Non-dimensionalized displacement.
$P_1$	The maximum angular velocity of the periodic trajectory in scaled coordinate.
$P_2$	The minimum angular velocity of the periodic trajectory in scaled coordinate.
$P_3$	The critical angular velocity when the cart begins to keep stationary.
$F_x$	Force applied on the ball in the horizontal direction.
$F_y$	Force applied on the ball in the vertical direction.
$N_0$	Normal load.
$F$	The friction function representing the friction force per unit of normal load.
$R_F$	Forward motion stage.
$R_B$	Backward motion stage.
$Y(\cdot)$	Regressor representing the nonlinear functions with unknown parameters.
$V(t)$	Lyapunov function.

**Lowercase Roman Letters**

$m$	Mass of the ball.
$l$	Length of the inverted pendulum.
$x$	Displacement of the cart.
$k$	Stiffness coefficient of the torsional spring.
$c$	Damping coefficient of the damper.
$g$	Gravitational acceleration.
$f_c$	Horizontal sliding friction between the system and the ground.
$f_p$	Motor viscous friction at the pivot.
$f_0$	The stiction force when the velocity of the system is zero.
$h$	Non-dimensionalized amplitude of the harmonic excitation.
$f_{max}$	The maximal static friction between the cart and the sliding ground.
$q_a$	Actuated sub-coordinate.
$q_p$	Un-actuated (Passive) sub-coordinate.
$q_0$	The initial state of the configuration variable.
$q_d$	The desired state of the configuration variable.

**Greek Letters**

$\theta$	Angular displacement of the pendulum from vertical.
$\mu$	Coefficient of the friction between robotic system and the ground.
$\Omega$	Frequency of the harmonic excitation.
$\rho$	Non-dimensionalized stiffness coefficient of the torsional spring.
$\nu$	Non-dimensionalized damping coefficient of the torsional spring.
$\omega$	Non-dimensionalized frequency of the harmonic excitation.

$\lambda$	Mass ratio.
$\omega_n$	Natural frequency of the driving pendulum.
$\hat{\xi}$	Average bristle deflection.
$\delta_0$	The stiffness coefficient of the bristle.
$\delta_1$	The damping coefficient of the bristle.
$\delta_2$	The viscous constituent of the resistant force.
$\theta_0$	Initial angular displacement of the pendulum.
$\dot{\theta}_d$	The desired periodic motion trajectory.

# Abbreviations

UMSs	Underactuated mechanical systems.
DOF	Dgrees of freedom.
PFL	Partial feedback linearization.
CPFL	Collocated partial feedback linearization.
MTTP	Minimum-time trajectory planning.
EC	Evolutionary computation.
FL	Fuzzy logic.
VDCs	Vibro-driven cart systems.
CPSs	Cart-pole systems.
COM	Centre of mass.
AM-GM	Arithmetic-geometric.
EPC	Elastically-joint actuated pendulum-driven cart-pole.
MMMS	Mobile micro-mechanical systems.
LM	The LuGre model.
EM	The Exponential model.
SMC	Sliding mode control.
VSC	Variable structure control.

## ABBREVIATIONS

---

AS	The acceleration stage.
DS	The deceleration stage.
VTOL	Vertical take off and landing.
IWP	Inertia-wheel pendulum.
TORA	Translational oscillator with rotational actuator.
UPOs	Unstable periodic orbits.
SCC	Semi-continuous control.
EBC	Energy-based control.
PVTOL	Planar vertical takeoff and landing.
AFSMC	Adaptive fuzzy sliding-mode control.
NNs	Neural networks.
RBFNN	Radial basis function neural network.

# Chapter 1

## Introduction

### 1.1 Background and Research Motivation

During the past decade, researchers all over the world have been attracted and involved in an interdisciplinary research field—robotics, seeking feasible solutions for a large scope from theoretical challenges (Albu-Schäffer and Petit, 2012; Ravichandran and Mahindrakar, 2011; Xin et al., 2013) and practical problems (Petković et al., 2013a; Shiriaev et al., 2014; Zhang et al., 2016) to potential applications (Fang et al., 2012; Huda and Yu, 2015; N. Sun et al., 2012). Besides the well-established industrial robots, tremendous applications have emerged from factory automation to field and service applications, for instance, surgical robots, unmanned vehicles, automated cranes, tele-operated machines, humanoid robots, rehabilitation robots.

The innovations arose in the design of robotic mechanisms that are capable of surpassing human beings in terms of efficiency, operation accuracy as well as flexibility have achieved promising outcomes in extensive fields of applications. However, from the perspective of control, theoretical and practical challenges have all along existed in the research of robotics in finding feasible control inputs for desired movements and compensating for internal model uncertainties and external

disturbances, such that higher controllability, manoeuvrability and adaptability to the uncertain environments can be realized.

Presenting fascinating variety of motion forms, nature has always been a source of ideas and inspirations for the robotics community (Habib, 2007). During the past few decades, applications of bio-inspired mobile systems have been extensively studied to undertake large scope of tasks in unstructured and hazardous environments. Towards this end, the major challenge has been converted to be the design of novel robotic systems and related control systems that inspired from the motion/behaviour of biological systems to improve the energy efficiency, to maintain autologous and exogenous compliant interactions, to enhance the adaptability to the dynamic environments. For instance, by considering the agile animals as multi-body systems integrated with actuators and intelligent, mobile sensors, particularly represent the relationship between animal's joint and muscle using viscoelastic property. Nevertheless, given such a nontrivial representation, the design of these complicated bio-inspired mobile systems has been proven to be considerably challenging. This thesis proposes a bio-inspired micro-robotic system with viscoelastic property, it can be used as a benchmark model for studying bio-inspired design and control of underactuated microrobotic systems.

Design of mechanism and actuation for those mechanical systems raises difficulties in how to achieve systematic methodology in a comprehensive way. For robotic systems such as industrial manipulators, the design concepts are mature, for instance, establishing the interconnection between different links and realizing joints actuation through electric, hydraulic or pneumatic actuators. However, this is not the case for many other kinds of robotic systems, in which some degrees of freedom (DOF) are absent by design or some passive elements are involved, have appeared to be influential to perform motions, which are richer in terms of energy efficiency, speed and agility (Chevallereau et al., 2013; Pfeifer et al., 2012; Zoso and Gosselin, 2012). The robotic systems have the feature above are known as underactuated mechanical systems (UMSs), which are defined with fewer independent control inputs  $m$  than the degree of freedom  $n$ , and as such  $k = n - m$  DOF cannot be

directly actuated. The terminology underactuation is referred to as the system which has a difference between the number of DOF and the number of control actions (Acosta et al., 2005). Studying underactuation in the context of locomotion, as reported in the seminal work (Spong, 1998), is likely to lead to an improved understanding of locomotion in biological systems. The applications of UMSs in real-life is extensive, including mobile robots (Z. Li et al., 2014), helicopters (Meza-Sánchez et al., 2011), underwater vehicles (Cui et al., 2010), legged robots (Ackerman and Seipel, 2013), aircrafts (Do, 2015), spacecrafts (Zou et al., 2011) and flexible systems (Wang et al., 2013). Synthesis of the control systems for UMSs, according to the Brockett's theorem (Brockett et al., 1983), is always challenging due to the non-holonomic property, complicated internal dynamics and unavailability of feedback linearizability. The existence of underactuation and other undesirable properties such as possessing an undetermined relative degree or being in a non-minimum phase, give rise to complex theoretical problems and less generality in which the conventional techniques are not directly applicable, particularly for the issues of trajectory planning and nonlinear control. Still, in spite of the challenges and difficulties, UMSs excel in performing complicated tasks with a reduced number of actuators, which in turns imply the increased manoeuvrability, optimized energy consumption as well as reduced cost. However, as recently reported in (Shiriaev et al., 2014), it is always challenging to find an appropriate way to describe and characterize performance of the non-collocated subsystem due to the underactuation and dynamic couplings.

Starting with this viewpoint, the motions with a repeated pattern at periodic intervals raise interests for various applications, for instance, walking or running of the biological systems under a regular pattern in their implementation. During the past few decades, significant devotions have been made from robotics and control communities towards the trajectory planning and nonlinear control of UMS, not just facing the theoretical challenges, but also towards the practical requirements. Among these studies, a class of UMSs that employ a pendulum or a system of pendulums attracts investigations to select different important nonlinear effects. Attentions have been extensively paid to the classical pendulum-like UMSs as

benchmarks, including the Acrobot (Xin and Yamasaki, 2012; A. Zhang et al., 2013), the Pendubot (Mathis et al., 2014; Ordaz et al., 2014; Xia et al., 2014; Xin et al., 2013), the cart-pole system (Peters et al., 2010; Yih, 2013), the crane systems (Ning Sun et al., 2012; Sun et al., 2013; X. Zhang et al., 2014), the TORA (translational oscillator with rotational actuator) systems (Celani, 2011), Furuta pendulum systems (Chang, 2010; Freidovich et al., 2007). Besides, numerous applications of such systems are known in engineering, for instance, in vibro-absorption problems (Shi and Parker, 2012), in trajectory tracking control of pendulum-driven capsule systems (Y. Liu et al., 2011; Yu et al., 2008a). However, making a periodic motion trajectory through feedback laws has been proved to be essential for nonlinear control. And describing and characterizing the coupling behaviour, which are difficult and challenging, are of vital importance particularly for efficient trajectory planning. This is owing to the coupling system dynamics that make the related analysis a difficult task. In this research, it is found that the underactuated system dynamics are susceptible to the elastic coefficient and viscous coefficient, which are vital factors for energy consumption. As such, it is plausible to design a geometric analysis-based approach to project the dynamics onto a hyper-manifold that is affected qualitatively by the control parameters. Then, the issue of trajectory planning is converted into geometric analysis and trajectory optimization. This thesis proposes a novel characterization algorithm towards the dynamic couplings, and designs kernel practical control indexes in associate with viscoelastic property and the jag problem, and therefore constructs an analytical motion trajectory.

For high fidelity engineering systems, accurate modelling or prediction of nonlinear friction force is a nontrivial while intractable aspect of scientific research. Conventionally, frictions are regarded as instabilities that need to be eliminated or compensated through control systems design. Conversely, for self-propelled robotic systems, friction plays pivotal roles in robot locomotion, the dynamic coupling between the driving mechanism and the robot are utilized to generate efficient stick-slip motions. Hence, accurate predictions of the dynamic interactions in the sticking, presliding and pure sliding regimes become crucial. Therefore, a robust friction model is required in practical engineering problems to capture several

experimentally observed dynamic phenomena reported in literature. Nevertheless, the static friction models solely consider the difference in velocities between two bodies in frictional contact, whilst the hysteretic loops and the drooping frictional characteristics in the regime with lower relative velocity are not captured. Therefore, this study proposes a combined physics-based and analytical-based approach to model the frictional dynamic interactions and identify the frictional limits for the static friction, the presliding regime and the pure sliding regime. It is the first time the dynamic frictional characteristics (non-reversible drooping and hysteretic) are studied towards the capsule systems. The proposed framework is an advisable benchmark to exploit the challenges in friction compensation and control of underactuated micro-robotic systems.

The complexity of control problem related to UMSs can be reduced when the objective is to stabilize merely a subset of the system's DOF. In the specialized literature, a great number of existing control system design for UMSs are based on the idea of linearization through partial feedback (Huda and Yu, 2015; Le et al., 2012, 2014; Lee et al., 2013; Terry and Byl, 2014; Wu and He, 2016). Although linear systems could be suitably applied to capture the nonlinear dynamics at a certain local operation range, globally stabilization of the underactuated dynamics are still unavailable under this approach. Besides, practical requirements are raised from the current applications, in which the adaptability of UMSs is extremely crucial when facing environments with matched and mismatched uncertainties. However, it is difficult to get an exact dynamic model due to the presence of frictions, unknown disturbances, time-varying parameters, etc. It is noted that the descriptions of dynamic couplings between the actuated and passive subsystems of UMSs are typically highly nonlinear. Therefore, it is plausible to consider the employment of approximation approaches to map the coupling between the torques applied at the actuated subsystem and the resulting accelerations of the passive subsystem, with the intent of achieving control globally. The state-of-art literatures indicate that only a few works have addressed the problem of trajectory tracking control of UMSs. Note also that very few reported studies on this subject have presented rigorous analysis of the closed-loop system trajectories. Therefore, the

problem of trajectory tracking control of a class of UMSs with uncertainties is an open problem and requires in-depth investigations. This thesis proposes novel schemes to extend and encompass the adaptive control schemes from fully actuated systems to underactuated systems. Mismatched disturbances are considered in this research which are omitted in most of existing methods for the tracking control of underactuated systems.

## **1.2 Aims and Objectives**

### **1.2.1 Research Aims**

In this research, the main focus is to address the problems that consider: (1) the proposal of a self-propelled robotic model drawing inspirations from the undulatory locomotion of nematode worm, (2) the planning of periodic motion trajectory that accommodates the bio-inspired viscoelastic property, (3) the prediction of dynamic compliance interactions that manipulate the stick-slip effects, and (4) the design of nonlinear and adaptive tracking control systems that can be used to accurately match the reference model in a finite-time horizon. A particular goal is to elaborate a framework that has the basis of the work presented here. Specifically, the aim of this research is to propose principles for: (1) design of motion principles for the bio-inspired robotic model, (2) systematic planning of periodic trajectory with bio-inspired viscoelastic property based on the dynamics of UMSs, (3) physical and analytical characterization of compliant interaction dynamics, and (4) design of nonlinear and adaptive tracking control systems.

### **1.2.2 Research Objectives**

The objectives of this research project are:

1. To investigate the state-of-art in the UMSs and bio-inspired approaches and identify the theoretical challenges and common difficulties (in Chapter 2).
2. To study control systems for UMSs with underactuation degree one using coordinate transformation and decoupling (in Chapter 3).

3. To study the structural control properties of partial integrability and complete integrability of UMSs with underactuation degree one (in Chapter 3).
4. To propose a novel self-propelled robotic model that draws inspirations from the undulatory locomotion of the nematode worm (in Section 4.2.1 of Chapter 4).
5. To propose a novel and systematic algorithm for trajectory planning and control for a class of UMSs with bio-inspired viscoelastic property (in Chapter 4).
6. To design 3D models and develop the prototype of the proposed vibro-driven model, and to conduct comparative experimental studies to verify the robotic model and motion principle (in Section 4.7 of Chapter 4).
7. To perform combined physics-based and analytical-based analysis for the vibro-driven capsule system and develop mathematical model of the frictional interaction dynamics (in Section 5.2 of Chapter 5).
8. To conduct analytical studies on the frictional interaction dynamics of the vibro-driven capsule system (in Section 5.3 of Chapter 5).
9. To extends and encompasses the adaptive control schemes to stabilize the state space of a class of underactuated systems (in Chapter 6).
10. To counteract matched and mismatched disturbances, and function approximation error of a class of underactuated systems (in Chapter 6).

### **1.3 Research Contributions**

Motivated by the aforementioned nontrivial challenges when confronting with the issues of modelling, bio-inspired design and bio-inspired control, trajectory planning and nonlinear control of the UMSs, this thesis specializes in the proposal of new benchmark models and development of novel algorithms for optimal and adaptive underactuated locomotion. The contributions are stated in detail below.

The main contributions of Chapter 3 are to formulate the control problems for trajectory planning and tracking control of 2-DOF UMSs with underactuation degree one and conduct coordination transformation and decoupling of a class of 2-DOF

UMSs with PFL and PFL-free. The control properties of partial integrability and complete integrability of 2-DOF Class I, II UMSs have been investigated with some propositions.

The main contributions of Chapter 4 are to propose a bio-inspired robotic model for underactuated vibro-driven microrobotic systems and to propose a novel geometric analysis-based trajectory planning approach with bio-inspired viscoelastic property. The main idea is to reduce the complexity and to characterize the coupling by imposing a harmonic drive and then to compute the dynamics projection onto a hyper-manifold, such that the issue of trajectory planning is converted into geometric analysis and trajectory optimization. An analytical two-stage velocity trajectory is developed based on the control indexes and dynamic constraints. A locomotion-performance index is proposed and evaluated to identify the optimal viscoelastic parameters. The trajectory is optimally parameterized through rigorous analytical-based analysis. Nonlinear tracking controllers are designed using collocated partial feedback linearization and variable structure control with an auxiliary control variable, respectively. For the sake of efficiency in progression and energy, the proposed method provides a novel approach in characterizing and planning motion trajectory for underactuated vibro-driven systems such that the optimal locomotion can be achieved.

The main contributions of Chapter 5 are to propose a novel model and to analysis and characterise the dynamic frictional interactions of underactuated vibro-driven capsule systems with bio-inspired viscoelastic actuation. Up to now, most investigations in frictional interactions towards capsule systems were confined into static or quasi-dynamic circumstance, where it is difficult to facilitate online utilization and control. In this chapter, it is the first time the dynamic frictional characteristics (non-reversible drooping and hysteretic) are studied towards the capsule systems. Primary attention is devoted to the modelling and characterization of frictional interaction dynamics using a combined physics-based and analytical-based approach, in a manner that non-reversible characteristic for static friction, presliding as well as pure sliding regimes are revealed, and the frictional

limit boundaries are identified. Subsequently, the studies are mainly focused on numerical analysis and comparison of friction-induced vibrational responses and qualitative changes triggered by the control parameters in capsule dynamics. It is found that the models predict periodic responses for the parameters considered and the average capsule velocity can be controlled through proper tuning of the control parameter around identified control points.

The main contributions of Chapter 6 are to propose adaptive control schemes for a class of UMSs with matched and unmatched disturbances. For fully actuated mechanical systems, adaptive stabilization of time-varying reference trajectories can be achieved (He et al., 2016b; Wang, 2016). However, the extension of these works to the underactuated case is not straightforward. This chapter extends and encompasses the adaptive control schemes to stabilize the state space of underactuated systems by designing auxiliary control variables that contain NN approximator and robust compensator. The parametric uncertainties, matched and unmatched external disturbances are considered in the controller design, which feature a generic model in the research of underactuated systems. The unmatched disturbances have been neglected in most of existing methods for the tracking control of underactuated systems. Robust compensators are designed to counteract matched and unmatched disturbances, and function approximation error of NNs and nonlinear frictions. The tracking error can be reduced as small as desired in finite time by selecting appropriate controller parameters.

## **1.4 Structure of the Thesis**

The organization of the thesis is summarized as follows.

Chapter 1 provides an introduction to the thesis. The background and research motivation for carrying out this study are explained, with reference to the state-of-art studies on UMSs. Subsequently, the overall aims and objectives, contributions of the study are stated. A list of publications is presented at the end of the chapter.

Chapter 2 presents a systematic review of relevant studies from the literature. Concentrations are mainly placed on six categories. Elaborate reviews of state-of-art

in modelling, bio-inspired design and bio-inspired motor/behaviour control, periodic trajectory planning and nonlinear control techniques are investigated. Four identified key directions are thoroughly investigated towards the bio-inspired behaviour/motor control of underactuated robotics: (1) active impedance modulation/control for compliance interactions; (2) appropriate mechanical feedback for self-stabilization; (3) optimized morphological design for behavioural variability, and (4) optimal dynamics control for motor control learning. Undulation locomotion and serpentine robotic systems are investigated in this chapter. Challenges and future research trends are summarized.

Chapter 3 studies nonlinear control problem of mechanical systems with underactuation degree one based on coordinate transformation of the UMSs with PFL and PFL-free approach. The control problems of trajectory planning and tracking control of UMSs are then formulated. The control properties of partial integrability and complete integrability of 2-DOF Class I, II UMSs are investigated by proposing some propositions.

Chapter 4 proposes a bio-inspired robotic model of underactuated microrobotic system, develops a novel geometric-analysis based trajectory planning algorithm in the presence of viscoelastic property and constructs two nonlinear tracking control schemes. The non-collocated dynamic constraints are considered into the control indexes, wherein the viscoelastic modelling of actuation interaction plays vital role in the optimal control of stick-slip propulsion and the energy efficacy. The two-stage motion trajectory is constructed and synthesized based on the control indexes and lag problem consideration in control practice. The coupling and qualitative variation patterns between the driving mechanism and the unactuated cart progression are identified through rigorous geometric analysis in the phase plane. The control indexes and constraints are evaluated analytically, and the synthesized trajectory is further optimized and tuned via rigorous analysis on the base of system dynamics. Two tracking control schemes are constructed with rigorous convergence analysis, wherein an auxiliary control variable is designed for the adaptive variable structure control of underactuated system in the presence of parametric uncertainties.

Asymptotic stability and convergence of time-varying reference trajectories for the system dynamics are shown by means of Lyapunov synthesis. The effectiveness and efficacy of the proposed approach are verified via numerical simulations. The robot design, experimental setup and experimental results are presented to validate the proposed robotic model and locomotion principle.

Chapter 5 studies the dynamic frictional characteristics for accurate prediction and control of a vibro-driven capsule model. A combined physics-based and analytical-based approach is proposed to the modelling and characterization of frictional interaction dynamics, as such, non-reversible characteristic for static friction, presliding as well as pure sliding regimes are revealed, and the frictional limit boundaries are identified. Subsequently, the studies are mainly focused on numerical analysis and comparison of friction-induced vibrational responses and qualitative changes triggered by the control parameters in capsule dynamics. The simulation results demonstrate good captions of experimentally observed frictional characteristics, quenching of friction-induced vibrations and satisfaction of energy requirements. The results suggested that the frictional interaction dynamics of the capsule systems for a wide range of vibrational behaviours can be predicted, and the vital importance of a concrete understanding and accurate description of the dynamic friction at the sliding substrate is highlighted.

Chapter 6 proposes a systematic adaptive control scheme for a class of UMSs with matched and unmatched disturbances. Coping with the internal uncertain dynamics and external disturbances, adaptive neural network control schemes are developed with auxiliary control variables to close the unactuated feedback loops. RBF neural networks is adopted to approximate the nonlinearities of the non-collocated subset, the adaptive control algorithm is constructed to estimate the neural networks approximation error and the bounded unmatched disturbance. The combination of variable structure control, NN approximation and adaptive approach makes the constructed new controller more robust, and such errors resulting from trajectory tracking, parameter uncertainties, unmatched external disturbances as well as NN approximation are compensated.

Chapter 7 summarizes the entire thesis and future researches. The research aims and objectives of the PhD project are revisited. The future works are presented for the further studies.

## 1.5 List of Publications

- [1] P. Liu, H. Yu and S. Cang, “Geometric analysis-based trajectory planning and control for underactuated capsule systems with viscoelastic property,” *Transactions of the Institute of Measurement and Control*, September 20, 2017.
- [2] P. Liu, H. Yu and S. Cang, “Trajectory synthesis and optimization of an underactuated microrobotic system with dynamic constraints and couplings,” *International Journal of Control, Automation and Systems*, conditionally accepted.
- [3] P. Liu, H. Yu and S. Cang, “Optimized adaptive tracking control for an underactuated vibro-driven microrobotic system,” *Nonlinear Dynamics*, under review.
- [4] P. Liu, H. Yu and S. Cang, “Modelling and analysis of dynamic frictional interactions of vibro-driven capsule systems with viscoelastic actuation,” *Advances in Engineering Software*, under review.
- [5] P. Liu, H. Yu and S. Cang, “Adaptive neural network tracking control for a class of underactuated systems with matched and mismatched disturbances,” *Nonlinear Dynamics*, under review.
- [6] P. Liu, H. Yu, and S. Cang, “Modelling and dynamic analysis of underactuated capsule systems with friction-induced hysteresis,” In: *Proceedings of the IEEE/RSJ International Conference on Intelligent Robots and Systems, 2016*, Daejeon KR, 9-14 October, pp. 549-554.
- [7] P. Liu, H. Yu, S. Cang and Luige Vladareanu, “Robots-assisted smart firefighting and interdisciplinary perspectives,” In: *Proceedings of the IEEE International Conference on Automation and Computing*, 2016, Colchester UK, 7-8 September, pp. 395-401.
- [8] P. Liu, H. Yu, and S. Cang, “On periodically pendulum-driven systems for underactuated locomotion: A viscoelastic jointed model,” In: *Proceedings of the IEEE International Conference on Automation and Computing*, 2015, Glasgow, UK, 11-12 September, pp. 1-6.
- [9] P. Liu, H. Yu, and S. Cang, “Modelling and control of an elastically joint-actuated cart-pole underactuated system,” In: *Proceedings of the IEEE International*

*Conference on Automation and Computing*, 2014, Cranfield, UK, 12-13 September, pp. 26-31.

## **Chapter 2**

# **Literature Review**

### **2.1 Introduction**

There has been a surge of researches in the field of bio-inspired underactuated robotic systems aiming at significant improvement of the behavioural performances of the robots. Bio-inspiration implies the understanding of principles underlying the behaviours of animals and humans and transfers these principles into the development of robots. Biological systems naturally perform dynamic behaviours in complex environment with fantastic energy efficacy, adaptability and robustness. Active dynamic compliance is created and enhanced from musculoskeletal system (joint-space) to external environment (task-space) amongst the underactuated motions. Whilst the underactuated robotic systems are still lagging behind, in that their self-organisation and overall tasks must be achieved by coordinating the subsystems and dynamically interacting with the environment. Towards the discrepancy of behaviour/motor control in biological and robotic systems, underactuated robotic systems have attracted significant attentions for manoeuvrable, efficient, and adaptive behaviours in the real world. One important question to raise is: How can we design control systems to achieve efficient locomotion, while adapt to dynamic conditions as the living systems do?

Underactuated systems are characterized with fewer independent control inputs than configuration variables. Basically, the terminology underactuation describes the property of a system to have an input vector with smaller dimension than the output vector, meaning that the DOF cannot be fully controlled. UMSs are extensively utilized in the real-life, such as mobile robots (Z. Li et al., 2014), helicopters (Meza-Sánchez et al., 2011), underwater vehicles (Cui et al., 2010), legged robots (Ackerman and Seipel, 2013), aircrafts (Do, 2015), spacecrafts (Zou et al., 2011) and underactuated manipulators (Z. Li et al., 2014). The origination of underactuation are generally diversified, including: (1) the natural dynamics of the system such as spacecraft, aircraft, helicopters, underwater vehicles; (2) by design for reduction of the cost or some practical purposes such as satellites with two thrusters and flexible-link robots; (3) be imposed artificially to create complex low-order nonlinear systems to gain insight into the control of high-order underactuated systems, e.g., the Pendubot (Xia et al., 2014), the Acrobot (A. Zhang et al., 2013), the TORA (Chen and Huang, 2012); and (4) the actuator failure.

It is emerging that the relatively slow evolution of control algorithms for UMSs unmatches the rapid development of sophisticated prototypes, this inconformity makes researchers and practitioners seek feasible solutions when control is supposed to be a vital part of integrally functioning UMSs. To achieve a thorough understanding of UMSs, it is necessary to scrutinize from the dynamic characterizations in the forms of modelling, trajectory planning and nonlinear control of UMSs over the past decade. On the other hand, the complexity is increased by the restricted control authority, resulting into the non-effectiveness of the well-established classical control techniques such as feedback linearizability and passivity. Furthermore, practical requirements are raised from the current applications, for instance, the adaptability of UMSs when facing environments with uncertainties. These difficulties motivate the researchers and engineers all over the world devoting their endeavours into the issues of nonlinear control, stabilization as well as periodic trajectory generation, etc. However, despite these extensive studies, there are a few particularly significant challenges that are related to the control of

nonlinear dynamics derived from autologous compliance interaction between the subsystems and exogenous physical interaction with the environment.

Although these problems and challenges are nontrivial, there are several potentially promising research directions which, we believe, significantly contribute to the progress in the exciting research domain of bio-inspired underactuated robotics. This chapter discusses four prevailing directions of research and technological challenges that will potentially lead to significant breakthroughs in dealing with bio-inspired underactuated systems. The references discussed in this chapter are selected with rationale for representing the critical information that delineate the state-of-art perspectives and addressing particular research issues and problems in underactuated systems. Figure 2.1 demonstrates the relationship of the four directions from the system level. The block region in purple presents the underactuated systems to be controlled, where the issues of modelling (in Section 2.2) and bio-inspired design (in subsection 2.3.1) are discussed. The block region in blue shows the trajectory planning module where the periodic reference trajectory is generated, this module is discussed in Section 2.4. The block region in green demonstrates the control system for underactuated robotic systems, the studies on bio-inspired control and nonlinear control system design are investigated in Subsection 2.3.2 and Section 2.5, respectively.

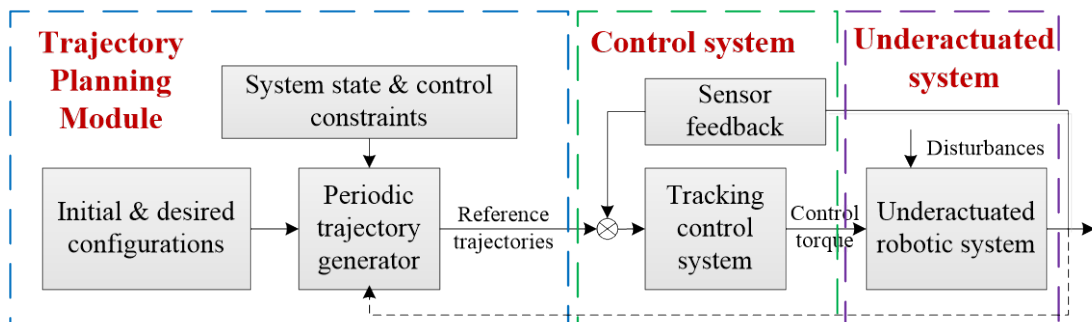


Figure 2.1 Block diagram of trajectory planning and control of underactuated robotic systems

This chapter starts with the reviews of the latest studies on issues of modelling, bio-inspired design and bio-inspired control, planning of periodic trajectory and control system design from Section 2.2 to Section 2.5. Subsequently, challenges and future research trends are summarized in Section 2.6. Finally, confronting these difficulties and challenges, a summary of contributions of this study is presented in Section 2.8 as a trigger of the following chapters.

## 2.2 Modelling of UMSs

Before the motion/trajectory planning and control law design, different analytical solutions for robotic application have been developed through the understanding of the fundamental first principles which precisely portray the robot dynamics. Generally, a set of differential equations are formulated from the basis of mathematical models whose solutions predict the evolution of the configuration variables in time in the presence of a given sequence of external generalized forces which referred to as control input torques. Based on the conventional procedure to model the Euler-Lagrangian mechanical systems as shown in Appendix A, this section aims to shed light on the state-of-art in modelling issue of UMSs.

Modelling of UMSs has been extensively investigated in various domains over the past decade, from prevailing benchmarks such as the cart-pole system (Peters et al., 2010; Yih, 2013) to novel underactuated systems (Huang et al., 2013; Huda and Yu, 2015; Liu et al., 2013b; Zhao et al., 2010). Most of the modelling studies have been conducted based on the model of fundamental Lagrangian mechanical system. However, many realistic and practical considerations have been simplified or omitted, for instance, modelling of the interactions with actuators, sensors, dynamic frictions, and (structured or unstructured) uncertainties and external disturbances. Towards this end, researchers have been trying to design plausible and efficient control systems that are able to guarantee the adaptability and robustness to the inaccuracies. Nevertheless, any achievement in adaptive and robust control becomes intractable due to the underactuated dynamics. Therefore, modelling of the UMSs in a systematic way becomes a nontrivial issue.

For high fidelity engineering systems, accurate modelling or prediction of nonlinear frictional dynamics has always been a nontrivial while intractable aspect of scientific research. Conventionally, frictional instabilities are required to be eliminated or compensated through efficiently designed controllers. Simplified static friction model using the Rayleigh dissipation function (see Figure 2.2 (b)) has been employed in a very few literatures (Minguzzi, 2015; Sarracino et al., 2013), in which the friction force was considered proportional to the velocity of the object. Subsequently, accompanied by the requirements of underactuated systems in the industrial applications, substantial efforts have been devoted to the modelling of more realistic frictions for practical control purposes (Armstrong-Helouvry, 2012; Freidovich et al., 2010; Lee et al., 2011; Na et al., 2014). The dynamic friction model proposed in these works normally refers to as the LuGre friction model, which is capable of reproducing some of the observed friction distinctive behaviour, such as hysteresis, Stribeck effect and Coulomb friction. A discontinuous friction model was applied on the unactuated joint in (Martínez and Álvarez, 2012) for a class of 2 DOF UMSs, which was based on the Coulomb friction model (Figure 2.2 (a)).

Recently, a modified nonlinear friction model based on the LuGre model utilized for the passivity-based control of UMSs was proposed in (Cornejo and Alvarez-Icaza, 2011). And the passivity-based control law together with the interconnection and damping assignment was successfully demonstrated by an underactuated double pendulum with friction effect. For more realistic application, the considerations of modelling the frictions need to be more practical. As promising underactuated microrobotic models, the capsule robotic systems have attracted significant interest in various applications such as medical assistance (Carpi et al., 2011; Ciuti et al., 2010; Huda and Yu, 2015; Tianjia Sun et al., 2012; C. Zhang et al., 2014a), pipeline inspection (Lai et al., 2010; Perelman and Ostfeld, 2013; Yusupov and Liu, 2016), maritime search (Matos et al., 2013), etc. For self-propelled capsule systems, friction plays pivotal roles in capsule propulsion and locomotion, particularly for the vibro-driven underactuated systems considered in this thesis, the dynamic coupling between the driving mechanism and the system body are utilized

to generate efficient stick-slip motions. Hence, accurate prediction of dynamic interactions in the sticking, presliding as well as pure sliding regimes becomes crucial.

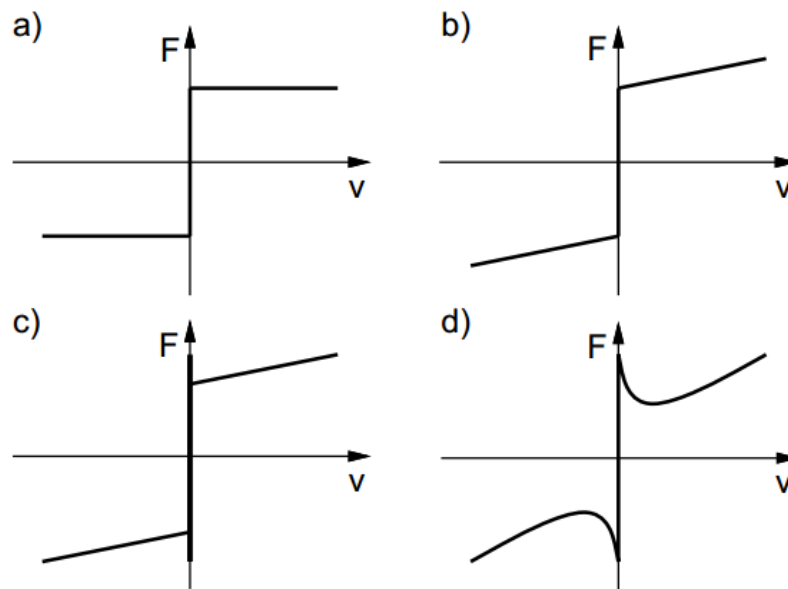


Figure 2.2 Friction models for locomotive systems: (a) the Coulomb model; (b) the Coulomb viscous damping model; (c) Stiction plus Coulomb and viscous friction; (d) seven-parameter model (Olsson et al., 1998).

The uncertainties and disturbances are other important issues need to be considered in modelling of UMSs, which contain parameter uncertainty, environmental noises and uncertain perturbations. The inclusion of disturbances and uncertainties in the system dynamics has always been one of the pivotal issues particularly in the control system design. During the past years, the development of control algorithms is accompanied with the deepening understanding and improving of robustness in the presence of various type of uncertainties and disturbances. Among them, most of the researches modelled the system dynamics considering relatively simple parameters with uncertain boundaries (Mohanty and Yao, 2011; Zeinali and Notash, 2010) and utilized robust control approach. More recently, the

issues of robust tracking control for an underactuated surface vessel with parameter uncertainties was addressed in (Yu et al., 2012). For nonholonomic mobile manipulators with an underactuated joint, adaptive motion/force control by dynamic coupling and output feedback is considered by (Li et al., 2010), in the presence of parametric and functional uncertainties. An integral sliding-mode controller was proposed in (Xu et al., 2014) on a two-wheeled mobile robot with the friction modelled as the combination of viscous friction and Coulomb friction. Most of the studies were conducted from the viewpoint of control, i.e. developing robust controllers for UMSs with uncertainties, however, relatively a few considerable works took this issue to the modelling stage.

To sum up, the issue of modelling of UMSs dynamics is still challenging in accurately represent the interactions with actuators, sensors, dynamic frictions, and (structured or unstructured) uncertainties and external disturbances.

## **2.3 Bio-Inspired Design and Bio-Inspired Control**

### **2.3.1 UMSs with Bio-Inspired Viscoelastic Property**

Nature has always been a source of inspirations and ideas for researchers and practitioners from robotics and control communities. The terminology bio-inspiration implies the understanding of fundamental principles that underlie the motions/behaviours of animals and humans and transfers these principles into development of robotic systems. For example, during walking, the muscles constantly change their stiffness and damping when the leg is swinging forward and the foot is put on the ground. This idea enables explorations in robotic systems with flexible elements—viscoelasticity to mimic the compliant motion of biological muscles.

During the past few decades, the effective utilizations of flexible elements into the robotic locomotion have attracted significant interests. The motivations are diverse, for instance, to build up safer interactions with humans (Argall and Billard, 2010; Ulmen and Cutkosky, 2010; Wolf et al., 2015), to improve the model accuracy

of the robotic systems (Moreira et al., 2014; Wang et al., 2013), to achieve higher level of manoeuvrability, high bandwidth mechanical compliance (Chanthasopeephan et al., 2014; Miyata et al., 2016), flexibility, agility, controllability, adaptability, and efficacy in fulfilling large scope of tasks in unstructured and hazardous environment (Greibenstein et al., 2011; Kolhe et al., 2013; Lam and Xu, 2011; Shang et al., 2011). The DLR hand arm system as shown in Figure 2.3 has Series Elastic Actuators (SEAs) that employ compliant and flexible elements (e.g., springs) at the joints.

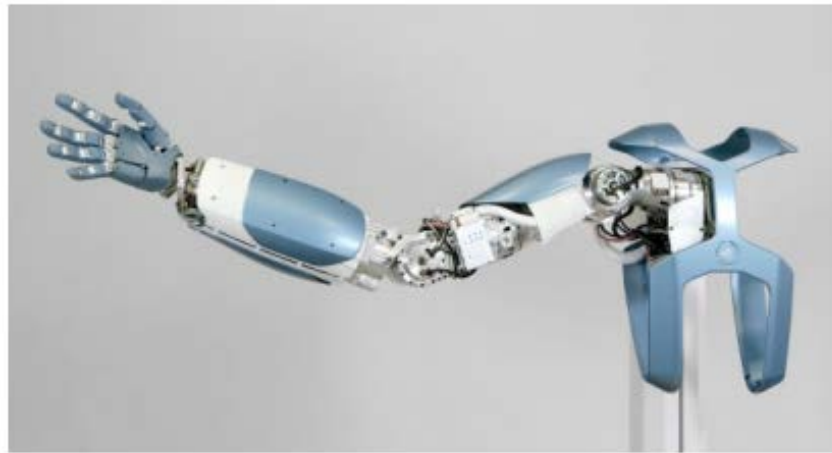


Figure 2.3 The DLR hand arm system (Greibenstein et al., 2011)

Extensive endeavours have been devoted to these research domains. The online estimation problem of transmission stiffness in robots driven by variable stiffness actuators in antagonistic or serial configuration was studied in (Flacco et al., 2012) without the need for joint torque sensing. A viscoelastic models were proposed in (Nguyen et al., 2014) for a soft robotic mechanism horizontally actuated by two dielectric elastomer actuators. To maximize the energy dissipated in transparent laminates under low velocity impact, a genetic algorithm was employed in (Antoine and Batra, 2015) to optimize a model built as thermo-elasto-visco-plastic materials. In the presence of hysteresis and friction, the impact on stiffness and damping characteristics of elastic robot joints were discussed in (Ruderman, 2012). To design

an optimal motion trajectory of flexible mobile manipulators, Pontryagin's minimum principle was adopted in (Korayem et al., 2012) and the optimal control issue was converted into a two point boundary value problem. However, for locomotive systems, the challenges are remained in how to achieve a systematic way of utilizing the system dynamics in the forms of optimally synthesized trajectory and effectively designed controller, particularly in the presence of viscoelasticity. Structural simple systems may behave rich system dynamics, and a tiny parameter variation may lead to qualitative changes of the system outputs.

Recently, along with the practical requirement of engineering applications and the rising research interest in nonlinear dynamics, the vibro-impact characteristic of active mechanisms have been widely applied to a large range of practical mechanical systems. During these applications, correlative relationships between the model parameters and dynamic performance can be achieved. Driven by external harmonic excitations, these implementations are capable of motions such as rectilinear (Liu et al., 2013a; Pavlovskaia et al., 2015), unidirectional (Pavlovskaia and Wiercigroch, 2003) and bidirectional (Liu et al., 2013b) by utilizing a periodically driven mass/inertia interacting with the main body. A newly developed three masses model was analysed and compared with a low dimensional model in (Pavlovskaia et al., 2015). More interestingly, the authors considered three main control parameters which were referred to as the applied static force, the amplitude and the frequency of the applied dynamics force, which were optimally chosen through the higher dimensional model simulations. As an practical application in robotics domain, the vibro-impact dynamics of a capsule robot was studied in (Liu et al., 2013b; Y. Liu et al., 2015), which consists of a capsule main body interacting with an internal mass driven by a harmonic excitation. It is revealed in (Liu et al., 2013b) that the system response are mainly periodic and the best progression can be determined by a careful choice of the system parameters. In the presence of various friction models, the qualitative changes in the capsule dynamics were studied in (Liu et al., 2013a) such that directional control of the system was achieved. Notably, the dynamic models developed by these works have been proved to be useful for uncovering the interactive dynamic performance of such systems in real-world

applications. Moreover, the related studies have contributed abundant information of the fundamental characteristics to the non-smooth motions of practical mechanical systems especially with impacts. It is important to note that most of these researches are, in nature, based on linear motions with the consideration of viscoelastic characteristic. However, for the systems that are intrinsically nonlinear, limited studies have been considered modelling, analysis and optimal parameter selection for active rotational motions with viscoelastic properties.

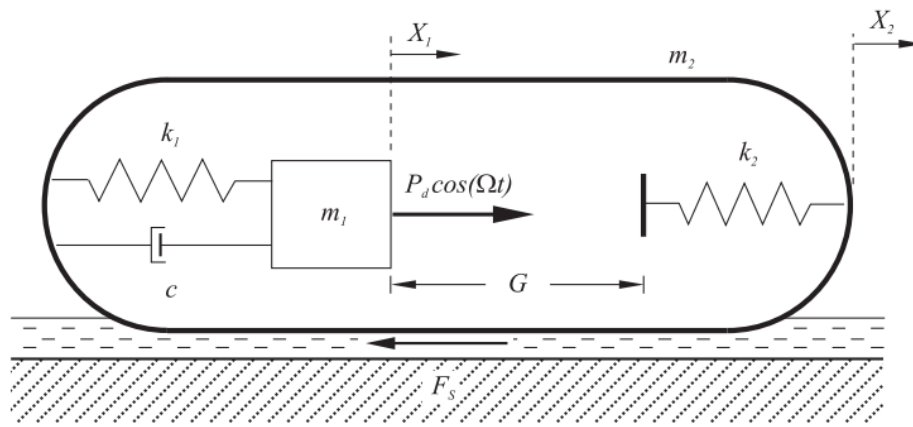


Figure 2.4 Physical model of the vibro-impact capsule system (Liu et al., 2013b)

It is well known that incorporated with nonlinear elements, harmonically excited mass-spring-damper systems behave complex dynamics in their motion near resonant conditions (Nayfeh and Balachandran, 2008). Particularly when a pendulum is introduced, its geometric nonlinearity initially coupled with the rotational motion naturally induces the occurrence of quadratic nonlinearities. Extensive investigations have been carried out from a perspective of utilizing the pendulum in real environment which needs to be stabilized or neutralized, for example, effective vibration control of absorbers (Harne, 2013; Li et al., 2013; Weber, 2014), balance control of suspension system (C.-J. Huang et al., 2010; Lee and Kim, 2010) and human standing posture (Insperger et al., 2013; Kanamiya et al., 2010), etc. However, the researches above are mainly restricted to the stability and dynamic behaviour of unforced systems, relatively few efforts have been devoted to

the nonlinear dynamic behaviour and efficient controller design of mobile mechanisms.

### **2.3.2 Bio-Inspired Behaviour/Motor Control**

Biological systems naturally exhibit energy efficient, robust and adaptive behaviours in complicated environment, whilst the robotic systems we have are still suffering from insufficient capabilities of sensory-motor and learning. To bridge the gap between biological and robotic systems in behaviour control, there has been a surge of research interest in underactuated robotic systems operating in the real world.

Due to the nature of UMSs, the behaviours of underactuated robots are constrained by their passive dynamics, which characterize the motion control in biological systems (Iida, 2009). The passive dynamics bring three advantages: (1) most of the behaviours of underactuated robots are regulated by passive dynamics due to less number of motors, e.g. Passive Dynamic Walkers (Y. Huang et al., 2010; Wang et al., 2010); (2) the locomotion velocity is plausible to be improved through exploiting the passive dynamics, and the limitation on maximum speed of each actuator can be sufficiently relaxed; (3) UMSs have simpler mechanical structures and therefore control architectures on account of less number of motors and sensors. Therefore, it is plausible that underactuated robots achieve controlled behaviours and self-adaptability as their biological counterparts through appropriate exploration in their passive dynamics.

#### *A. Active Impedance Modulation/Control for Compliance Interactions*

It is well-established that appropriate utilization of impedance modulation/control is able to improve the interaction ability of robotic systems through modulating high mechanical impedance. Over the years, it has attracted significant research interests in the domains where the robotic systems are required to work in close vicinity or interact with the unknown and dynamic environments or humans.

Active impedance modulation/control is when an actuator mimics the impedance behaviour using software control. Based on the measured output state, a correction is calculated by the controller and set by the (stiff) actuator. An advantage

of controlled impedance is that it can adapt both the damping and stiffness (contributing to the impedance of the system) online and this in a theoretical infinite range and with infinite speed (Vanderborght et al., 2013). A novel human-like learning controller to interact with unknown environments was proposed in (Yang et al., 2011), which can deal with unstable situations that are typical of tool use and gradually acquire a desired stability margin. (Hussain et al., 2013) presented an adaptive impedance control scheme adapts the robotic assistance according to the disability level and voluntary participation of human subjects. An impedance model with virtual force was considered in (Yang et al., 2013) to design the model reference control of robot dynamics, which provides a kind of cushion effect (compliance) for better user experience.

Noted that the determination of the architecture of active impedance control is dramatically related to specific application and required performance of impedance regulation. The specifications include, naming a few, stability bandwidth, desired impedances, passivity, working frequency, and other mechanical and electrical features of the robotic systems.

#### *B. Appropriate Mechanical Feedback for Self-Stabilization*

Mechanical feedback is an important and useful notion that proposed and studied by many researchers from various fields of biological research. Its main idea is that many mechanical processes in biology effectively act to assist in the self-stabilization of tasks, and therefore, serve functionally as a first level of feedback control (Seipel, 2011). Using neural feedback has been proved insufficient to control many tasks of biological systems, and therefore more appropriate perspectives in feedback control in neuro-mechanical systems are needed when designing bio-inspired robot and control system architectures.

It is plausible that the motions of underactuated robot are able to be mechanically regulated through appropriate design inspired from the biological systems. Mechanical feedback for self-stabilization in periodic motions has been proved applicable to different kinds of underactuated robot models. The study in (Collins et al., 2005) based on the Passive Dynamic Walker is a good example as

shown in Figure 2.5, which can walk on level ground and induce behaviour patterns with small active power sources substituted for gravity. More interestingly, the undesired motion deviations due to the robot-environment interactions can be mechanically regulated.

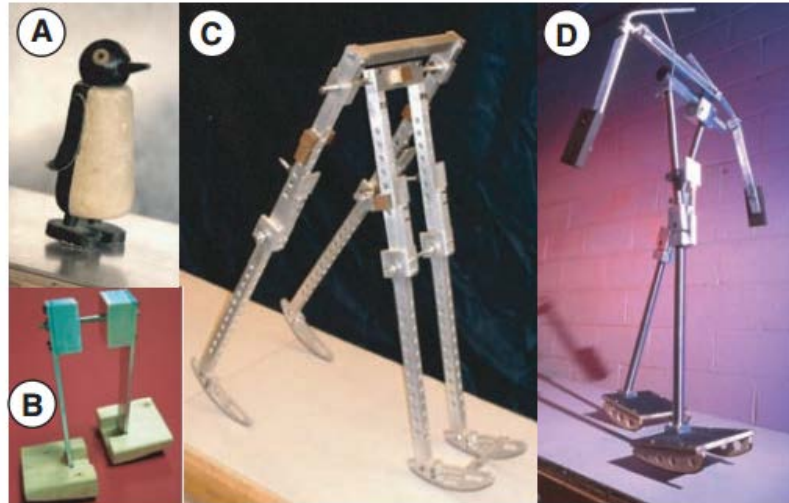


Figure 2.5 Bipedal robots based on passive-dynamic walkers (Collins et al., 2005)

### *C. Optimized Morphological Design for Behavioural Variability*

The nonlinear dynamics of underactuated robots that derived from their morphological constraints have attracted many research interests in to the modest control system design. Morphology plays a vital role in underactuated systems with respect to the behavioural variability, since many UMSs merely capable of limited periodic behavioural patterns (Iida, 2009).

The study in (Collins et al., 2015) demonstrates reduction of the energy cost of human walking through designing and utilization of an unpowered exoskeleton. A lightweight elastic device was designed as shown in Figure 2.6 that acts in parallel with the user's calf muscles, off-loading muscle force and thereby reducing the metabolic energy consumed in contractions. Interestingly, there is no mechanical work is done by the actuators, and the springs store and return energy through the

fact that the kinetic and potential energy of the body remain constant on average. A powered prosthetic ankle joint was designed in (Grimmer et al., 2016) for walking and running as shown in Figure 2.7. The active spring design improve the motion/behavioural variability in certain range and relax the limitations in positive work output of passive walking and running feet. These studies demonstrate how various kinds of motion/behaviour can be created through the robot nonlinear dynamics that are significant in the motion adaptability as well. It is noted that not only behavioural variability is achieved through appropriate computational procedure of the motor control, but also it is dramatically determined by the interaction dynamics with simple motor action and the reaction force from the environment.

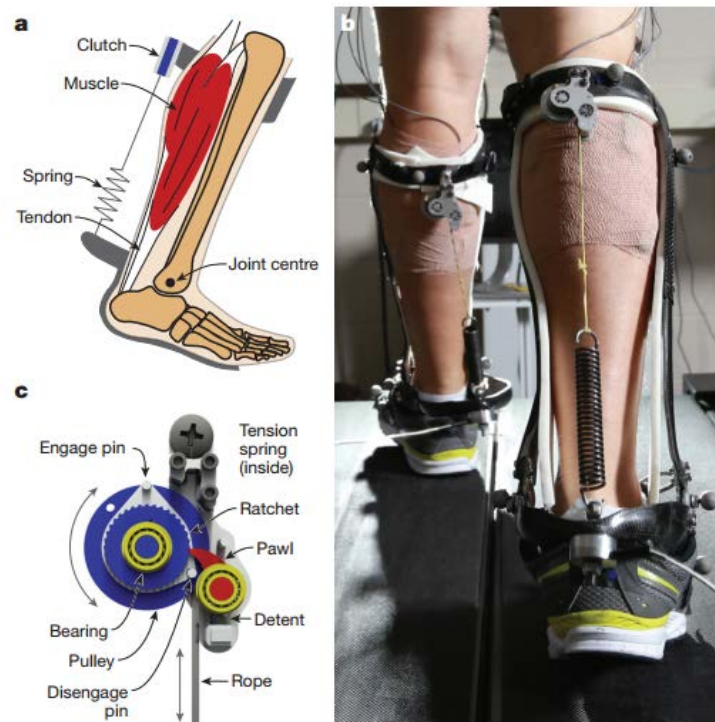


Figure 2.6 Unpowered exoskeleton design (Collins et al., 2015)

One of the interesting challenges is how to generate desired and substantially different motor/behaviour patterns through appropriate design and control of the morphological parameters, e.g., coefficient of elasticity and viscosity. As such, new

optimal motion control schemes are to be constructed with energy efficiency and adaptability.

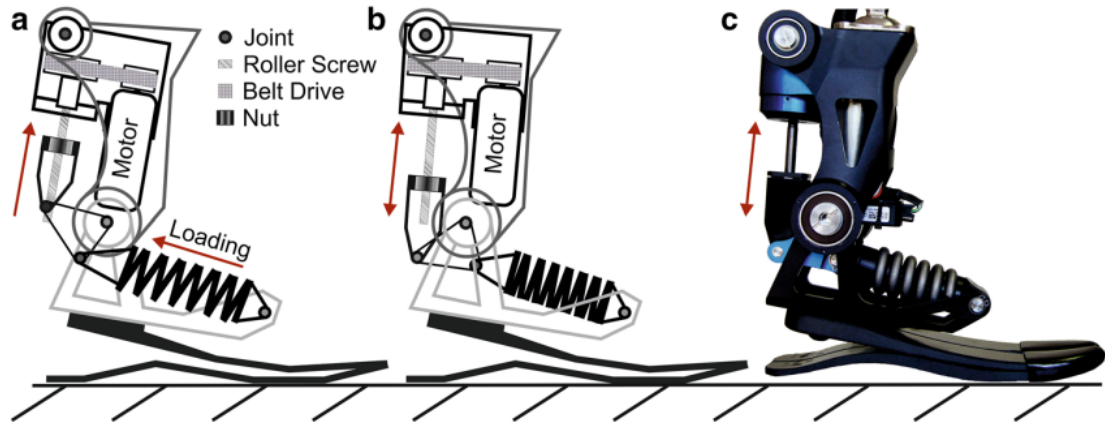


Figure 2.7 Springactive Walk-Run ankle (Grimmer et al., 2016)

#### *D. Optimal Dynamics Control for Motor Control Learning*

The appropriate design of mechanical feedback for self-stabilization has been proved to be of great significance in the research of underactuated robotics, whilst the challenge in kinematic trajectory control is still an intractable issue due to the unactuated/passive dynamics. Towards this control problem, there has been a rising interest in utilization of computational optimization, which is able to tackle with the automatic reasoning of nonlinear dynamics through evaluation of single scalar value. A novel approach to reinforcement learning for parameterized control policies based on the framework of stochastic optimal control with path integrals was studied in (Theodorou et al., 2010). A method that learns to generalize parametrized motor plans by adapting a small set of global parameters was studied in (Kober et al., 2012), called meta-parameters. The arm reaching dynamics was thoroughly explored in (Huang et al., 2012) to achieve reductions of metabolic cost during motor learning as shown in Figure 2.8. A method to learn discrete robot motions from a set of demonstrations was presented in (Khansari-Zadeh and Billard, 2011), global asymptotic stability at the target was guaranteed through defining of sufficient conditions.

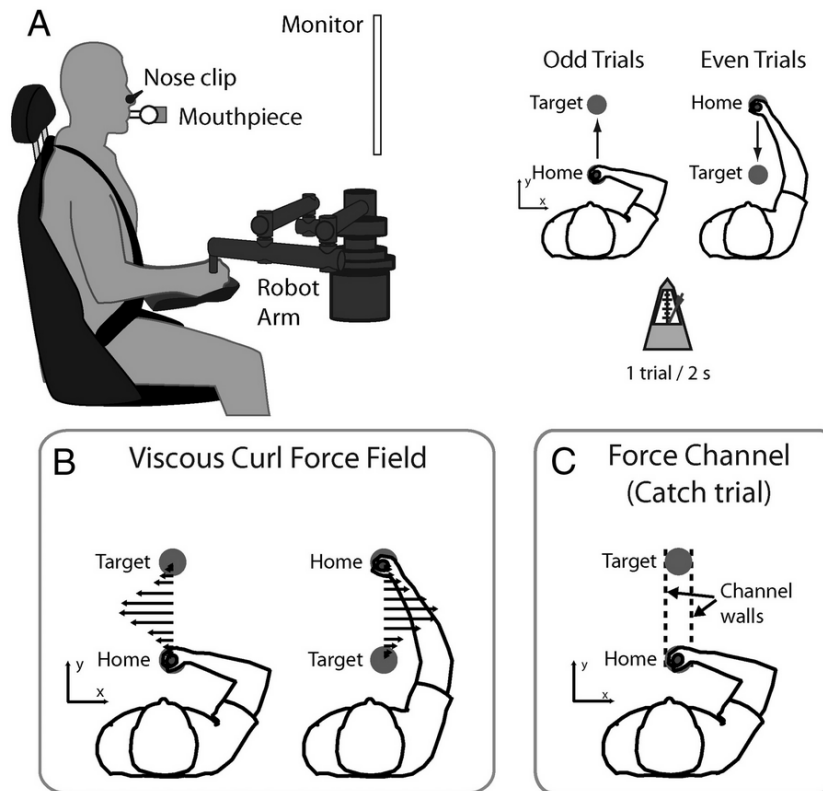


Figure 2.8 Arm reaching experiment setup and force fields (Huang et al., 2012)

The cutting-edge researches on motor control learning including control and trajectory planning have demonstrated significant preliminary steps in bio-inspired control of underactuated robotic systems, whilst there are several challenging issues need to be uncovered. The reduction of the number of trial-and error iterations is the nontrivial and intractable one. Towards this end, it is plausible to explore the design of more generalized state representations, and improvement in autonomy of mechanical model generation of the robot itself (Bongard et al., 2006).

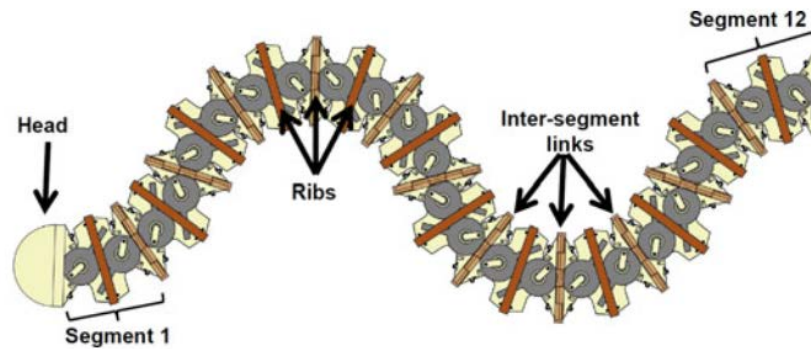
### 2.3.3 Undulatory Locomotion and Serpentine Robotic Systems

Movement is one of the vital existential requirements of microbial and animal life on the earth. Many terrestrial animals adopt limbs to support their weight and to cope with the gravitational forces. Some smaller animals have employed a great number of forms that keep them close to the ground or even underground to

minimise the effects of gravity. Whilst flying, subterranean and marine animals have to deal with various kinds of physical environments.

Undulatory locomotion is a primitive and relatively simple mode of locomotion that relies on the generation and propagation of waves along the animal body. It is remarkably widespread across a wide range of biological systems from motile bacteria and worms to snakes. It is evident that the body's interplay with the physical environment is the key to undulatory locomotion. Various forms of undulations are adopted by animals, which can be categorized into direct (same as the motion direction) or retrograde (opposite to the motion direction), horizontal or vertical, and longitudinal or transverse. Generally speaking, retrograde waves are used to propagate opposite to the motion direction such that the body move in a given direction. Specifically, the environment applies forward forces to the body if the body wave travels backward. For example, some worms and protozoa, when their body is moving forwards or backwards, have their body lined with so-called 'bristles' that jut out at right angles to the long axis and act as paddles to generate sufficient drag forces.

It is evident that undulatory locomotion is typically constrained by frictional or drag forces of the physical environment rather than the gravitational forces. Significant endeavours have been made in the development of robotic systems with undulatory locomotion that is inspired from worms or snakes (Boyle et al., 2013; Liljebäck et al., 2012; Memon et al., 2014; Mohammadi et al., 2014), e.g., the worm-inspired robot as shown in Figure 2.9. These systems typically consist of a chain of rigid segments linked by articulated joints actuated by motors and normally restricted to planar bending motions. They propel themselves by changing their body configurations. The snake robot Anna Konda (Liljebäck et al., 2006; Transeth et al., 2008) is a typical example that is able to push against external obstacles apart from a flat ground and capable of obstacle-aided locomotion. There are also some robotic systems using alternative actuation systems such as pneumatics (Liljebäck et al., 2005; Transeth et al., 2009) and shape-memory alloys (Liu and Liao, 2004; Yuk et al., 2011).



(a) Top-down 2-D schematic of the robot



(b) Physical robot

Figure 2.9 Worm-inspired robot (Boyle et al., 2013)

The forward propulsion by means of undulatory locomotion requires the actuators are controlled in a manner that the propulsive wave propagates along the robot body, this feature is significantly different from the traditional wheeled, legged or tracked robotic systems whose forward motion is obtained simply by driving the motors on the wheel or leg. Therefore, undulatory locomotion has the potential capabilities of robustness and versatility with suitably designed control systems.

Undulatory rectilinear motion can be generally partitioned in two different forms: rectilinear motion using vertical waves as shown in Table 2.1 and rectilinear motion using expanding/contracting segments as shown in Table 2.2.

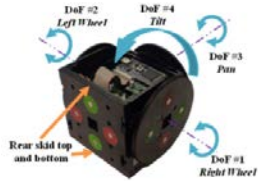
Table 2.1 Undulation-based bio-inspired robots using vertical waves

<b>Robots/Features</b>	<b>Bionic target</b>	<b>Locomotion types</b>	<b>Sensors</b>	<b>Power supply</b>	<b>Examples</b>
<b>Inchworm robots</b>	Inchworm	Extension & flexion; Autonomous.	Tactile, infrared	Tethered	(Felton et al., 2013; Koh and Cho, 2013; Qiao et al., 2013; Wang et al., 2014)
<b>Snake robots</b>	Snake	Obstacle-aided ; Autonomous.	Visual camera	Tethered	(Liljebäck et al., 2006; Liljebäck et al., 2012; Mohammadi et al., 2014; Transeth et al., 2008)
<b>Reconfigurable robots</b>	Snake	Sinusoid serpentine -like; Rolling track; Caterpillar-like	Visual camera	Electric al module	 (Eckenstein and Yim, 2012, 2014)
<b>Modular robots</b>	Snake	Serpentine -like; climbing, swimming & crossing gaps; Autonomous.	Video camera	Tethered	 ("Biorobotics Lab," n.d.)

To sum up, it is plausible that underactuated robots achieve controlled behaviours and self-adaptability as their biological counterparts through appropriate exploration in their passive dynamics. Viscoelastic property helps understanding the efficient, compliant and adaptive behaviours of biological systems through bio-inspired design of the underactuated robotic systems, the problem is how to realize optimal morphological design such that the behavioural variation can be

increased while maintaining fascinating characteristics of underactuated robotic systems? Besides, compliant interactions can be obtained through active impedance modulation/control, self-stabilization can be realized by appropriate mechanical feedback using passive dynamics and motor learning is important preliminary steps in bio-inspired control of underactuated systems.

Table 2.2 Undulation-based bio-inspired robots using linear expansion

Robots/Features	Bionic target	Locomotion type	Sensors	Power supply	Examples
<b>Slim Slime robot</b>	Snake	Snake-like creep; Snail-like pedal wave; Lateral rolling & pivot turning; Autonomous.	Visual camera	Tethered	 (Wright et al., 2012)
<b>Planar inchworm robot</b>	Inchworm/Snake	Snake-like creep; Autonomous.	Visual camera	Tethered	 Planar Walker (Chen and Yeo, 2003)
<b>Self-Reconfigurable robots</b>	Snake	Contracting/expanding; Connecting/disconnecting from neighbouring modules; Autonomous.	Not reported	Electrical module	 SMORES (Davey et al., 2012)

## 2.4 Periodic Trajectory Planning

Trajectory planning is a terminology that extensively used in robotics and control communities, which generally includes motion planning and trajectory optimization for the process of finding a feasible trajectory to fulfil certain tasks that minimizes or maximizes some measure of performance within prescribed constraint boundaries.

The concentrations on periodic trajectory planning are twofold depending on the dimensions of the input space. For the mechanical systems whose DOF is equivalent to the dimensions of the input space (referred to as fully-actuated systems), the procedure of trajectory planning falls into the task of generating trajectories that integrally reveals the system dynamics and satisfies specific constraints, for instance, bounded input torques, constraints in various motion stages, obstacles avoidance in the work space. In terms of the motion execution, the feedback linearization technique which shed light on the tracking issue of a predesigned reference trajectory is convenient to be extended to more general cases. On the other hand, when the reduced dimensions of the input space appear, the underactuation is an essential factor needs to be considered, which makes finding a feasible trajectory for a specific task highly nontrivial. Moreover, it becomes more complicated in the presence of nonholonomic dynamic constraints (Li and Canny, 2012).

Towards the issue of trajectory planning for UMSs, extensive efforts have been made in diverse ways. A feedback motion-planning algorithm was proposed by (Tedrake et al., 2010) to efficiently evaluate regions of attraction for smooth non-linear systems, which utilized rigorously computed stability regions to build a sparse tree of LQR-stabilized trajectories. Optimized adaptive control and neural network-based trajectory generation was studied in (Yang et al., 2013) for a class of wheeled inverted pendulum (WIP) models of vehicle systems for dynamic balance and motion tracking of desired trajectories. The proposed control method considers the presence of various uncertainties, including both parametric and functional uncertainties. An optimal offline minimum-time trajectory planning (MTTP) approach for underactuated overhead cranes was proposed in (X. Zhang et al., 2014) as shown in Figure 2.10, which simultaneously considers various constraints,

including the bounded swing angle for the payload, bounded velocity, acceleration, and even jerk for the trolley. A point-to-point motion planning algorithm was presented in (Zoso and Gosselin, 2012) that is based on the natural frequency of the pendulum-like free motion with unconstrained degree of freedom. The virtual holonomic constraint approach was utilized in (Meza-Sánchez et al., 2011) to generate the feasible periodic motion along a path founded through the computation of the reduced-order dynamics. Towards the nonholonomic constraints and nonlinear dynamic coupling, (Ryu and Agrawal, 2010) used a special inertia distribution on the manipulator arm to achieve the differential flatness property of mobile manipulators, such that the issues of trajectory planning and control were addressed. However, dynamic constraints and the evaluation of objective function may result in computational complexity and subsequent slow convergence, particularly in the presence of higher DOF and higher degrees of underactuation.

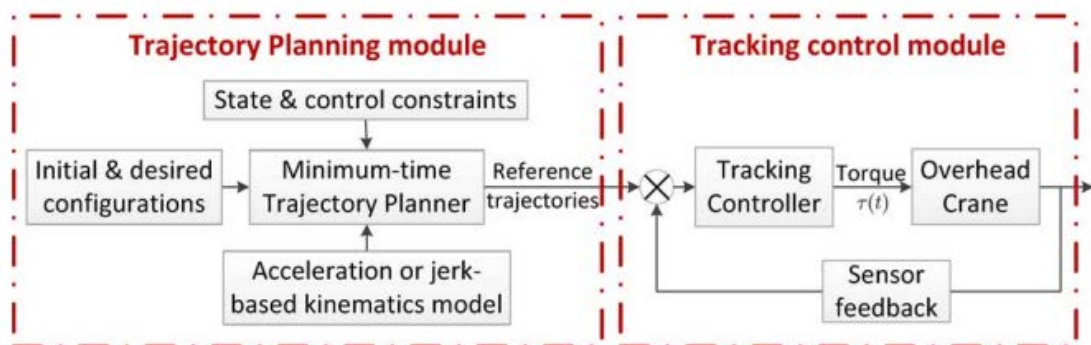


Figure 2.10 Block diagram for planning and control of overhead crane

Systems (X. Zhang et al., 2014)

Kinematic coupling was elaborately considered in (Ning Sun et al., 2012) to plan the motion trajectory of overhead crane systems with the objectives of smooth trolley transportation and small payload swing. An anti-swing mechanism was developed into an S-shape reference trajectory based on analytical studies on the coupling behaviour between the payload and the trolley. The combined trajectory was tuned through a designed iterative learning scheme to ensure precise trolley

positioning. The trajectory planning scheme proposed in this study (as shown in Figure 2.11) was proved to be robust against payload variations, and it guarantees accurate trolley positioning and efficient swing elimination. However, globally describing and characterizing the coupling behaviour including kinematic and dynamic couplings, which are of vital importance particularly for efficient trajectory planning, are still difficult and challenging tasks for underactuated robotic systems.

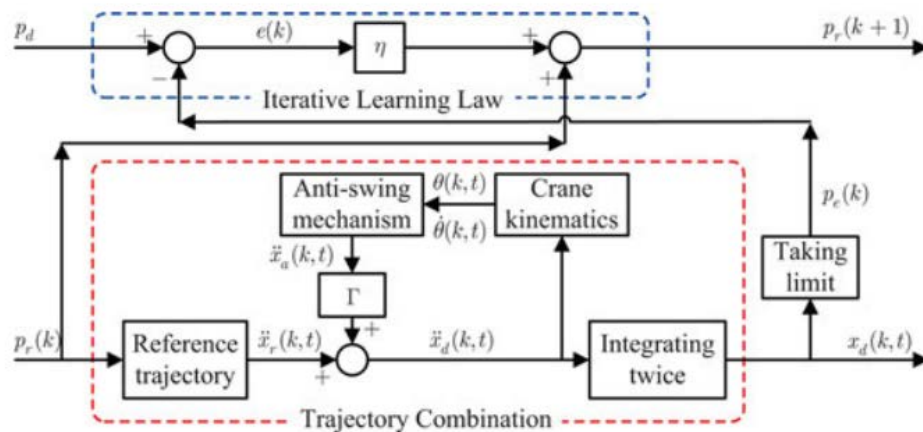


Figure 2.11 Overall block diagram for trajectory planning in the  $k$ th iteration (Ning Sun et al., 2012)

Motion behaviours are important aspect to the trajectory of underactuated systems. A behaviour-based control approach was proposed in (Huda et al., 2014) for the trajectory tracking control of an underactuated planar capsule robot. The basis behaviours and required behaviour-sets to track the trajectory were elaborately defined in this study. Four motion behaviours, four switching behaviours and one stationary behaviour were proposed for the motion trajectory generation. A selection algorithm was designed to determine the appropriate behaviour-set to track each piece of the trajectory. Nevertheless, the issue of robustness to uncertainties and external disturbances were not investigated.

There have been a rising research interests in employing limit cycle reshaping/control for trajectory planning of underactuated robots. This approach is

motivated by various practical engineering applications whose motion behaviours are repetitively, for instance, walking (Hu et al., 2011; Tlalolini et al., 2011), running (Haldane et al., 2013; Karssen and Wisse, 2011), etc. Limit cycles are periodic trajectories defined on the phase space, accordingly the utilization of limit cycles can be regarded as curve tracking in the phase space. The common difficulty exists in the determination of the existence of limit cycles for a given set of differential equations. It is also challenging to plan these periodic orbits as feasible trajectory candidates which can be served as the dynamic behaviour of the closed-loop system. The utilization of limit cycle control falls in to the existence of limit cycles and the orbital stability analysis. Confronting both tasks, Poincaré map analysis is a popular and promising approach. The method of Poincaré sections and return maps has been widely used to determine the existence and stability of periodic orbits in a broad range of system models. Poincaré maps are able to sample the solution of a system according to an event-based or time-based rule, and then evaluate the stability properties of equilibrium points (or fixed points) of the sampled system. Periodic solutions correspond to fixed points in Poincaré map. The stability of the periodic solutions can be guaranteed through the stability of the fixed points in Poincaré map which is determined by the eigenvalues of the Poincaré map linearized about these points. Inspired by this idea, extensive studies have been carried out, for example, (Erez and Todorov, 2012; Freidovich et al., 2009; Gregg et al., 2010; Grizzle et al., 2001; Manchester et al., 2011; Plestan et al., 2003; Shkolnik et al., 2010).

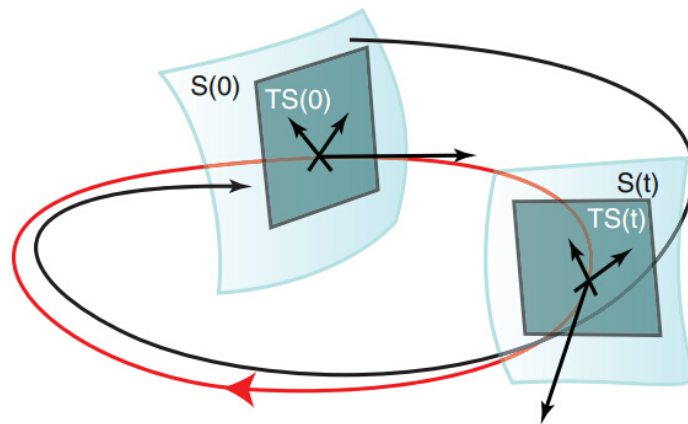


Figure 2.12 A visualization of Poincaré surfaces and transverse linearization of a periodic orbit (red) and a trajectory converging to it (black) (Manchester et al., 2011)

The comparison among trajectory planning algorithms based on key features is demonstrated in Table 2.3.

To sum up, underactuated systems have reduced dimensions of the input space, thus underactuation is an essential factor needs to be considered, which makes finding a feasible trajectory for a specific task highly nontrivial. Moreover, it becomes more complicated in the presence of nonholonomic dynamic constraints (Li and Canny, 2012). Describing and characterizing the coupling behaviour including kinematic and dynamic couplings, which are of vital importance particularly for efficient trajectory planning, are still difficult and challenging tasks for underactuated robotic systems.

Table 2.3 Comparison among trajectory planning algorithms for UMSs based on key features

<b>Algorithms/ Features</b>	<b>Controlled system</b>	<b>Objectives</b>	<b>Novelty</b>	<b>Coping with uncertainties</b>	<b>Holonomic/ Nonholonomic constraints</b>	<b>Dynamic coupling</b>	<b>Kinematic coupling</b>	<b>Example</b>	<b>Comments/ Demerits</b>
Feedback motion planning	Constrained nonlinear system	To build a sparse tree of LQR-stabilized trajectories	LQR trees; Sums-of-squares method	No	No	No	No	(Tedrake et al., 2010)	Randomized motion planning
NN-based trajectory generation	WIP	Dynamic balance and motion tracking	Optimized trajectory model	Yes	Yes	No	No	(Yang et al., 2013)	Implicitly controlled passive dynamics
MTTP	Overhead cranes	Minimum-time trajectory planning	State and control constraints	Yes	No	No	No	(X. Zhang et al., 2014)	Off-line trajectory planning
Point-to-point planning	Cable-suspended robot	Regulation of prescribed poses	Natural frequency of unconstrained DOF	No	No	No	No	(Zoso and Gosselin, 2012)	Unconstrained motion dynamics
Periodic motion planning	Underactuated helicopter	Tracking of prescribed motion trajectory	Virtual constraints-based approach	Yes	Yes	No	No	(Meza-Sánchez et al., 2011)	Control problem of linearized system
Kinematic coupling-based planning	Overhead cranes	Accurate trolley positioning	S-shape reference trajectory with coupling	No	No	No	Yes	(Ning Sun et al., 2012)	Off-line trajectory planning
Behaviour-based planning	Planar capsule robot	Tracking of predefined behaviour-sets	Basis behaviours design	Yes	No	No	No	(Huda et al., 2014)	Off-line trajectory planning
Controlled Invariants	UMSs	Creation of invariants via feedback	Reduction and representation of dynamics	No	Yes	No	No	(Shiriaev et al., 2014)	Virtual holonomic constraints

## 2.5 Nonlinear Control Systems Design

The control of UMSs is an active domain of research in robotics and control engineering, which generates interesting topics and requires systematic nonlinear approaches. The difficulties of designing controller for UMSs are originated from the nature of underactuation, which results in the partially linearizable feedback. Some well-established approaches and properties of nonlinear systems such as feedback linearizability and passivity are not directly applicable in the presence of UMSs. The traditional approaches to nonlinear control laws design are, for instance, backstepping (Cheng et al., 2012; Hu et al., 2012; Taheri et al., 2014; Wai and Muthusamy, 2014), forwarding (Krupinski et al., 2012; Wang and Kosuge, 2012), predictive control (Ge et al., 2012; Oh and Sun, 2010; Yan and Wang, 2012), and SMC (J. Huang et al., 2010; Hwang et al., 2014; Xu et al., 2014; Yu et al., 2012). This is resulted from the fact that these approaches are unable to transform UMSs into cascade nonlinear systems. During the past decade, considerable nonlinear control algorithms have been developed for the underactuated characteristics based on passivity, feedback linearization, Lyapunov theory, etc. However, nonlinear control systems design for UMSs is still regarded as a major open challenge (Ashrafiuon et al., 2010; Jiang, 2010; Liu and Yu, 2013; Pfeifer et al., 2012; Xin and Liu, 2014).

### 2.5.1 Classification

Based on the introduction in Section 2.1, this subsection concentrates on the underactuation due to the origination that imposed artificially to create complex low-order nonlinear systems for gaining insight into the control of higher order UMSs. These systems are classified into two types in (Olfati-Saber, 2000) according to the object to be controlled, which are named as Type-I systems and Type-II systems.

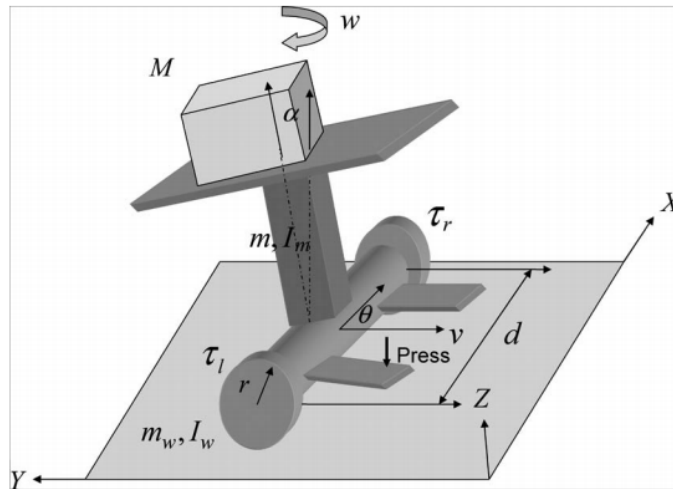


Figure 2.13 The 3-DOF WIP model scheme (Yang et al., 2013)

Type-I systems is defined as the UMSs that contain a pendulum or a system of pendulums, such as the Acrobot, the Pendubot, the IWP (inertia-wheel pendulum) system as shown in Figure 2.13, the rotating pendulum system, the cart-pole system, etc. Based on the system properties, the main control objective is to regulate the configuration variables asymptotically convergence to the set-point references. Two essential issues have been facing towards these UMSs. The first one is devoted to swing the pendulum from the hanging position to the upright position (Huang et al., 2015; Tao et al., 2010; Xin and Yamasaki, 2012). The second issue is dealing with the problem of upward pendulum stabilization (Adhikary and Mahanta, 2013; Ramirez-Neria et al., 2014; Ravichandran and Mahindrakar, 2011), including stabilizing the system around its unstable equilibrium point, on condition that the pendulum is initially above the horizontal plane, or lies inside an open vicinity of zero, i.e. the attraction region of the closed-loop system. Numerous control schemes have been developed, e.g. Bang-Bang Control (Damadi et al., 2011; Kim and Turner, 2014; X. Zhang et al., 2014), Fuzzy Logic (Chang et al., 2013; Hwang et al., 2014; Z. Li et al., 2014; Petković et al., 2013b), energy based (Xin and Yamasaki, 2012), state feedback based (Anvar et al., 2010), Sliding Mode (Man and Lin, 2010), Backstepping, PID adaptive (Li and Xu, 2010), Time Optimal (Jiang and Jiang, 2012), Switching (Ibanez et al., 2013), Neural Network (Zhang et al., 2011), Prediction (Mills et al., 2009), etc. The issues of trajectory planning and optimized adaptive control was investigated in (Yang et al., 2013) for a class of WIP vehicle models. Under the control objective of shaping the controlled vehicle dynamics with

minimized motion tracking errors and angular accelerations, the linear quadratic regulation optimization approach was employed to achieve an optimal reference model. Variable structure technique was used for adaptive control to guarantee the reference model to be accurately matched in a finite-time horizon, even in the presence of internal and external uncertainties. Interestingly, a neural network-based adaptive generator of implicit control trajectory of the tilt angle was proposed to indirectly manipulate the forward velocity.



Figure 2.14 The VTOL aircraft (Hua et al., 2013)

Type-II systems is defined as the UMSs that contain car-like subsystems such as the mobile robot (yue et al., 2010), VTOL aircraft (Hua et al., 2013) as shown in Figure 2.14, UAV (Raffo et al., 2011), underwater vehicles (Cui et al., 2010), etc. The control objectives of these kind of UMSs are to regulate the configuration variables asymptotically convergence to the predesigned trajectories. This trajectory tracking problem has twofold cases: kinematic tracking or dynamic tracking which is depended on whether the systems is represented by a kinematic or dynamic model. Some studies have been made on the kinematic tracking issue, for instance, (Chwa, 2011; Ghommam et al., 2010; Ghommam and Saad, 2014; M. Huang et al., 2010). However, considering the tracking problem in a dynamics point of view is more realistic and practical than its kinematic counterpart, which needs to be uncovered elaborately.

## 2.5.2 Control Algorithms

**Definition 2.1.** The set of DOF of UMSs can be partitioned into two subsets (Spong, 1998), which referred to as collocated subset with its cardinality contains the actuated DOF and equals the number of control inputs; and non-collocated subset accounts for the remaining non-actuated DOF.

### A. Partial Feedback Linearization

Partial feedback linearization (PFL) is an interesting property which can be applied for the control of UMSs. For UMSs with symmetry, the authors proposed natural global changes of coordinates according to the Lagrangian of the system that transform nonlinear models into strict feedback ones. PFL approach is presented in detail as follows.

**Lemma 2.1** (Spong et al., 2006): Consider the actuated configuration vector  $q_2$  in equation (A.11), there exists a global invertible change of control in the form below

$$u = \alpha_1(q)\tau + \beta_1(q, \dot{q}) \quad (2.1)$$

that partially linearizes the dynamics of equation (A.11) in the following form

$$\dot{q}_1 = p_1 \quad (2.2a)$$

$$\dot{p}_1 = f_0(q, p) + g_0(q)\tau \quad (2.2b)$$

$$\dot{q}_2 = p_2 \quad (2.2c)$$

$$\dot{p}_2 = \tau \quad (2.2d)$$

where  $\alpha_1(q)$  is a  $m \times m$  positive-definite symmetric matrix and

$$f_0(q, p) = -D_{11}^{-1}(q)h_1(q, \dot{q}) \quad (2.3a)$$

$$g_0(q) = -D_{11}^{-1}(q)D_{12}(q) \quad (2.3b)$$

The procedure of PFL using Lemma 2.1 is named as the collocated partial linearization, which copes with the dynamics of the actuated configuration vector. The advantages of the PFL are both a conceptual and a structural simplification of the control problem. It is always used as an initial simplifying step for reduction and control of underactuated systems, regardless of the method used for decoupling of

the actuated and unactuated subsystems. There are a few control approaches, such as energy-based control (EBC), adaptive control, and SMC have been developed based on the PFL technique.

### *B. Energy-Based Control*

EBC is one of the most popular control approaches for UMSs particularly for the set-point regulation problem. This idea is originated from the energy existing in the system dynamics. Obtaining the derivative of total energy (Liu and Yu, 2013) gives

$$\dot{H}(q, \dot{q}) = \dot{q}^T [B(q)u - \frac{\partial p(\dot{q})}{\partial \dot{q}}] \leq \dot{q}^T B(q)u \quad (2.4)$$

where  $\dot{H}(q, \dot{q})$  denotes the total energy of the systems,  $p(\dot{q})$  is the dissipation term of UMSs,  $B(q)$  is the input force matrix. (2.4) implies that the system is passive with respect to the input  $u$  and output  $\dot{q}$ . As an essential characteristic of UMSs, the passivity enables the stable origin and existence of feedback control law for  $\dot{H}(q, \dot{q}) \leq 0$ . Therefore, passivity has always been a main property considered in energy-based control. The main idea of passivity-based control is to regulate the total energy of the system to the equivalent value of a desired equilibrium.

Most EBC algorithms integrate with the PFL technique to deal with the swing-up control of the pendulum-like (Type-I) UMSs. Energy-based swing-up control was studied in (Xin and Yamasaki, 2012) for a remotely driven Acrobot which is a 2-link planar robot with the first link being underactuated and the second link being remotely driven by an actuator mounted at a fixed base through a belt. The global motion analysis was conducted based on the behaviour of the closed-loop solution and the stability of the closed-loop equilibrium points. An energy coupling-based output feedback control scheme was proposed in (Sun et al., 2013) for 4 DOF overhead cranes with saturated input constraints. The concept of virtual payloads was introduced with a designed energy storage function to efficiently explore the crane dynamics. A new energy shaping control design was presented in (Albu-Schäffer and Petit, 2012) for a class of underactuated systems including flexible joint robots, Series Elastic Actuators, and Variable Impedance Actuated Robots. Passivity property was utilized to conduct Lyapunov-based analysis for

arbitrarily low feedback gains. Interestingly, non-collocated feedback was considered for the control scheme to shape the kinetic energy of the system.

### *C. Sliding Mode Control/Variable Structure Control*

In the control system construction, uncertainty is a common but intractable problem to be considered, particularly for UMSs. One of the notable forms is the discrepancies between the practical system and the theoretical model built up through some well-established principles. These discrepancies are mainly due to the unmodeled dynamics, parameter uncertainty and external disturbances. Therefore, adaptability and robustness have attracted significant interests from the control engineering community in the past decade. Among them, two of the main approaches are adaptive control (Dydek et al., 2013; Gribovskaya et al., 2011; He et al., 2016a; Park et al., 2010; Sun et al., 2011) and robust control (Fallaha et al., 2011; Fateh, 2012; Islam and Liu, 2011; Kolhe et al., 2013; Soltanpour et al., 2014).

Robust control aims to make the system insensitive to all uncertainties using a fixed structure, but is only suitable for coping with small uncertainties. On the other hand, adaptive control uses on-line identification in which either the system parameters are identified using the predictive errors, or the controller parameters are adjusted using tracking errors. It is applicable to a wide range of parameter variations, but is sensitive to the unstructured uncertainties.

The difficulty of control law designs for UMSs results from the reduced dimension of the input space, and it becomes folded when taking uncertainty into consideration. Thus, the control of UMSs with uncertainty has been received extensive attentions. One interesting approach is Sliding Mode Control (SMC), which is a specific type of Variable Structure Control (VSC). This method has been successfully applied to various UMSs. For example, an adaptive neural network sliding-mode controller design approach with decoupled method was proposed by (Hung and Chung, 2007), which presented a simple way to achieve asymptotic stability for a class of fourth-order nonlinear systems. SMC was employed to stabilize a class of underactuated systems which are in cascaded form in (Xu and Özgüner, 2008). A novel SMC method was introduced by (Park and Chwa, 2009)

based on the coupling sliding surface, the semi-globally asymptotically stable zero dynamics over the upper half-plane was generated. A cascade adaptive fuzzy sliding-mode control (AFSMC) scheme including inner and outer control loops is investigated in (Wai et al., 2008) for the stabilizing and tracking control of a nonlinear two-axis inverted-pendulum servomechanism. Hybrid controller design is developed by (Martinez et al., 2008) for a class of 2-DOF underactuated mechanical systems with dry friction in the joints. It is noted that both of the unactuated and actuated joints were regulated, and the convergence of error dynamics and robustness to small variations of Coulomb friction coefficients were guaranteed. A robust-velocity-tracking scheme was proposed in (J. Huang et al., 2010) using two SMC methods to deal with the parametric uncertainties and external disturbances. To suppress the pendulum sway motion of an offshore container crane in load/unload operations, (Ngo and Hong, 2012) designed a new mechanism for anti-sway control through a sliding surface design. Taking into consideration of frictions and uncertainties, A hierarchical sliding-mode under-actuated control scheme was developed in (Hwang and Wu, 2013) for trajectory tracking of a differential mobile robot. Direct and indirect reference inputs were elaborately planned with separately defined sliding surfaces for the collocated and non-collocated subsystems.

#### *D. Soft Computing-based Learning and Approximation*

Despite the sustained active research on control of underactuated robotics over the past decades, the key technical problems such as adaptive learning of varying nonlinear dynamics, the improvement of robustness, and the removal of effects of unmodeled dynamics, external disturbances and uncertainties remain to be the main research issues that have attracted consecutive attention. Extensive researches have been carried out towards these issues. One of the prevailing objectives is to make the existing controller more intelligent. Soft computing is regarded as one of the key future intelligent systems technologies and has been studied and applied in addressing different kinds of practical problems. As shown in Figure 2.15, it contains various advanced techniques such as Neural Networks (NNs), Fuzzy Logic

(FL), Evolutionary Computation (EC), which are paradigms for mimicking human intelligence and smart optimization mechanisms observed in the nature to solve problems that are too large or too complex to be solved with traditional techniques (Yu and Kaynak, 2009).

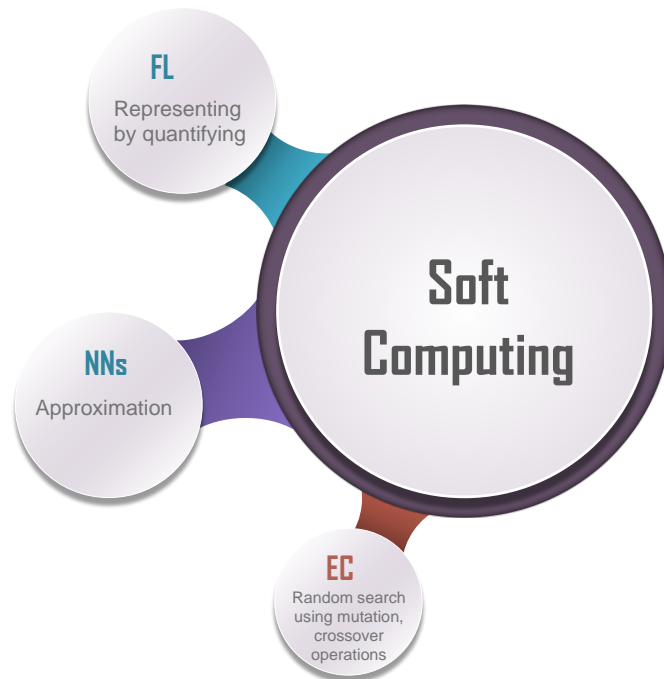


Figure 2.15 Soft computing techniques

The structure of NNs is inspired by observed processes in natural networks of brain neurons as shown in Figure 2.16. The learning process is conducted by adjusting the weights which represent the interconnection strength of neurons based on specific learning algorithms. NNs have an inherent learning ability and are able to approximate a nonlinear continuous function to arbitrary accuracy. As such, a surge of researches has been devoted using NNs-based approach for underactuated robot control. An active adaptive NNs-based controller for WIP models was proposed in (Yang et al., 2014), wherein NN scheme was utilized for motion control of the actuated subsystem, and the passive subsystem was indirectly controlled through the dynamic coupling with the planar forward motion of its actuated

counterpart. The energy-based controller integrated with radial basis function (RBF) NN compensation was developed in (Xia et al., 2014) to swing up the Pendubot. In this study, NNs was employed to compensate the effect of dynamic friction of the system. Multiple underactuated underwater vehicles were considered in (Cui et al., 2010), where the leader-follower formation control system was proposed using NNs to approximate model parametric uncertainties and unknown disturbances for the follower.

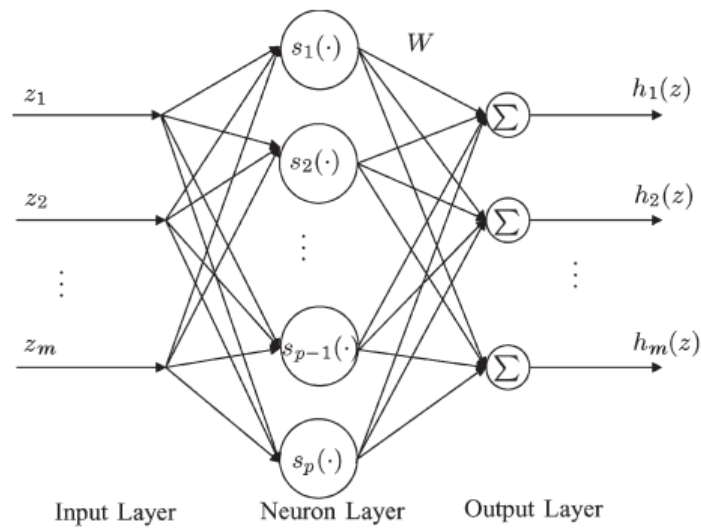


Figure 2.16 Structure of the RBF neural network

FL is a form of multivalued logic derived from fuzzy set theory to address vague instead of precise reasoning, wherein the degree of truth of a statement is ranging from zero to one. Fuzzy systems provide an alternative representation framework to present problems which are difficult to be expressed using deterministic and probabilistic mathematical models. As such, FL is chosen as one of the prevailing approximator for the control problems of UMSs. Nonholonomic mobile manipulator (as shown in Figure 2.17) was considered in (Z. Li et al., 2014) in the presence of parametric and functional uncertainties, and designed an adaptive control for the actuated subsystem using FL approximation. The reference trajectory was developed through FL-based motion generator, and the unactuated subsystem is

indirectly controlled through dynamic coupling. A Takagi-Sugeno-type FL controller was presented in (Xu et al., 2013) for a two-wheeled mobile robot to facilitate position control of the wheels while keeping the pendulum around the upright position. The proposed FL controller synthesizes the heuristic knowledge and the model information of the considered system. The output parameters of the controller are chosen through comparison of the output with a linear controller at certain operating points, which avoids the tedious manual tuning work.

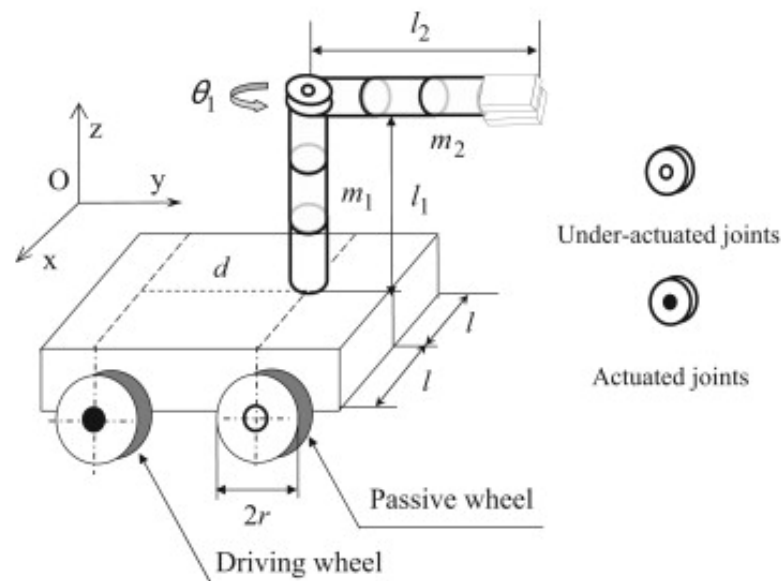


Figure 2.17 The mobile underactuated manipulator (Z. Li et al., 2014)

To sum up, nonlinear control systems design for underactuated systems is still regarded as a major open challenge (Ashrafiuon et al., 2010; Jiang, 2010; Liu and Yu, 2013; Pfeifer et al., 2012; Xin and Liu, 2014). The existence of underactuation and other undesirable properties like possessing an undetermined relative degree or being in a non-minimum phase, give rise to complex theoretical problems and less generality in which conventional techniques are not directly applicable.

Table 2.4 Comparison among nonlinear control algorithms for UMSs based on key features

<b>Algorithms/ Features</b>	<b>Properties</b>	<b>Adaptability to uncertainties</b>	<b>Robustness to disturbances</b>	<b>Merits</b>	<b>Limitations/ Demerits</b>	<b>Examples</b>
<b>PFL</b>	Linearization for dynamics of the actuated/unactuated configuration vector	Poor	Poor	A conceptual and a structural simplification of the control problem	Low-level control	(Huda and Yu, 2015; Le et al., 2014; Wu and He, 2016; H. Yu et al., 2008)
<b>EBC/ Passivity -based control</b>	Regulation of the total energy to the equivalent value of a desired equilibrium state	Weak	Weak	Investigation in passive dynamics	Conditions of passivity need to be satisfied	(Cornejo and Alvarez-Icaza, 2011; Vakil et al., 2011; Valentinis et al., 2015; Venkatesh et al., 2013; Xin and Yamasaki, 2012)
<b>SMC/VSC</b>	Alteration of the dynamics by applying discontinuous control signal	Good	Good	Robust to input disturbances	Control input chattering; Assumption of known uncertainty bounds	(Hwang and Wu, 2013; Ngo and Hong, 2012; Soltanpour et al., 2014; Yu et al., 2012)
<b>NNs-based control</b>	Approximation of nonlinear continuous function	Good	Good	Learning ability; Arbitrary approximation	Design of the NN structure; Determination of the NN parameters	(Xia et al., 2014; Yang et al., 2013, 2014)
<b>FL-based control</b>	Representation of nonlinear continuous function by quantification	Good	Good	Learning ability; Arbitrary approximation	Design of fuzzy rules	(Hwang et al., 2014; Petković et al., 2013b; Wai et al., 2008; Yue et al., 2016; Zhang et al., 2011)

## 2.6 Challenges and Future Trends

### 2.6.1 Theoretical Challenges and Common Difficulties

Based on the investigations in modelling, bio-inspired design and bio-inspired control, trajectory planning and nonlinear control of UMSs, we may observe that the evolutions of relevant techniques are relatively slower than the speed of development of sophisticated robotic prototypes. This drives us wonder that why this discrepancy exists when the above technical issues are supposed to be significant aspects of integrally functioning of UMSs. It is hypothesized that this is due to several challenges that are inherent to UMSs.

**Analysis of frictional interaction dynamics** As discussed in Section 2.2, for high fidelity engineering systems, accurate modelling or prediction of nonlinear friction force is a nontrivial while intractable aspect of scientific research. Conventionally, the frictional instabilities are required to be eliminated or compensated through efficiently designed controllers. For instance, the practical engineering problems historically reside in the circumstances where robust friction models with instabilities are essentially required. Therefore, accurate predictions of friction-induced dynamic responses in sticking, presliding as well as pure sliding regimes become crucial. Several friction models with an arbitrary degree-of-complexity (i.e. numbers of parameters to be identified and controlled) have been proposed in literature which incorporates varying physical phenomena corresponding to friction. However, an accurate representation of friction for given practical applications of UMSs is required to capture several experimentally observed dynamic phenomena reported in literature. The static friction models are merely determined by the relative velocity between surfaces in frictional contact, and the dropping friction characteristics in the low relative velocity regime and the hysteretic loops are not captured.

**Optimal morphological design with bio-inspired viscoelastic property** As discussed in Subsection 2.3.1, UMSs have a couple of beneficial properties

including mechanical self-stability, energy efficiency and manoeuvrability, however, there still remain some challenges that are related to optimal morphological design process of nonlinear mechanical dynamics and their robust and accurate control. To realize efficient trajectory planning and tracking control, bio-inspired morphology constraints need to be elaborately considered, such that the behavioural variation can be increased while maintaining fascinating characteristics of underactuated robotic systems.

**Efficient operation/locomotion** It implies efficient operation/locomotion during each motion cycle in terms of travelling distance and energy consumption, either for the Type-I UMSs (Kolhe et al., 2013; Mathis et al., 2014) that are fastened to the environment or, type-II UMSs that are designed to move and interact with the environment (Cristofaro et al., 2014; Pereira et al., 2014). The operation/locomotion index is typically set as distance-optimal or energy-optimal, as such, the challenges become how to generate optimal trajectory and how to design effective control system to satisfy the designed index.

**Dynamic coupling characterization with system performance** Describing and characterizing the coupling behaviour, which are difficult and challenging, are of vital importance particularly for efficient trajectory planning. Unfortunately, a majority of reported results in the literature, such as (Li et al., 2006; 2014; Yu et al., 2008), are mainly devoted to the couplings characterization in part of the motion stage, the underactuated (passive) motion stage is usually neglected. This is mostly owing to the underactuated kinematic and dynamic coupling behaviours and the relevant analysis is a difficult and challenging task. Towards trajectory construction, it is worth mentioning that there are several significant studies for overhead cranes systems based on phase plane analysis of crane kinematics (Sun et al., 2011, 2012), whilst as locomotion systems, the locomotion-performance indexes (e.g., average locomotion velocity, energy efficiency) were not examined. Indeed, it is a tough task to achieve steady-state periodic motion of the driving mechanism and efficient system performance simultaneously.

**Planning of optimal motion trajectories** Generating periodic motions that can be seen in various natural locomotion of biological systems has always been a challenging issue. UMSs have reduced dimensions of the input space, thus underactuation is an essential factor needs to be considered, which makes finding a feasible trajectory for a specific task highly nontrivial. Moreover, it becomes more complicated in the presence of nonholonomic dynamic constraints (Li and Canny, 2012) and viscoelastic property (Korayem et al., 2012).

**Dealing with uncertainties and disturbances** Uncertainties in system dynamics are critical and challenging issues either for control design or for trajectory planning of the UMSs, including structured and unstructured uncertainties and time-varying matched and unmatched external disturbances. As such, the construction of adaptive control schemes or approximator-based (e.g., NNs, FL) approaches tends to be promising solutions. However, the uncertainty lies in different loops requires different treatments, especially in the non-collocated subset that is unmatched with the control action, which is nontrivial and intractable for adaptive control system design.

## 2.6.2 Trends and Future Directions

Through the investigations into the characteristics and state-of-arts of UMSs and bio-inspired approaches, it is apparent that studying on UMSs is meaningful and significant and has always been a popular and active domain of research in robotics and control communities. Based on the investigations, several essential research issues, trends and promising future research directions of UMSs are summarized and presented as follows.

**Novel bio-inspired design and development** With increasing requirements in real life, current machines and equipment become unable to satisfy new applications and new explorations. What can be further developed based on the current framework of UMSs to deal with the presence of new issues in real-life control systems? For example, the tasks of monitoring, sensing and intervention in narrow and restricted space such as pipeline that are inaccessible to human beings require the robot to undertake minimally invasive operation/locomotion. The robot therefore

needs to adopt some principles inspired from animals that excel in moving in such environments. Therefore, novel bio-inspired design and development of UMSs are required for a natural understanding of motion/behaviour principles of biological systems, the achievement in diversified motion/behaviour patterns of underactuated robotic systems. It is believed that this is a promising research direction of UMSs in applications in military, healthcare, medical assistance, industry, etc.

#### **Accurate modelling and prediction of dynamic frictional interactions**

Friction plays an important part in the motion of UMSs, however, it is easily ignored or simplified in the works during the past decades. Moreover, the investigation of nonlinearities of the friction effects is still open. Therefore, attentions are to be paid to the characterization of frictional dynamics. Besides, investigations from the viewpoint of chemical and material science are also promising directions to characterize the dynamic interactions with the environment.

#### **Analysis of underactuated dynamics with bio-inspired viscoelastic property**

For locomotive UMSs, there has always been a lack of thorough understanding of system dynamics and their efficient utilization. Therefore, efforts are to be made in how to achieve a systematic way of utilizing system dynamics in the forms of optimally synthesized trajectories and effectively designed controllers, particularly when bio-inspired viscoelastic elements are employed. Moreover, to the best of our knowledge, for the systems consisting of a pendulum or a system of pendulums that are essentially nonlinear, unfortunately, there is little analytical research.

#### **Optimal planning of periodic motion trajectories**

Dynamical underactuated locomotion of robotic systems corresponds to the existence of limit cycles in the state space of the UMSs. The generation of periodic motion trajectory and the design of controllers that induce limit cycles, while a challenge in its own right, are made significantly even more difficult by the aforementioned difficulties. The objectives of optimal planning are typically containing time-optimal, distance-optimal and energy-optimal. Therefore, attentions are to be paid to how to construct the periodic motion trajectories and how to design efficient control laws that induces limit cycle locomotion and holds stability.

**Adaptive control in the presence of matched and unmatched uncertainties** It is well-established that tracking control has always been a vital control issue of UMSs due to unknown unactuated trajectory, less control actuator, and nonlinear behaviour, etc. Compared with their fully-actuated counterparts, challenges still remain in trajectory tracking control of UMSs, particularly in the presence of matched and unmatched uncertainties. When the dynamic parameters are uncertain or unknown in practice, and kinematics relationship is not accurate, what adaptive control scheme is feasible for this nonlinear system where linear parameterization does not hold and linear structured adaptive control scheme is not valid.

## 2.7 Conclusion

This chapter has presented the state-of-art in UMSs and bio-inspired approaches over the past decade, including the research problems of modelling, bio-inspired design principles and bio-inspired motor/behaviour control approaches, periodic trajectory planning, and nonlinear control systems. Most of the modelling studies were conducted based on the model of fundamental Lagrangian mechanical system. Realistic and practical considerations need to be emphasized, for instance, models of the interactions with actuators, sensors, dynamic interactions with the environment, dynamic frictions, and (structured or unstructured) uncertainties and external disturbances.

Flexible element—viscoelasticity is of vital significance to understand the compliant motion/behaviour of the biological muscles and biological system. The challenges are remained in how to achieve a systematic way of utilizing the system dynamics in the forms of optimally synthesized trajectory and effectively designed controller, particularly in the presence of bio-inspired viscoelastic property. The passive dynamics of underactuated robotic systems have three advantages: (1) most of the behaviours of underactuated robots are regulated by passive dynamics due to less number of motors; (2) the locomotion velocity can be improved through exploiting the passive dynamics, and the limitation on maximum speed of each actuator can be sufficiently relaxed; (3) UMSs have simpler mechanical structures

and therefore control architectures because less number of motors and sensors. Therefore, by appropriate exploration in the passive dynamics, underactuated robots can achieve controlled behaviours and self- adaptability as their biological counterparts through appropriate exploration in their passive dynamics. Motor control learning including control and trajectory planning are significant preliminary steps in bio-inspired control of underactuated robotic systems. As such, four identified key directions have been thoroughly investigated towards the bio-inspired behaviour/motor control of underactuated robotics.

Periodic trajectory planning generally includes motion planning and trajectory optimization for the process of finding a feasible trajectory for the underactuated robots to fulfil certain tasks that minimizes or maximizes some measure of performance within prescribed constraint boundaries. The underactuation is an essential factor needs to be considered, which makes finding a feasible trajectory for a specific task highly nontrivial. Moreover, it becomes more complicated in the presence of nonholonomic dynamic constraints.

This chapter also emphasizes on the nonlinear control problem of UMSs. The existence of underactuation gives rise to complex theoretical problems and less generality in which classical control techniques are not applicable. Global controllability and uncertainties are key issues for the nonlinear control system design of underactuated systems. The local controllability of the system can be obtained if the linearization of a nonlinear system at an equilibrium point is controllable. In the presence of uncertainties and disturbances, the linear parameterization does not hold and linear structured adaptive control scheme is not valid due to the inaccurate kinematics relationship. There are mainly two types of control problems for UMSs: stabilization control and trajectory tracking control. Extensive researches have been done towards the stabilization, however, trajectory tracking is still challenging. This research investigates the trajectory tracking problem of UMSs.

## Chapter 3

# Control Systems for 2-DOF UMSs with Underactuation Degree One

### 3.1 Introduction

In this chapter, the control problems are formulated for a class of 2-DOF UMSs with underactuation degree one, the structural control properties are investigated for the ease of control systems construction. The system is of underactuation degree one, as defined in (Acosta et al., 2005), if the difference between the number of DOF and the number of control actions is one. The difficulties lie in the fact that reduced input space is less than the number of the system configuration to be controlled. Generally speaking, there are three typical control problems towards UMSs:

1. Feedback stabilization: given a desired equilibrium configuration  $q_d$ , the control objective is to design a feedback control law that makes equilibrium state  $q = q_d$  and  $\dot{q} = 0$  asymptotically stable;
2. Trajectory planning: given an initial state  $(q_0, \dot{q}_0)$  and a final desired state  $(q_d, \dot{q}_d)$ , the control objective is to design a feasible trajectory  $q_d(t)$  that joins the initial and the final states.

3. Trajectory tracking: given a feasibly designed trajectory  $q_d(t)$ , the control objective is to construct a feedback control system that makes the trajectory tracking error  $e(t) = q_d(t) - q(t)$  converges to zero asymptotically.

It is well-established that for fully actuated mechanical systems, the number of control inputs is equal to the dimension of the configuration manifold, thus these control problems are always solvable with convenient solutions. Specifically, for set-point stabilization and trajectory tracking, there always exists a nonlinear static state feedback that can transform the system into a linear controllable form. As for trajectory planning, any trajectory  $q_d(t)$  with arbitrary boundary velocities is feasible to interpolate  $q_0(0)$  and  $q_d(t)$  only if the condition of  $q(t)$  is twice differentiable is satisfied. On the other hand, the mechanical systems with underactuation are the systems that the number of control inputs is less than the dimension of their configuration manifold. However, most studies on underactuated systems focus on set-point regulation, such as swing-up of the Acrobot (Xin and Yamasaki, 2012), the Pendubot (Xia et al., 2014), and the cart-pole system (Yih, 2013), etc.

This chapter is devoted to study the control problems for 2-DOF UMSs with 1-DOF unactuated. The structural control properties are investigated for the ease of control systems construction. The issues of trajectory planning and tracking control are studied. The contributions of this chapter are summarized as follows:

1. Coordination transformation and decoupling of a class of 2-DOF UMSs with PFL-free approach in the cascade form to satisfy the pure feedback condition;
2. Formulating the control problems of trajectory planning and trajectory tracking towards 2-DOF UMSs;
3. Studying the structural control properties of partial integrability and complete integrability.

This chapter is organized as follows. Coordinate transformation of UMSs with PFL and PFL-free approaches are investigated in Section 3.2. In Section 3.3, the

control problems of feedback stabilization, trajectory planning and trajectory tracking for UMSs are formulated. In Section 3.4, some important structural control properties are investigated with emphasis on the partial and complete integrability. Finally, conclusions are given in Section 3.5.

## 3.2 Coordinate Transformations of 2-DOF UMSs

The PFL algorithm discussed in the previous chapter is utilized for coordinate transformation that facilitates control system design. In this section, decoupling of a class of 2-DOF UMSs with PFL and PFL-free are studied to formulate the control problems. The reason behind this consideration is that 2-DOF systems are well-established as benchmarks for the investigations in nonlinear control problems of UMSs, for instance, the cart-pole system, Acrobat, and Pendubot system. The transformation of 2-DOF underactuated dynamics with PFL is firstly studied, and then a system model transformation with PFL-free is presented.

### 3.2.1 Transformation with PFL

Based on the partially linearized dynamics (2.2), the following 2-DOF UMSs in general chained form is considered

$$\dot{q}_1 = p_1 \quad (3.1a)$$

$$\dot{p}_1 = f_0(q, p) + g_0(q)\tau \quad (3.1b)$$

$$\dot{q}_2 = p_2 \quad (3.1c)$$

$$\dot{p}_2 = \tau \quad (3.1d)$$

where  $q = [q_1 \ p_1 \ q_2 \ p_2]^T$  is the state vector defined in the  $Q$ -space for the sake of simplicity. It is noted that the control input exists in the two subsystems. Applying the coordinate transformation (Olfati-Saber, 2002) as

$$w_1 = q_1 - \int_0^{q_2} g_0(s) ds$$

$$w_2 = p_1 - g_0(q)p_2$$

$$w_3 = q_2$$

$$w_4 = p_2 \quad (3.2)$$

Subsequently, in the space defined by the state vector  $w = [w_1 \ w_2 \ w_3 \ w_4]^T$ , the dynamics of (3.1) can be obtained through the time derivative of (3.2), we have

$$\begin{aligned} \dot{w}_1 &= \dot{q}_1 - \frac{d}{dt} \int_0^{q_2} g_0(s) ds \\ &= p_1 - \frac{d}{dt} \int_0^{w_3} g_0(s) ds \\ &= w_2 + g_0(w)w_4 - \frac{d}{dt} \int_0^{w_3} g_0(s) ds \\ \dot{w}_2 &= \dot{p}_1 - g_0(q)\dot{p}_2 - \frac{dg_0(q)}{dt} p_2 \\ &= f_0(q, p) + g_0(q)\tau - \frac{dg_0(q)}{dt} p_2 - g_0(q)\tau \\ &= f_0(w) - \frac{dg_0(w)}{dt} w_4 \\ \dot{w}_3 &= \dot{q}_2 = p_2 = w_4 \\ \dot{w}_4 &= \dot{p}_2 = \tau \end{aligned}$$

Put them collectively as

$$\dot{w}_1 = w_2 + g_0(w)w_4 - \frac{d}{dt} \int_0^{w_3} g_0(s) ds \quad (3.3a)$$

$$\dot{w}_2 = f_0(w) - \frac{dg_0(w)}{dt} w_4 \quad (3.3b)$$

$$\dot{w}_3 = w_4 \quad (3.3c)$$

$$\dot{w}_4 = \tau \quad (3.3d)$$

As a result, it can be concluded that the decoupling is effective, as after the coordinate transformation from Q-space to W-space, there is no control signal  $\tau$  exists in (3.3a) and (3.3b).

### 3.2.2 Transformation with PFL-Free Approach

The complete feedback linearization of UMSs, according to the Brockett's theorem, is always unavailable. In Subsection 3.2.1, the transformation with PFL decouples the actuated subsystem into a double integrator. In this subsection, 2-DOF UMSs are transformed into a model with PFL-free approach.

Consider the generic model of a class of 2-DOF UMSs in the form of (A.11) and after some reorganisation, gives

$$D_{pp}(q)\ddot{q}_p + D_{pa}(q)\ddot{q}_a + H_p(q, \dot{q}) = 0 \quad (3.4a)$$

$$D_{ap}(q)\ddot{q}_p + D_{aa}(q)\ddot{q}_a + H_a(q, \dot{q}) = \tau \quad (3.4b)$$

where  $q = [q_p \ q_a]^T \in R^2$ ,  $H_p(q, \dot{q}) = C_{pp}(q, \dot{q})\dot{q}_p + C_{pa}(q, \dot{q})\dot{q}_a + G_p(q)$  and  $H_a(q, \dot{q}) = C_{ap}(q, \dot{q})\dot{q}_p + C_{aa}(q, \dot{q})\dot{q}_a + G_a(q)$ .

From (3.4), we have

$$\ddot{q}_p = -D_{pp}^{-1}(q)D_{pa}(q)\ddot{q}_a - D_{pp}^{-1}(q)H_p(q, \dot{q}) \quad (3.5)$$

Substitute (3.5) into (3.4b), gives

$$D_{ap}(-D_{pp}^{-1}D_{pa}\ddot{q}_a - D_{pp}^{-1}H_p) + D_{aa}\ddot{q}_a + H_a = \tau \quad (3.6)$$

Take some convenient mathematical calculations, we have

$$\ddot{q}_a = f_a(q, \dot{q}) + g_a(q)\tau \quad (3.7)$$

where

$$f_a(q, \dot{q}) = (D_{aa} - D_{ap}D_{pp}^{-1}D_{pa})^{-1}[D_{ap}D_{pp}^{-1}H_p(q, \dot{q}) - H_a(q, \dot{q})]$$

$$g_a(q) = (D_{aa} - D_{ap}D_{pp}^{-1}D_{pa})^{-1}$$

Subsequently, substitute (3.7) into (3.5) to obtain

$$\begin{aligned} \ddot{q}_p &= -D_{pp}^{-1}D_{pa}[f_a(q, \dot{q}) + g_a(q)\tau] - D_{pp}^{-1}H_p(q, \dot{q}) \\ &= -D_{pp}^{-1}D_{pa}f_a(q, \dot{q}) - D_{pp}^{-1}H_p(q, \dot{q}) - D_{pp}^{-1}D_{pa}g_a(q)\tau \end{aligned}$$

Then  $\ddot{q}_p$  can be described in the form as

$$\ddot{q}_p = f_p(q, \dot{q}) + g_p(q)\tau \quad (3.8)$$

where

$$f_p(q, \dot{q}) = -D_{pp}^{-1}D_{pa}f_a(q, \dot{q}) - D_{pp}^{-1}H_p(q, \dot{q})$$

$$g_p(q) = -D_{pp}^{-1}D_{pa}g_a(q)$$

Put (3.7) and (3.8) collectively to represent the system as

$$\ddot{q}_a = f_a(q, \dot{q}) + g_a(q)\tau \quad (3.9a)$$

$$\ddot{q}_p = f_p(q, \dot{q}) + g_p(q)\tau \quad (3.9b)$$

Define the state vector as  $q = [q_1 \ p_1 \ q_2 \ p_2]^T = [q_p \ \dot{q}_p \ q_a \ \dot{q}_a]^T$ , we therefore have the system model in the  $Q$ -space as

$$\dot{q}_1 = p_1 \quad (3.10a)$$

$$\dot{p}_1 = f_p(q, p) + g_p(q)\tau \quad (3.10b)$$

$$\dot{q}_2 = p_2 \quad (3.10c)$$

$$\dot{p}_2 = f_a(q, \dot{q}) + g_a(q)\tau \quad (3.10d)$$

It is apparent that there are differences between the system model represented by (3.10) and the one described by (3.1) in Subsection 3.2.1. From (3.1c) and (3.1d), the actuated subsystem becomes a double integrator after the transformation with PFL, whilst with PFL-free transformation, nonlinearities arise in the actuated subsystem as shown in (3.10c) and (3.10d). Besides, the control signal of the actuated system in (3.1) has the constant coefficient 1, whilst the one in (3.10) is with the nonlinear coefficient  $g_a(q) = -D_{pp}^{-1}D_{pa}g_a(q)$ . As a result, the decoupling approach utilized in (3.2) is not applicable here. Therefore, a new transformation is considered as follows

$$w_1 = q_1 - \int_0^{q_2} \frac{g_p(s)}{g_a(s)} ds$$

$$w_2 = p_1 - \frac{g_p(q)}{g_a(q)} p_2$$

$$\begin{aligned} w_3 &= q_2 \\ w_4 &= p_2 \end{aligned} \quad (3.11)$$

Then, in the space defined by the new state vector  $w = [w_1 \ w_2 \ w_3 \ w_4]^T$ , the system dynamics described by (3.10) can be obtained through the time derivative of (3.11), gives

$$\begin{aligned} \dot{w}_1 &= \dot{q}_1 - \frac{d}{dt} \int_0^{q_2} \frac{g_p(s)}{g_a(s)} ds \\ &= p_1 - \frac{d}{dt} \int_0^{w_3} \frac{g_p(s)}{g_a(s)} ds \\ &= w_2 + \frac{g_p(w)}{g_a(w)} w_4 - \frac{d}{dt} \int_0^{w_3} \frac{g_p(s)}{g_a(s)} ds \end{aligned} \quad (3.12a)$$

$$\begin{aligned} \dot{w}_2 &= \dot{p}_1 - \frac{g_p}{g_a} \dot{p}_2 - \frac{d(g_p/g_a)}{dt} p_2 \\ &= f_p(q, p) + g_p(q)\tau - \frac{d\left(\frac{g_p}{g_a}\right)}{dt} p_2 - \frac{g_p}{g_a} [f_a(q, \dot{q}) + g_a(q)\tau] \\ &= f_p(w) - \frac{g_p(w)}{g_a(w)} f_a(w) - \frac{d\left[\frac{g_p(w)}{g_a(w)}\right]}{dt} w_4 \end{aligned} \quad (3.12b)$$

$$\dot{w}_3 = \dot{q}_2 = p_2 = w_4 \quad (3.12c)$$

$$\dot{w}_4 = \dot{p}_2 = f_a(q, \dot{q}) + g_a(q)\tau \quad (3.12d)$$

Allocate the dynamics equations collectively as

$$\begin{aligned} \dot{w}_1 &= w_2 + \frac{g_p(w)}{g_a(w)} w_4 - \frac{d}{dt} \int_0^{w_3} \frac{g_p(s)}{g_a(s)} ds \\ \dot{w}_2 &= f_p(w) - \frac{g_p(w)}{g_a(w)} f_a(w) - \frac{d\left[\frac{g_p(w)}{g_a(w)}\right]}{dt} w_4 \\ \dot{w}_3 &= w_4 \\ \dot{w}_4 &= f_a(w) + g_a(w)\tau \end{aligned} \quad (3.13)$$

It is noted that the system dynamics in the  $W$ -space as shown in (3.13) only contains one control input  $\tau$ . The actuated subsystem in the  $W$ -space shares the same form with the one in the  $Q$ -space as shown in (3.10), while more complexities appear in the unactuated subsystem in the  $W$ -space. As such, the following definitions are given as

$$\begin{aligned}
 d_1(w) &= \frac{g_p(w)}{g_a(w)} w_4 - \frac{d}{dt} \int_0^{w_3} \frac{g_p(s)}{g_a(s)} ds \\
 d_2(w) &= f_p(w) - \frac{g_p(w)}{g_a(w)} f_a(w) - \frac{d \left[ \frac{g_p(w)}{g_a(w)} \right]}{dt} w_4 - w_3 \\
 d_3(w) &= 0 \\
 d_4(w) &= f_a(w)
 \end{aligned} \tag{3.14}$$

Substitute (3.14) into (3.13), we have the system dynamics in the  $W$ -space as

$$\begin{aligned}
 \dot{w}_1 &= w_2 + d_1(w) \\
 \dot{w}_2 &= w_3 + d_2(w) \\
 \dot{w}_3 &= w_4 + d_3(w) \\
 \dot{w}_4 &= d_4(w) + g_a(w)\tau
 \end{aligned} \tag{3.15}$$

From (3.15), it is plausible to design a control system to stabilize the system in the  $W$ -space through the unique control input  $\tau$  in the actuated subsystem. It is obvious that  $d_1(w)$  and  $d_2(w)$  could be with high complexities such that the accurate forms are difficult to achieve. One plausible approach is to consider them as nonlinear uncertainties in the system, while they enter the system from the unactuated subsystem, meaning that they are unmatched with the control input. As a result, conventional control schemes are not feasible and applicable in this circumstance. In this thesis, an adaptive controller is firstly designed in this chapter to cope with the parametric uncertainties through realisation of the online update of the parameter values.

### 3.3 Control Problem Formulation

In Section 3.2, coordinate transformations and decoupling for a class of 2-DOF UMSs with PFL and PFL-free approaches are investigated. In this section, the existence of uncertainties is studied to formulate the problem of control system design. Specifically, Subsection 3.3.1 demonstrates that, when the system model is transformed and decoupled with PFL, no uncertainty is contained in the system and needs to be coped with. In this circumstance, the control problem is solely confined into feedback stabilization, trajectory planning or trajectory tracking scheme design for UMSs without uncertainties.

On the other hand, it is shown in Subsection 3.3.2 that the system with PFL-free transformation and decoupling generally allows the existence of uncertainties in the  $Q$ -space that features a generic significance of UMSs. As such, considerations in advanced control need to be taken to cope with the uncertainties. Finally, formulation of the control problems for  $n$ -th order UMSs is given in Subsection 3.3.3.

#### 3.3.1 2-DOF UMSs Control System Design with PFL

From Figure 3.1, the coordinate transformation and decoupling with PFL of the system from  $Q$ -space to  $W$ -space is summarized. The system dynamics in the  $Q$ -space and the  $W$ -space are represented by (3.1) and (3.3), respectively. The transformation law is described by (3.2). In the  $Q$ -space, one control signal  $\tau$  appears in both actuated and unactuated subsystems that formulate the underactuated dynamics; whilst in the  $W$ -space,  $\tau$  only appears in the actuated subsystem that demonstrates the effectiveness of the decoupling.

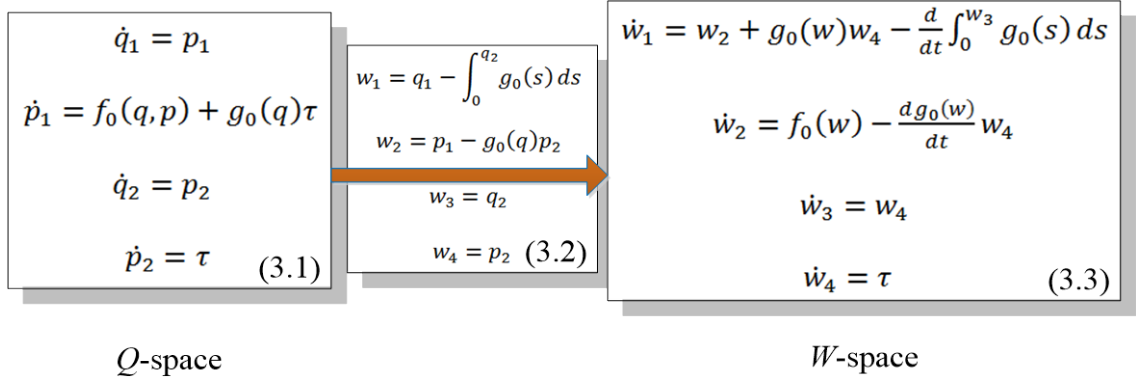


Figure 3.1 The coordination transformation and decoupling of a class of 2-DOF UMSs with PFL approach

It is evident that no uncertainty is contained in  $g_0(q) = D_{pp}^{-1}(q)D_{pa}(q)$  as seen from (3.1b), which guarantees the realizability of the coordinate transformation. It is noted that when using PFL, one assumption that all system parameters are known is given to facilitate the linearization of the system into a double integrator. In this regard, no uncertainty is contained in  $f_0(q, p)$  either. This in turn implies that the following term needs to be known

$$\mathcal{L} = (D_{aa} - D_{ap}D_{pp}^{-1}D_{pa})^{-1} [H_a(q, \dot{q}) - D_{ap}D_{pp}^{-1}H_p(q, \dot{q})] \quad (3.16)$$

From the definition in (A.10), (3.16) is a function of  $H_a(q, \dot{q})$  and  $H_p(q, \dot{q})$ , and therefore it is a function of the matrixes  $C(q, \dot{q})$  and  $G(q)$ . The initial matrix  $D(q)$  is also needed to be available to obtain  $\mathcal{L}$ . Therefore, it is concluded that the system in *Q*-space does not contain any uncertainty when PFL is utilized.

### 3.3.2 2-DOF UMSs Control with PFL-Free Design

From Figure 3.2, the coordinate transformation and decoupling with PFL-free design of the system from *Q*-space to *W*-space is summarized. The system dynamics in the *Q*-space and the *W*-space are represented by (3.10) and (3.13), respectively. The transformation law is described by (3.11). In the *Q*-space, one control signal  $\tau$

appears in both actuated and unactuated subsystems that formulate the underactuated dynamics; whilst in the  $W$ -space,  $\tau$  only appears in the actuated subsystem that demonstrates the effectiveness of the decoupling.

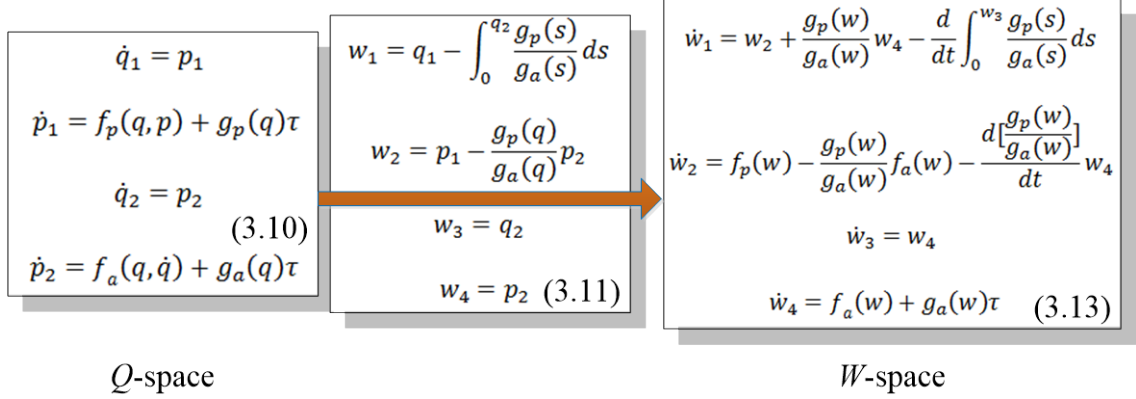


Figure 3.2 The coordination transformation and decoupling of a class of 2-DOF UMSs with PFL-free approach

It is observed from the coordinate transformation law (3.11) that it contains both  $g_p(q) = -D_{pp}^{-1} D_{pa} g_a(q) (D_{aa} - D_{ap} D_{pp}^{-1} D_{pa})^{-1}$  and  $g_a(q) = (D_{aa} - D_{ap} D_{pp}^{-1} D_{pa})^{-1}$ , which have to be known. This in turn implies that the inertia matrix  $D(q)$  is not able to contain uncertainties. Nevertheless, both  $f_p(q, p)$  and  $f_a(q, p)$  in (3.10) can be independently transformed, therefore their availability can be guaranteed. Considering their precise forms as follows that

$$\begin{aligned} f_p(q, \dot{q}) &= -D_{pp}^{-1} D_{pa} f_a(q, \dot{q}) - D_{pp}^{-1} H_p(q, \dot{q}) \\ f_a(q, \dot{q}) &= (D_{aa} - D_{ap} D_{pp}^{-1} D_{pa})^{-1} [D_{ap} D_{pp}^{-1} H_p(q, \dot{q}) - H_a(q, \dot{q})] \end{aligned}$$

As a result, the matrixes  $H_p(q, \dot{q})$  and  $H_a(q, \dot{q})$  may have uncertainties. This in turns indicates that the matrixes  $C(q, \dot{q})$  and  $G(q)$  may be unknown to us. Therefore, in this thesis, the system model without going through PFL approach is also considered in the presence of uncertainties to facilitate adaptive control scheme design.

### 3.3.3 Control Problem Formulation

#### A. Trajectory Planning

Trajectory planning for fully-actuated robotic systems consists of constructing a trajectory that satisfies system dynamics and various constraints, such as limitations in control torques and velocities, obstacle avoidance in the work space. As these systems are feedback linearizable at the motion execution level, thus the task of trajectory tracking of a constructed motion trajectory can be done by conventional approaches. However, robotic systems with passive (unactuated) DOF are generally restricted in feasible motions and their dynamics are typically not feedback linearizable, and the determination of efficient and optimal trajectories is a tough task. Thus, trajectory planning for UMSs is a highly nontrivial task due to the dynamic constraints. There is apparently a need for analytical approaches that simplify the motion trajectory planning and quantify the dynamic properties along the planned motions.

Consider the 2-DOF UMSs dynamics as

$$\begin{aligned} D_{11}(q)\ddot{q}_1 + D_{12}(q)\ddot{q}_2 + H_1(q, \dot{q}) &= 0 \\ D_{21}(q)\ddot{q}_1 + D_{22}(q)\ddot{q}_2 + H_2(q, \dot{q}) &= \tau \end{aligned}$$

Then the problem of trajectory planning is formulated as follows:

**Control Problem 3.1.** Given a final time  $T > t_0$  for one motion cycle and two system states  $q_1$  and  $q_2$ , given arbitrary initial and final states, construct a feasible and optimal motion trajectory for the actuated subsystem that satisfy the above system dynamics and second-order dynamic constraints (motion-dependent velocity and acceleration constraints), and the optimization objectives of travel displacement and energy consumption can be achieved.

In this thesis, a novel trajectory planning algorithm is proposed for a class of 2-DOF UMSs as outlined in Section 3.5 and detailed in Chapter 4. The main idea is to reduce complexity and to characterize coupling by imposing a harmonic drive and then to compute the dynamics projection onto a hyper-manifold, such that the issue

of trajectory planning is converted into geometric analysis and trajectory optimization problems.

### B. Trajectory Tracking Control

Synthesis of the tracking control systems for UMSs, according to the Brockett's theorem, is always challenging due to the nonholonomic property, complicated internal dynamics and unavailability of feedback linearizability. Based on the absence and presence of uncertainties and disturbances, the tracking control problems studied in this thesis are two-folded.

**Control Problem 3.2.** Consider the UMSs in the following form

$$D_{nn}(q)\ddot{q}_n + D_{nc}(q)\ddot{q}_c + C_n(q, \dot{q})\dot{q}_n + G_n(q) = 0 \quad (3.17a)$$

$$D_{cn}(q)\ddot{q}_n + D_{cc}(q)\ddot{q}_c + C_c(q, \dot{q})\dot{q}_c + G_c(q) = \tau \quad (3.17b)$$

where the subscripts “c” and “n” respectively indicate collocated and non-collocated.

Suppose that the control objective is to let the system to follow a prescribed desired motion trajectory, in other words, to drive the system states  $q = [q_c, q_n]^T$  to follow a prescribed path  $q_{cd}$  and  $q_{nd}$ , respectively, and assume that  $q_{cd}$  and  $q_{nd}$  are bounded in norm ( $\|q_{cd}\|_\infty \leq \vartheta_1$ ,  $\|q_{nd}\|_\infty \leq \vartheta_2$  with  $\vartheta_i, i = 1, 2$  be the positive upper bounds of the desired reference trajectories) and uniformly continuous on  $\mathcal{R}^+$ , and homogeneously on the same set, its first and second order derivatives are well-defined, bounded and uniformly continuous.

Introducing the trajectory tracking error as

$$\tilde{q}_c = q_c - q_{cd}, \quad \tilde{q}_n = q_n - q_{nd} \quad (3.18)$$

It is noted that the design of  $\vartheta_1$  and  $\vartheta_2$  has to satisfy the zero dynamics as

$$D_{nc}(q)\ddot{\vartheta}_1 + D_{nn}(q)\ddot{\vartheta}_2 + C_{nc}(q, \dot{q})\dot{\vartheta}_1 + C_{nn}(q, \dot{q})\dot{\vartheta}_2 + G_n(q) = 0 \quad (3.19)$$

The tracking control problem is solvable if we can construct appropriate continuous or discontinuous time-varying feedback controllers, given prescribed

motion trajectories  $q_{cd}$  and  $q_{nd}$ , such that the closed loop system is globally asymptotically stable.

In this thesis, this control problem will be investigated in Chapter 4, where the tracking error dynamics asymptotically stabilized.

**Control Problem 3.3.** Consider the UMSs with parametric uncertainties and external disturbances in the following form

$$D_{cc}(q, \alpha)\ddot{q}_c + D_{cn}(q, \alpha)\ddot{q}_n + C_{cc}(q, \dot{q}, \alpha)\dot{q}_c + C_{cn}(q, \dot{q}, \alpha)\dot{q}_n + G_c(q, \alpha) + F_{vc}(\alpha)\dot{q}_c + F_{cc}(q, \dot{q}, \alpha) + \tau_{dc} = \tau \quad (3.20a)$$

$$D_{nc}(q, \alpha)\ddot{q}_c + D_{nn}(q, \alpha)\ddot{q}_n + C_{nc}(q, \dot{q}, \alpha)\dot{q}_c + C_{nn}(q, \dot{q}, \alpha)\dot{q}_n + G_n(q, \alpha) + F_{vn}(\alpha)\dot{q}_n + F_{cn}(q, \dot{q}, \alpha) + \tau_{dn} = 0 \quad (3.20b)$$

with  $q = [q_1, \dots, q_n]^T \in \mathcal{R}^n$  describes the vector of generalized configurations,  $\alpha \in \mathcal{R}^p$  is the vector of the unknown parameters of the system mainly including the base initial parameters and possible loading parameters ( $p$  indicates the number of uncertain parameters),  $D(q, \alpha) \in \mathcal{R}^{n \times n}$  is a symmetric, positive definite inertial matrix,  $C(q, \dot{q}, \Phi) \in \mathcal{R}^n$  is the vector of centripetal and Coriolis matrix,  $G(q, \Phi) \in \mathcal{R}^n$  is the gravitational torque/force,  $F_v(\alpha) \in \mathcal{R}^{n \times n}$  denotes the viscous friction coefficients which is a positive definite matrix,  $F_c(q, \dot{q}, \alpha) \in \mathcal{R}^n$  models the nonlinear friction torques,  $\tau_d$  denotes bounded unknown disturbances and unmodeled dynamics.

Let the reference trajectory for the actuated and unactuated subsystems be described by the vector-valued functions  $\|q_{cd}\|_\infty \leq \vartheta_1$  and  $\|q_{nd}\|_\infty \leq \vartheta_2$ , respectively, and assume that these functions are bounded in norm and uniformly continuous on  $\mathcal{R}^+$ , and homogenously on the same set, its first and second order derivatives are well-defined, bounded and uniformly continuous. Introducing the trajectory tracking error as

$$\tilde{q}_c = q_c - q_{cd}, \quad \tilde{q}_n = q_n - q_{nd} \quad (3.21)$$

which is to be asymptotically stabilized to zero without the knowledge of the system parameters  $\alpha$ .  $\vartheta_1$  and  $\vartheta_2$  are positive upper bounds of the desired reference trajectories. Noted that the design of  $\vartheta_1$  and  $\vartheta_2$  must satisfy the zero dynamics as

$$\begin{aligned} D_{nc}(q, \alpha)\ddot{\vartheta}_1 + D_{nn}(q, \alpha)\ddot{\vartheta}_2 + C_{nc}(q, \dot{q}, \alpha)\dot{\vartheta}_1 + C_{nn}(q, \dot{q}, \alpha)\dot{\vartheta}_2 + G_n(q, \alpha) \\ + F_{vn}(\alpha)\dot{\vartheta}_2 + F_{cn}(q, \dot{q}, \alpha) + \tau_{dn} = 0 \end{aligned} \quad (3.22)$$

The tracking control problem is solvable if we can construct appropriate continuous or discontinuous time-varying feedback controllers, given prescribed motion trajectories  $q_{cd}$  and  $q_{nd}$ , such that the all the error signals in the closed loop system is globally asymptotically or exponentially stable.

### 3.4 Control Properties of UMSs with 2-DOF

In this section, some of the structural control properties of UMSs are investigated for the ease of facilitating feasible solutions towards the control problems formulated in Section 3.3.

#### 3.4.1 Constraint Integrability

The integrability of constraints is one of the important control properties to be determined. If the constraints are completely integrable, some algebraic relations between the generalized coordinates can be obtained, such that the system dimension can be reduced through eliminating some of the generalized coordinates. Based on the integrability status of UMSs, the following definition is given

**Definition 3.1.** (Raffaella and Oriolo, 2003) (**Partial Integrability and Complete Integrability**) The  $(n-m)$ -dimensional second-order differential constraint expressed by the unactuated subsystem in (A.11) is partially integrable to a set of  $n_1$  ( $0 < n_1 < n - m$ ) first-order differential constraints

$$h_1(q, \dot{q}) = 0$$

or even completely integrable to a set of  $n_2 \leq n_1$  holonomic constraints

$$h_2(q) = 0$$

**Definition 3.2. (Holonomy and Non-holonomy)** An underactuated system is defined as holonomic if the constraint is completely integrable; it is defined as nonholonomic if the constraint is partially integrable or non-integrable.

Consider the 2-DOF UMSs with configuration vector  $q = [q_1 \ q_2]^T$ , and the system has kinetic symmetry with respect to  $q_1$ , in other words, only  $q_2$  is contained in the inertial matrix, the system dynamics is in the following Class-I,II form (Olfati-Saber, 2000)

$$D_{11}(q_2)\ddot{q}_1 + D_{12}(q_2)\ddot{q}_2 + D'_{11}(q_2)\dot{q}_1\dot{q}_2 + D'_{12}(q_2)\dot{q}_2^2 - G_1(q_1, q_2) = u_1 \quad (3.23a)$$

$$D_{21}(q_2)\ddot{q}_1 + D_{22}(q_2)\ddot{q}_2 - \frac{1}{2}D'_{11}(q_2)\dot{q}_1^2 + \frac{1}{2}D'_{22}(q_2)\dot{q}_2^2 - G_2(q_1, q_2) = u_2 \quad (3.23b)$$

where  $G_i(q_1, q_2) = -\frac{\partial V(q)}{\partial q_i}$ ,  $i = 1, 2$ ,  $V(q)$  denotes the potential energy of the system, the prime (') represent  $\frac{d}{dq_2}$ .

#### A. Partial Integrability

**Proposition 3.1.** Given the underactuated system dynamics as (3.23), the second-order dynamic constraint is not integrable if  $u_2 = 0$ .

**Proof.** Consider the underactuated system dynamics as (3.23) with  $u_1 = u \neq 0$  and  $u_2 = 0$ . Then the dynamic equation of the unactuated subsystem is given by

$$D_{21}(q_2)\ddot{q}_1 + D_{22}(q_2)\ddot{q}_2 - \frac{1}{2}D'_{11}(q_2)\dot{q}_1^2 + \frac{1}{2}D'_{22}(q_2)\dot{q}_2^2 - G_2(q_1, q_2) = 0 \quad (3.24)$$

It is noted that no input control signal appears in (3.24), it therefore can be regarded as a second-order dynamic constraint containing generalized coordinates and their first and second-order time derivatives.

Take the following generic form for the first-order constraints as

$$f(\dot{q}, q, t) = 0 \quad (3.25)$$

Taking differentiation of (3.25) with respect to  $t$ , gives

$$\frac{\partial f}{\partial \dot{q}}\ddot{q} + \frac{\partial f}{\partial q}\dot{q} + \frac{\partial f}{\partial t} = 0 \quad (3.26)$$

For (3.24) to be integrable, it must have the equivalent structure with (3.26). Considering that  $t$  does not exist explicitly in (3.24), it is plausible that the term  $\frac{\partial f}{\partial t}$  enters the system as a constant. Then we have

$$f(\dot{q}, q, t) = f_1(\dot{q}, q) + c_1 t \quad (3.27)$$

Taking differentiation of (3.27) with respect to  $t$ , gives

$$\frac{\partial f_1}{\partial \dot{q}} \ddot{q} + \frac{\partial f_1}{\partial q} \dot{q} + c_1 = 0 \quad (3.28)$$

Setting  $\ddot{q} = 0$ , from (3.24) and (3.28), we have

$$\frac{\partial f_1}{\partial \dot{q}} = [D_{21}(q_2) D_{22}(q_2)], \quad c_1 = -G_2 \quad (3.29)$$

It is noted that only  $q_2$  is contained in the inertia matrix, thus  $\dot{q}$  must appear linearly in  $f_1(\dot{q}, q)$ . Accordingly, the following equation is obtained

$$f(\dot{q}, q, t) = D_{21}(q_2)\dot{q}_1 + D_{22}(q_2)\dot{q}_2 + f_2(q) - G_2 t \quad (3.30)$$

Taking differentiation of (3.30) with respect to  $t$ , gives

$$D_{21}(q_2)\ddot{q}_1 + D_{22}(q_2)\ddot{q}_2 + D'_{21}(q_2)\dot{q}_1\dot{q}_2 + D'_{22}(q_2)\dot{q}_2^2 + \frac{\partial f_2}{\partial q} \dot{q} - G_2 = 0 \quad (3.31)$$

Comparing (3.31) with (3.24), the following equation is yielded

$$\frac{\partial f_2}{\partial q} \dot{q} = -\frac{1}{2}D'_{11}(q_2)\dot{q}_1^2 - \frac{1}{2}D'_{22}(q_2)\dot{q}_2^2 - D'_{21}(q_2)\dot{q}_1\dot{q}_2 \quad (3.32)$$

It is evident that (3.32) violates (3.30) due to the fact that  $\dot{q}$  is not contained in  $f_2(q)$ . This is the end of the proof. ■

**Proposition 3.2.** Given the underactuated system dynamics as (3.23), the second-order dynamic constraint (3.24) is partially integrable with the integral form of

$$f(\dot{q}, q, t) = D_{11}(q_2)\dot{q}_1 + D_{12}(q_2)\dot{q}_2 - G_1 t + c_2$$

(where  $c_2$  is a constant related to  $f_2(q)$  to be determined from the system initial conditions) if and only if the following conditions hold:

- (1)  $u_1 = 0$  and  $u_2 = u \neq 0$ ;
- (2) the initial matrix does not contain the unactuated state variable  $q_1$ ;
- (3) the gravitational term in subsystem (3.23a) is constant.

**Proof. (Necessity)**

Consider the underactuated system dynamics as (3.23) with  $u_1 = 0$  and  $u_2 = u \neq 0$ , then the second-order dynamic constraint becomes

$$D_{11}(q_2)\ddot{q}_1 + D_{12}(q_2)\ddot{q}_2 + D'_{11}(q_2)\dot{q}_1\dot{q}_2 + D'_{12}(q_2)\dot{q}_2^2 - G_1 = 0 \quad (3.33)$$

Following the procedure from (3.25) to (3.28), we have

$$\frac{\partial \mathcal{f}_1}{\partial \dot{q}} = [D_{11}(q_2) \ D_{12}(q_2)], \quad c_1 = G_1 \quad (3.34)$$

Accordingly, the following expression of (3.25) is obtained

$$\mathcal{f}(\dot{q}, q, t) = D_{11}(q_2)\dot{q}_1 + D_{12}(q_2)\dot{q}_2 + \mathcal{f}_2(q) - G_1 t \quad (3.35)$$

Taking differentiation of (3.35) with respect to  $t$ , gives

$$D_{11}(q_2)\ddot{q}_1 + D_{12}(q_2)\ddot{q}_2 + D'_{11}(q_2)\dot{q}_1\dot{q}_2 + D'_{12}(q_2)\dot{q}_2^2 + \frac{\partial \mathcal{f}_2}{\partial q} \dot{q} - G_1 = 0 \quad (3.36)$$

Comparing (3.36) with (3.33), the following equation is yielded as

$$\frac{\partial \mathcal{f}_2}{\partial q} \dot{q} = 0 \quad (3.37)$$

It is evident from (3.37) that  $\mathcal{f}_2(q)$  is constant. Therefore, if the integrability of (3.33) can be obtained, from (3.35) and (3.37), we have the following integral form

$$\mathcal{f}(\dot{q}, q, t) = D_{11}(q_2)\dot{q}_1 + D_{12}(q_2)\dot{q}_2 - G_1 t + c_2 \quad (3.38)$$

**(Sufficiency)**

Assuming Proposition 3.2 is hold, then the second-order dynamic constraint becomes

$$D_{11}(q_2)\ddot{q}_1 + D_{12}(q_2)\ddot{q}_2 + D'_{11}(q_2)\dot{q}_1\dot{q}_2 + D'_{12}(q_2)\dot{q}_2^2 - G_1 = 0 \quad (3.39)$$

Taking integration of (3.39) with respect to  $t$ , gives

$$[D_{11}(q_2)\dot{q}_1 + D_{12}(q_2)\dot{q}_2 - G_1 t]_{t_0}^t = 0 \quad (3.40)$$

where  $t_0$  is the initial time.

Rewriting (3.40) in the following form as

$$D_{11}(q_2)\dot{q}_1 + D_{12}(q_2)\dot{q}_2 - G_1 t + c_2 = 0 \quad (3.41)$$

where  $c_2 = -D_{11}(q_2)|_{t=t_0}\dot{q}_1|_{t=t_0} - D_{12}(q_2)|_{t=t_0}\dot{q}_2|_{t=t_0} - G_1 t|_{t=t_0}$ .

This is the end of the proof. ■

### B. Complete Integrability

Propositions and discussions have been given for the partial integrability of the constraint above, in this subsection, conditions for (3.40) to be further integrated are investigated. The following definitions are given at the first place:

**Definition 3.3. (1-Distribution mapping)** The smooth mapping  $\Delta: q \mapsto \Delta(q)$  is the 1-distribution with respect to the constraint that assigns a linear subspace of  $\Delta(q)$  to each configuration variables  $q$ .

**Definition 3.4. (Lie bracket)** let  $f$  and  $g$  be two arbitrary vector fields, the Lie bracket  $[f, g]$  is the vector field of

$$\frac{\partial g}{\partial q} f - \frac{\partial f}{\partial q} g$$

where each column of  $\frac{\partial g}{\partial q}$  and  $\frac{\partial f}{\partial q}$  is partial of velocity with respect to the configuration variable  $q$ .

**Definition 3.5. (Involutivity closure)** The closure  $\bar{\Delta}$  of the distribution  $\Delta$  is involutive closure under the vector field of Lie bracket.

**Definition 3.6. (Distribution involutivity)** A distribution is involutive if it is closed under the vector field of Lie bracket.

Therefore, the following proposition is proposed for the conditions of complete integrability.

**Proposition 3.3.** Given the underactuated system dynamics as (3.23), the second-order dynamic constraint (3.24) is completely integrable with the integral form

$$\mathfrak{D}(q) - \frac{1}{2} G_1 t^2 + c_2 t + c_3 = 0 \quad (3.43)$$

(where  $\frac{\partial \mathfrak{D}(q)}{\partial q} = D_p$ ,  $D_p(q) = [D_{11}(q) \ D_{12}(q)]$  is a Pfaffian constraint that satisfies  $D_p(q)\dot{q} = 0$  and  $c_3$  is a constant determined by the system initial condition) if and only if the following conditions hold:

- (1) the constraint (3.24) is partially integrable;
- (2) the distribution  $\Delta$  of  $D_p(q)\dot{q} = 0$  is involutive.

**Proof.** Consider the following Pfaffian Constraint as

$$D_p(q)\dot{q} = 0 \quad (3.42)$$

Note that for any  $q$ , (3.42) determines a 1-dimensional linear subspace  $\Delta(q)$  which is the null-space of matrix  $D_p(q)$ . Introducing the following theorem as

**Theorem 3.1. (Frobenius's Theorem)** (Oriolo and Nakamura, 1991) A distribution  $\Delta$  is integrable if and only if it is involutive.

From Theorem 3.1, the distribution of (3.41) is 1-dimensional and involutive, it then can be concluded that is (3.41) always integrable, and it can be further integrated in to the following form

$$\mathfrak{D}(q) - \frac{1}{2} G_1 t^2 + c_2 t + c_3 = 0 \quad (3.43)$$

where  $\frac{\partial \mathfrak{D}(q)}{\partial q} = D_p$  and  $c_3$  is a constant determined by the system initial condition.

This is the end of the proof. ■

**Remark 3.1.** The partial integrability and complete integrability of system constraint are important control properties to be determined for UMSs. If these

properties are identified, the system dimension can be reduced and the system model is simplified through eliminating some of the generalized coordinates.

### **3.5 Conclusion**

In this chapter, control of mechanical systems with underactuation degree one has been studied. The study is based on the coordinate transformation of the UMSs with PFL or PFL-free approach. The control problems of trajectory planning and tracking control of UMSs are then formulated. The control properties of partial integrability and complete integrability of 2-DOF Class I, II UMSs have been investigated with some propositions. In this thesis, a trajectory planning scheme will be proposed for underactuated vibro-driven cart systems with bio-inspired viscoelastic property in Chapter 4. The planned motion trajectory is based on a rest-to-rest motion, wherein the unactuated subsystem is controlled by the planned trajectory of the actuated subsystem. Trajectory tracking control schemes will be studied for vibro-driven cart systems with and without parametric uncertainties in Chapter 4, respectively. Generically, a tracking control scheme coping with UMSs with parametric uncertainties and external disturbances will be studied in Chapter 6.

## **Chapter 4**

# **Geometric Analysis-Based Trajectory Planning and Tracking Control**

### **4.1 Introduction**

Vibro-driven cart systems (VDCs), as typical UMSs, have become an increasingly important domain of research and received significant attentions from control and robotics communities (Bolotnik and Figurina, 2008; Fang and Xu, 2011; Huda et al., 2014; Huda and Yu, 2015; Kim et al., 2010, 2007; Wang et al., 2008). These systems are energetically involved in several fields of application working in restricted space and vulnerable media, such as minimally invasive diagnosis and intervention, engineering diagnosis, pipeline inspection, seabed exploration and disaster rescues. Nevertheless, describing and characterizing feasible motions and trajectories and nonlinear control are still challenging tasks for underactuated VDCs.

The primary objectives of trajectory planning for autonomous VDCs are optimal travel distance and fast average travel velocity. Towards this end, one of the key issues is the motion principles and actuation mechanisms, which determine the capabilities, performance, and in particular, the energy consumption and degrees of autonomy of VDCs. Conventional motion mechanisms have been designed and utilized via mimicking the earth-worm progression (Wang et al., 2008), canoe

paddling (Kim et al., 2010), magnetic field (Ciuti et al., 2010; Yim et al., 2014), etc. The internal force-static friction principle (Yamagata and Higuchi, 1995) is well-established in the literature of VDCs researches (Bolotnik and Figurina, 2008; Fang and Xu, 2011; Huda et al., 2014; Huda and Yu, 2015; Kim et al., 2010, 2007; Liu et al., 2014; Wang et al., 2008). The primary principle is that the rectilinear locomotion of VDCs can be achieved via an internally vibration-driven mass interacting with the main body and simultaneously, overcoming the resistance forces acting at the contacting surface. Generally speaking, one cycle of operation contains two fundamental stages: fast motion stage and slow motion stage. Specifically, the internal mass is driven at relatively high acceleration and the capsule body can move via the coupling behaviour in fast motion stage. Then, the capsule is terminated and the internal mass returns to the desired location through the interaction between the driving force and friction in slow motion stage.

In recent years, intensive researches have been conducted to the optimal periodic control modes of the internal driving mechanism, namely velocity-controlled mode (Lee et al., 2008; Li et al., 2006; Su et al., 2009; H. Yu et al., 2008) and acceleration-controlled mode (Fang and Xu, 2011; Yu et al., 2011). The minimal energy solution is obtained in (Li et al., 2006) to generate a four step motion pattern. An optimal controller is designed with an experimental comparison in (Lee et al., 2008). Yu et al (H. Yu et al., 2008) propose a six-step motion strategy based on optimal selection of trajectory parameters. A novel four-step acceleration profile is proposed in (Yu et al., 2011) for the motion control of capsubots. The stick-slip effect is considered by Fang et al (Fang and Xu, 2011) to optimize the parameters of the internal controlled mass under the objective of maximal average steady-state velocity of the system. It is well-established that the VDCs dynamics can be generally partitioned into two parts, namely collocated (actuated driving subsystem) and non-collocated (passive cart subsystem) dynamics, which are strongly coupled. It is also evident that friction plays pivotal roles in the propulsion and locomotion for self-propelled VDCs. In the fast motion stage, the system is propelled to move back and forth under the effects of underactuated dynamics and nonlinear friction, which contributes the net progressions. Therefore, globally

describing and characterizing the coupling behaviour, which are difficult and challenging, are of vital importance particularly for efficient trajectory planning. Unfortunately, a majority of reported results in the literature, such as (Li et al., 2006; 2014; Yu et al., 2008), are mainly devoted to the couplings in the slow motion stage, optimal control of the fast underactuated motion is usually neglected. This is mostly owing to the underactuated kinematic coupling behaviour and the relevant analysis is of much difficulty. Towards trajectory planning and control, there exist some studies for overhead cranes systems based on phase plane analysis of crane kinematics (Sun et al., 2011, 2012), however for locomotion systems, the locomotion-performance indexes (e.g., average locomotion velocity, energy efficiency) were not examined. Besides, it is always a tough task to achieve steady-state periodic motion of the driving mechanism and efficient progression of the cart simultaneously. In this research, an optimized trajectory model is proposed by geometric analysis method to characterize the coupling dynamics and identify the qualitative variation laws in fast motion stage in a manner that the designed control (locomotion-performance) indexes can be met. The main idea is to reduce complexity and to characterize coupling by imposing a harmonic drive and then to compute the dynamics projection onto a hyper-manifold, such that the issue of trajectory planning is converted into geometric analysis and trajectory optimization.

Most of the published studies on VDCs mainly focus on the optimization of the trajectory parameters in such a manner that the maximal average velocity can be obtained. Indeed, the operational environment can be very dynamic and the system may subject to parameter uncertainties. In this regards, overly unsupervised oscillations or even chaotic motions induced by the system control parameters would dramatically reduce the efficiency and lead to risks of severe jerk and potential damages to the actuators. Thus, the control parameters of VDCs are essential elements for the steady-stage system response and therefrom, for the efficient trajectory planning. Nevertheless, this nontrivial consideration has not been taken in any of the existing studies on the trajectory planning problems of underactuated VDCs. Besides, in control practice, it is well-established that the smart actuators (e.g. piezoelectric actuators, shape memory alloys) may experience

lag problem (certain delay in time such as hysteresis) originated from magnetic, ferromagnetic and ferroelectric materials, which may occur between the application and the removal of a force (Hassani et al., 2014; Iyer et al., 2005; Tan and Baras, 2004; Wang and Su, 2006). It is particularly true when sudden changes in velocity/acceleration burst in. This is the circumstance in which the motion principle of VDCs resides. To drive the cart via the coupling behaviour, the internal mechanism has to be initiated by the actuator with relatively higher velocity/acceleration. Besides, the interaction between the actuator and the driving mechanism needs to be characterized such that practical engineering requirements can be met. Nevertheless, these technical issues and relevant solutions have not been reported in the literature of trajectory planning.

In this chapter, the issues of trajectory planning and tracking control are studied using a novel VDC model that employs combined tangential-wise (linearly along the direction of motion) and norm-wise vibrations for bidirectional underactuated locomotion, which features a generic significance in the studies on VDCs. In contrast to the conventional cart-pole systems (CPSs), the control input is applied at the pendulum pivot, instead of the force on the cart in the horizontal direction. More importantly, CPSs address the set-point stabilization problem, whilst the proposed system is to make the cart track a desired (designed) trajectory by actuating the inverted pendulum. It is worth mentioning that the interaction between the actuator and the driving pendulum is characterized by a viscoelastic pair of torsional spring and viscous damper. It is the first time that the viscoelastic elements are introduced into the trajectory planning of VDCs to model the nontrivial interaction and to explore the feasibilities of improving the energy efficacy. As such, a novel geometric analysis-based trajectory planning approach is proposed, the main idea is to reduce complexity and to characterize coupling by imposing a harmonic drive and then to compute the dynamics projection onto a hyper-manifold, such that the issue of trajectory planning is converted into geometric analysis and trajectory optimization. Based on the trajectory planning approach studied in Chapter 3, this chapter will concretely investigate the nonlinear geometric-based approach on the VDCs with viscoelastic property. The proposed VDCs model is an advisable benchmark to

exploit the challenges in trajectory planning and tracking control of UMSs. Main contributions of this chapter are as follows:

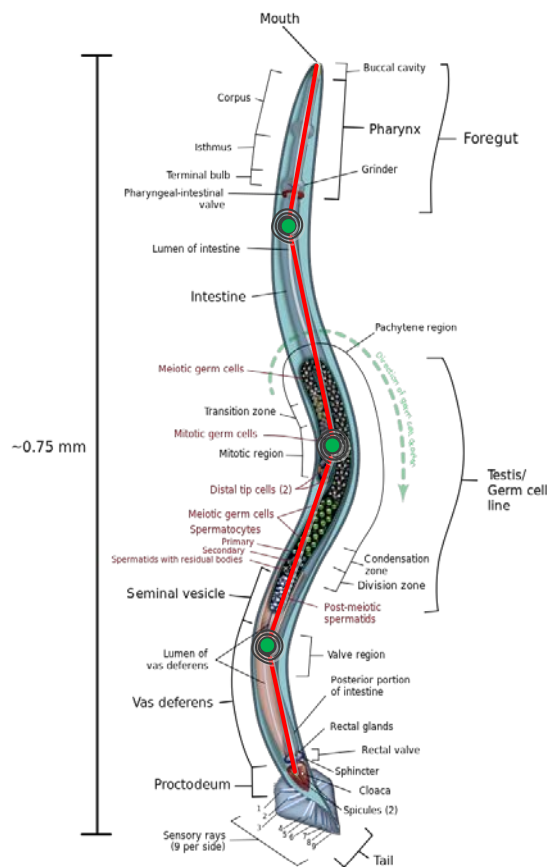
1. Proposing a bio-inspired robotic model utilizing undulatory self-propulsion with viscoelastic property;
2. Designing a characterization algorithm towards the underactuation-induced dynamic couplings using the nonlinear geometric analysis approach;
3. Proposing kernel practical control indexes in the presence of viscoelastic property and jag problems, and construct an analytical motion trajectory with improved energy efficacy and characteristics in continuity and smoothness, which facilitate design of the tracking controller;
4. Identifying qualitative variation laws of the viscoelastic parameter such that the system performance can be evaluated beforehand;
5. Developing an analytical parameterization algorithm for optimization of the trajectory parameters;
6. Constructing closed-loop feedback and adaptive control laws for trajectory tracking.

The outline of this chapter is organized as follows. First, the description and dynamic modelling of the VDC system is presented in Section 4.2. Then the problem formulation is given in Section 4.3. The geometric analysis-based trajectory planning algorithm is studied in Section 4.4. In Section 4.5, trajectory tracking control algorithms are constructed. Simulation results are provided and discussed in Section 4.6 to establish the verification of the performance of the proposed system. The 3D design, experimental setup and experimental results are presented in Section 4.7 to demonstrate and validate the locomotion of the proposed VDC model. Finally, conclusions are given in Section 4.8.

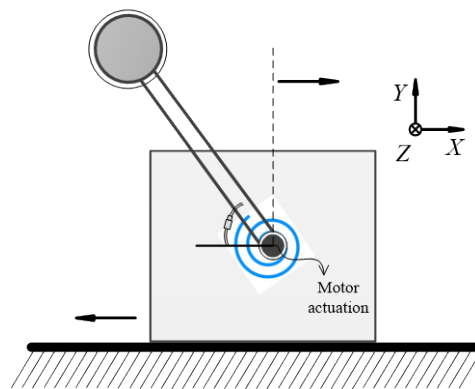
## 4.2 System Description and Mathematical Modelling

### 4.2.1 Bio-Inspired Self-Propelled Robotic Model with Viscoelastic Property

In this thesis, a self-propelled robotic model is proposed as shown in Figure 4.1 (b) by drawing inspiration of the undulatory locomotion of the nematode worm in low Reynolds environments (Figure 4.1(a)). From the figure, the nematode worm can be split up into segments, including frictionless two-dimensional joints (as the dots in green) between weightless pendulums (as the rods in red).



(a)



(b)

Figure 4.1 The biological inspiration: (a) a four-segment *C. elegans* nematode (“Nematode,” 2017); (b) the proposed two-segment bio-inspired self-propelled model with viscoelastic property

The internal fluid pressure of the worm is utilized through the viscoelastic property in the joint-space to form a firm but flexible actuated segment. Muscles of the worm act as simple passive actuators. The combination of the bio-inspired viscoelastic property of the muscles makes the worm quite compliant and allows the body to passively accommodate external constraints that physically increases the robustness of the locomotion system. The pendulum is employed as the first segment and the robot body is adopted as the second segment. Two segments are connected through an articulated joint with viscoelastic property. Undulations are propagated from the rotating pendulum to the robot body. It is noted that the nematode worm moves through undulation by pushing the obstacles around that relatively restricted applications into robotic design. In the proposed model, however, the unidirectional property of the ground is utilized as an always-existing ‘obstacle’ for the robot to propel itself through interactions with the physical environment, as such, the above limitation of the nematode worm is relaxed. Note also that propagation of undulations can vary in kinematic parameters such as coefficient of elasticity and viscosity, frequency, wavelength, amplitude. When characterizing the transition as a function of the environment, the qualitative behaviour changes need to be explicitly controlled against possible variations in the worm’s autologous and

exogenous microscopic physical environments. Therefore, a geometric-analysis based method is used to characterise the viscoelasticity of the bio-inspired model in this Chapter, and a prediction and analysis framework will be proposed to characterize the frictional interaction dynamics in Chapter 5.

The proposed model has extensive applications such as capsule robots for minimally invasive diagnosis and intervention, autonomous systems for pipeline inspections, exploration for firefighting operations, etc.

### 4.2.2 Vibro-Driven Cart System and Mathematical Modelling

The bio-inspired self-propelled model contains a pendulum and a platform. A DC motor is mounted at the pivot on the platform to rotate the pendulum. The nonlinear interaction between the actuator and the pendulum is described by a linear viscoelastic pair of torsion spring and damper. The system works as follows. The platform is propelled over a surface rectilinearly via the interaction between the drag forces and the horizontal sliding friction, resulting into alternative sticking and slipping locomotion. Meanwhile, the elastic potential energy is stored and released alternatively in compatible with contraction and relaxation of the torsional spring. The motion of the platform starts with static state, and it moves when the magnitude of resultant force applied on its body in the horizontal direction exceeds the maximal value of friction force. This model is developed to exploit advisable friction control approach and stick-slip vibration to generate a periodic progression where the platform and the driving pendulum synchronize their motion harmoniously.

Based on the proposed model in Subsection 4.2.1, a VDC system is shown in Figure 4.2. The wheels are passive with no actuation. The parameters of the system are defined as follows.  $M$  and  $m$  are the masses of the cart and the ball, respectively.  $l$  is the length from the pivot to the Centre of Mass (COM) of the ball,  $\mu$  is the friction coefficient between the platform and ground,  $k$  and  $c$  are elastic coefficient of the torsion spring and viscous coefficient of the damper, respectively.  $f_c$  denotes the horizontal sliding friction between the system and the ground.  $f_p$  represents the motor viscous friction at the pivot.  $\theta$  is the angular displacement measured from the vertical,  $x$  is the displacement of the platform measured from the initial position,  $\tau$

is the control torque applied to the pendulum by the DC motor. In what follows, for the sake of brevity,  $s_\theta$ ,  $c_\theta$  and  $S_{\dot{x}}$  will be employed to denote the trigonometric function  $\sin\theta$ ,  $\cos\theta$  and the signal function  $Sign(\dot{x})$ , respectively.

The main difference between the proposed model and the conventional cart-pole system is that the force is applied at the pivot to rotate the pendulum, which induces trajectory planning and tracking issues rather than the swinging-up or set-point stabilization problems. As an energy storage element, a torsional spring is employed to improve the energy efficacy through carefully designed motion trajectory of the pendulum which will discuss in Section 4.4.

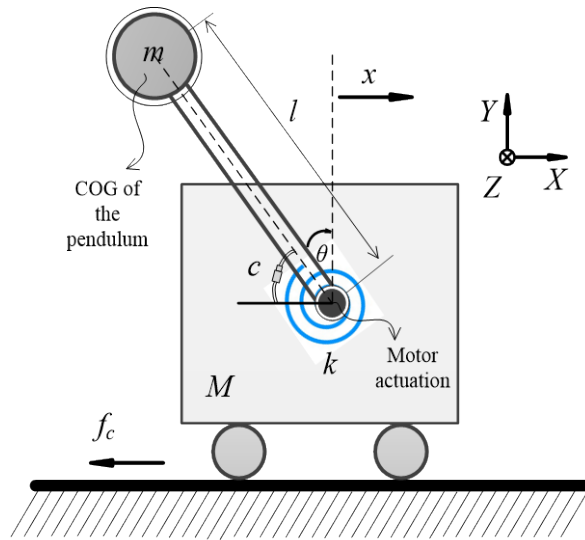


Figure 4.2 Schematic of the vibro-driven cart system

Definitions of the sticking phase and the slipping phase are given as follows:

**Definition 4.1.** The sticking phase is the moment when the magnitude of resultant force applied on the cart in the horizontal direction is less than the maximal static friction force. The cart keeps stationary in this phase.

**Definition 4.2.** The slipping phase is the instant when the magnitude of resultant force applied on the cart in the horizontal direction is larger than the maximal static

friction force. When this condition is met, the sticking phase is annihilated and the cart starts to move.

From the above definitions, it is evident that friction plays a vital role for optimal control of the stick-slip locomotion. Prior to the mathematical modelling of the proposed model, the following assumptions are given

**Assumption 4.1.** The mass of the inverted pendulum is omitted comparing to the mass of the bob on its tip, thus the mass of the pendulum is centralized at the ball.

**Assumption 4.2.** The COM of the cart coincides with the pivot axis such that the moment of inertia of the base can be omitted.

**Assumption 4.3.** The motion of the cart is constrained on X-Y plane and no motion is allowed in the Z direction.

**Assumption 4.4.** The Coulomb friction is assumed to act as the resistance force between the system and the sliding surface, gives

$$f_c = \begin{cases} \mu(M + F_y)S_{\dot{x}}, & \text{for } \dot{x} \neq 0 \\ f_0, & \text{for } \dot{x} = 0 \end{cases} \quad (4.1)$$

where  $F_y$  is the internal reaction forces applied on the pendulum by the platform in the vertical direction,  $f_0$  denotes the stiction force when the velocity of the cart is zero.

Assume the moment of inertia  $I = ml^2$ . The ball's position is uniquely described by  $x_b$  and  $y_b$ , chosen as the deflection of the geometric centre of the ball referenced from the medial axis. The position and velocity of the ball are given by

$$x_b = x - ls_{\theta}, \quad y_b = lc_{\theta} \quad (4.2a)$$

$$\dot{x}_b = \dot{x} - l\dot{\theta}c_{\theta}, \quad \dot{y}_b = -l\dot{\theta}s_{\theta} \quad (4.2b)$$

Based on the Newton's law, let  $F = [F_x \ F_y]^T$  and  $N = [N_x \ N_y]^T$  be the internal reaction forces applied on the pendulum by the platform and the viscoelastic element, respectively. We have

$$F = \begin{bmatrix} F_x \\ F_y \end{bmatrix} = \begin{bmatrix} m\ddot{x}_b \\ m\ddot{y}_b + mg \end{bmatrix} + \begin{bmatrix} N_x \\ N_y \end{bmatrix} = \begin{bmatrix} -m\ddot{x} + ml\ddot{\theta}c_{\theta} - ml\dot{\theta}^2s_{\theta} + N_x \\ mg - ml\dot{\theta}^2c_{\theta} - ml\ddot{\theta}s_{\theta} + N_y \end{bmatrix} \quad (4.3)$$

where  $N_x = (k\theta + c\dot{\theta})c_\theta/l$  and  $N_y = -(k\theta + c\dot{\theta})s_\theta/l$ .

Based on the assumptions and definitions, the governing equations of the proposed model are then derived using Euler-Lagrangian's method described as

$$\frac{d}{dt} \frac{\partial L(q_i, \dot{q}_i)}{\partial \dot{q}_i} - \frac{\partial L(q_i, \dot{q}_i)}{\partial q_i} + f = Q_i \quad i = 1, 2 \quad (4.4)$$

where  $q_i(t) = [\theta \ x]^T, i = 1, 2$  represents the system state vector.  $L(q_i, \dot{q}_i) = E(q_i, \dot{q}_i) - V(q_i)$  is the Lagrangian function,  $E$  and  $V$  respectively denote the kinetic energy and potential energy,  $f$  describes the resistant and dissipated forces,  $Q_i$  is the generalized externally applied force or moment. The detailed expression for  $E$ ,  $V$ ,  $f$  and  $Q_i$  are given by

$$E = \frac{1}{2}M\dot{X}^2 + \frac{1}{2}m[(\dot{X} - l\dot{\theta}\cos\theta)^2 + (-l\dot{\theta}\sin\theta)^2] \quad (4.5a)$$

$$V = \frac{1}{2}k\theta^2 + mgl\cos\theta \quad (4.5b)$$

$$f = \begin{bmatrix} f_p \\ f_c \end{bmatrix} = \begin{bmatrix} c\dot{\theta} \\ f_c \end{bmatrix}, \quad Q_i = \begin{bmatrix} u \\ 0 \end{bmatrix} \quad (4.5c)$$

Therefore, the underactuated dynamics of the VDC model are derived as

$$D(q)\ddot{q} + C(q, \dot{q})\dot{q} + K(q)q + G(q) = Bu + f \quad (4.6)$$

where  $D(q) \in \mathcal{R}^{2 \times 2}$  is the inertia matrix,  $C(q, \dot{q}) \in \mathcal{R}^{2 \times 2}$  denotes the Centripetal-Coriolis matrix,  $K(q) \in \mathcal{R}^{2 \times 2}$  is the generalized stiffness matrix,  $G(q) \in \mathcal{R}^{2 \times 1}$  represents the gravitational torques,  $u \in \mathcal{R}^1$  denotes the control input applied to the system. The details of the aforementioned variables are shown as follows

$$D(q) = \begin{bmatrix} ml^2 & -mlc_\theta \\ -mlc_\theta & (M+m) \end{bmatrix}, \quad C(q, \dot{q}) = \begin{bmatrix} 0 & 0 \\ mls_\theta\dot{\theta} & 0 \end{bmatrix}, \quad K(q) = \begin{bmatrix} k & 0 \\ 0 & 0 \end{bmatrix},$$

$$G(q) = [-mgl s_\theta \ 0]^T, \quad B = [1 \ 0]^T, \quad f = [-c\dot{\theta} \ -f]^T \quad (4.7)$$

where  $g \in \mathcal{R}^+$  is the gravitational acceleration.

The model dynamics are component of a actuated subsystem (pendulum) and a passive subsystem (cart), wherein the latter one composes the system kinematics that captures the coupling behaviour between the driving pendulum and the cart. The coupling behaviour and nonlinearity are resulted from the nonlinear frictions and the trigonometric functions.

**Remark 4.1.** The contact interface is anisotropic, and asymmetry characteristic may arise due to physical and structural inconsistency of system parameters. It is plausible that the stiction force  $f_0$  exists with its value range falling into the threshold of the Coulomb friction  $[-\mu(M + F_y)S_{\dot{x}}, \mu(M + F_y)S_{\dot{x}}]$ . This results from the sticking motion and largely relying on the magnitudes of the external forces. In this chapter, we assume that there is no friction force applied on the cart when it keeps stationary ( $\dot{x} = 0$ ). The study on dynamic frictions will be reported in Chapter 5.

Harmonic excited forces are typically adopted to generate periodic motions for capsule systems as studied in (Liu et al., 2013a, 2013b). On this occasion, forward and backward motions can be generated and controlled via proper tuning of the control parameters. Utilizing the harmonic force  $u = A\cos(\Omega t)$  with amplitude  $A$  and frequency  $\Omega$  to excite the pendulum and introducing the characteristic time scale  $\omega_n = \sqrt{g/l}$  and the characteristic length  $x_0 = g/\omega_n^2$ , the nondimensional equations of motion of the system can be obtained as

$$[\mathbb{D}]\{\ddot{\mathfrak{X}}\} + [\mathbb{C}]\{\dot{\mathfrak{X}}\} + [\mathbb{K}]\{\mathfrak{X}\} + [\mathbb{G}] + [\mathbb{F}_\delta] = \{\mathbb{U}\}u_d \quad (4.8)$$

where  $[\mathbb{D}] = \begin{bmatrix} 1 & -c_\theta \\ -c_\theta & \lambda + 1 \end{bmatrix}$ ,  $[\mathbb{C}] = \begin{bmatrix} 0 & 0 \\ s_\theta \dot{\theta} & 0 \end{bmatrix}$ ,  $[\mathbb{K}] = \begin{bmatrix} \rho & 0 \\ 0 & 0 \end{bmatrix}$ ,  $[\mathbb{G}] = \begin{bmatrix} -s_\theta \\ 0 \end{bmatrix}$ ,  $\{\mathbb{U}\} = \begin{bmatrix} 1 \\ 0 \end{bmatrix}$  and  $[\mathbb{F}_\delta] = \begin{bmatrix} v\dot{\theta} \\ f' \end{bmatrix}$ ,  $u_d = hc_{\omega\tau}$  and  $f' = \mu[(\lambda + 1) - s_\theta\ddot{\theta} - c_\theta\dot{\theta}^2 - (\rho\theta + v\dot{\theta})s_\theta]S_{\dot{x}}$ .

The derivations above are conducted with respect to the dimensionless time  $\tau = \omega_n t$  and the configuration variables are transformed to  $\{\mathfrak{X}\} = [\xi_1 \ \xi_2]^T = [\theta \ X]^T$ . The dot ( $\cdot$ ) in (4.8) denotes the derivative in dimensionless time coordinate. The rest of the non-dimensional quantities are defined as

$$\begin{aligned} X &= x/x_0, \lambda = M/m, \omega = \Omega/\omega_n, \\ \rho &= k/(ml^2\omega_n^2), v = c/(ml^2\omega_n), h = A/(ml^2\omega_n^2) \end{aligned} \quad (4.9)$$

**Remark 4.2.** Nondimensionalization of the governing equations can simplify the analysis of the model through searching the dimensionless groups which control its solution patterns. Under the dimensionless coordinate, the physical meanings of the control parameters are captured as:  $\lambda$  is the mass ratio,  $\rho$  and  $v$  respectively denote the normalized elastic and viscous coefficients,  $h$  and  $\omega$  are the normalized excitation amplitude and frequency.

**Remark 4.3.** The control action is a rotational torque at the pivot. Due to the fact that the motion of the cart cannot be directly controlled, the proposed model is an interesting mechanical system with underactuation degree one. For motion systems, such as the proposed one, the friction between the cart and the surface plays a key role in the locomotion of the entire system. The optimal control of the friction will be investigated in trajectory planning in Section 4.4.

## 4.3 Problem Formulation and Trajectory Planning

### 4.3.1 Problem Formulation

A typical time history of system performance after initial transients is presented in Figure 4.3, showing the cart displacement and pendulum angular velocity. It is evident that the net cart displacement during one cycle of excitation  $\mathbf{R}$  is mainly determined by the ramp edges of the harmonic force in forward motion stage  $\mathbf{R}_F$ . However, such periodic motions are essentially not optimal, since for each motion cycle, the forward displacement obtained in  $\mathbf{R}_F$  is partly counteracted in the forthcoming backward motion stage  $\mathbf{R}_B$ , and excessive energy are consumed due to the backward journey.

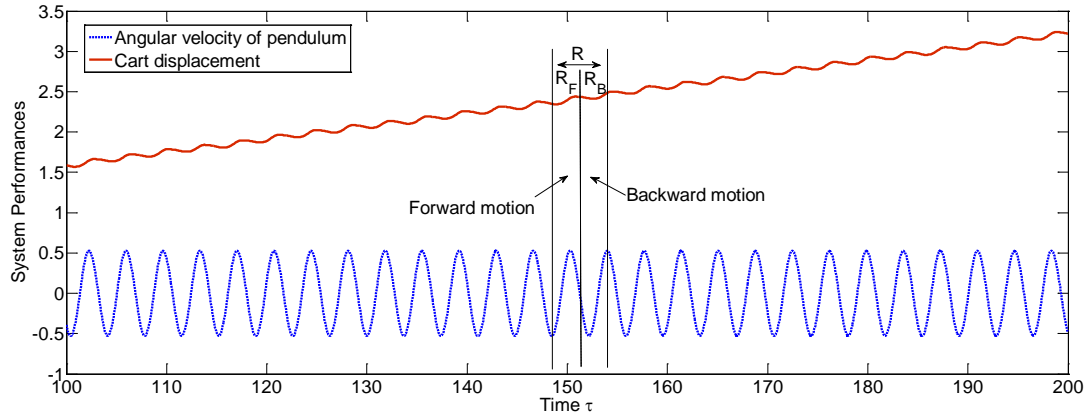


Figure 4.3 Time histories of typical steady-state system performance

Therefore, a two-stage motion trajectory needs to be constructed that optimally utilizes the ramp edges of the harmonic excitation in the forward motion stage and thereafter, sufficiently neutralize the backward motions via optimal control of the sticking phase and friction. The definitions are given as follows:

**Definition 4.3. (Initialization Stage and Re-initialization Stage)** One cycle of progressive motion begins and ends with the initialization and re-initialization stages, respectively. In the initialization stage, the pendulum together with the torsional spring are constrained and kept stationary at a predesigned negative angle to the opposite direction of the retraction of spring, which stores potential energy such that more mechanical power is provided to system; at the end of the motion, the pendulum gradually returns to the initial position, the system then is reinitialized with stored elastic energy.

**Definition 4.4. (Progressive Stage)** driving the pendulum with higher angular acceleration incorporating with the release of the elastic energy stored in the torsion spring that leads the cart to overcome the maximal static friction to generate a slipping motion ( $\dot{X} \neq 0$ ).

**Definition 4.5. (Restoring Stage)** returning the pendulum to initial position slowly to restore potential energy and prepare for the next cycle, the resultant force exerting

on cart in the horizontal direction is less than the maximum dry friction, that is, the cart is kept in the sticking phase in this stage ( $\dot{X} = 0$ ).

Based on practical control indexes and dynamic constraints associated with the stick-slip locomotion of the cart, the following principles are designed as objectives to be achieved to construct an optimal motion trajectory for the driving pendulum:

**Principle 4.1.** For each motion cycle, the pendulum is constrained rotating within an advisable angle range, indicating that the upper and lower boundaries are given as

$$|\theta(\tau)| \leq \theta_0 \quad (4.10)$$

where  $\theta_0$  is the prescribed angular displacement of the driving pendulum.

**Principle 4.2.** The angular velocity and angular acceleration of the driving pendulum need to be placed within bounded ranges, given by

$$|\dot{\theta}(\tau)| \leq v_\theta, \quad |\ddot{\theta}(\tau)| \leq a_\theta \quad (4.11)$$

where  $v_\theta \in \mathcal{R}^+$  and  $a_\theta \in \mathcal{R}^+$  are the absolute boundary values of angular velocity and acceleration, respectively.

**Principle 4.3.** The cart is contacting with the sliding surface, in order to achieve a non-bounding motion, the constraint for the contact force needs to be satisfied, which means the contact force has to be always greater than zero, gives

$$(\lambda + 1) - s_\theta \ddot{\theta} - c_\theta \dot{\theta}^2 - (\rho\theta + v\dot{\theta})s_\theta > 0 \quad (4.12)$$

**Principle 4.4.** The cart has to be remained stationary after one cycle of forward motion to wait for the return of pendulum. In this occasion, the force of the driving pendulum applied on the cart in the horizontal direction has to be less than the maximal static friction, gives

$$|c_\theta \ddot{\theta} - s_\theta \dot{\theta}^2 + (\rho\theta + v\dot{\theta})c_\theta| \leq \mu[(\lambda + 1) - s_\theta \ddot{\theta} - c_\theta \dot{\theta}^2 - (\rho\theta + v\dot{\theta})s_\theta] \quad (4.13)$$

**Remark 4.4.** Principles 4.1 and 4.2 are associated with the collocated subsystem which is prone to control and convenient to achieve, whilst Principles 4.3 and 4.4 are of vital importance for the non-collocated cart locomotion and energy efficacy.

Therefore, as one major contribution, both principles are explicitly considered through the nonlinear geometric analysis method.

### 4.3.2 Periodic Trajectory Synthesis and Construction

In this subsection, the periodic motion principles are designed for synthesizing of the rotating pendulum and the viscoelastic components. In this thesis, it is considered that the existence of viscoelasticity is equivalent to the existence of a periodic trajectory manifold with corresponding arguments. Consequently, we analyse the motion generation of the VDC system by planning the rate of changes of pendulum angular position.

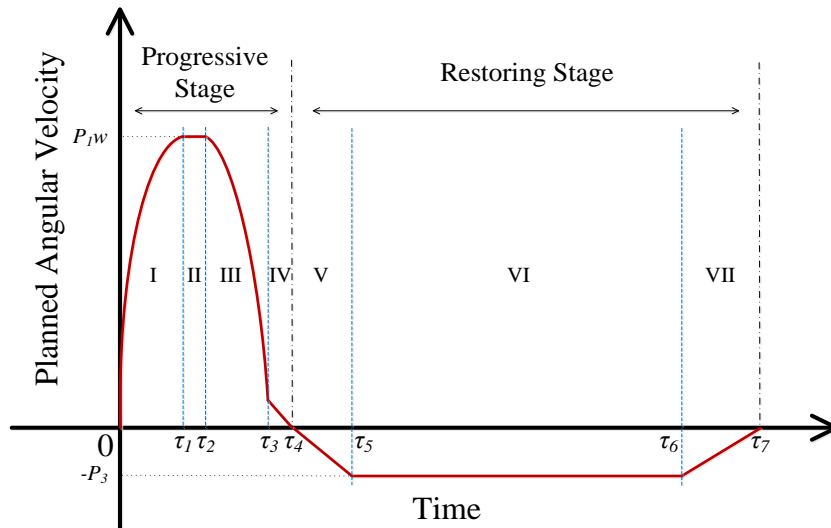


Figure 4.4 Schematic profile for the synthesized velocity trajectory

The proposed model, in nature, is an underactuated system with non-collocated actuation and sliding friction, which means the pendulum can be directly controlled whilst the progression of the cart is in the indirect feedback loop. Thus, the objective of trajectory synthesis is to generate the periodic motion to drive the VDC system moving rectilinearly only by utilizing the rotational torque. Thus, we are motivated to consider the characteristic of viscoelasticity in trajectory synthesis.

Therefore, Figure 4.4 depicts the proposed two-stage velocity trajectory based on the indexes, objectives and synchronization considerations. As stated in the introduction, the actuator may experience lag problem, in this regard, we are motivated to introduce a transition function to cope with this problem and to synchronize the motion trajectory.

The synthesized trajectory is described as

$$\dot{\theta}(\tau) = \begin{cases} P_1 \omega S_{\omega\tau}, & \tau \in [0, \tau_1) \\ P_1 \omega, & \tau \in [\tau_1, \tau_2) \\ P_1 \omega S_{\omega\tau - \tau_2}, & \tau \in [\tau_2, \tau_3) \\ \frac{\tau_3 - \tau}{\tau_3 - \tau_2} P_2, & \tau \in [\tau_3, \tau_4) \\ \frac{\tau_3 - \tau}{\tau_4 - \tau_3} P_3, & \tau \in [\tau_4, \tau_5) \\ -P_3, & \tau \in [\tau_5, \tau_6) \\ \frac{\tau_6 - \tau}{\tau_5 - \tau_6} P_3, & \tau \in [\tau_6, \tau_7) \end{cases} \quad (4.14)$$

where  $P_1 \omega$  and  $P_3$  are upper and lower trajectory boundaries, respectively.  $P_2$  is the critical boundary when the cart keeps stationary,  $\omega$  is the frequency of excitation.

Obviously, a parametric selection procedure is needed to obtain the time-varying reference motion trajectory (4.14), and accordingly a series of parameters including the time durations  $\tau_1 \sim \tau_7$ , the maximum angular velocity of the periodic trajectory in scaled coordinate  $P_1$ , its minimum counterpart  $P_2$  as well as the critical angular velocity  $P_3$  when the cart begins to keep stationary. This optimal selection procedure will be investigated in Section 4.4.

The explicit description of the synthesized desired angular velocity profile of the driving pendulum is as follows:

**Initialization.**  $\tau = 0$  :  $\theta(\tau) = \theta_{min} = -\theta_0$  ,  $X(\tau) = 0$  ,  $\dot{\theta}(\tau) = 0$  ,  $\dot{X}(\tau) = 0$  ,  $\ddot{\theta}(\tau) = 0$  ,  $\ddot{X}(\tau) = 0$  The pendulum together with the torsion spring is kept stationary at a predesigned negative angle  $-\theta_0$  to the opposite direction of the retraction of spring, which stores potential energy such that more mechanical power will be injected into the system.

**Phase I.**  $\tau \in (0, \tau_1)$ :  $\theta(\tau) = \theta > 0$ ,  $X(\tau) = x$ ,  $\dot{\theta}(\tau) > 0$ ,  $\dot{X}(\tau) > 0$ ,  $\ddot{\theta}(\tau) \gg 0$ ,  $\ddot{X}(\tau) > 0$  The torque motor begins to actuate under the synchronized angular velocity and simultaneously the stored potential energy is released from the stretched torsion spring, which results in a motion with maximal angular acceleration of the pendulum dragging the cart moving forward with a high acceleration.

**Phase II.**  $\tau \in [\tau_1, \tau_2)$ :  $\theta(\tau) = \theta > 0$ ,  $X(\tau) = x$ ,  $\dot{\theta}(\tau) > 0$ ,  $\dot{X}(\tau) > 0$ ,  $\ddot{\theta}(\tau) = 0$ ,  $\ddot{X}(\tau) > 0$  It is noted that once the potential energy is released, a short period of time is required to let the potential energy fully transfer into kinetic energy, which leads to a more efficient energy consumption. Thus, a short period of uniform motion of the pendulum is designed. During this period, the pendulum swings forward with the maximal angular velocity while driving the base accelerating continuously.

**Phase III.**  $\tau \in [\tau_2, \tau_3)$ :  $\theta(\tau) = \theta > 0$ ,  $X(\tau) = x$ ,  $\dot{\theta}(\tau) > 0$ ,  $\dot{X}(\tau) > 0$ ,  $\ddot{\theta}(\tau) < 0$ ,  $\ddot{X}(\tau) < 0$  The torque actuation exerts an opposing force under the synchronized angular velocity together with the contractility of the torsion spring, leading to a forward deceleration motion of the pendulum and the cart.

**Phase IV.**  $\tau \in [\tau_3, \tau_4)$ :  $\theta(\tau) = \theta_{max} > 0$ ,  $X(\tau) = x \rightarrow 0$ ,  $\dot{\theta}(\tau) \rightarrow 0$ ,  $\dot{X}(\tau) = 0$ ,  $\ddot{\theta}(\tau) < 0$ ,  $\ddot{X}(\tau) = 0$  In this phase, a slow deceleration motion of the pendulum results in the stationary of the cart, which is subjected to the constraints under the dissipative force lie in the sliding surface and the pivot. Moreover, the angular displacement of the pendulum is constrained at  $\theta_{max}$  to avoid over-actuation and system failure.

**Phase V.**  $\tau \in [\tau_4, \tau_5)$ :  $\theta(\tau) = \theta < 0$ ,  $X(\tau) = x$ ,  $\dot{\theta}(\tau) < 0$ ,  $\dot{X}(\tau) = 0$ ,  $\ddot{\theta}(\tau) < 0$ ,  $\ddot{X}(\tau) = 0$

Phase V is designed to be a short duration that a relatively low angular acceleration of the pendulum is generated while keeps the base stands still.

**Phase VI.**  $\tau \in [\tau_5, \tau_6)$ :  $\theta(\tau) = \theta < 0$ ,  $X(\tau) = a\Delta x$ ,  $\dot{\theta}(\tau) = -P_3 < 0$ ,  $\dot{X}(\tau) = 0$ ,  $\ddot{\theta}(\tau) = 0$ ,  $\ddot{X}(\tau) = 0$  A uniform angular velocity of the pendulum is designed for gradually stretching the torsion spring such that enough potential energy is restored

for the coming cycle. The base remains stationary in this stage.  $a\Delta x$  represents the net displacement of the cart after the  $a^{th}$  cycle.

**Phase VII.**  $\tau \in [\tau_6, \tau_7)$ :  $\theta(\tau) = \theta < 0$ ,  $X(\tau) = a\Delta x$ ,  $-P_3 < \dot{\theta}(\tau) < 0$ ,  $\dot{X}(\tau) = 0$ ,  $\ddot{\theta}(\tau) > 0$ ,  $\ddot{X}(\tau) = 0$  In phase VII, a low angular acceleration motion is generated in a short duration to accelerate the pendulum while the cart keeps stationary.

**Re-initialization.**  $\tau = 0$ :  $\theta(\tau) = \theta_{min} = -\theta_0$ ,  $X(\tau) = a\Delta x$ ,  $\dot{\theta}(\tau) = 0$ ,  $\dot{X}(\tau) = 0$ ,  $\ddot{\theta}(\tau) = 0$ ,  $\ddot{X}(\tau) = 0$  When the pendulum reaches to the initial angle, the torsional spring is constrained to  $\theta_{min}$  such that enough elastic energy is stored for the coming new cycle.

## 4.4 Nonlinear Geometric Analysis-based Trajectory Planning

**Definition 4.6.** Poincaré maps: one considers a periodic orbit with initial conditions within a section of the space, samples the solution of a system according to an event-based or time-based rule, and then evaluates the stability properties of equilibrium points (or fixed points) of the sampled system (Westervelt et al., 2007).

It is evident from (4.12) and (4.13) that Principles 3 and 4 are susceptible to elastic coefficient  $\rho$  and viscous coefficient  $\nu$ , which are vital factors for energy consumption. In this section, a novel approach is explored to characterize the coupling and identify the qualitative variation laws of the control parameters in the form of system performance, such that the optimal control parameters are selected beforehand and fed into parameterisation of the motion trajectory. Concretely, when the control indexes and non-collocated dynamic constraints are considered, the proposed geometric analysis-based trajectory planning algorithm is given by

**Algorithm 4.1.** Construction and optimization of motion trajectory

**Step 1.** Compute and project the underactuated dynamics onto the dimensionless phase plane and Poincaré maps through nonlinear geometric analysis approach;

**Step 2.** Describe and characterize coupling between the collocated and non-collocated subsystems, and identify the optimal control parameters through qualitative variation laws against the system locomotion-performance index;

**Step 3.** Characterize the dynamic constraints for stick-slip progression through rigorous analytical analysis towards underactuation and internal coupling;

**Step 4.** Compute the trajectory boundaries;

**Step 5.** Optimize and parameterize the planned trajectory for each phase with identified optimal control parameters from Step 2, characterized conditions for optimal stick-slip progression from Step 3 and computed trajectory boundaries from Step 4.

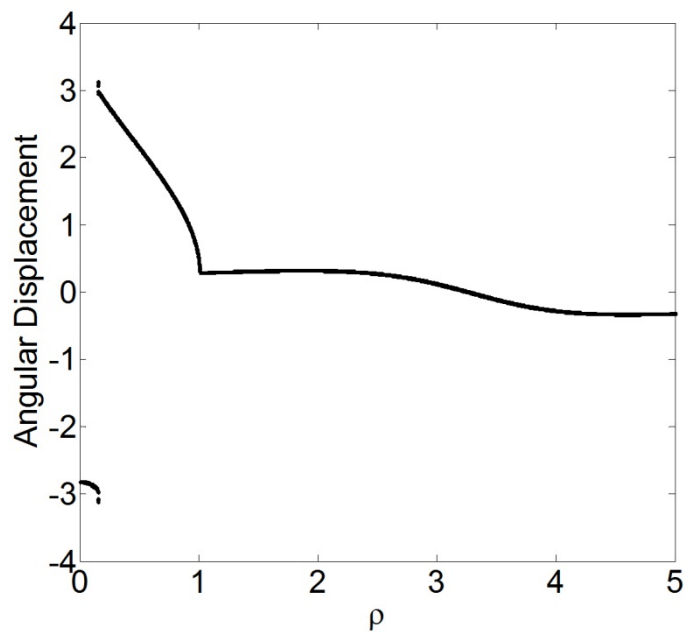
**Remark 4.5.** Poincaré maps can sample the solution of a system according to an event-based or time-based rule, and then evaluate the stability properties of equilibrium points (or fixed points) of the sampled system. The proposed algorithm utilizes the knowledge from both collocated and non-collocated subsystems to facilitate efficient locomotion of the proposed model. The computation and projection of dynamics onto an induced hyper-manifold of the closed-loop system enables convenient analysis and characterization of the underactuated couplings.

#### **4.4.1 Coupling Characterization and Viscoelastic Parameter Identification**

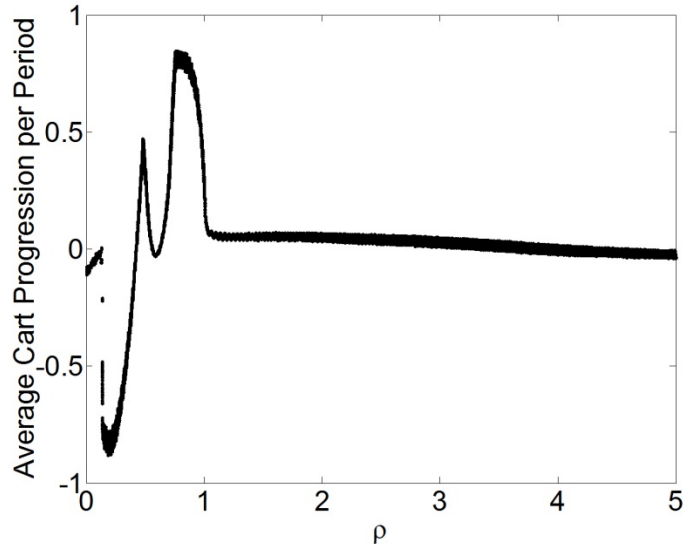
In dynamical systems, geometric representations of the qualitative changes in the dynamic behaviour induced by tiny smooth variations of the system parameter can be achieved through bifurcations, which give rise to the creations and annihilations of equilibria as well as the periodic solutions. The advantage is that it employs a visual interpretation of how the dynamic behaviours are affected by the system parameters and how the stability of solutions changes accompanied by the varying parameters. The main objective of the proposed VDC system is to be capable of rectilinear motion by utilizing the rotational torque, in the presence of friction or resistance force from the contacting environment. The solutions in this section are numerically

calculated using a modified first-order Euler's method, for identifying the most suitable qualitative motion for the forward progression of the VDC system.

In this following, coupling behaviour and qualitative variation laws induced by the viscoelastic parameters for the progressive stage are firstly characterized and identified. From the viewpoint of energy, it is evident that efficient utilizations of potential energy stored in the spring and dissipative energy in the dampers are crucial factors for energy efficacy. The average progression per period is characterized geometrically to examine the locomotion-performance index.



(a) Angular displacement



(b) Average cart progression per period

Figure 4.5 Qualitative variation laws of  $\rho$  obtained for  $h = 0.8$ ,  $\omega = 1.7$ ,  $v = 0.8$  and  $\lambda = 3.6$

The qualitative variation law of elastic coefficient  $\rho$  is presented in Figure 4.5. The effects of  $\rho$  on the pendulum and the cart subsystems are shown in Figures 4.5 (a) and 4.5 (b), respectively. It is also observed in Figure 4.5 (a) that a grazing of angular displacement occurs at  $\rho = 0.25$ , and thereafter the angular displacement largely decreases as  $\rho$  increases. As a locomotion system, the average locomotion speed is of vital importance, in this regard, the average cart progression per period of excitation is characterized and shown in Figure 4.5 (b), in which the global maximum and minimum average progressions points are recorded at  $\rho = 0.9$  and  $\rho = 0.25$ , respectively. A pair of local maximal and minimal points of average progressions is also identified at  $\rho = 0.65$  and  $\rho = 0.75$ . Time histories of the cart displacements for  $\tau \in [370,400]$  are presented in Figure 4.6 to verify the identified variation laws. It indicates that for a smaller coefficient at  $\rho = 0.1$ , the spring is insufficient to generate enough force to enhance the cart progression, accordingly the cart moves in vibrational motion around the starting point. Similarly, for a larger coefficient at  $\rho = 2.0$ , the spring becomes sufficiently 'hard' to trap the VDC progression. For the values in between, the spring either contributes to the forward

motions of the cart (e.g.  $\rho = 0.7, 0.9$ ), or drags it backwards in the negative direction (e.g.  $\rho = 0.3, 0.25$ ).

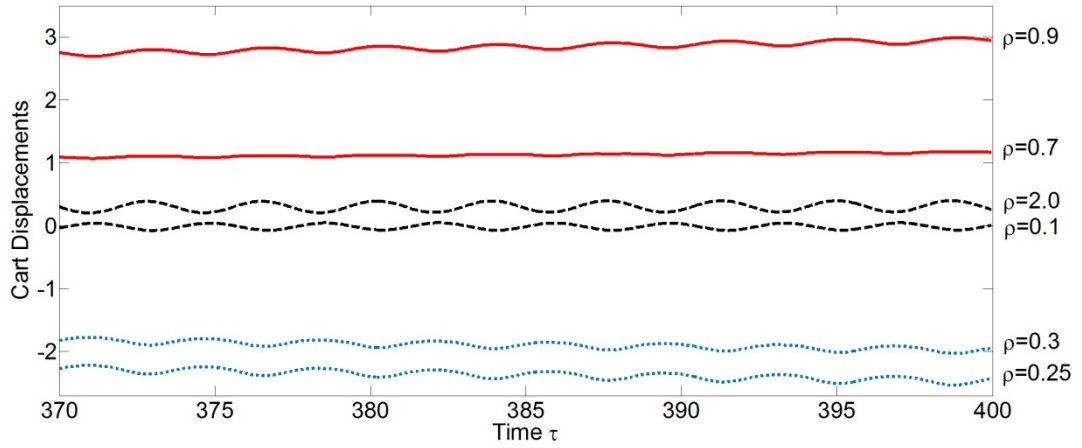
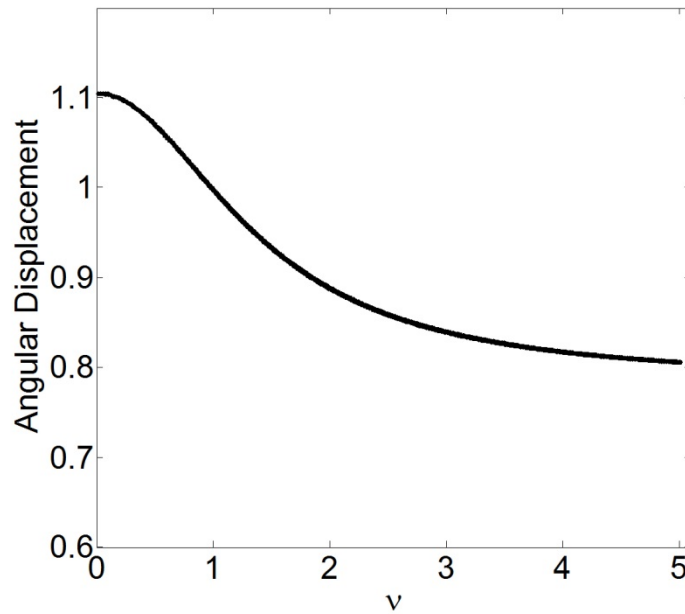
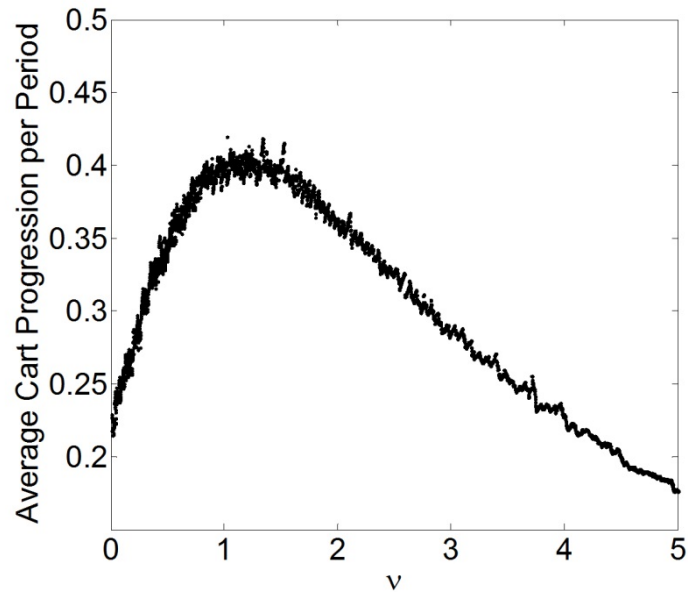


Figure 4.6 Time histories of the cart displacements



(a) Angular displacement



(b) Average cart progression per period

Figure 4.7 Qualitative variation laws of  $v$  obtained for  $h = 0.8$ ,  $\omega = 1.7$ ,  $\rho = 0.9$  and  $\lambda = 3.6$

Figure 4.7 presents the qualitative variation law of viscous coefficient  $v$ . From Figure 4.7 (a), it is observed that as  $v$  increases, the angular displacement decreases monotonously. However, it seems insufficient to identify and conclude the effects of  $v$  on the VDC performance through the observation on the pendulum subsystem. Therefore, the average cart progression per period of excitation is portrayed in Figure 4.7 (b), where the maximum average progression point is recorded at  $v = 1.3$ . Interestingly from Figure 4.7 (b), it is noted that for value  $v \in (0, 1.3]$ , the cart progression increases monotonically as  $v$  augments; on the other hand, for  $v \in (1.3, 5.0]$ , the viscosity acts negative roles by decreasing the cart's forward progression. The identified optimal viscous value is critical for the system and controller design. Time histories of cart displacements for  $\tau \in [370, 400]$  are presented in Figure 4.8 to verify the qualitative variation laws.

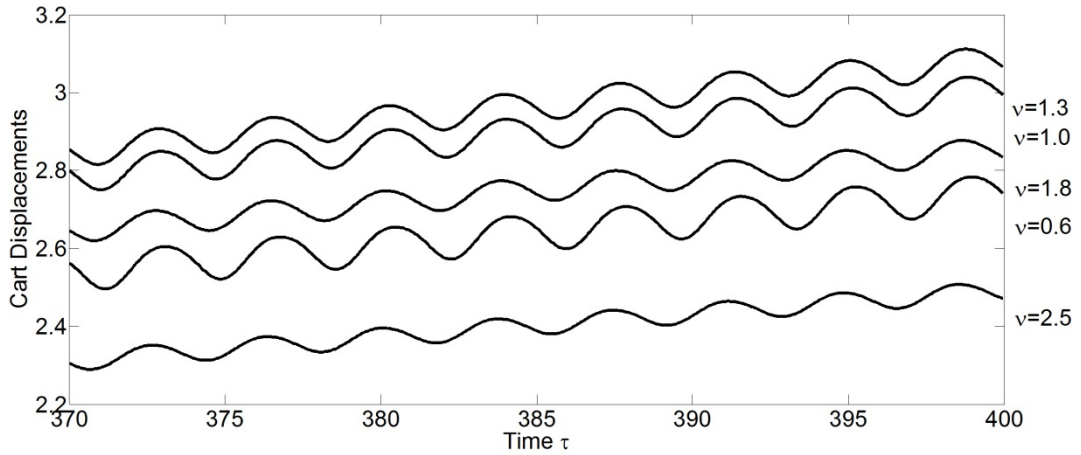


Figure 4.8 Time histories of the cart displacements

**Remark 5.** As shown in Figures 4.5 (a) and 4.7 (a), the performance of the collocated subsystem is convenient to be evaluated using conventional approaches via the affined projection, whilst it is a challenging task to evaluate the non-collocated subsystem. The proposed approach enables characterization of the internal dynamic couplings such that the cart performance can be evaluated beforehand through the locomotion-performance index. The optimal values of viscoelastic parameters can be identified conveniently.

From Figures 4.6 and 4.8, it is shown that the existence of backward motions decreases the locomotion efficacy. To sufficiently suppress the effect of backward motions, the sticking phase needs to be controlled at the restoring stage through the dynamic interactions with friction, which will be discussed in the following subsections.

#### 4.4.2 Dynamic Constraints Characterization

Conventional motion planning approaches is not directly applicable to the cart subsystem which is non-collocated, as a result, the dynamic constraints (4.12) and (4.13) imposed on the system locomotion need to be fully considered when planning

an efficient nominal forced trajectory. The following propositions are given to characterize the constrained stick-slip motions.

*A. Constraint for the Non-Bounding Motion (Phase I to Phase VII)*

The cart is contacting with the sliding surface, a constraint for the contact force need to be satisfied for the whole system to achieve a non-bounding motion, in other words, the contact force has to be greater than zero, which gives an inequality constraint in scaled coordinate as

$$F_y = (\lambda + 1) - \sin\theta\ddot{\theta} - \cos\theta\dot{\theta}^2 - \rho\theta\sin\theta > 0, \tau \in [\tau_1, \tau_7) \quad (4.17)$$

**Proposition 4.1.** From Principle 3, the non-bounding motion for the cart can be achieved if the following condition is satisfied

$$\dot{\theta}^2 |(\ddot{\theta} + \rho\theta + v\dot{\theta})| < \varpi^2/2 \quad (4.18)$$

where

$$\varpi = \lambda + 1$$

**Proof.** From Principle 4.3, we have

$$(\ddot{\theta} + \rho\theta + v\dot{\theta})s_\theta + \dot{\theta}^2 c_\theta < (\lambda + 1) \quad (4.19)$$

Using the auxiliary angle formula and enlarging the inequality gives a sufficient condition as

$$\sqrt{(\ddot{\theta} + \rho\theta + v\dot{\theta})^2 + \dot{\theta}^4} < (\lambda + 1) \quad (4.20)$$

Then through the AM-GM inequality theorem yields

$$\sqrt{2\dot{\theta}^2(\ddot{\theta} + \rho\theta + v\dot{\theta})} < (\lambda + 1) \quad (4.21)$$

Therefore, we have

$$\dot{\theta}^2 |(\ddot{\theta} + \rho\theta + v\dot{\theta})| < (\lambda + 1)^2/2 \quad (4.22)$$

■

*B. Constraint for the Non-Sliding Motion (Phase VI to Phase VII)*

In this duration, the cart remains stationary on the ground without any sliding. Thus the force of the inverted pendulum applied on the base in the horizontal direction has to be less than the maximal static friction, that is,

$$|F_x| \leq \mu F_y, \tau \in [\tau_5, \tau_7) \quad (4.23)$$

which gives a non-dimensionalized inequality constraint as

$$|\cos\theta\ddot{\theta} - \sin\theta\dot{\theta}^2 + \rho\theta\cos\theta| \leq \mu[(\lambda + 1) - \sin\theta\ddot{\theta} - \cos\theta\dot{\theta}^2 - \rho\theta\sin\theta]$$

Furthermore, the interactive force from vertical  $F_y$  is implicitly restricted to be non-negative under the constraint above, which essentially in virtue of the unidirectional property of the ground.

**Proposition 4.2.** From Principle 4, the sticking motion for the platform in the restoring stage will be achieved if the following condition is satisfied

$$\ddot{\theta} + \dot{\theta}^2 + \rho\theta + v\dot{\theta} \leq \varpi\vartheta \quad (4.24)$$

where

$$\varpi = \lambda + 1, \vartheta = \mu/\sqrt{\mu^2 + 1}$$

**Proof.** Utilizing the forces in horizontal and vertical directions, removing the absolute value sign and considering one side of the inequality that

$$c_\theta\ddot{\theta} - s_\theta\dot{\theta}^2 + (\rho\theta + v\dot{\theta})c_\theta \leq \mu[(\lambda + 1) - s_\theta\ddot{\theta} - c_\theta\dot{\theta}^2 - (\rho\theta + v\dot{\theta})s_\theta] \quad (4.25)$$

Reorganizing the formulation above, we have

$$(\mu s_\theta\ddot{\theta} + c_\theta\ddot{\theta}) + (\mu c_\theta\dot{\theta}^2 - s_\theta\dot{\theta}^2) + [\mu(\rho\theta + v\dot{\theta})s_\theta + (\rho\theta + v\dot{\theta})c_\theta] \leq \mu(\lambda + 1) \quad (4.26)$$

Using the auxiliary angle formula and enlarging the inequality gives a sufficient condition as

$$\sqrt{\mu^2 + 1}(\ddot{\theta} + \dot{\theta}^2 + \rho\theta + v\dot{\theta}) \leq \mu(\lambda + 1) \quad (4.27)$$

Therefore, we have

$$\ddot{\theta} + \dot{\theta}^2 + \rho\theta + v\dot{\theta} \leq \mu(\lambda + 1)/\sqrt{\mu^2 + 1} \quad (4.28)$$

#### 4.4.3 Trajectory Boundaries Computation

Based on the constraints analysed above, the boundary conditions are defined below

$$\theta(\tau)|_{\tau=\tau_0} = \theta(\tau)|_{\tau=\tau_7} = -\theta_0 < 0, \theta(\tau)|_{\tau=\tau_3} = \theta_0, \dot{\theta}(\tau)|_{\tau=\tau_0} = 0,$$

$$\dot{X}(\tau)|_{\tau=\tau_0} = \dot{X}(\tau)|_{\tau=\tau_3} = \dot{X}(\tau)|_{\tau=\tau_7} = 0$$

Integrating VDC dynamics (4.8) once along one full motion cycle, we have

$$\begin{aligned} (\lambda + 1)\dot{X} + \mu(\lambda + 1)S_{\dot{X}}\tau - \dot{\theta}c_{\theta} - \mu\dot{\theta}s_{\theta}S_{\dot{X}} - \mu\rho S_{\dot{X}} \int_0^{\tau} \theta s_{\theta} d\tau - \int_0^{\tau} \mu\rho h c_{\omega\tau} s_{\theta} S_{\dot{X}} d\tau \\ + \mu v S_{\dot{X}} \left( \theta s_{\theta} - \int_0^{\tau} \theta c_{\theta} d\tau \right) - \int_0^{\tau} \mu v h \omega s_{\omega\tau} s_{\theta} S_{\dot{X}} d\tau - C_1 = 0 \end{aligned} \quad (4.31)$$

The optimal values of elastic coefficient  $\rho$  and viscous coefficient  $v$  are identified using the qualitative analysis in the previous section. Recalling the desired periodic motion profile, in the duration  $[0, \tau_3]$ ,  $P_2$  can be obtained through integral calculation of (4.8) under the consideration of  $\theta_0$  that if  $c_{\theta} + \mu s_{\theta} \neq 0$ . We have

$$P_2 = \dot{\theta}(\tau)|_{\tau=\tau_3} = \frac{1}{c_{\theta_0} + \mu s_{\theta_0}} [\mu(\lambda + 1)\tau_3 - \mu\rho \int_0^{\tau_3} \theta s_{\theta} d\tau + \mu v (\theta s_{\theta} - \int_0^{\tau_3} \theta c_{\theta} d\tau)] \quad (4.32)$$

Furthermore, the following relationships can be obtained utilizing the conservation of the energy demonstrated in Figure 4.3

$$\int_0^{\tau_1} P_1 \omega_1 s_{\omega\tau} d\tau + P_1 \omega_1 (\tau_2 - \tau_1) + \int_{\tau_2}^{\tau_3} P_1 \omega_1 s_{\omega_1 \tau - \tau_2} d\tau - \frac{1}{2} P_2 \left[ \frac{N\pi}{\omega_1} + \tau_2 - \tau_3 \right] \quad (4.33)$$

$$\frac{1}{2}(-P_3)[(\tau_7 - \tau_4) + (\tau_6 - \tau_5)] = \frac{1}{2}P_2(\tau_4 - \tau_3) + 2\theta_0 \quad (4.34)$$

Therefore, the lower and critical trajectory boundaries are obtained as

$$P_2 = \frac{2P_1[1 - c\omega_1\tau_1 + \omega_1(\tau_2 - \tau_1) + c\omega_1\tau_2 - c\omega_1\tau_3 - \tau_2]^{-4\theta_0}}{N\pi/\omega_1 + \tau_2 - \tau_3} \quad (4.35)$$

$$P_3 = \frac{4\theta_0 + P_2(\tau_4 - \tau_3)}{(\tau_7 - \tau_4) + (\tau_6 - \tau_5)} \quad (4.36)$$

#### 4.4.4 Trajectory Optimization and Parameterization

**Theorem 4.1.** Consider the VDC system (4.8) with viscoelastic property and the planned trajectory (4.14) with dynamic constraints (4.10) - (4.13), if the trajectory parameters are chosen as

$$\begin{aligned} \tau_1 &= \frac{\varpi^2}{2(P_1\omega)^3} - v, \tau_2 = \omega\tau_3 - \arcsin \frac{P_2}{P_1\omega}, \tau_3 = \frac{N\pi}{\omega}, \\ \tau_4 &= -\frac{P_2}{\varpi\vartheta - P_2^2 - \rho P_2\tau_3 - vP_2} + \tau_3, \tau_5 = \frac{\varpi\vartheta - P_3^2 - vP_3}{\rho P_3}, \\ \tau_6 &= \frac{[4\theta_0 + \tau_4(P_2 + 2P_3) - P_2\tau_3]}{2P_3} \text{ and } \tau_7 = (4\theta_0 - P_2\tau_3 + P_2\tau_4 + 2P_3\tau_5)/2P_3 \\ \tau_6 &= \frac{[4\theta_0 + \tau_4(P_2 + 2P_3) - P_2\tau_3]}{2P_3} \text{ and } \tau_7 = (4\theta_0 - P_2\tau_3 + P_2\tau_4 + 2P_3\tau_5)/2P_3 \end{aligned} \quad (4.37)$$

Then the following properties hold:

- (1) the planned trajectory (4.14) is analytical;
- (2) Principles 4.1-4.4 are satisfied;
- (3) the time per period of locomotion can be evaluated beforehand as  $T_{total} = \sum_{i=1}^7 \tau_i$ .

**Proof.** To optimally parameterize the motion trajectory, the dynamic constraints are explicitly utilized with the identified optimal viscoelastic parameters  $\rho$  and  $v$ . Specifically, for *Phase I*, from *Proposition 4.1*, we have

$$\dot{\theta}^2(\tau_1)|(\ddot{\theta}(\tau_1) + \rho\theta(\tau_1) + v\dot{\theta}(\tau_1))| < \varpi^2/2 \quad (4.38)$$

where  $\dot{\theta}(\tau_1) = P_1\omega$ ,  $\ddot{\theta}(\tau_1) = 0$  and  $\theta(\tau_1) = P_1\omega\tau_1$ . The upper boundary of *Phase I* is obtained as

$$\tau_1 = (\frac{\varpi^2}{2(P_1\omega)^3} - v)/\rho \quad (4.39)$$

The formulation for *Phase II* can be described as  $P_1\omega s_{\omega\tau_3-\tau_2} = P_2$ , accordingly its duration can be derived as

$$\tau_2 = \omega\tau_3 - \arcsin_{P_2/P_1\omega} \quad (4.40)$$

In view of the synchronization and smoothness consideration, the motion trajectory is designed to reach the amplitude of harmonic excitation at time  $\tau_1$  and keep it till time  $\tau_2$ , and duration of this phase has to be half of the excitation period, which gives the duration *Phase III* as

$$\tau_3 = N\pi/\omega \quad (4.41)$$

During *Phase IV*, the cart is kept stationary which allows a recovery process without any backward motion. Applying *proposition 4.2* at time  $\tau_3$ , gives

$$\ddot{\theta}(\tau_3) + \dot{\theta}(\tau_3)^2 + \rho\theta(\tau_3) + v\dot{\theta}(\tau_3) \leq \varpi\vartheta \quad (4.42)$$

where  $\theta(\tau_3) = P_2\tau_3$ ,  $\dot{\theta}(\tau_3) = P_2$  and  $\ddot{\theta}(\tau_3) = -P_2/(\tau_4 - \tau_3)$ .

Then the duration  $\tau_4$  can be obtained as

$$\tau_4 = -P_2/(\varpi\vartheta - P_2^2 - \rho P_2\tau_3 - vP_2) + \tau_3 \quad (4.43)$$

In terms of *Phase V*, applying *Proposition 4.2* at time  $\tau_5$ , we have

$$\ddot{\theta}(\tau_5) + \dot{\theta}(\tau_5)^2 + \rho\theta(\tau_5) + v\dot{\theta}(\tau_5) \leq \varpi\vartheta \quad (4.44)$$

where  $\ddot{\theta}(\tau_5) = 0$ ,  $\dot{\theta}(\tau_5) = P_3$ ,  $\theta(\tau_5) = P_3\tau_5$ .

Accordingly, the maximal boundary of *Phase V* is calculated as

$$\tau_5 = (\varpi\vartheta - P_3^2 - \nu P_3)/\rho P_3 \quad (4.45)$$

Further relationship can be achieved in the duration of  $[\tau_4, \tau_5]$  as

$$P_2(\tau_5 - \tau_4) = P_3(\tau_4 - \tau_3) \quad (4.46)$$

As for the trajectory profile for *Phase VI* and *Phase VII*, it is noted that the durations of  $[\tau_4, \tau_5]$  and  $[\tau_6, \tau_7]$  are accordant based on the design objectives, gives

$$\tau_5 - \tau_4 = \tau_7 - \tau_6 \quad (4.47)$$

Combining (4.46) with (4.35), we have

$$\tau_6 = [4\theta_0 + \tau_4(P_2 + 2P_3) - P_2\tau_3]/2P_3 \quad (4.48)$$

$$\tau_7 = (4\theta_0 - P_2\tau_3 + P_2\tau_4 + 2P_3\tau_5)/2P_3 \quad (4.49)$$

The trajectory parameterisation procedure (4.38) - (4.49) directly indicate the analytical property of the planned trajectory (4.14) and satisfaction of Principles 4.1 and 4.2. The utilization of Propositions 4.1 and 4.2 indicate the satisfaction of Principles 4.3 and 4.4. Property (3) can be directly shown by adding the trajectory durations from (4.39), (4.40), (4.41), (4.43), (4.45), (4.48) and (4.49), i.e.,  $T_{total} = \sum_{i=1}^7 \tau_i$ .

**Remark 4.12.** It is noted that the trajectory planning scheme proposed in this work can be adopted either in the open-loop control system design or as feedforward segment in the closed-loop control system formulation of the VDC systems. Admittedly, it is nearly impossible to implement trajectory planning algorithm merely in an open-loop control system to cope with the unexpected uncertainties (e.g. unstructured and unmodeled dynamics, external disturbances). Indeed, the proposed approach may be combined with advanced control schemes (e.g., robust and adaptive paradigms) to enhance robustness to disturbances and adaptability to parametric uncertainties with guaranteed performance of the proposed algorithm. The closed-loop feedback control and adaptive control of the proposed system will be studied in the next section.

## 4.5 Trajectory Tracking Control System Design

In this section, we design the controller for the proposed system based on the control algorithms proposed in Chapter 3. The aim is to allow the pendulum trajectory to effectively track the periodic motion profile only by applying the torque actuation as the control input at the pivot of the pendulum. Based on the absence and presence of parametric uncertainties, two tracking control schemes are constructed. Specifically, the objective of designing the trajectory tracking controllers is two-folded. Firstly, to verify the superior performance of the VDC system with the proposed trajectory planning algorithm and to make convenient comparison with the conventional approach, a closed-loop feedback control scheme is designed using collocated PFL approach. On the other hand, an adaptive variable structure trajectory tracking control algorithm is constructed to cope with the parametric uncertainties.

### 4.5.1 Closed-Loop Feedback Control Scheme

Based on the dynamic model in (4.8) and after some calculations, we have

$$\left(1 - \frac{1}{\lambda+1} c_\theta^2\right) \ddot{\theta} + \frac{1}{\lambda+1} [c_\theta (s_\theta \dot{\theta}^2 + f')] - s_\theta + \rho\theta + v\dot{\theta} = u_d \quad (4.50)$$

Define the trajectory tracking error and its derivatives as

$$\tilde{\theta} = \theta - \theta_d, \quad \dot{\tilde{\theta}} = \dot{\theta} - \dot{\theta}_d \quad \text{and} \quad \ddot{\tilde{\theta}} = \ddot{\theta} - \ddot{\theta}_d \quad (4.51)$$

**Remark 4.13.** It is noted that the duration of each motion phase is fixed, using equations of motion (4.8) and the planned trajectory (4.14), the prior knowledge of desired cart and pendulum trajectory for each sampling time can be obtained by convenient computation.

Substituting (4.51) into (4.50) and conducting appropriate mathematical manipulation, we have the following system dynamics

$$\left(1 - \frac{1}{\lambda+1} c_\theta^2\right) \ddot{\tilde{\theta}} = u_d - \frac{1}{\lambda+1} [c_\theta (s_\theta \dot{\theta}^2 + f')] + s_\theta - \rho\theta - v\dot{\theta} - \left(1 - \frac{1}{\lambda+1} c_\theta^2\right) \ddot{\theta}_d \quad (4.52)$$

Utilising the CPFL technique for the system dynamics in (4.52), a feedback linearizing controller can be designed as

$$u_d = \left(1 - \frac{1}{\lambda + 1} c_\theta^2\right) \ddot{\theta}_d + \frac{1}{\lambda + 1} [c_\theta (s_\theta \dot{\theta}^2 + f')] - s_\theta + \rho \theta + v \dot{\theta} - K_v \left(1 - \frac{1}{\lambda + 1} c_\theta^2\right) \dot{\tilde{\theta}} - K_p \left(1 - \frac{1}{\lambda + 1} c_\theta^2\right) \tilde{\theta} \quad (4.53)$$

where  $K_v$  and  $K_p$  are positive control gains selected by the designer.

Substituting (4.53) into system (4.52) and after some convenient calculations, the closed-loop system can be obtained in the following form

$$\ddot{\tilde{\theta}} + K_v \dot{\tilde{\theta}} + K_p \tilde{\theta} = 0 \quad (4.54)$$

Therefore, it is evident through the Routh-Hurwitz criterion that the system stability is guaranteed.

#### 4.5.2 Adaptive Robust Control Scheme with an Auxiliary Variable

This subsection considers the condition with parametric uncertainties that the system base parameters are unknown. The main difficulty exists in the nonlinearity of collocated inverse dynamics *w.r.t.* the base parameters, which makes the applications of conventional adaptive control algorithms not directly available. The main idea in this thesis is to introduce an auxiliary control variable to closure the non-collocated subsystem and to construct online adaptive algorithms to estimate the system parameter values such that the tracking error and estimation error signals in the closed-loop system converge to zero asymptotically.

In the following, new vector variables are defined as

$$\varrho = \begin{bmatrix} \varrho_\theta \\ \varrho_x \end{bmatrix} = \dot{q}_d - \Lambda \tilde{q} = \begin{bmatrix} \dot{\theta}_d - \Lambda_\theta \tilde{\theta} \\ \dot{X}_d - \Lambda_x \tilde{X} \end{bmatrix} \quad (4.55a)$$

$$\delta = \begin{bmatrix} \delta_\theta \\ \delta_x \end{bmatrix} = \begin{bmatrix} \dot{\theta} - \varrho_\theta \\ \dot{X} - \varrho_x \end{bmatrix} = \begin{bmatrix} \dot{\tilde{\theta}} + \Lambda_\theta \tilde{\theta} \\ \dot{\tilde{X}} + \Lambda_x \tilde{X} \end{bmatrix} \quad (4.55b)$$

where  $\delta$  denotes the filtered error signal and describes the measure of tracking accuracy,  $\varrho$  is referred to as vector of the reference trajectory,  $\Lambda = [\Lambda_\theta \Lambda_X]^T$  are positive constants selected by designers and denoting for the bandwidth of the first-order filter.

Alongside the definitions in (4.60), two sliding variables  $\delta_\theta$  and  $\delta_X$  are designed for the collocated and non-collocated subsystems, respectively. The dynamics in terms of the sliding variables can be derived from (4.8) and (4.55) as

$$M \begin{bmatrix} \dot{\delta}_\theta \\ \dot{\delta}_X \end{bmatrix} + C \begin{bmatrix} \delta_\theta \\ \delta_X \end{bmatrix} = \begin{bmatrix} T + N_\theta(t) \\ N_X(t) \end{bmatrix} \quad (4.56)$$

where  $N_\theta(t)$  and  $N_X(t)$  represent nonlinear functions with unknown base parameters detailed as follows:

$$\begin{aligned} N_\theta(t) &= -ml^2 \dot{\varrho}_\theta + mlc_\theta \dot{\varrho}_X - k\theta - c\dot{\theta} + mgl s_\theta \\ &= [\dot{\varrho}_\theta - c_\theta \dot{\varrho}_X \theta \dot{\theta} - s_\theta] [ml^2 \ ml \ k \ c \ mgl]^T = -Y_\theta \alpha_\theta \end{aligned}$$

$$\begin{aligned} N_X(t) &= mlc_\theta \dot{\varrho}_\theta - (M + m) \dot{\varrho}_X - \mu NS_X - mls_\theta \dot{\varrho}_\theta \\ &= [-c_\theta \dot{\varrho}_\theta \ \dot{\varrho}_X \ NS_X \ s_\theta \dot{\varrho}_\theta] [ml \ (M + m) \ \mu \ ml]^T = -Y_X \alpha_X \end{aligned}$$

**Remark 4.13.** The filtered error dynamics (4.56) satisfies Properties 4.1 and 4.2.

Accounting for the parametric uncertainty existing in  $Y_\theta \alpha_\theta$  and  $Y_X \alpha_X$ , the following theorem presents an adaptive variable structure control scheme, based on the filtered error dynamics in (4.56), that ensure the adaptive asymptotic convergence of the closed loop signals.

**Theorem 4.2.** Consider the VDC system modelled by (4.8) and introduce an auxiliary variable  $\eta$ . If the following control system is designed to the underactuated VDC system with parametric uncertainty

$$u = T_c + T_n \quad (4.57a)$$

$$T_c = Y_\theta \hat{\alpha}_\theta - K_1 \delta_\theta \quad (4.57b)$$

$$\begin{aligned} T_n &= -sgn(\delta_\theta) \|\delta_X\| |\eta| - K_2 sgn(\delta_\theta) \|\delta_X\| - \frac{(\eta + 1) \delta_\theta \delta_X^T K_3 \delta_X}{\|\delta_\theta\|^2 + \beta} \\ &\quad - \frac{(\eta - 1) \delta_\theta \|\delta_X^T Y_X\| \hat{\alpha}_X}{\|\delta_\theta\|^2 + \beta} \end{aligned}$$

(4.57c)

$$\dot{\eta} = \eta^{\frac{2n+2}{2n+1}} \frac{\|\delta_\theta\|^2}{\|\delta_\theta\|^{2+\beta}} (K_3 \|\delta_X\|^2 + \|\delta_X^T Y_X\| \hat{\alpha}_X) \quad (4.57d)$$

with the adaptation laws

$$\dot{\hat{\alpha}}_\theta = -\Gamma_1 Y_\theta \delta_\theta, \quad \dot{\hat{\alpha}}_X = -\Gamma_2 Y_X \delta_X \quad (4.57e)$$

where the subscripts “c” and “n” indicate the collocated and non-collocated, respectively.  $K_1 \in \mathcal{R}^1$ ,  $K_2, K_3 \in \mathcal{R}^1$  are diagonal, constant positive definite matrices,  $\Gamma_1 \in \mathcal{R}^1$  and  $\Gamma_2 \in \mathcal{R}^1$  are positive definite matrices determining the rate of adaptation.  $\beta > 0$  is a selected small constant.  $\tilde{\alpha}_\theta(t) = \hat{\alpha}_\theta(t) - \alpha_\theta(t)$  and  $\tilde{\alpha}_X(t) = \hat{\alpha}_X(t) - \alpha_X(t)$  are parameter estimation errors. Then the following conclusions hold:

- (1) The system is globally asymptotically stabilized;
- (2) All signals in the closed-loop system are bounded and uniformly continuous ;
- (3) The asymptotical convergence of the error signals are guaranteed.

**Proof.** Consider the following Lyapunov candidate function as

$$V = \frac{1}{2} \delta^T D \delta + \frac{1}{2} \tilde{\alpha}_\theta^T \Gamma_1^{-1} \tilde{\alpha}_\theta + \frac{1}{2} \tilde{\alpha}_X^T \Gamma_2^{-1} \tilde{\alpha}_X + \frac{2n+1}{2n} \eta^{\frac{2n}{2n+1}} \quad (4.58)$$

Differentiating both sides of (4.58) and substituting the control laws (4.57), yields

$$\begin{aligned} \dot{V} &= \delta^T D \dot{\delta} + \frac{1}{2} \delta^T \dot{D} \delta + \dot{\hat{\alpha}}_\theta^T \Gamma_1^{-1} \tilde{\alpha}_\theta + \dot{\hat{\alpha}}_X^T \Gamma_2^{-1} \tilde{\alpha}_X + \eta^{\frac{-1}{2n+1}} \dot{\eta} \\ &= \delta^T \left( \begin{bmatrix} T - Y_\theta \alpha_\theta \\ -Y_X \alpha_X \end{bmatrix} - C \delta \right) + \frac{1}{2} \delta^T \dot{D} \delta + \dot{\hat{\alpha}}_\theta^T \Gamma_1^{-1} \tilde{\alpha}_\theta + \dot{\hat{\alpha}}_X^T \Gamma_2^{-1} \tilde{\alpha}_X + \eta^{\frac{-1}{2n+1}} \dot{\eta} \end{aligned}$$

Adopting the Property A.2 and substituting the auxiliary control variable in (4.57c) with its evolving law (4.57d), we have

$$\dot{V} = \delta^T \begin{bmatrix} T - Y_\theta \alpha_\theta \\ -Y_X \alpha_X \end{bmatrix} + \delta^T \left( \frac{1}{2} \dot{D} - C \right) \delta + \dot{\hat{\alpha}}_\theta^T \Gamma_1^{-1} \tilde{\alpha}_\theta + \dot{\hat{\alpha}}_X^T \Gamma_2^{-1} \tilde{\alpha}_X + \eta^{\frac{-1}{2n+1}} \dot{\eta}$$

$$\begin{aligned}
 &= \delta^T \begin{bmatrix} Y_\theta \hat{\alpha}_\theta - K_1 \delta_\theta - \text{sgn}(\delta_\theta) \|\delta_x\| |\eta| - K_2 \text{sgn}(\delta_\theta) \|\delta_x\| - \\ \frac{(\eta + 1) \delta_\theta \delta_x^T K_3 \delta_x}{\|\delta_\theta\|^2 + \beta} - \frac{(\eta - 1) \delta_\theta \|\delta_x^T Y_x\| \hat{\alpha}_x}{\|\delta_\theta\|^2 + \beta} - Y_\theta \alpha_\theta \\ -Y_x \alpha_x \end{bmatrix} + \hat{\alpha}_\theta^T \Gamma_1^{-1} \tilde{\alpha}_\theta \\
 &\quad + \hat{\alpha}_x^T \Gamma_2^{-1} \tilde{\alpha}_x + \eta^{\frac{-1}{2n+1}} \dot{\eta} \\
 &= [\delta_\theta^T \ \delta_x^T] \begin{bmatrix} Y_\theta \hat{\alpha}_\theta - K_1 \delta_\theta - \text{sgn}(\delta_\theta) \|\delta_x\| |\eta| - K_2 \text{sgn}(\delta_\theta) \|\delta_x\| - \\ \frac{(\eta + 1) \delta_\theta \delta_x^T K_3 \delta_x}{\|\delta_\theta\|^2 + \beta} - \frac{(\eta - 1) \delta_\theta \|\delta_x^T Y_x\| \hat{\alpha}_x}{\|\delta_\theta\|^2 + \beta} - Y_\theta \alpha_\theta \\ -Y_x \alpha_x \end{bmatrix} + \hat{\alpha}_\theta^T \Gamma_1^{-1} \tilde{\alpha}_\theta \\
 &\quad + \hat{\alpha}_x^T \Gamma_2^{-1} \tilde{\alpha}_x + \eta^{\frac{-1}{2n+1}} \dot{\eta} \\
 &= -\delta_\theta^T K_1 \delta_\theta - \delta_\theta^T \text{sgn}(\delta_\theta) \|\delta_x\| |\eta| - K_2 \delta_\theta^T \text{sgn}(\delta_\theta) \|\delta_x\| - \frac{(\eta + 1) \|\delta_\theta\|^2 \delta_x^T K_3 \delta_x}{\|\delta_\theta\|^2 + \beta} \\
 &\quad - \frac{(\eta - 1) \|\delta_\theta\|^2 \|\delta_x^T Y_x\| \hat{\alpha}_x}{\|\delta_\theta\|^2 + \beta} - \delta_x^T Y_x \alpha_x + \hat{\alpha}_x^T \Gamma_2^{-1} \tilde{\alpha}_x + \eta^{\frac{-1}{2n+1}} \dot{\eta} \\
 &= -\delta_\theta^T K_1 \delta_\theta - \delta_\theta^T \text{sgn}(\delta_\theta) \|\delta_x\| |\eta| - K_2 \delta_\theta^T \text{sgn}(\delta_\theta) \|\delta_x\| - \frac{(\eta + 1) \|\delta_\theta\|^2 \delta_x^T K_3 \delta_x}{\|\delta_\theta\|^2 + \beta} \\
 &\quad - \frac{(\eta - 1) \|\delta_\theta\|^2 \|\delta_x^T Y_x\| \hat{\alpha}_x}{\|\delta_\theta\|^2 + \beta} - \delta_x^T Y_x \alpha_x + \hat{\alpha}_x^T \Gamma_2^{-1} \tilde{\alpha}_\theta \\
 &\quad + \frac{\eta \|\delta_\theta\|^2}{\|\delta_\theta\|^2 + \beta} (K_3 \|\delta_x\|^2 + \|\delta_x^T Y_x\| \hat{\alpha}_x) \\
 &\leq -\delta_\theta^T K_1 \delta_\theta - \delta_\theta^T \text{sgn}(\delta_\theta) \|\delta_x\| |\eta| - K_2 \delta_\theta^T \text{sgn}(\delta_\theta) \|\delta_x\| - \frac{\|\delta_\theta\|^2 K_3 \|\delta_x\|^2}{\|\delta_\theta\|^2 + \beta} \\
 &\quad + \frac{\|\delta_\theta\|^2}{\|\delta_\theta\|^2 + \beta} \|\delta_x^T Y_x\| \hat{\alpha}_x - \delta_x^T Y_x \alpha_x + \hat{\alpha}_x^T \Gamma_2^{-1} \tilde{\alpha}_x \\
 &\leq -\delta_\theta^T K_1 \delta_\theta - \delta_\theta^T \text{sgn}(\delta_\theta) \|\delta_x\| |\eta| - K_2 \delta_\theta^T \text{sgn}(\delta_\theta) \|\delta_x\| - \frac{\|\delta_\theta\|^2 K_3 \|\delta_x\|^2}{\|\delta_\theta\|^2 + \beta} \\
 &= -\delta_\theta^T K_1 \delta_\theta - \|\delta_\theta\| \|\delta_x\| |\eta| - K_2 \|\delta_\theta\| \|\delta_x\| - \frac{\|\delta_\theta\|^2 K_3 \|\delta_x\|^2}{\|\delta_\theta\|^2 + \beta} \\
 &\leq -K_1 \|\delta_\theta\|^2 - \frac{\|\delta_\theta\|^2 K_3 \|\delta_x\|^2}{\|\delta_\theta\|^2 + \beta} \leq 0
 \end{aligned} \tag{4.59}$$

From the definition of Lyapunov function  $V(t)$  in (4.58), it is lower bounded by zero and decreases for any nonzero  $\delta$  as shown from (4.59). It is evident from the above mathematical proof that the global uniform boundedness of the filtered tracking error of collocated subsystem  $\delta_\theta$  and non-collocated subsystem  $\delta_X$ , the parameter estimation errors  $\tilde{\alpha}_\theta$  and  $\tilde{\alpha}_X$  are guaranteed. From the definition and assumption 1 of filtered tracking error  $\delta$ , it is evident that  $\delta$  is bounded. The boundedness of control input is obvious from (4.57). It can be conclude that  $\delta = [\delta_\theta \ \delta_X]^T \in L_2^n \cap L_\infty^n$ , and it is obvious that  $\dot{\delta} \in L_\infty^n$  from (4.55), thus, based on Barbalat's Lemma,  $\delta_\theta$  and  $\delta_X$  are continuous and  $\delta_\theta \rightarrow 0, \delta_X \rightarrow 0$  as  $t \rightarrow \infty$ , and  $\eta \in L_\infty$ . From (4.57), it can be shown that  $\tilde{\alpha}_\theta \in L_\infty^p$ . This in turns implies that, based on the Property 3.1 and (4.55),  $\dot{\delta} \in L_\infty^n$ ,  $\ddot{q} = [\ddot{q}_\theta \ \ddot{q}_X]^T \in L_\infty^n$  and  $\tilde{q} = [\tilde{q}_\theta \ \tilde{q}_X]^T \in L_\infty^{2n}$ . Therefore,  $\tilde{q}_\theta$  and  $\tilde{q}_X$  are uniformly continuous and  $\tilde{q} = [\tilde{q}_\theta \ \tilde{q}_X]^T \in L_\infty^{2n}$ , it is proofed that  $\tilde{q} \rightarrow 0$  as  $t \rightarrow \infty$ . ■

**Remark 3.3.** Based on the stability analysis, the feedback signal  $K_2 \text{sgn}(\delta_\theta) \|\delta_X\|$  designed in (4.57) enhances the robustness of the system. Beneficial from this inclusion, the trajectory tracking error will converge to zero in the presence of parametric uncertainties.

## 4.6 Simulation Results

In this section, a number of numerical simulations are conducted to verify the performance and efficiency of the proposed trajectory planning scheme and the adaptive tracking control scheme. In particular, the advantages of the planned trajectory such as smooth transition in progressive stage, superior efficiency in progression and energy consumption are presented. In the simulation, the rationality of the parameter values selection in this section is specified as follows: the system parameter values are configured from the studies in literature as reported in (Li et al., 2006; Y. Liu et al., 2008, 2011) as  $M = 0.5 \text{ kg}$ ,  $m = 0.138 \text{ kg}$ ,  $l = 0.3 \text{ m}$ ,  $g = 9.81 \text{ m/s}^2$ ,  $\mu = 0.01 \text{ N/ms}$  and the system natural frequency  $\omega_n = 5.7184 \text{ rad/s}$ . Then, based on the optimal selection algorithms in Section 4, the

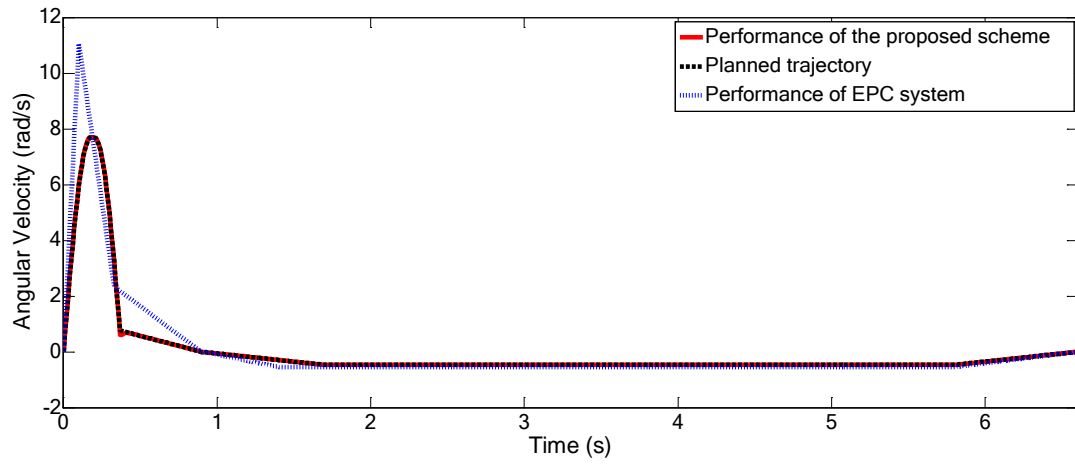
control parameters are configured as  $k = 0.36 \text{ Nm/rad}$  and  $c = 0.0923 \text{ kgm}^2/\text{srad}$  to obtain optimal steady-state motion. The initial conditions are set as  $\theta(0) = \theta_0 = \pi/3$ ,  $\dot{\theta}(0) = 0$ ,  $x(0) = 0$  and  $\dot{x}(0) = 0$ .

Firstly, in the absence of parametric uncertainty, comparative studies are performed with (Liu et al., 2014) (referred to as EPC system), in which a two-stage velocity trajectory is proposed using conventional approach with heristically chosen control parameters. To make convenient comparison, control scheme (4.53) is employed. Based on the trajectory planning algorithms in Section 4.4, the parameters for the constructed trajectory (4.14) and the trajectory in (Liu et al., 2014) are detailed in Table 4.1.

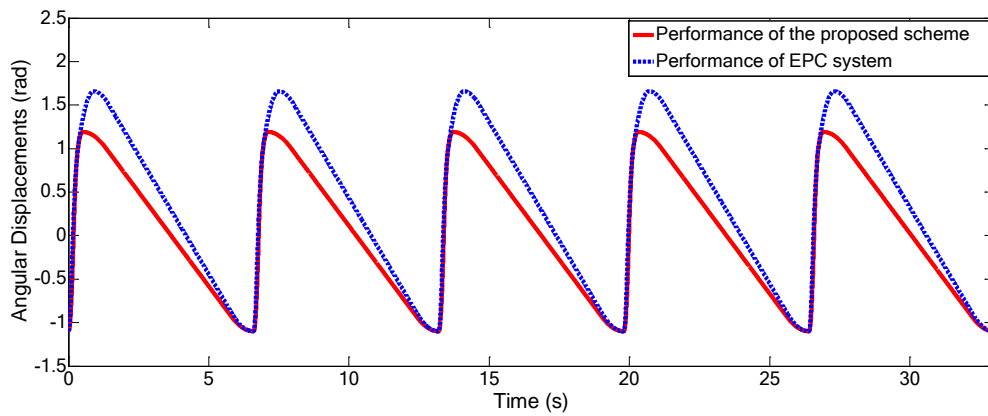
Table 4.1 Trajectory parameters for numerical simulation (s)

Trajectories	$t_1$	$t_2$	$t_3$	$t_4$	$t_5$	$t_6$	$t_7$
Trajectory in EPC	0.1	0.33	0.9	1.4	5.8	6.6	NA
Trajectory (10)	0.133	0.195	0.275	0.9	1.7	5.8	6.6

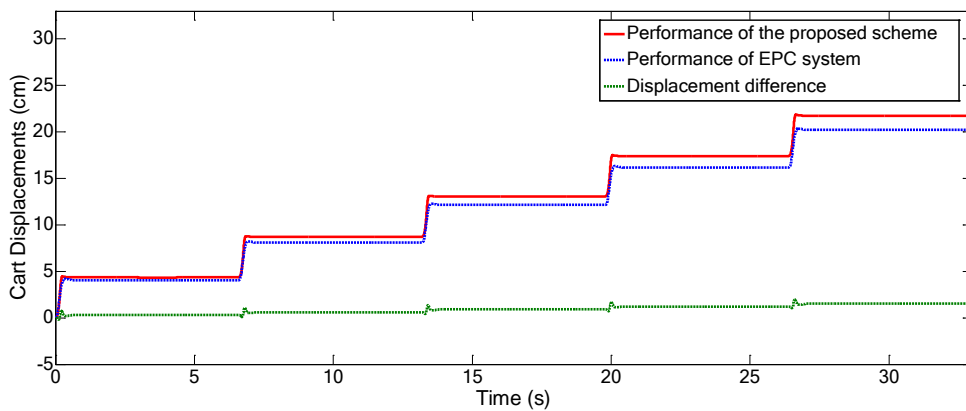
The simulation results are presented in Figure 4.9. It can be clearly observe from Figure 4.9(a) that the maximum angular velocity using the proposed method is about 7.8 rad/s, which is lower than the EPC system with 11 rad/s. The synchronized trajectory present better transient performance in terms of the overshoot and the maximum pendulum swing is about  $68.75^\circ$  ( $17.1^\circ$  smaller than the EPC system). These results have good agreements with the trajectory planning indexes and principles. The average velocity with the proposed trajectory calculated from Figure 4.9(c) for the first five cycles is 0.642cm/s, whereas it is 0.629cm/s for the EPC system. The transition functions inserted into progressive stage guarantee the smooth transition and thereafter a lower maximum input torques as shown in Figure 4.9(d) (0.5367 Nm compared with 0.6246 Nm of EPC system). This directly evidents a superior performance in energy efficacy. The backward motions are sufficiently supressed as can be seen from Figure 4.9(c). The results concludes that the friction-indcued stick-slip motions are precisely controlled through the proposed trajectory planning scheme, in a manner that the superior performance are guaranteed.



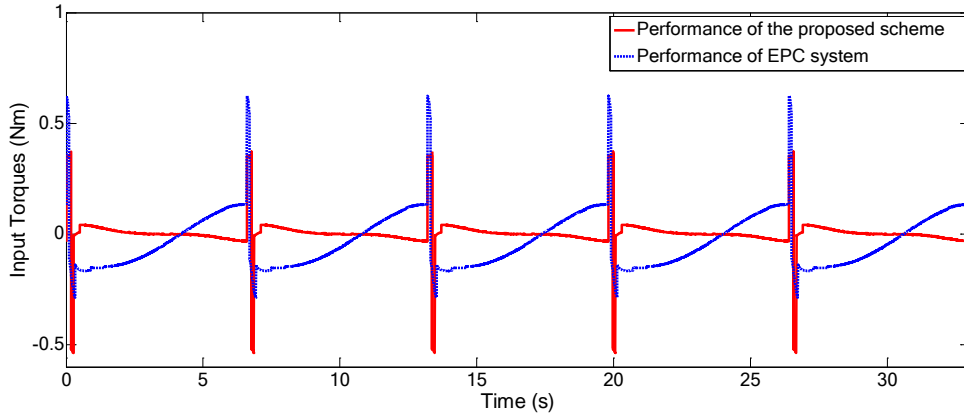
(a) Trajectory tracking performance



(b) Time histories of angular displacements for five motion cycles



(c) Time histories of cart displacements for five motion cycles

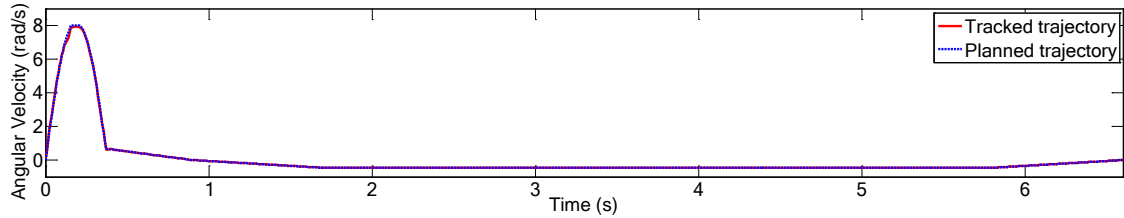


(d) Time histories of input torques for five motion cycles

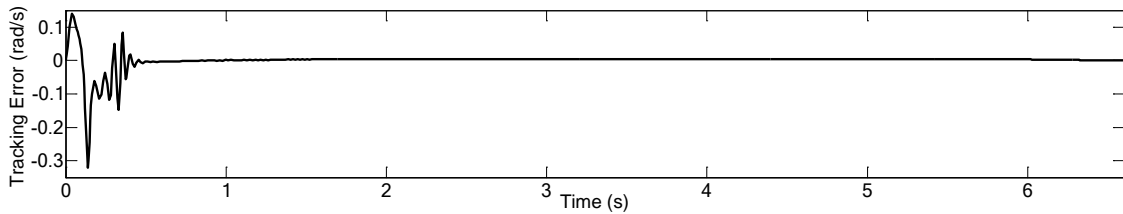
Figure 4.9 Simulation results of the proposed method (red solid line) and conventional method in EPC (blue dashed line)

Subsequently, the adaptive tracking control scheme in (4.57) are evaluated in the presence of parametric uncertainty. The mass of the cart  $M$  and the friction coefficient  $\mu$  are assumed uncertain with known bounds, i.e.,  $0.45kg \leq M \leq 0.55kg$  and  $0.009 N/ms \leq \mu \leq 0.011N/ms$ . This is under the consideration that the mass of cart body may vary when working in the environment with high degree of viscosity, and the cart may be glued on environmental component such as water, mud, mucus, etc. And the sliding friction coefficient is undergoing changes at different substrate. The bandwidth of the first-order filter is set as  $\Lambda = [\Lambda_\theta \ \Lambda_x]^T = [12 \ 30]^T$ . The control gain used in the simulation are chosen to be  $K_1 = 1.3$ ,  $K_2 = 10$  and  $K_3 = 50$ . As a result, the associated base parameters are  $\alpha_\theta = [0.01424, 0.0414, 0.36, 0.0923, 0.40527]^T$  and  $\alpha_x = [0.0414, 0.638, 0.01, 0.0414]^T$ . The adaptation gains are chosen as  $\Gamma_1 = 0.1$  and  $\Gamma_2 = 0.1$ . The simulation result of trajectory tracking performance of the adaptive variable structure control scheme (4.5) are shown in Figure 4.10. The planned collocated trajectory (4.14) (red dashed line), the simulated trajectory (black solid line) in Figure 4.10(a) and the trajectory tracking error in Figure 4.10(b) are portrayed. It can be observed that the driving pendulum tracks the planned trajectory accurately and the maximum angular velocity is about 7.9 rad/s. The figure illustrates the effectiveness of the designed

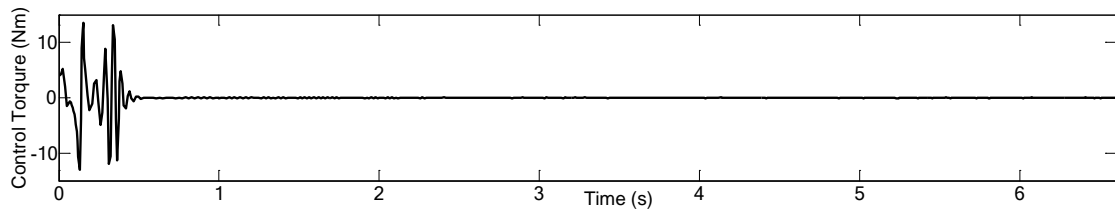
control scheme. It is clear to see that the asymptotic convergence of the tracking error is achieved.



(a) Trajectory tracking performance with tracked trajectory (black solid line) and planned trajectory (red dashed line)



(b) Trajectory tracking error



(c) Control torque

Figure 4.10 Simulation results of control scheme (4.57) under parametric uncertainty

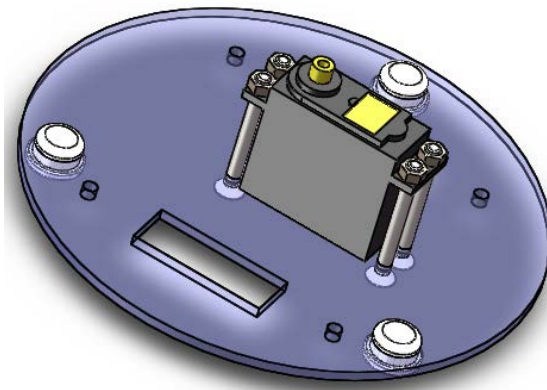
## 4.7 Robot Design and Experimental Results

In this section, the 3D design of the the vibro-driven cart system, experimental setup and some preliminary results are presented.

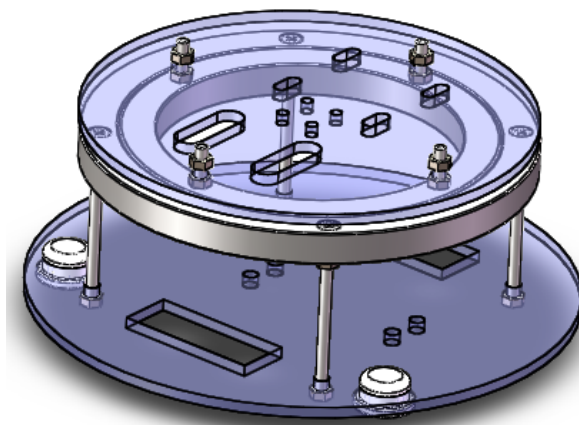
### 4.7.1 3D Robotic System Design

The 3D robotic model for the vibro-driven system is built through SolidWorks (as shown in Figure 4.11), in which the connections between each component are detailed. The system contains two layers, the lower layer is contacting with the

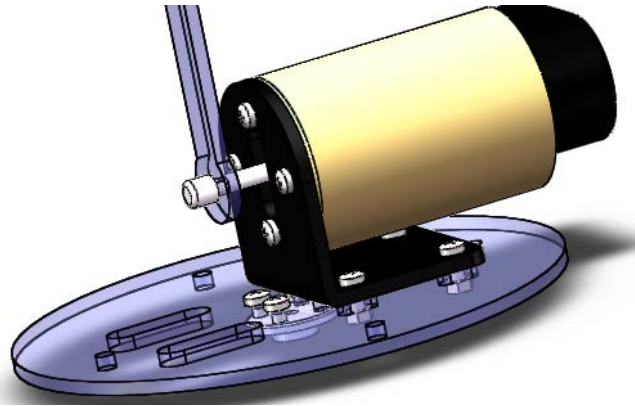
ground and the upper layer is linked with a rotating pendulum. The system contains one DC servo motor as the main actuation mechanism and one steering engine for two-dimensional locomotion. A steering engine is fixed with the lower layer as shown in Figure 4.11(a) such that the direction of the robot on the flat plane can be adjusted to facilitate a two-dimensional locomotion. Two layers are firmly fixed together through four bearings as can be seen from Figure 4.11(b). From Figure 4.11(c), a DC motor is installed and fixed on the upper layer. Alternative holes are designed for the mass ball as shown in Figure 4.11(d) such that the length and inertia of the pendulum becomes adjustable.



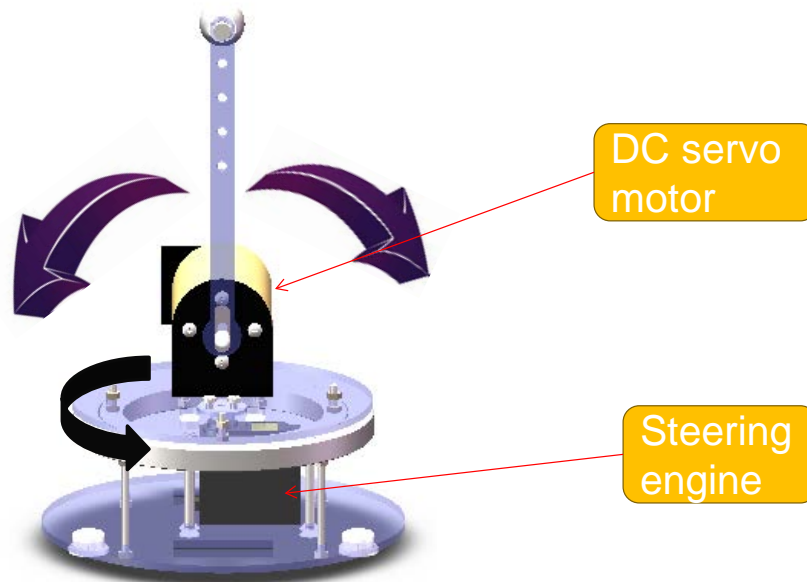
(a) The lower layer (chassis)



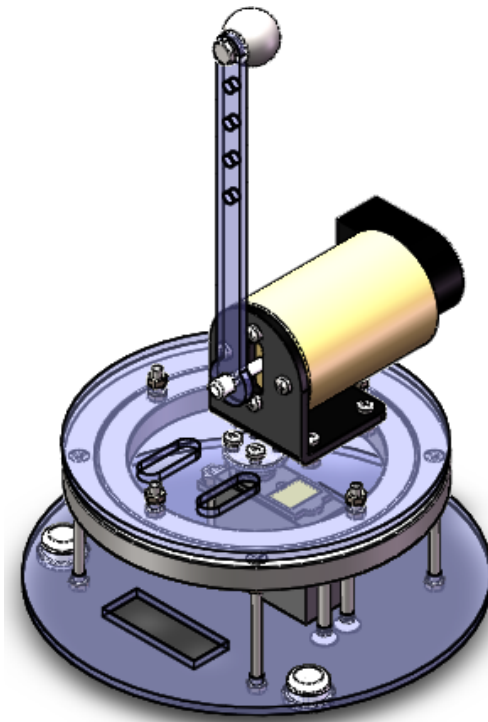
(b) The connected layers



(c) Motor installation



(d) The motor and steering engine



(e) The overall system

Figure 4.11 The 3D prototype of the vibro-driven system

### 4.7.2 Experiment Setup

In this subsection, the experimental setup of the vibro-driven system is presented. The objective of the experiment here is to demonstrate and validate the proposed robotic model and its mobility. The experimental components of the vibro-driven system are shown in Figure 4.12. As shown in Figure 4.12(a), a DC servo motor driver RMDS-102 (“RMDS,” n.d.) is employed to drive the DC motor. RMDS-102 is a high-performance DC motor driver which has 15 pins and 13 of them are used in this study. MT1 and MT2 connect the positive and negative terminal of the DC servo motor, respectively. CHB, +5V, CHA and GND are connected with the servo motor encoder. CANL and CANH are connected with corresponding pins in the controller. RS232 is used as communication mode. The main function of the motor is to control the rotation of the pendulum within a certain angular range, therefore the angular position and angular velocity need to be controlled. A DC servo motor produced by Globe Motor (“Globe Motors,” n.d.) as shown in Figure 4.12(d) is used

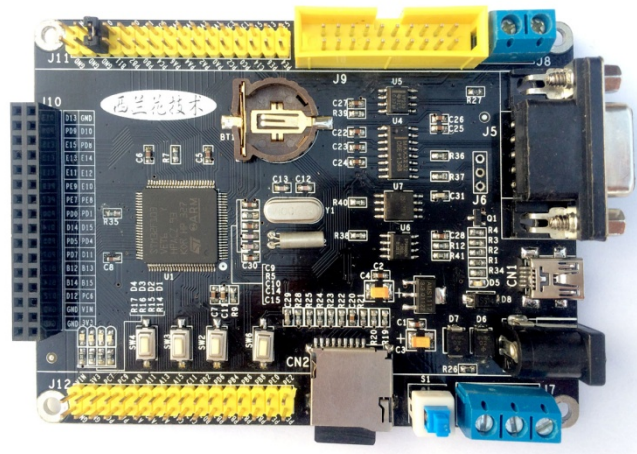
to rotate the pendulum. It has a double-channel encoder. A steering engine MG995 (“Shenzhen Zvepower Technology Co., Ltd.,” n.d.) as shown in Figure 4.12(b) is used to steering system on the flat plane. It is noted that in this study, the main function of the steering engine is to control the rotation of the platform, therefore it is required to operate/rotate in a lower velocity. A STM32 Series microcontroller STM 32VET6 (“STMicroelectronics,” n.d.) is used as the main controller as shown in Figure 4.12(c). The linear motor can be connected to the motion controller through wires and a connector. The motion controller provides power to the linear DC motor.



(a) DC servo motor driver



(b) Steering engine



(c) Controller



(d) Globe motor

Figure 4.12 Experimental components of the vibro-driven system



Figure 4.13 Experimental rig of the vibro-driven system

Acrylic plates are used as materials for the upper and lower plates and the pendulum rod, which are shaped through laser cutting machine. During the assembly of the experimental rig, clearance fit is realised through fixed joints of nuts and bolts. The assembled experimental rig is shown in Figure 4.13. The main controller, motor driver and battery are not installed on-board to reduce the overall weight during locomotion.

### 4.7.3 Motor Controller PID Tuning

The DC servo motor controller RMDS-102 has the function of PID tuning. When tuning the PID parameters, the DC servo motor is connected with the motor controller, which is directly communicated with the upper computer through RS232 interface. Therefore, the parameters are tuned through the communications between the upper computer and the motor controller.

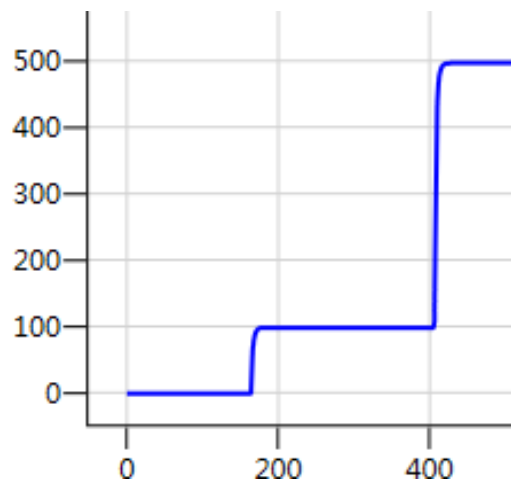
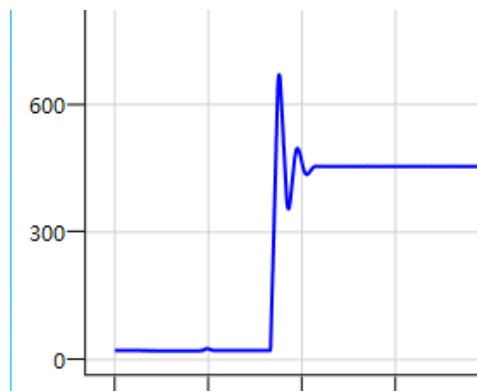


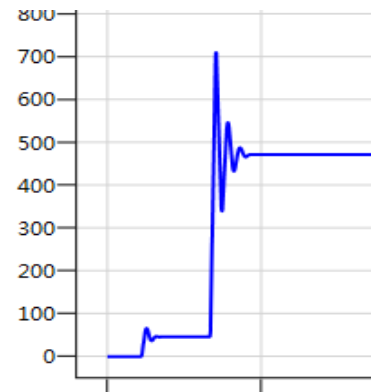
Figure 4.14 Motor no-load response curve

Motor control is a relatively simple task when the DC servo motor is in no-load condition, and the control parameters are accurate. The motor response curve in no-load condition is shown in Figure 4.14, it is evident that the motor has a fast response in this circumstance, the PD parameters are chosen as  $P=10$ ,  $D=200$ . When the motor output shaft is merged with an inverted pendulum, the load of the motor is in an eccentric state where the moment of inertia is changing. Besides, the inverted

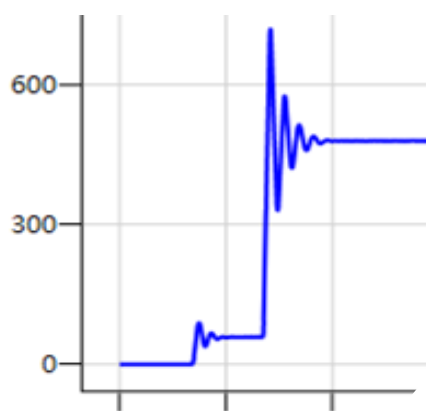
pendulum is operating in the vertical plane, thus the gravity has an influence on the control of the motor. Figure 4.15 demonstrates the motor position response curves under certain parameter conditions. It can be concluded from the curves that the elimination of influence of gravity on the motor control is a tough task. The reason behind is the existence of the eccentric state of the robotic system, and the effect of gravity on the motor has different directions when the pendulum is rotating in the left and right half of the vertical plane.



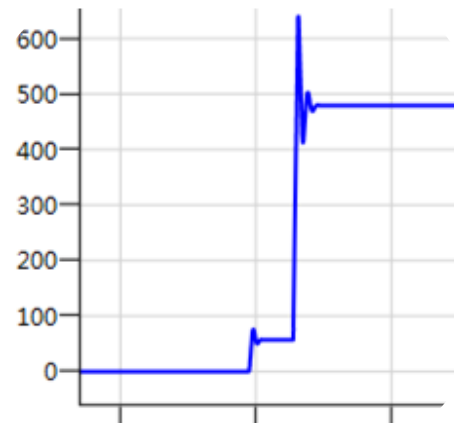
(a)  $P=10, D=200$



(b)  $P=15, D=200$



(c)  $P=20, D=200$



(b)  $P=20, D=400$

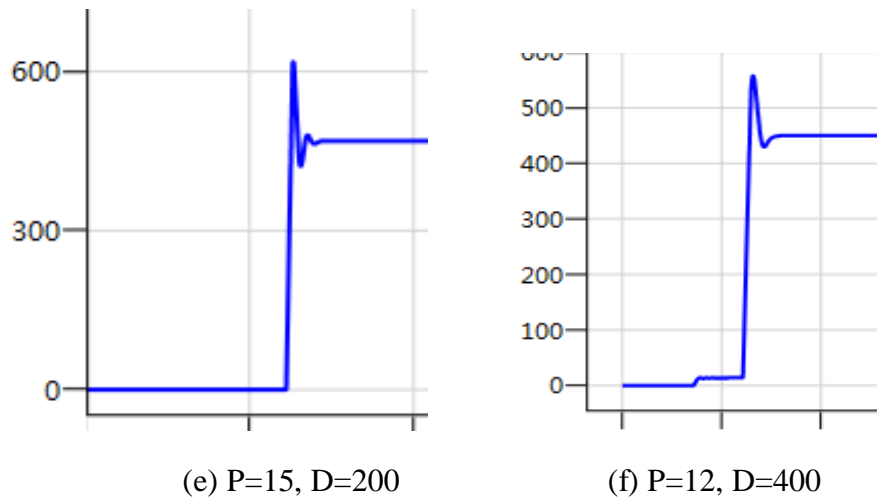


Figure 4.15 Motor position response curves under certain parameter conditions.

#### 4.7.4 Experiment Results

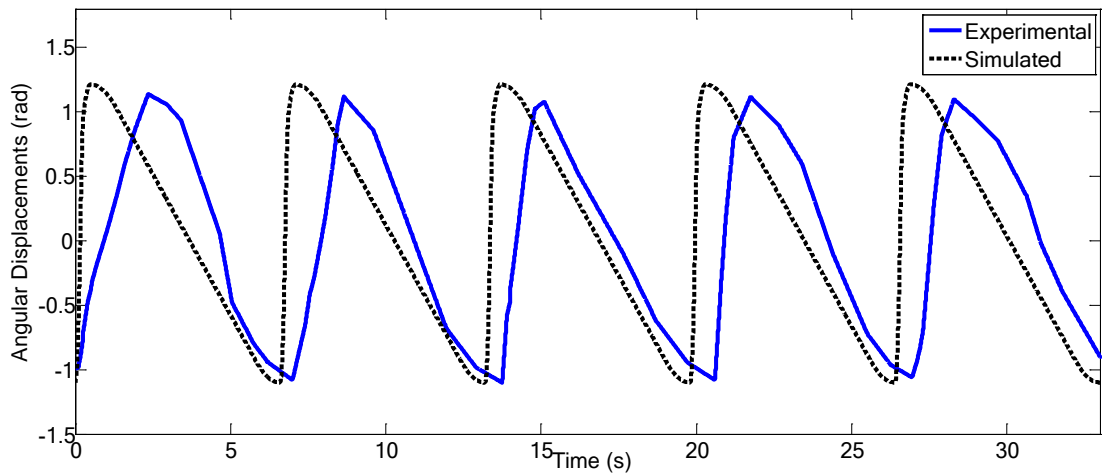
Preliminary experiments have been done to validate the proposed robotic model and locomotion principle. The motion controller powers and controls the movement of the pendulum. The motion controller is programmed through a PC and the program is transferred to the motion controller memory through RS232 cable at a baud rate of 57600. When the motion controller is powered the program is executed and the pendulum moves accordantly. Parameters of the vibro-driven system are listed as follows: mass of the cart is 0.523kg, mass of the pendulum is 0.119kg, length of the pendulum is 0.145m. The cart moves by the input signal from the driver. Input ports of the driver board are connected to the computer. Passive wheels with encoders are implemented to the cart to measure the distance that the cart travels. Quadrature encoders configured to count on both rising and falling A and B channel edges, therefore they are attached to the motor shaft and the cart wheels and position data is sampled with an angular resolution of  $0.18^\circ$  to output the positions. The encoders measure the displacements of the pendulum and the cart. The pendulum is fixed at a starting angle and travels in an anti-clockwise motion. The encoder positions of the pendulum and the cart wheels are stored in the memory of the motion controller.

When the motion controller is connecting with the PC, the position data are captured and imported into the Excel for analysis and scaling.

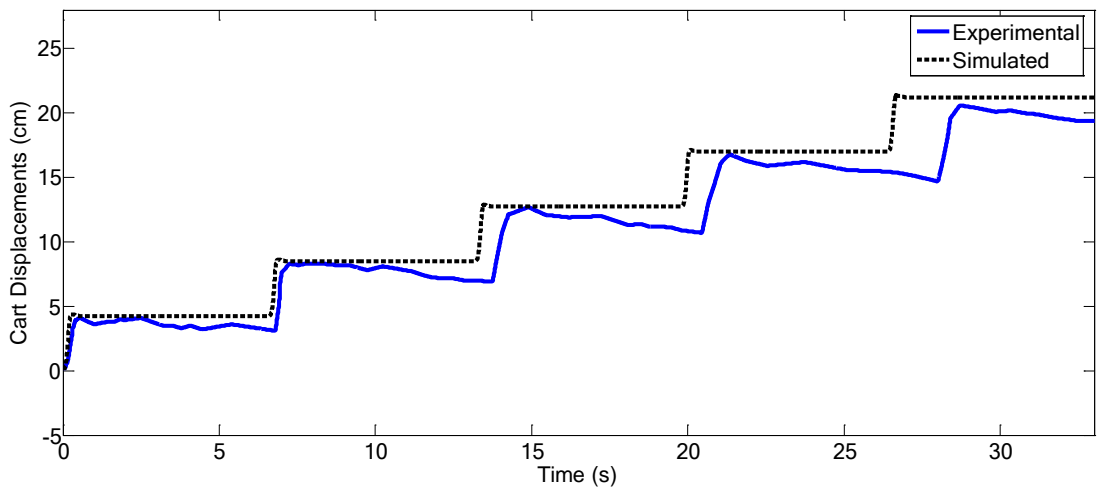
Figures 4.16(a) and 4.16(b) demonstrate the comparison of the experimental results with the simulation results. Figure 4.16(a) is drawn from the experimental data (blue solid line) and simulated data (black dashed line) for the movement of the pendulum. Figure 4.16(b) is portrayed from the experimental (blue solid line) and simulated data (black dashed line) for the locomotion of the cart on the dry surface of a wooden table. From the figures, we can clearly observe that the pendulum rotates in a certain angular range and the cart travels about 19.8cm during five motion cycles. It can be observed that although there are some differences between the simulated and the experimental results, the motion pattern of the robotic system follows the designed locomotion model. The experimental results of the pendulum and cart displacements are slightly delayed comparing to the simulation results. From Figure 4.16(b), we see that the cart experiences a delay of about 2s after five motion cycles in the experiments than the desired and simulation results. It is also observed from the figure that the backward motions (during restoring stage) of the cart for each cycle does not completely neutralized, meaning that after the progressive stage, the cart moves slightly toward the opposite direction. However, noted also that the experimental trajectories have similar pattern as the desired and simulation trajectories.

Possible reasons that lead to these discrepancies are summarized as follows: (1) we adopt a simplified friction model (the Coulomb friction model) in the simulation, in which the viscous friction and Stribeck effect are omitted. The Coulomb model is a static model, whilst in the experiment and text, the friction could be more complicated and dynamic which relies not only on the velocity of the cart. (2) we only consider the cart's dynamics, however, the dynamics of the actuator and the sensors are not considered in the system model and simulation. This makes the developed responses of the pendulum and the cart in the experiments slower than that in the simulation and thereafter a delay in the trajectory following is observed.

However, the preliminary experimental results have demonstrated the effectiveness of the proposed model and locomotion principle.



(a) Angular displacements of the pendulum



(b) Displacements of the cart

Figure 4.16 Comparison of experiment (blue solid line) and simulation (black dashed line) results of the vibro-driven cart system

In order to minimize the discrepancy between the experimental and simulation studies, a more practical robotic model is under development that incorporates the actuator dynamics, sensor dynamics and a dynamic and robust friction model. It is also clearly necessary to identify the practical values and test the capability of adaptability and robustness of the proposed control algorithms in physical system. The effectiveness of the proposed algorithms is demonstrated using analytical studies, numerical simulations and preliminary experimental works. It is also of great significance to apply the design ideas and main findings to more real environment applications, such as embedded the bio-inspired model into a capsule shell and conduct field tests on various surfaces in different environment. Several aspects of future works are summarized as follows:

(1) Identification of the bio-inspired viscoelastic parameters and comparison with the theoretical studies in this research, including the coefficients of the elasticity and viscosity;

(2) The real-time position feedback control and evaluation of the computational complexity. This will take into consideration of both the collocated subsystem (pendulum angle) and the non-collocated subsystem (cart displacement). To realise real-time implementation, an online optimal trajectory generator will be developed based on improvement of the proposed off-line trajectory control model. An evaluation of computational complexity of the proposed algorithm will be conducted through real-time implementation.

(3) Trajectory tracking of the robots on the surfaces with different friction coefficients, identification of the friction parameters, particularly in the tubular environments such as the gas and water pipes to test the performance of the adaptive control systems.

## 4.8 Conclusion

In this chapter, we studied the issues of trajectory planning, optimization and tracking control of a novel 2-DOF bio-inspired VDC system with viscoelastic property. The bio-inspired self-propulsion has been elaborately described with a proposed robotic model. As one of the distinguished features of the proposed model, the key role of viscoelasticity has been revealed. Towards this end, in the first place in section 4.2, the mathematical model was established to describe the natures of non-collocated actuation and sliding friction of the proposed model.

The problem of trajectory generation and synthesis was investigated in section 4.3. A two stages motion trajectory was planned for the driving pendulum with seven phases. On the other hand, the employment of viscoelastic property in the system dynamics drives us to consider the characteristic of viscoelasticity into the generation of desired periodic motion trajectory. Towards this end, a synchronization and smoothness procedure was introduced.

In Section 4.4, the geometric analysis-based trajectory planning algorithm was proposed and investigated in detail. The main idea is to reduce complexity and to characterize coupling by imposing a harmonic drive and then to compute the dynamics projection onto a hyper-manifold, such that the issue of trajectory planning is converted into geometric analysis and trajectory optimization. The non-collocated dynamic constraints were firstly considered into the control indexes, wherein it is found that characterization of viscoelastic interaction plays vital role in the optimal control of stick-slip propulsion and the energy efficacy. The qualitative variation laws of the control parameters were studied and identified through geometric and dynamic analysis. The dynamic coupling was characterized through rigorous analysis on the Poincaré maps. The two-stage analytical motion trajectory was constructed based on the control indexes and dynamic constraints, which were evaluated analytically, and the trajectory was optimized and parameterized via rigorous analysis.

In section 4.5, two trajectory tracking control schemes have been constructed. A closed-loop feedback controller was designed for the system with accurate model. An adaptive controller was proposed for the system with unknown base parameters, wherein an auxiliary control variable is designed to closure the non-collocated feedback loop. Asymptotic stability and convergence of time-varying reference trajectories for the system dynamics are shown by means of Lyapunov synthesis. The trajectory of the actuated sub-coordinate can be directly controlled through only one actuated DOF of the robot. The un-actuated (passive) part of the generalized coordinate, in turn, demonstrates the dynamic interaction between the trajectory of the actuated sub-coordinate and the dynamic behaviour of the proposed VDC system.

Extensive simulation results were presented in Section 4.6 to verifying the effectiveness and evaluating the performances of proposed trajectory planning and tracking control approaches. The simulation was implemented in two cases. Firstly, in the absence of parametric uncertainty, comparative studies are performed with EPC system, in which a two-stage velocity trajectory is proposed using conventional approach with heuristically chosen control parameters. The results conclude that the friction-induced stick-slip motions are precisely controlled through the proposed trajectory planning scheme, in a manner that the superior performance is guaranteed. Subsequently, the adaptive tracking control scheme is evaluated in the presence of parametric uncertainty. The results illustrate the effectiveness of the designed control scheme. The asymptotic convergence of the tracking error is achieved. On the other hand, under the parametric uncertainty, the adaptive control scheme shows better tracking performances than the conventional method.

The 3D design, experimental setup and experimental results were presented in Section 4.7 to demonstrate and validate the locomotion of the proposed VDC model. From the experimental results, the proposed robotic model has been shown, and the proposed robotic model and locomotion principles of the system have been validated. Comparison of the experiment and the simulation results has been given and precisely discussed. The system is propelled over a surface rectilinearly via the

interaction between the driving pendulum and the horizontal sliding friction, resulting into alternative sticking and slipping locomotion.

## **Chapter 5**

# **Analysis and Characterization of Dynamic Frictional Interactions**

### **5.1 Introduction**

Mobile Micro-Mechanical Systems (MMMS) that move overcoming the environmental resistance as a result of internal autogenetic forces have been the topics of active scientific research in robotics and control communities in recent years (Bolotnik and Figurina, 2008; Chernous'ko, 2005; Chernous'ko, 2011; Li et al., 2006; Zhan and Xu, 2015; C. Zhang et al., 2014b). These systems, with hermetic structure and smooth surface, have extensive potential applications in medical endoscopy, engineering diagnosis, disaster rescues and seabed exploration, etc. Irrespective of the complex gear case and external protruding components, they are simple in mechanical structure and prone to control. As a result, they provide a promising insight into the proper designs of the dynamical model of MMMS and bionic-robotic systems. The primary principle is that rectilinear locomotion can be achieved through an internally vibration-driven mass interacting with main body, overcoming the resistance forces acting at the contacting surface. This feature enables the feasibility and applicability of so-called capsule systems that work in

restricted space and vulnerable media such as pipeline inspection in a narrow tube, minimally invasive inspection and drug delivery inside a human body (Fang and Xu, 2011; Li et al., 2006; Liu et al., 2013a). For high fidelity engineering systems, accurate modelling or prediction of nonlinear friction force is a nontrivial while intractable aspect of scientific research. Conventionally, frictional instabilities are required to be eliminated or compensated through efficiently designed controllers. For instance, robust friction models are essentially required in practical engineering problems. Conversely, for self-propelled capsule systems, friction plays pivotal roles in capsule propulsion and locomotion, particularly for the vibro-driven underactuated system considered in this chapter, the dynamic coupling between the driving mechanism and the capsule are utilized to generate efficient stick-slip motions. Hence, accurate predictions of the dynamic interactions in the sticking, presliding as well as pure sliding regimes become crucial.

Various friction models with an arbitrary degree-of-complexity (i.e. numbers of parameters to be identified and controlled) have been proposed in the literature which incorporates different physical phenomena corresponding to friction. Threefold of requirements (Al-Bender and Swevers, 2008) for the models are conventionally perused: simple to facilitate online utilization, sophisticate to describe all frictional characteristics, and limited number of parameters to be identified. The Coulomb friction is the simplest model describing as a function of the difference in velocities between contacting bodies (Armstrong-Hélouvry et al., 1994), and it has been extensively adopted to study the motion of capsule systems (Chernous'ko, 2002; Fang and Xu, 2011; Huda and Yu, 2015; Li et al., 2006; Liu et al., 2013b). Some significant studies on stick-slip motions of a single-module vibration-driven locomotion system have been devoted in (Fang and Xu, 2013; H. B. Fang, 2010). Recently, an analytical frictional resistance model of a capsule endoscope inside an intestine was investigated in (Kim et al., 2007), which considers the contact geometry and viscoelasticity of the lubricants on intestine surface and revealing the stress relaxation characteristics of intestine resulted in lower frictional force as the speed of capsule decreased. In (Zhang et al., 2012), viscoelastic deformation of intestinal wall, viscous friction and Coulomb frictions were

considered for a capsule robot inside an intestine, and the model prediction results was verified experimentally fitting into the situation in which the capsule velocity is below a sufficiently small value ( $20\text{mm s}^{-1}$ ). It is plausible that the capsule moves as a stick-slip pattern with small magnitude of average velocity, and the environmental features such as viscoelasticity and villus-like structure inside the intestine affect the friction characteristics. However, an accurate representation of the dynamic frictional interaction for given practical applications of capsule systems is required to capture several experimentally observed dynamic phenomena reported in literature. The static friction models solely consider the relative velocity between the surfaces in frictional contact, and the drooping friction characteristics in low relative velocity regime and the hysteretic loops are not captured. These motivate the study here to model and analyse the dynamic interactions through the dominant components containing the static friction, presliding, breakaway force, stick-slip motion, the Stibek effect, friction memory and the hysteretic effect.

The drooping characteristic occurs when friction force falls into dynamic situations and is conventionally considered as a function of relative velocity of contacting bodies. The friction force becomes a single-valued function under this circumstance where reversible drooping is initiated to drive the friction force following the same path during the acceleration stage (AS) and the deceleration stage (DS). Nevertheless, conventional considerations do not have comprehensive agreements with the latter experimental observations in the unsteady environmental conditions (e.g. oscillations in relative velocity). Observed also in some engineering investigations that the friction curve may be a multi-valued velocity function and the friction force follows diverse ways for AS and DS to form a non-reversible curve (Becker and Mahin, 2013; Biswas and Chatterjee, 2014; Neis et al., 2011; Outirba and Hendrick, 2014; Stefański et al., 2006; Wojewoda et al., 2008). The reason behind is the temporal lag between respective changes in relative velocity and the friction force. Both clockwise (i.e. the friction force for AS is greater than that for DS) and anticlockwise drooping loops have been observed in pure sliding regime in engineering applications. Besides, ascribing to the spring-like-behaviour-induced contacting compliance between the asperities, hysteretic loops have been detected

experimentally during the regime of presliding (Casini et al., 2012; Giannini et al., 2011). This gives rise to the phenomena of velocity overshooting between the bodies in contact during the initiation of stick-slip motion.

Towards the friction-induced vibrations, single DOF mass-spring-damper systems resting on a moving belt are well-adopted in literature to explore the experimentally observed friction characteristics (Hetzler et al., 2007; Saha et al., 2015). And also a majority of researches place their considerations on 2 DOF tangential-wise (typically linearly along the direction of motion) (Fang and Xu, 2011; Huda and Yu, 2015; Liu et al., 2013b; Y. Liu et al., 2015; Zhan and Xu, 2015) or norm-wise (Chowdhury and Helali, 2008; Pavlovskaia et al., 2015) vibrations with respect to the substrates. These ideas for self-propelled micro-mechanisms/robots have been well-employed. However, the combined (nonlinear) tangential-wise and norm-wise vibrations could perform as a pivotal propulsion mechanism for bidirectional locomotion which has not been reported in literature. It sheds light on a generic significance for the studies on capsule systems. Note also that towards the nonlinear friction, there are several seminal studies in the literature (Fang and Xu, 2011, 2012, Liu et al., 2013a, 2013b; Y. Liu et al., 2015). These works are mainly focusing on the qualitative changes induced by control parameters with static (Fang and Xu, 2011, 2012) or quasi-dynamic friction (Liu et al., 2013a, 2013b; Y. Liu et al., 2015) models. However, dynamic friction model and therefore friction-induced responses in sticking, presliding and pure sliding regimes have not been reported. And the previous analyses are mainly restricted into numerical rather than analytical investigations. And also in most studies on capsule dynamics such as (Liu et al., 2013c, 2013b, 2015), for ease of numerical studies, the qualitative behaviour for the initial transient were omitted (the first 100 cycles in (Liu et al., 2013b) and 200 cycles in (Liu et al., 2013b) and (Liu et al., 2015)). However, the transient response is a vital performance index to evaluate how quickly and accurately a dynamic system responds to changes.

This chapter considers combined tangential-wise and norm-wise vibro-driven capsule systems for underactuated locomotion. The nonlinear interaction between

actuator and driving pendulum is characterized by a viscoelastic pair of torsional spring and viscous damper. Viscoelastic property is a promising feature for future bio-inspired robots, which enables efficient locomotion through natural oscillations. Many animals are able to reduce the metabolic cost of running considerably by utilizing the viscoelastic properties of muscles, tendons, and bones distributed in their bodies (Alexander et al., 1985) and limbs (Dimery et al., 1986; McMahon, 1985). The study on relations between viscoelastic parameters and the system performance is beyond the scope of the thesis and will be reported in due course. Motivated by the experimental findings in the literature, the thesis studies the frictional forces described by the LuGre model (De Wit et al., 1995) (LM) and the Exponential model (Armstrong-Hélouvry et al., 1994) (EM). In the literature, there is a lack of understandings of dynamic frictional interactions between the capsule system and the substrate, towards this end, the non-reversible characteristics of friction force (drooping and hysteresis) are studied. The dynamic interactions are firstly modelled using a combined physics-based and analytical-based approach. Thereafter, the frictional limits for the static friction, presliding regime as well as pure sliding regime are identified. Dynamic analysis of the friction-driven vibrational responses is then conducted and the qualitative variations laws induced by the control parameter are identified. The analytical and numerical results have good agreements with the seminal findings in the literature. The proposed work is an advisable benchmark to exploit the challenges in friction compensation and control of underactuated micro-robotic systems.

The rest of the chapter is organized as follows. Section 5.2 provides the mathematical modelling of capsule system and frictional interactions. Analysis of dynamic interactions is presented in Section 5.3. Finally, conclusions are outlined in Section 5.4.

## 5.2 Mathematical Modelling

### 5.2.1 System Description

Consider a 2-DOF capsule model as shown in Figure 5.1. The system contains a pendulum (with length  $l$  and mass  $m$ ) and a platform (with mass  $M$ ) merged with a rigid massless capsule shell. A vibration actuator is mounted on the platform at the pivot and connected with the pendulum. The movable pendulum is connected with the capsule body and driven by a prescribed harmonically excited force generated by the actuator. The actuator model is simplified here and the interconnection between pendulum and capsule is represented by a linear viscoelastic pair of torsional spring with stiffness coefficient  $k$  and viscous damper with damping coefficient  $c$ .  $\theta$  and  $x$  respectively denote the absolute displacements of the driving pendulum and the capsule. It is assumed that the mass of pendulum is centralized at the ball and the centre of mass of the platform coincides with the pivot axis. And assume also that the sliding friction force  $F_2$  between the capsule and substrate is applied along the X-axis.

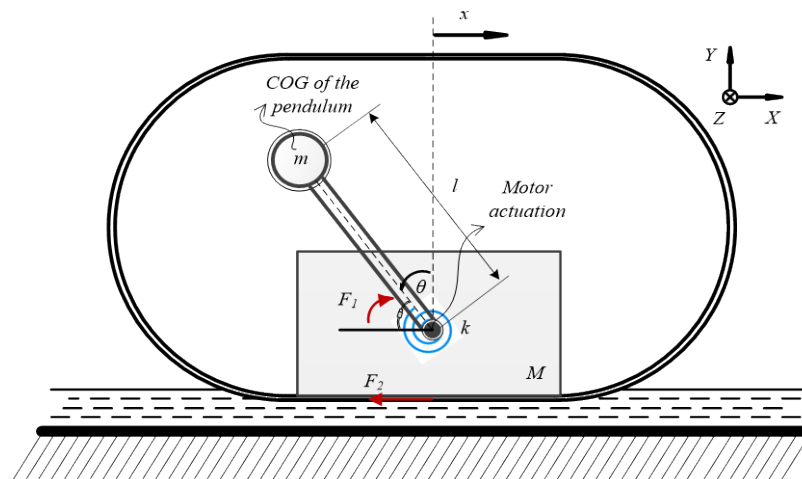


Figure 5.1 Schematic of the vibro-driven underactuated encapsulated system

The propulsion mechanism is on the strength of interaction between the centripetal torques excited by the platform-mounted vibration actuator and the

friction torques at the substrate. The capsule is propelled over a surface rectilinearly through this interaction. Meanwhile, the elastic potential energy is stored and released alternatively in compatible with the contraction and relaxation of the torsional spring. The pendulum is rotated back and forth and drives the capsule move via dynamic couplings. The capsule motion begins with static state, and it moves when the resultant force applied in the horizontal direction exceed the threshold of static friction force at the contacting surface. It is termed as the sticking phase when the above condition is not satisfied. At the instant when the condition is met, the sticking phase is annihilated and the capsule moves progressively, which falls into the fast motion called the pure sliding phase. The capsule model is developed to exploit advisable friction control approaches to manipulate the stick-slip effect and generate optimal steady-state progressive motions, in which the capsule and the driving pendulum synchronize their motion harmoniously.

### 5.2.2 Dynamic Model

Based on the derivation procedure presented in Section 4.2 of Chapter 4, the equations of motion of the encapsulated system are derived using Euler-Lagrangian method as

$$ml^2\theta'' - ml\cos\theta x'' - mgl\sin\theta + k\theta + c\theta' = A\cos(\Omega t) \quad (5.1)$$

$$-ml\cos\theta\theta'' + (M + m)x'' + ml\sin\theta\theta'^2 + N_0F = 0 \quad (5.2)$$

where  $A$  and  $\Omega$  are the amplitude and frequency of the harmonic force,  $N_0F$  is the friction force at the substrate,  $N_0$  is the normal load and  $F$  is the friction function representing the friction force per unit of normal load.

Introducing characteristic time scale  $\omega_n = \sqrt{g/l}$  and characteristic length  $x_0 = g/\omega_n^2$  to facilitate convenient analysis, we have the following non-dimensional motions of equation as

$$\theta'' - \cos\theta X'' - \sin\theta + \rho\theta + \nu\theta' = h\cos(\omega\tau) \quad (5.3)$$

$$-\cos\theta\theta'' + (\lambda + 1) X'' + \sin\theta\theta'^2 + Nf = 0 \quad (5.4)$$

The prime ( ' ) in (5.3) and (5.4) denotes the derivative in the normalized time coordinate  $\tau = \omega_n t$ . The rest of the non-dimensional quantities are defined as  $X = x/x_0$ ,  $\lambda = M/m$ ,  $\rho = k/(ml^2\omega_n^2)$ ,  $v = c/(ml^2\omega_n)$ ,  $h = A/(ml^2\omega_n^2)$ ,  $\omega = \Omega/\omega_n$  and  $N = N_0/(ml\omega_n^2)$ .

**Remark 5.1.** In the normalized coordinate, the physical meanings of the control parameters are captured as:  $\lambda$  represents the mass ratio,  $\rho$  and  $v$  respectively denote the dimensionless spring and damping coefficients,  $h$  and  $\omega$  are dimensionless excitation amplitude and frequency.

### 5.2.3 Modelling and Characterization of the Frictional Interaction Dynamics

#### *A. The Physics-Based Analysis*

Friction arises at the physical interface between contact surfaces of different bodies in relative motions. It is plausible that the substrate is composed of a great number of tiny contacts on the surface irregularities, and the spring-like limit for a microscopic part of contacting area is far larger than that for bulk object. This consideration enables the feasibility that the contacting surfaces could have relative motion within a sufficiently small distance without destroying the transitory connections. And also the stretched irregularities gradually exert the elastic force to predominate the resisting friction force. It is noted that the above truisms have different patterns of manifestation governed by the relative velocity between contacting bodies. The reason behind is the bonds may remain undisrupted for a period of time. The time is equivalent to the maximum extension of the micro-connections divided by the average velocity (McMillan, 1997). For the relative velocity near zero, the hysteretic effect would appear, resulting from the tiny movement between the two bodies in the phase of sticking, which is also named as micro-slip. The increasing number of bonds being disrupted in a time period would be associated with an increasing friction force at a sufficiently fast average velocity. Hence, characteristics of the nonlinearity near zero relative velocities would be the

most significant to introduce the hysteretic effect, which is originated from the random distribution and size of asperities between the contacting bodies.

Figure 5.2 demonstrates that the capsule model rests on the horizontal plane and is driven by a pendulum relative to the substrate with a velocity of  $X'(\tau)$ . For sufficiently small driving force in the horizontal direction, it is apparent that the interface between the capsule and the surface falls into sticking regime. The stiction force results from the tension in conjoint irregularities. The brush-like surface illustration represents the evolution of junction deflections between different asperities, as well as the tension on these connections. Nevertheless, as the driving force increases, the capsule is capable of moving, with the displacement larger than the maximum extension of the connections. From Figure 5.2(a), the capsule is initially standing still and the connections are un-tensioned with no friction torque resisting the motion. In Figure 5.2(b), after a short period of time under anticlockwise motion of the pendulum, relative velocity of the capsule is appeared to be slightly positive, and the bonds remain intactness. The threshold will be met during the sticking phase via opposing torque of the friction force.

At this critical boundary as depicted in Figure 5.2(c), the capsule starts to slip with a kinematic friction force thereafter, which is characterized by a dramatic decrease. The clockwise motion of pendulum results into a deceleration of the capsule to a slightly positive velocity whilst it would keep slipping since the bonds need some time to reform (see Figure 5.2(d)). When the capsule decelerates through  $X'(\tau) = 0$ , see Figures 5.2(e) and (f), the connections are reformed and the sticking phase is arrived again. Backward motions of the capsule follow the argument through Figures 5.2(g) to (j). Following the above discussions, Figure 5.3 shows the curve of friction force as a function of average capsule velocity.

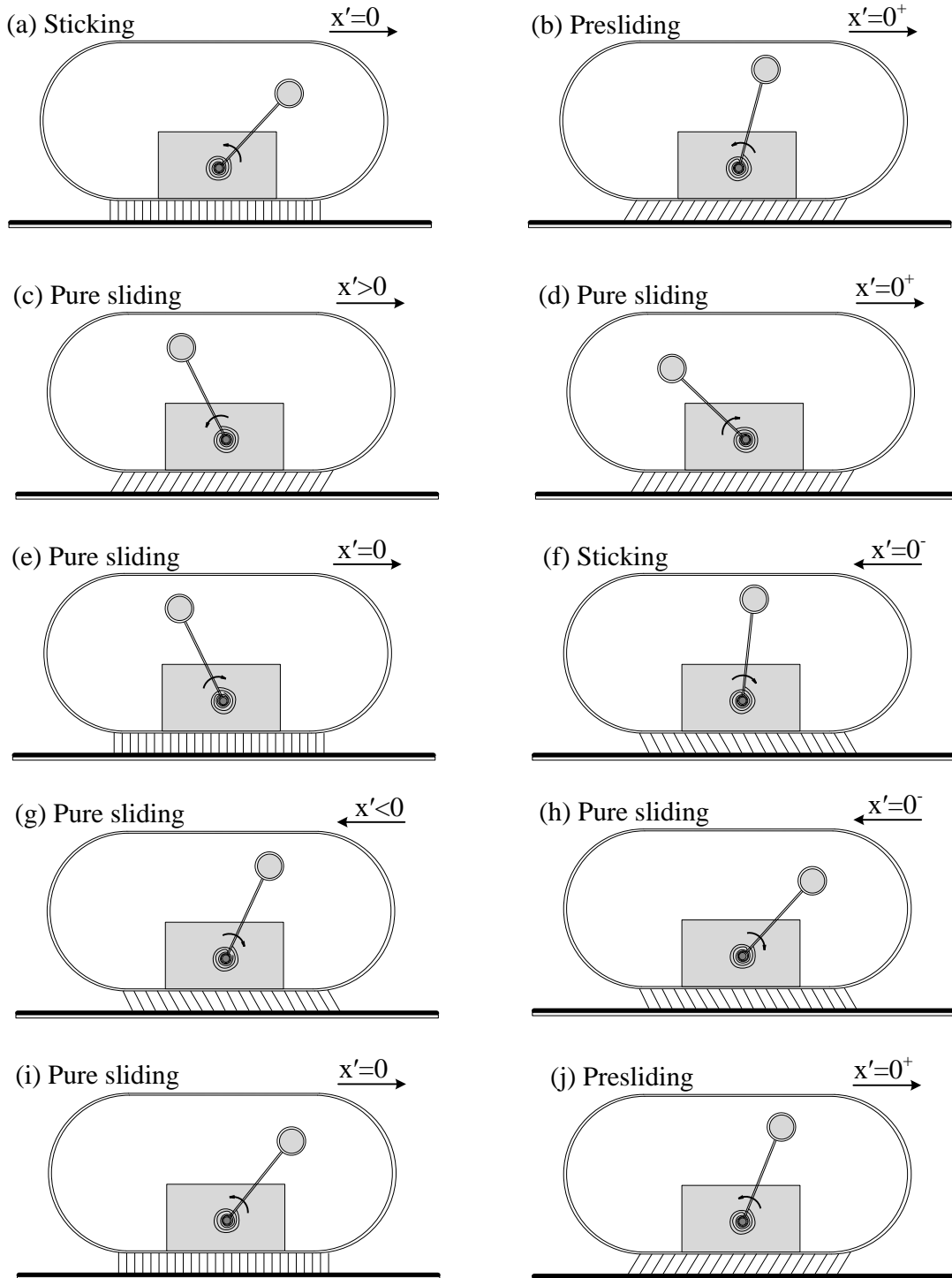


Figure 5.2 Schematic of the capsule motion with interface deformation

The arguments above is based on the consideration that the friction force solely depends on the relative velocity of the contacting surfaces (Armstrong-Hélouvy et al., 1994), i.e.  $f(\tau) = f(X'(\tau))$ , which results in the reversible characteristic of the friction force (black solid line) (McMillan, 1997) shown in Figure 5.3. This means the capsule slips back onto a lately travelled path where new asperities might have been reformed. This is originated from the unique value for a given relative velocity during the AS and DS. However, for dynamic frictional circumstance, it is necessary to consider the state variable(s) along with the average velocity  $X'(\tau)$ . The state variable may have different values for one relative velocity during AS and DS since they evolve with time by the description of differential equations. The arrows in green clearly depict the different acceleration and deceleration paths that the capsule follows, and accordingly a clockwise hysteric loop in the pure sliding regime is characterised.

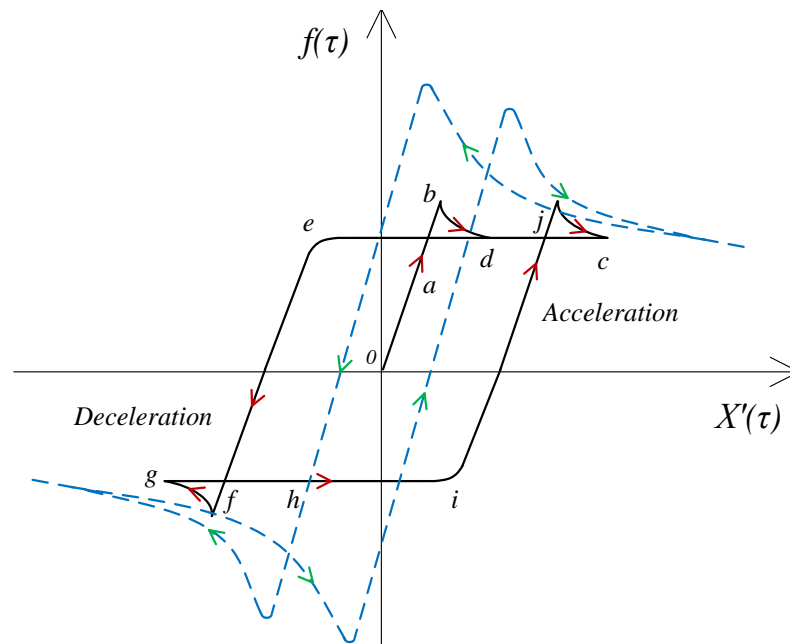


Figure 5.3 Schematic of the reversible (black solid line) (McMillan, 1997) and non-reversible (blue dashed line) characteristics of the friction forces

**Remark 5.2.** The phenomenon described above introduces non-reversible characteristic of the friction force which is demonstrated by different friction values during AS and DS (blue dashed line in Figure 5.3). Therefore, the friction-velocity curve following different paths for AS and DS gives rise to the hysteretic loops, such as the non-reversible friction characteristic for forced vibrations as shown in Figure 5.3. Up to now, most investigations in frictional interactions towards capsule systems were confined into static or quasi-dynamic circumstance, where it is difficult to facilitate online utilization and control. This study aims to fill in the research gaps of modelling and analysing the dynamic interactions between the mobile capsule systems and the substrate.

### *B. The Friction Models*

In this study, two friction models (LM and EM) are employed as first approximations for describing the tribological interactions between the capsule and the locomotion substrate in the tangential direction. LM (De Wit et al., 1995) models the spring-like bristles with damping using surface asperities existing between the contacting bodies. Thus, both of micro-slip in the presliding regime (tiny displacement) and the Stribeck effect in the pure sliding regime (large displacement) are included in the dynamic model. The bristles deform and reform alternatively affected by the external force, and certainly the friction force is the result related to the resultant bristles' deflection and a linear viscous term associated with the relative velocity. The average bristle deflection  $\hat{\xi}$  is employed as an additional and internal variable. Hence, the friction force  $f$  features two state variables, and  $f = f_{LM}(\hat{\xi}, X')$  is described as

$$f_{LM}(\hat{\xi}, X') = \delta_0 \hat{\xi} + \delta_1 \frac{d\hat{\xi}}{dt} + \delta_2 X' \quad (5.5)$$

where  $\hat{\xi}$  is the average bristle deflection,  $\delta_0$  and  $\delta_1$  are the stiffness and damping coefficients of the bristle, and  $\delta_2$  describes the viscous constituent of the resistant force. The evolution of the average bristle deflection is governed by

$$\frac{d\hat{\xi}}{d\tau} = X' \left( 1 - \frac{\delta_0 \hat{\xi}}{g(X')} \operatorname{sgn}(X') \right) \quad (5.6)$$

where  $g(X') = N(\eta_c + \Delta\eta e^{-(X'/v_s)^\alpha})$  dominates the Stribeck effect,  $\Delta\eta = \eta_s - \eta_c$ ,  $\eta_s$  and  $\eta_c$  respectively denote the level of static friction and the minimum level of Coulomb friction,  $v_s$  represents the critical Sticbeck velocity and  $\alpha$  is the slope parameter to be tuned ( $g(X')$  is referred to as the Gaussian friction model when  $\alpha = 2$ ).

The second friction model (Hinrichs et al., 1998) is employed to define the friction force  $f = f_{EM}(X')$  induced by EM

$$f_{EM}(X') = N(\eta_c + \Delta\eta e^{-(a|X'|)}) \operatorname{sgn}(X') \quad (5.7)$$

The equations of motion are allocated in state-space. Define state vectors in extended phase spaces including the evolutionary vector  $\hat{\xi}$  as: for the capsule system with LM  $S_1 := (y_1, y_2, y_3, y_4, y_5) \in \mathfrak{R}^{5 \times 1} := (\theta, \theta', X, X', \hat{\xi}) \in \mathfrak{R}^{5 \times 1}$ ; for the capsule system with EM  $S_2 := (y_1, y_2, y_3, y_4) \in \mathfrak{R}^{4 \times 1} := (\theta, \theta', X, X') \in \mathfrak{R}^{4 \times 1}$ . Decoupling and reorganizing (5.3) and (5.4), and incorporating with (5.5) and (5.7), the state-space representation in compatible with the defined state vector is derived as

$$\begin{bmatrix} y_1' \\ y_2' \\ y_3' \\ y_4' \\ y_5' \end{bmatrix} = \begin{bmatrix} 0 & 1 & 0 & 0 & 0 \\ A_{21}/B & A_{22}/B & 0 & 0 & 0 \\ 0 & 0 & 0 & 1 & 0 \\ A_{41}/B & A_{42}/B & 0 & 0 & 0 \\ 0 & 0 & 0 & A_{54} & A_{55} \end{bmatrix} \begin{bmatrix} y_1 \\ y_2 \\ y_3 \\ y_4 \\ y_5 \end{bmatrix} + \begin{bmatrix} 0 \\ \Delta_1/B \\ 0 \\ \Delta_2/B \\ 0 \end{bmatrix} \quad (5.8)$$

where  $A_{21} = -\rho(\lambda + 1)$ ,  $A_{22} = -v(\lambda + 1) - \sin y_1 \cos y_1 y_2$ ,  $A_{41} = -\rho \cos y_1$ ,  $A_{42} = -v \cos y_1 - \sin y_1 y_2$ ,  $B = \lambda + 1 - \cos^2 y_1$ .  $\Delta_1 = (\lambda + 1)h \cos(\omega\tau) + (\lambda + 1)\sin y_1 - Nf \cos y_1$ ,  $\Delta_2 = \cos y_1 h \cos(\omega\tau) + \cos y_1 \sin y_1 - Nf$ . For the capsule with LM,  $A_{54} = 1$ ,  $A_{55} = -\sigma_0 y_4 \operatorname{sgn}(y_4)/g(y_4)$ ,  $f = f_{LM}(y_4, y_5) = \delta_0 y_5 + \delta_1 y_5' + \delta_2 y_4$  and  $g(y_4) = N(\eta_c + \Delta\eta e^{-(y_4/v_s)^2})$ ; For the capsule with EM,  $A_{54} = 0$ ,  $A_{55} = 0$  and  $f = f_{EM}(y_4) = (\eta_c + \Delta\eta e^{-(a|y_4|)}) \operatorname{sgn}(y_4)$ .

**Remark 5.3.** The additional state  $\hat{\xi}$  in  $S_1$  is the distinctive factor that governs the evolution of the dynamic friction forces, however, there limited studies in the

literature on how  $\hat{\xi}$  manipulates the dynamic frictional characteristics (e.g., drooping) of capsule systems during presliding and pure sliding. In this regard, the role of  $\hat{\xi}$  will be studied elaborately in the thesis.

*C. Dynamic Frictional Limit Analysis*

The microscopic elastic limits for the sticking, the presliding and the pure sliding phases are depicted in Figure 5.4. The friction at the sticking phase acts like springs which have been observed experimentally in the literatures. During the sticking, there exists a presliding displacement as shown in Figure 5.4(b) which can be approximated by linear function of the static friction. The breakaway occurs when a critical force is reached as shown in Figure 5.4(c) and simultaneously, the micro-connections are disrupted. Conventional studies on the friction-induced capsule dynamics are mainly restricted into either numerical analysis (Liu et al., 2013a, 2013b) or analytical analysis (Fang and Xu, 2011, 2012) of the static or quasi-dynamic frictions, which are practically unattainable. In the thesis, we study the frictional limit analytically to reveal the non-reversible characteristic for the static friction, the presliding regime as well as the pure sliding regime, and the frictional limit boundaries are identified.

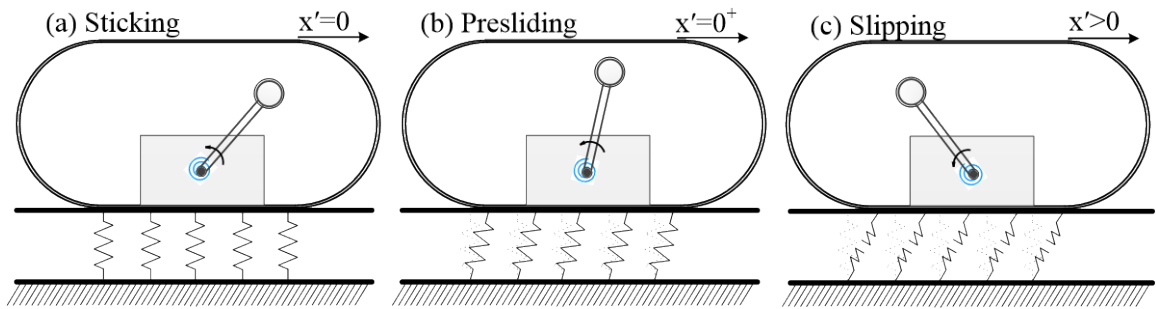


Figure 5.4 Schematic of the microscopic elastic limit for sticking, presliding and pure sliding phases

From the friction models studied, it is apparent that to create slipping between the two contacting bodies, the friction force is initially strapping both parties together such that only microscopic deformations of the interface are initiated. As stated, the micro-connections would be disrupted until a limit of the friction is satisfied.  $g(X')$  describes that, for quasi-static phase wherein no macroscopic sliding exists, the bristle deflection evolved with state variable  $\hat{\xi}$  enlarges proportionally with the friction force. The critical condition for the bristles to break free is satisfied when  $\hat{\xi} = g(X'(\tau))$ . Consequently, the maximum static friction force is obtained at the conditions of  $X''(\tau) = 0$  and  $\hat{\xi}' = 0$ , and accordingly we have

$$g(X') = \frac{N}{\delta_0} (\eta_c + (\eta_s - \eta_c) e^{-(X'/v_s)^\alpha}) \quad (5.9)$$

where  $\eta_s$  denotes the maximum static friction in the presence of quasi-static motion.

When the steady-state sliding is initiated, meaning that a relative sliding motion occur between the two contacting bodies, the deflecting rate of the bristles is held at zero ( $\hat{\xi}' = 0$ ). The friction force and its derivative are yielded as

$$f = \delta_0 g(X') + \delta_2 X' = N(\eta_c + (\eta_s - \eta_c) e^{-(X'/v_s)^\alpha}) + \delta_2 X' \quad (5.10)$$

$$\frac{\partial f}{\partial X'} = -\alpha N \frac{X'^{\alpha-1}}{v_s^\alpha} (\eta_s - \eta_c) e^{-(X'/v_s)^\alpha} + \delta_2 \quad (5.11)$$

Comparing to the Stribeck velocity  $v_s$ , the first term on the right side of the above equation is negligible under the assumption that the capsule has sufficiently small or large average velocity. Consequently, it is reasonable to make supposition that for the sliding phase, two offset values of the average velocity labelled as  $X'_l$  (lower velocity) and  $X'_h$  (higher velocity) are created. For the value range  $X'(\tau) \in (0, X'_l)$  as well as  $X'(\tau) \in (X'_h, X'_{max})$  ( $X'_{max}$  represents the maximum velocity the capsule can achieve), the friction force as a function of average velocity is a monotonically increasing curve. On the other hand, for the velocity belongs to  $X'(\tau) \in (X'_l, X'_h)$ , a monotonically decreasing curve is obtained. At the offset points  $X'(\tau) = X'_l$  and  $X'(\tau) = X'_h$ , the slope of the curve becomes zero. This finding will be verified in the numerical analysis in Section 5.3. To obtain the values of  $X'_l$  and  $X'_h$  analytically, (5.11) is solved by letting  $\partial f / \partial X' = 0$ , and then we have

$$-\alpha N \frac{X'^{\alpha-1}}{v_s^\alpha} (\eta_s - \eta_c) e^{-(X'/v_s)^\alpha} + \delta_2 = 0 \quad (5.12)$$

It is noted that the lower velocity point  $X'(\tau) = X'_l$  is supposed to have a sufficiently small magnitude, since the velocity is extremely low, by setting  $(X'/v_s)^\alpha = 0$ , we have

$$X'_l = v_s \left[ \frac{\delta_2 v_s}{\alpha N (\eta_s - \eta_c)} \right]^{1/(\alpha-1)} \quad (5.13)$$

For the higher velocity point  $X'(\tau) = X'_h$ , it is considered that the value of  $X'_h$  stays adjacent to the value of the Stribeck velocity  $v_s$  within a sufficiently small boundary. Therefore, it can be obtained recursively as

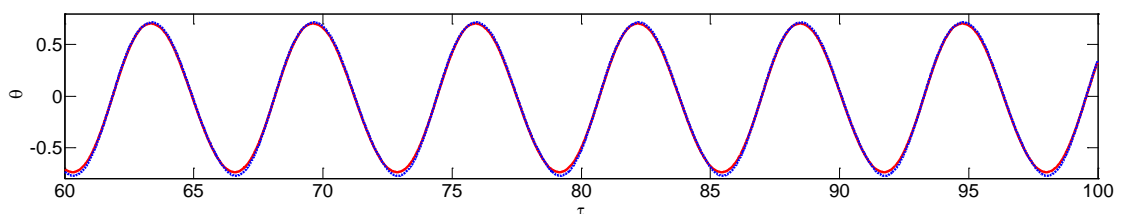
$$\left( \frac{X'_h}{v_s} \right)_{n+1} = \left\{ \ln \left[ \left( \frac{\alpha N (\eta_s - \eta_c)}{\delta_2 v_s} \right)^{1/(\alpha-1)} \left( \frac{X'_h}{v_s} \right)_n \right] \right\}^{1/2} \quad (5.14)$$

### 5.3 Analysis of Frictional Interaction Dynamics

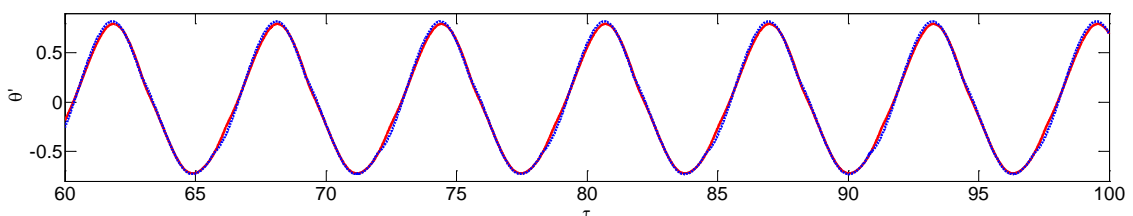
In this section, interaction dynamic responses of the capsule models with LM and EM are firstly analysed to reveal the nonlinear friction characteristics. Subsequently, effects of the control parameters are studied closely to identify the parameter dependence and the qualitative variation laws in capsule dynamics. The Gaussian friction model is adopted in this study as the exponential term in LM, i.e.,  $\alpha = 2$ . The rationality of the parameters chosen in this section is specified as follows: the parameter values for LM and EM are configured from the dynamic friction studies in literature as reported in (Chatterjee, 2007; Olsson et al., 1998; Saha et al., 2015) ( $\delta_0 = 100$ ,  $\delta_1 = 10$ ,  $\delta_2 = 0$ ,  $N = 1$ ,  $\eta_c = 0.15$ ,  $\eta_s = 0.45$ ,  $v_s = 0.1$  and  $\alpha = 10$ ); the control parameter values and initial conditions of state variables are selected based on our works on identification of qualitative variation laws induced by control parameters ( $y_1(0) = \pi/3$ ,  $y_2(0) = 0$ ,  $y_3(0) = 0$ ,  $y_4(0) = 0$  and  $y_5(0) = 0.0026$ ). The numerical studies in this section are based on the system dynamics (5.8).

### 5.3.1 The Responses of Friction-Induced Vibrations

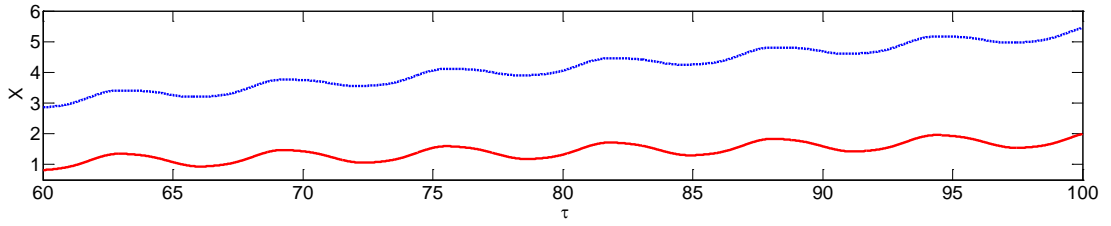
The dynamic response with LM and EM in time domain are shown in Figures 5.5 and 5.6. Both models have negative slope characteristic which guarantees the system stability. EM can describe the Stribeck effect, however, it is a static friction model, in which no hysteretic behaviour is shown. LM falls into the categories of dynamic models and is qualified for predicting the hysteretic loops. The friction-induced dynamic responses for capsule systems with LM and EM are depicted in Figure 5.5. The capsule with LM exhibits similar variation patterns to the one with EM in angular displacement  $\theta$ , angular velocity  $\theta'$ , capsule displacement  $X$  and capsule velocity  $X'$ . The main difference exists at the transitions between the sticking phase and the pure sliding phase. Influenced by the hysteretic characteristic of the friction force in the regime of presliding, the relative velocity does not completely drop to zero in sticking phase as depicted in Figure 5.5(d). It is noted that, in the absence of the hysteretic loop in EM in the presliding regime, the sticking phase poses a greater influence on EM than LM that the capsule velocity fluctuates around zero in such phase. It is observed from Figures 5.5(c) and 5.5(d) that the capsule gains a higher average velocity and larger displacement with EM than with LM, the reason behind is that the energy loss in the hysteretic loop is avoided with EM.



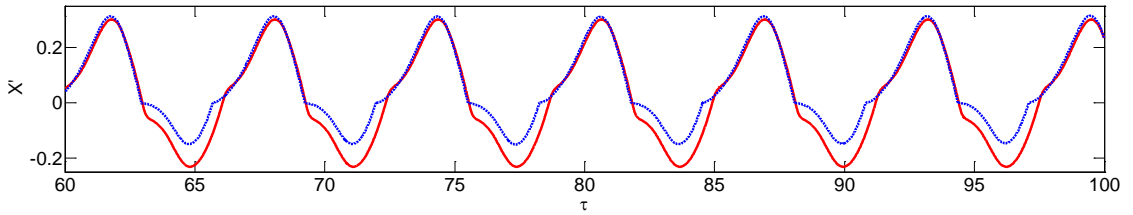
(a) Angular displacements



(b) Angular velocities



(c) Capsule displacements

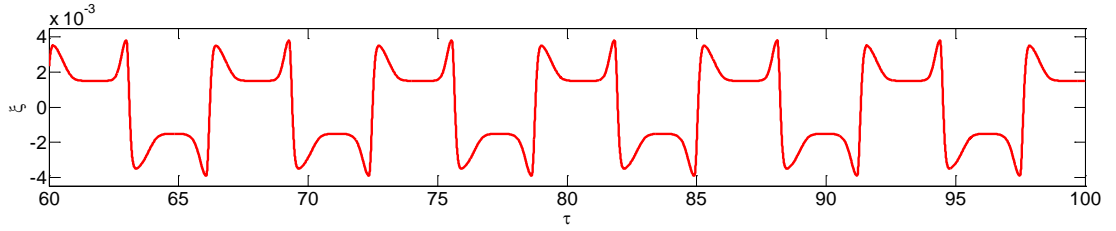


(d) Capsule velocity

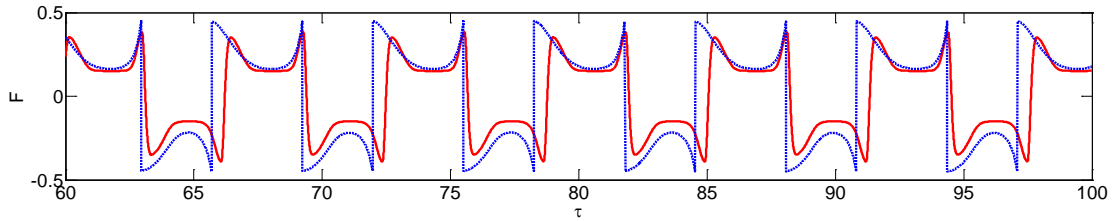
Figure 5.5 Friction-induced dynamic response with LM (red solid lines) and EM (blue dashed lines): (a) angular displacements  $\theta$ , (b) angular velocities  $\theta'$ , (c) capsule displacements  $X$  and (d) capsule velocity  $X'$ , obtained for  $\lambda = 2.5$ ,  $\rho = 2.0$  and  $v = 1.0$

Figure 5.6 shows that dynamic responses of internal state variable  $\hat{\xi}$  and friction force  $f$  exhibit same variation law, indicating that the evolution of  $f$  is governed by  $\hat{\xi}$ . Specifically,  $\hat{\xi}$  decreases dramatically from a certain value at the onset of sticking phase and then increases monotonically to reach the same absolute value in opposite direction, and vice versa. The value of average bristle deflection  $\hat{\xi}$  varies in both presliding and pure sliding regimes. It decreases with time in AS and subsequently increases with time in DS, repeatedly. This is directly originated from function  $g(X')$ , which governs the evolution of internal state variable  $\hat{\xi}$ . The abrupt decline of friction force as described in Figure 5.6(b) manifests the onset of the sticking phase, after which the friction force increases monotonically in the sticking phase to reach the magnitude of the static friction force. These are how  $\hat{\xi}$  manipulates the drooping characteristic in the pure sliding regime and the hysteretic behaviour in both presliding and pure sliding regimes. Interestingly, these findings in friction-induced vibrations confirm the results reported in (Astrom and

Canudas-De-Wit, 2008; Chatterjee, 2007; Saha et al., 2015), in which fully-actuated systems are studied. Since the capsule systems considered here are underactuated and the friction has indirect connection with the input, it is evident and verify the results presented here.



(a) Internal state variable  $\hat{\xi}$

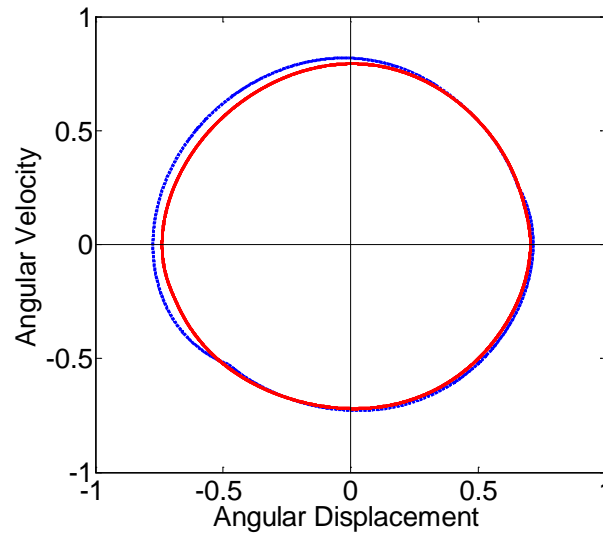


(b) Friction forces  $f$

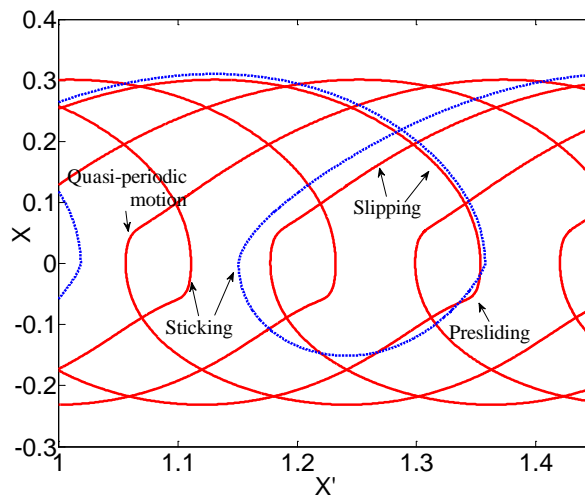
Figure 5.6 Friction-induced dynamic responses with LM (red solid lines) and EM (blue dashed lines): (a) internal state variable  $\hat{\xi}$  and (b) friction forces  $f$ , obtained for  $\lambda = 2.5$ ,  $\rho = 2.0$  and  $v = 1.0$

The examination on phase plane of the pendulum subsystem ( $\theta$  and  $\theta'$ ) and the capsule subsystem ( $X$  and  $X'$ ) are shown in Figure 5.7. It is clear to observe that the limit cycle of capsule system with EM is relatively larger in size compared to its counterpart with LM. The reason behind this phenomenon is the energy loss originated from the hysteresis characteristic of the friction force with LM. In both Figures 5.7(a) and 5.7(b) the step occurs in the loops when the relative velocity of capsule passes through zero and the friction falls into a stage of quasi-static. They portray slight discontinuities where imperfect overlap exists between the end and the beginning of limit cycle. The motion depicted here is not strictly periodic, whilst the phase portraits shown in Figure 5.7 are confined to reside within finite boundaries,

thus the motion in this stage is classified as quasi-periodic, which is associated with the hysteretic characteristic in the friction model.



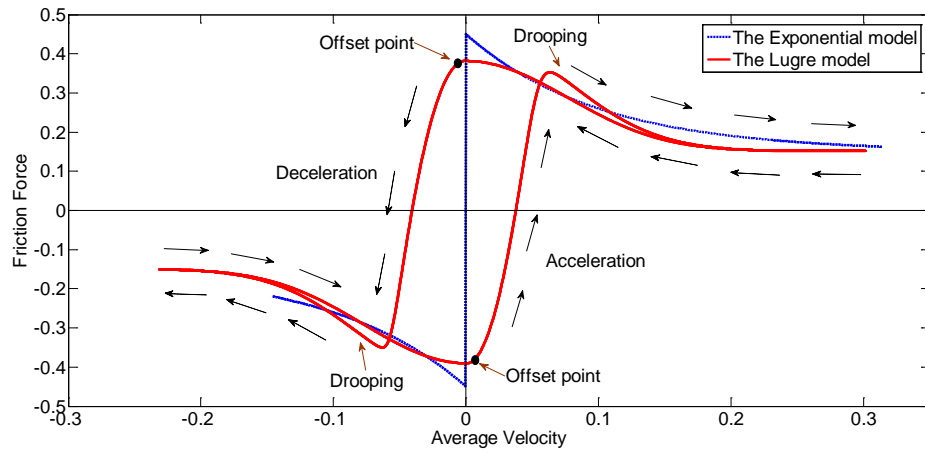
(a)



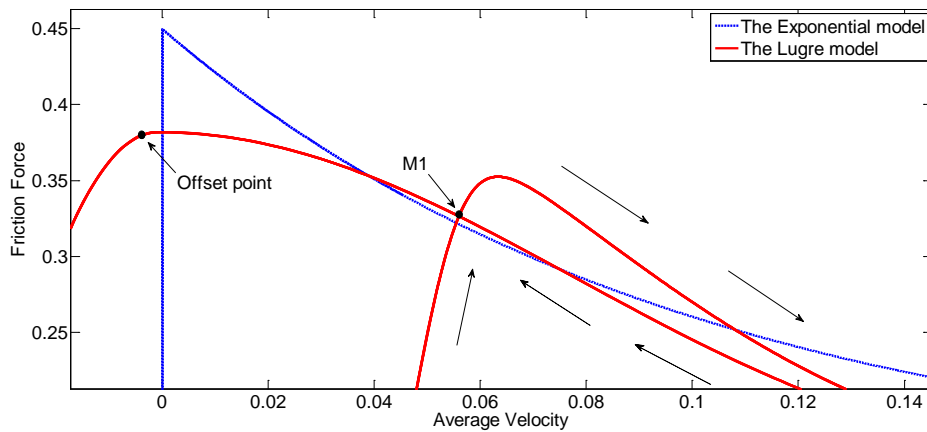
(b)

Figure 5.7 Phase portraits for capsule systems with EM (blue dashed lines) and LM (red solid lines): (a) the pendulum subsystem and (b) the capsule subsystem, obtained for  $\lambda = 2.5$ ,  $\rho = 2.0$  and  $\nu = 1.0$

The hysteretic loops shown in Figure 5.8 are associated with the friction force as a function of average capsule velocity. The friction force with respect to EM is depicted in blue dash line for comparison, which apparently does not show any hysteretic behaviour. This cross-validates the findings in Figures 5.5 and 5.6 wherein relatively higher frequency of oscillations in time coordinates with EM than that with LM are observed. Under the same parameter values of the Coulomb friction level  $\eta_c$ , the stiction force level  $\eta_s$  and the Stribeck velocity  $v_s$ , the maximum friction force in case of LM is lower than that for EM. The reason is that the dimension of limit cycle associated with LM is reduced. The arrows marked in Figure 5.8 demonstrate the changes of friction force with respect to the variation of average velocity for LM. It is observed in Figure 5.8 that during pure sliding regime for both forward and backward motions, irrespective of the regime near zero, the friction force is of relatively larger magnitude in AS than that in DS. Therefore, a clockwise hysteretic loop is taken place in pure sliding regime. On the other hand, the situation near zero relative velocity is totally different, wherein the magnitude of friction force in DS is relatively higher than that in AS. AS and DS are represented by the arrows associated with the increasing and decreasing values of relative velocity, respectively. Moreover, there exist offset points on the hysteretic curves near the regime of zero relative velocity when the friction force changes from small displacement to large displacement in AS and DS, respectively.  $M_1$  is the boundary point between presliding and pure sliding regimes for the forward motion of the capsule. The capsule escapes from presliding regime and enters into pure sliding regime at this point. The friction force firstly increases to a certain value within the maximal value of the Exponential friction force, then decreases monotonically along with the augmented average velocity, and subsequently overlaps with DS. The friction force between  $M_1$  and the terminal point for AS is always larger than that for DS. The situation between the offset point and  $M_1$  is reversed. More interestingly, the curves of LM and EM are almost coincided around  $M_1$ .



(a) Friction curves



(B) Enlarged friction curves

Figure 5.8 Friction forces for capsule systems with EM (blue dashed lines) and LM (red solid lines) obtained for  $\lambda = 2.5$ ,  $\rho = 2.0$  and  $v = 1.0$

### 5.3.2 Influence of the Control Parameters

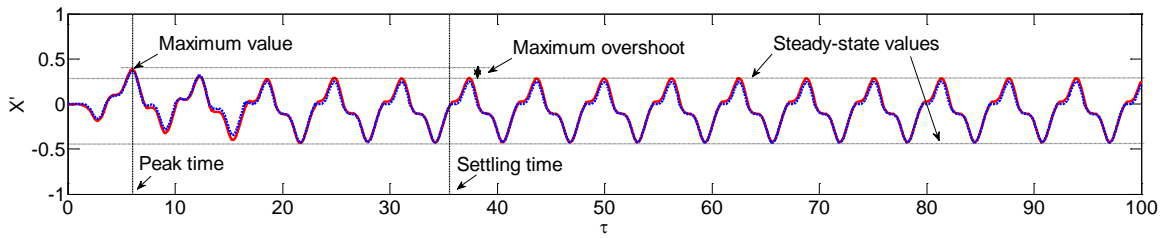
The solutions and their stabilities play a vital role in determining the transient response and a proper tuning of the control parameters will improve the system performance and avoid undesirable responses. The capsule system moves from the

origin, thus its average velocity is bounded and is capable of revealing the qualitative changes in the system responses. The average velocity  $X'$  is plotted as a function of mass ratio  $\lambda$  to reveal the parameter dependence. The comparison of transient responses under variation of amplitude  $h$  and frequency  $\omega$  of excitation are firstly discussed.

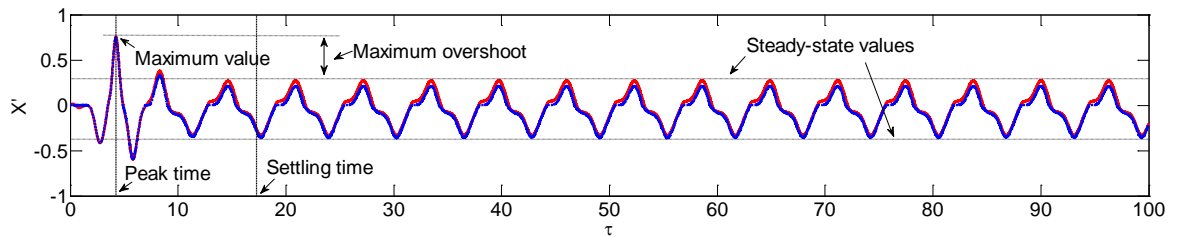
#### *A. Analysis of the System Transient Responses*

The transient response of dynamic systems is one of the vital performance indexes to evaluate how quickly and accurately a dynamic system responds to changes. The settling time is defined as the time after which the output is within a specified percentage of value around the steady-state value (2% is adopted in the thesis). For the capsule system considered, the time required from initiation to steady-state motion is determined by the values of the control parameters. In this subsection, a sequence of numerical simulations is conducted to make comparison of the system transient responses under varying control parameters.

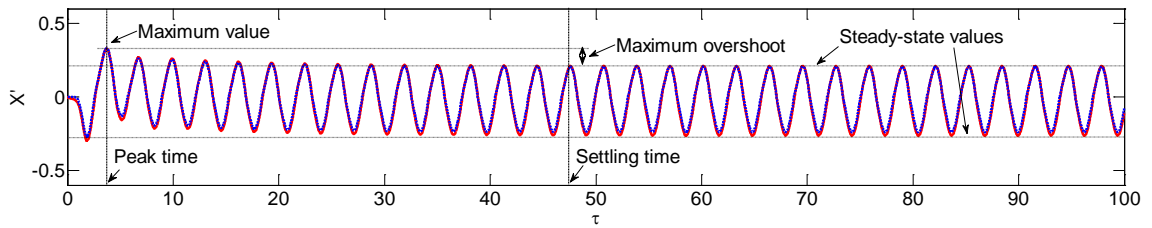
The comparisons of transient responses are shown in Figure 5.9. The velocity increases and decreases monotonically with time and reaches steady-state values for stable motion. It is observed in Figures 5.9(a) and 5.9(b) that the maximum value of the capsule velocity in the initial transient increases from 0.4 to 0.75 in compatible with the increase of the amplitude, which leads to a rising of maximum overshoot accordantly. However, the steady-state values slightly decrease from 0.285 to 0.275 as the same trend of the peak time, and the settling time is shortened dramatically by 18 unit of dimensionless time for amplitude with larger magnitude. The variation of the frequency is depicted in Figures 5.9(a) and 5.9(c), it is observed that as the frequency increases, the maximum velocity value varies from 0.4 to 0.33 with a decreasing in the steady-state value to 0.213, which indicates an increasing in the maximum overshoot. The peak time is slightly reduced whilst the settling time is augmented approximately by 10 unit of dimensionless time for higher value of frequency.



(a)  $h = 1.5, \omega = 1.0$



(b)  $h = 2.5, \omega = 1.0$



(c)  $h = 1.5, \omega = 2.0$

Figure 5.9 Transient responses under the variation of amplitude and frequency of excitation with LM (red solid lines) and EM (blue dashed lines): (a)  $h = 1.5, \omega = 1.0$ , (b)  $h = 2.5, \omega = 1.0$  and (c)  $h = 1.5, \omega = 2.0$ , obtained for  $\lambda = 2.5, \rho = 2.0$  and  $\nu = 1.0$

### B. Analysis of Parameter Dependence on the Mass Ratio

The numerical study taken the mass ratio  $\lambda$  as the branching parameter is presented in Figure 5.10, wherein the average velocity is projected as a function of  $\lambda$  for capsule systems with LM (red dotted) and EM (blue dotted).

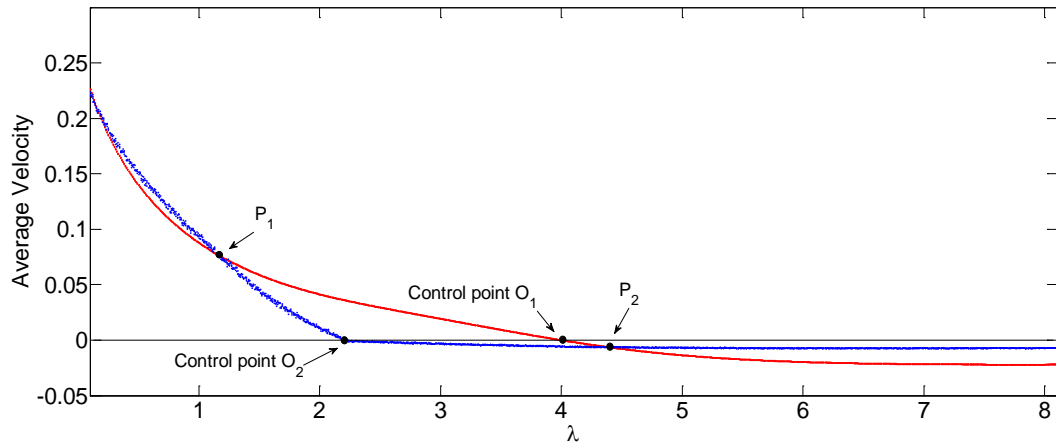
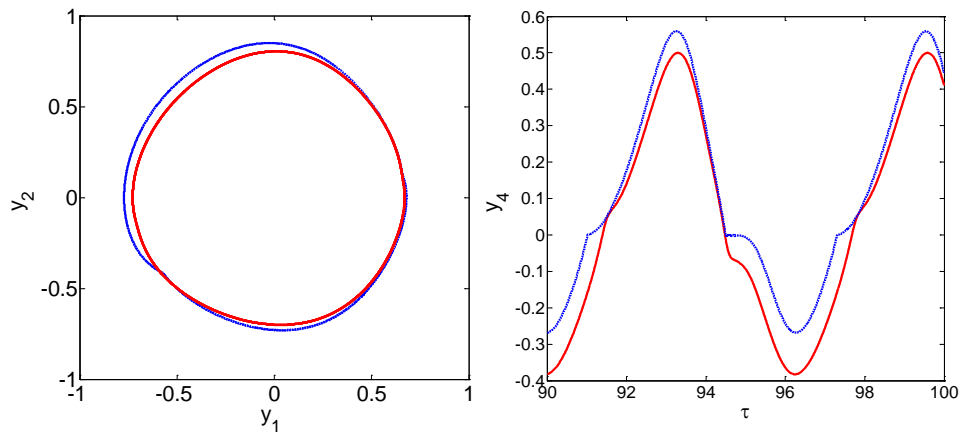


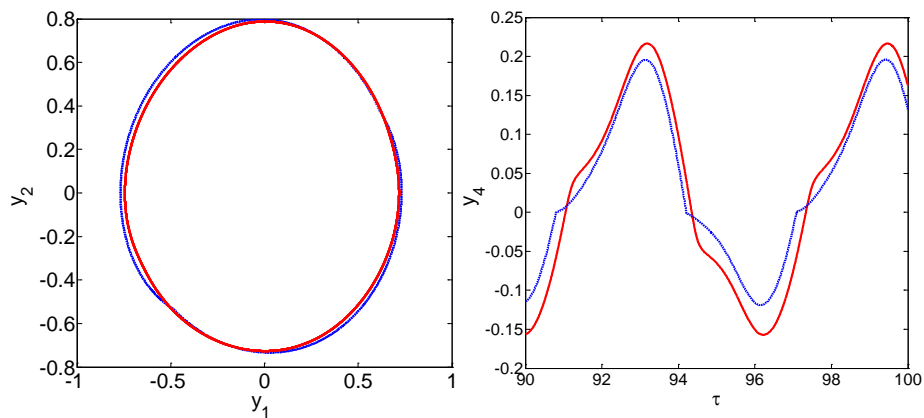
Figure 5.10 Bifurcation diagrams for capsule systems with LM (red dotted) and EM (blue dotted) constructed under variation of mass ratio  $\lambda$ , obtained for  $h = 1.8$ ,  $\omega = 1.0$ ,  $\rho = 4.0$  and  $v = 1.2$

It is noted from Figure 5.10 that periodic system responses are predicted for  $\lambda$  considered here. And both of the curves have the characteristic of negative slope, wherein the magnitude of the negative slope for LM is comparatively smaller than that for EM. Numerical study also shows that the average velocity of the capsule, with both friction models, decreases monotonically along with the increase of  $\lambda$  for  $\lambda \in [0.01, 8.1]$ . Boundary points at  $P_1$  ( $\lambda = 1.18$ ) and  $P_2$  ( $\lambda = 4.36$ ) are identified which differ the performances of capsules with LM and EM in average velocity. Before the boundary point  $P_1$ , the capsule with EM has a relatively higher average velocity than that with LM. For the mass ratio between points  $P_1$  and  $P_2$  ranged as  $\lambda \in [1.18, 4.36]$ , the situation is completely reversed, wherein the magnitude of average velocity with LM is higher than that with EM. After point  $P_2$  for  $\lambda \in [4.36, 8.1]$ , EM overtakes the situation again with velocity near zero in negative direction. As can be seen in Figure 5.10, the capsule has positive average velocities for  $\lambda \leq 4.0$  and  $\lambda \leq 2.2$  with LM and EM, respectively. Negative average velocities are observed for  $\lambda \in [4.0, 8.1]$  with LM and for  $\lambda \in [2.2, 8.1]$  with EM.

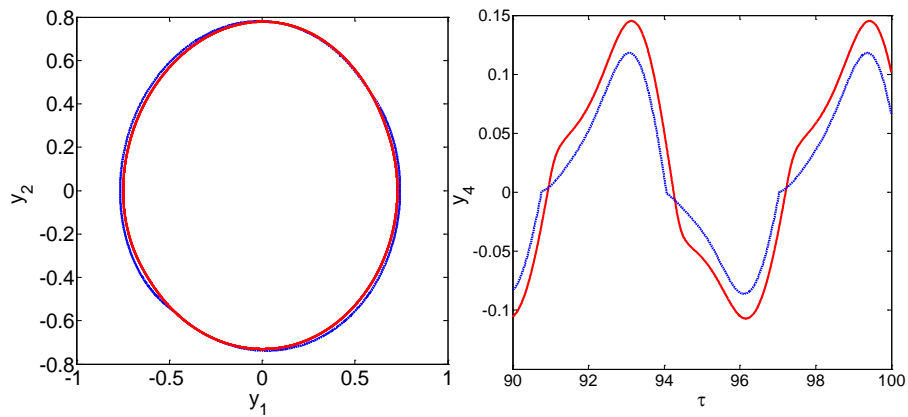
The trajectory of driving pendulum on phase plane and time histories of capsule velocity are recorded in Figure 5.11. It is noticed that with the two models, the capsule has larger positive velocities for every period of excitation for  $\lambda \leq 4.0$  and  $\lambda \leq 2.2$ , and as  $\lambda$  increases, the magnitude of velocity dramatically declines in the positive direction. Therefore, the average velocities of the capsule are reduced below zero. It is also noted that the average velocity of the capsule can be controlled through tuning  $\lambda$  around the control point  $O_1$  at  $\lambda = 4.0$  for LM and around the control point  $O_2$  at  $\lambda = 2.2$  for EM.



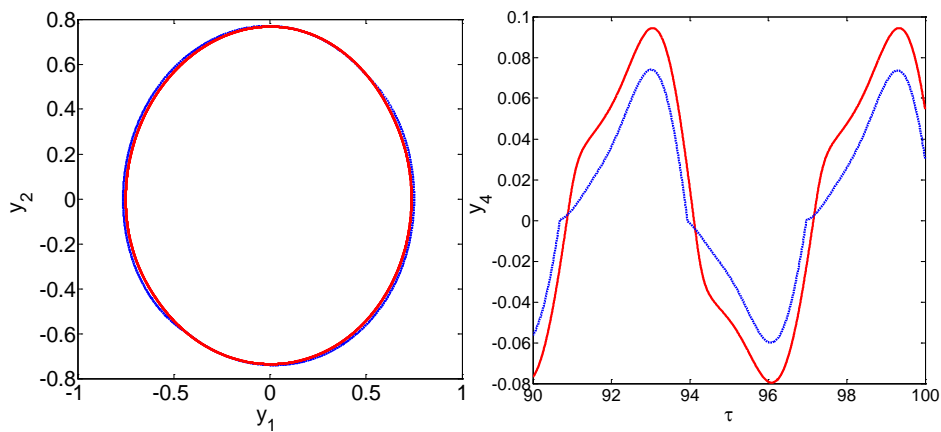
(a)  $\lambda = 0.5$



(b)  $\lambda = 2.5$



(c)  $\lambda = 4.0$

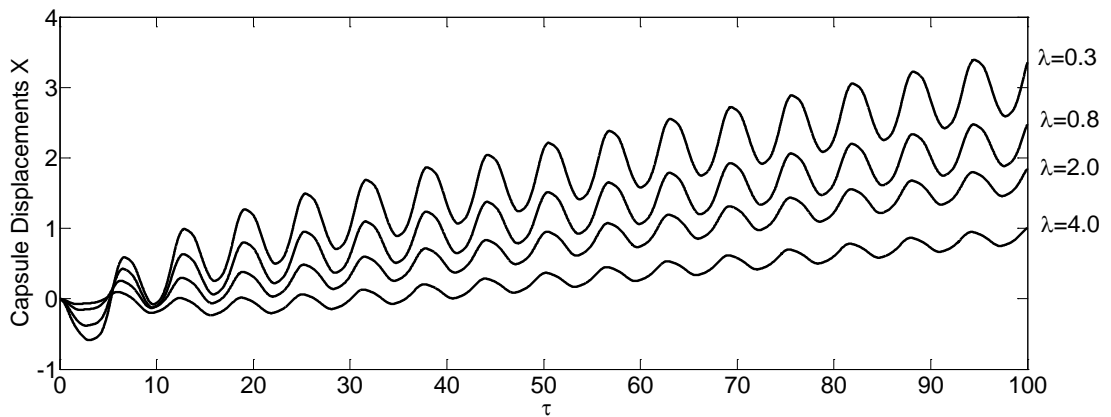


(d)  $\lambda = 6.0$

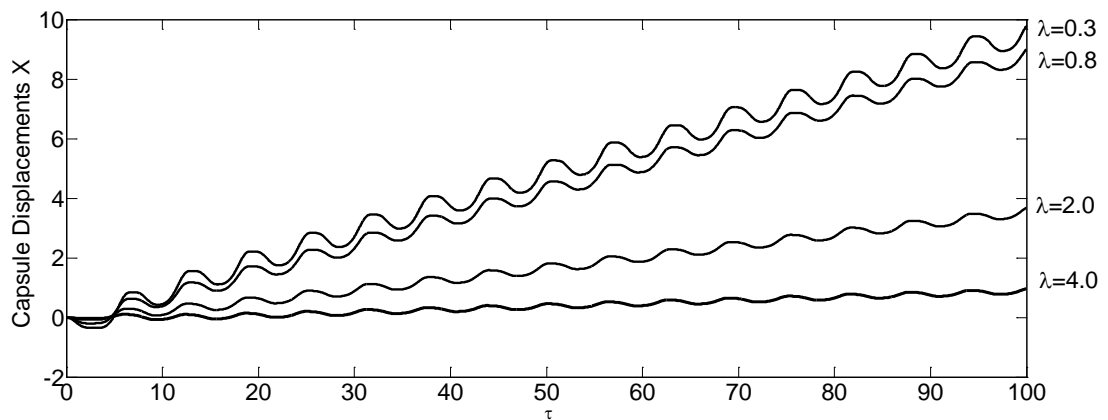
Figure 5.11 Trajectories on phase plane for the pendulum subsystem ( $y_1$  and  $y_2$ ) and on time coordinate for the capsule subsystem (progressive velocity  $y_4$ ), with LM (red solid lines) and EM (blue dashed lines): (a)  $\lambda = 0.5$ , (b)  $\lambda = 2.5$ , (c)  $\lambda = 4.0$  and (d)  $\lambda = 6.0$ , obtained for  $h = 1.8$ ,  $\omega = 1.0$ ,  $\rho = 4.0$  and  $v = 1.2$

Comparison of capsule progressions under variation of  $\lambda$  is shown in Figure 5.12. It is clearly observed that, for the capsule systems with LM and EM, both their progressions decrease monotonically in compatible with the augmentation of  $\lambda$ . Similarly, the amplitude of the displacement curves reduces as  $\lambda$  increases. On the

other hand, towards an increasing mass ratio, capsule displacement with EM exerts a greater decline rate than that with LM. The reason behind is the difference in the negative slopes of the average velocity curves as stated previously.



(a) Capsule displacements with LM



(b) Capsule displacements with EM

Figure 5.12 Time histories of capsule displacements under varying mass ratio ( $\lambda = 0.8, 2.0$  and  $4.0$ ): (a) with LM and (b) with EM, obtained for  $h = 1.8$ ,  $\omega = 1.0$ ,  $\rho = 4.0$  and  $v = 1.2$

## 5.4 Conclusions

Locomotion of the proposed vibro-driven capsule systems relies on the inherently nonlinear effects of dynamic frictions. The nonlinear friction forces are capable of triggering dynamic interactions between the systems and the contacting substrate. The friction models have negative slope characteristic which guarantees the stability of the system. The main difference exists in the transitions between the sticking phase and the pure sliding phase. As discussed in Section 5.3, influenced by the hysteretic characteristic of the friction force in the presliding regime, the relative velocity does not completely reduce to zero in the sticking phase. The capsule gains a higher average relative velocity and farther displacement with EM since energy loss in the hysteretic loop is avoided via the independence of the evolution of the internal variable  $\hat{\xi}$ . It is observed that  $\hat{\xi}$  decreases dramatically from a certain value at the onset of the sticking phase and then increases monotonically to reach the same absolute value in the opposite direction, and vice versa. The role of  $\hat{\xi}$  in manipulating the drooping characteristic in the pure sliding regime and the hysteretic behaviour in both of the presliding and pure sliding regimes has been precisely discussed. It is observed that during the pure sliding regime for both forward and backward motions, the friction force is of relatively larger magnitude in AS than that in DS to form a clockwise hysteretic loop in the pure sliding regime, and the situation is reversed near zero relative velocity. The parameter dependence studies have revealed that the interaction models predict periodic responses for the parameters considered. The average velocity of the capsule decreases monotonically along with the increase of the mass ratio  $\lambda$ , and control action can be applied through proper tuning of the control parameters. The studies on the capsule dynamics show the desirability of LM than EM in almost all the evaluations of the performance. The performance evaluations used for comparison of the friction models contain the capabilities of the caption of experimentally observed frictional characteristics, the quenching of friction-induced vibrations as well as the energy requirements.

## **Chapter 6**

# **Adaptive Control Systems for a Class of UMSs**

### **6.1 Introduction**

This chapter presents adaptive control systems for trajectory tracking of a class of UMSs with uncertainties and external disturbances, to obtain stability and convergence of time-varying reference trajectories for the system dynamics. The overall set of DOF is partitioned into two subsets, which referred to as collocated and non-collocated subsets. The cardinality of the collocated subset, which contains the actuated DOF, equals the number of control inputs. The non-collocated subset accounts for the unactuated (passive) DOF. As a result, the control objective is typically defined as the stabilization of either subset to desired values. The collocated and non-collocated adaptive control problem of UMSs is still a major concern for the control community. The main difficulty originates from the nonlinearity of the collocated and non-collocated inverse dynamics with respect to the base parameters, which prevents the direct application of existing prevailing adaptive control schemes. As a matter of fact, the collocated inverse dynamics is no longer linear with respect to the base parameters when expressed independently from the non-collocated accelerations. The existence of underactuation and other undesirable properties such as possessing an undetermined relative degree or being

in a non-minimum phase, give rise to complex theoretical problems and less generality in which conventional techniques are not directly applicable, particularly for the issues of trajectory planning and tracking control. Synthesis of the control systems for UMSs, according to the Brockett's theorem, is always challenging due to the nonholonomic property, complicated internal dynamics and unavailability of feedback linearizability. In addition, the lack of actuation along with model uncertainties and matched and unmatched disturbances that include external disturbances and unmodeled dynamics significantly complexify the control problem associated with UMSs.

The complexity of control problem related to UMSs can be reduced when the objective is to stabilize merely a subset of the system's DOF. In the specialized literature, a great number of existing control system design for UMSs are based on the idea of linearization through partial feedback (Huda and Yu, 2015; Le et al., 2012, 2014; Lee et al., 2013; Terry and Byl, 2014; Wu and He, 2016). Although linear systems could be suitably applied to capture the nonlinear dynamics at a certain local operation range, globally stabilization of the underactuated dynamics are still unavailable under this approach. Other prevailing techniques such as inverse dynamics (Blajer et al., 2011; Mistry et al., 2010), sliding mode/variable structure (Hwang et al., 2014; Xu et al., 2014; Yue et al., 2016), energy/passivity-based approaches (Cornejo and Alvarez-Icaza, 2011; Valentinis et al., 2015; Xin et al., 2013) have been extensively exploited. Furthermore, practical requirements are raised from the current applications, in which the adaptability of UMSs is extremely crucial when facing environments with uncertainties. For instance, microrobotic systems operating in restricted space and vulnerable media for minimally invasive diagnosis, sensing and risk intervention in pipeline inspection, endoscopic assistance, underwater exploration, etc. However, it is difficult to get an exact dynamic model due to the presence of frictions, unknown disturbances, time-varying parameters, etc. As a result, adaptive control of generic underactuated systems has received great attentions from the control community. The leader-follower formation control problem of underactuated autonomous surface vehicles in the presence of uncertainties and ocean disturbances is studied in (Peng et al., 2013), the control

system is developed using neural network and dynamic surface control technique. An adaptive fuzzy hierarchical sliding mode control system is designed for uncertain underactuated systems in (Hwang et al., 2014), where different layers of sliding surface are constructed to cope with the uncertainties and disturbances and fuzzy models are designed to approximate the nonlinearities.

It is evident that the descriptions of dynamic couplings between the actuated and passive subsystems of UMSs are typically highly nonlinear. Therefore, it is plausible to consider the employment of approximation approaches to map the coupling between the torques applied at the actuated subsystem and the resulting accelerations of the passive subsystem, with the intent of achieving control globally. As such, in this chapter, nonlinear control approach is investigated by employing multi-layer neural networks (NNs). NNs have versatile features such as learning capability mapping and parallel processing. An attractive feature of NNs is that their synaptic weights are online updated without any off-line learning phases. NNs have been widely used in various robotic systems to address the stabilization problem (Cong and Liang, 2009; Sazonov et al., 2003; Sprangers et al., 2015), where the robustness property of NNs was demonstrated using either simulations or real-time experiments. The problem of tracking control of robotic systems using NNs has attracted extensive attentions. A stochastic adaptive optimal control system was designed and applied to the Pendubot system in (J. Li et al., 2014) and also applied to a WIP system in (Yang et al., 2014). An adaptive neural network controller was designed in (He et al., 2016) for the robotic system with full-state constraints containing the Moore-Penrose inverse term. Two adaptive NN decentralized output feedback control schemes were designed for a class of systems with immeasurable states and unknown time delays in (Tong et al., 2011). In (Mohareri et al., 2012), adaptive tracking control for a nonholonomic wheeled mobile robot with unknown parameters and uncertain dynamics was studied. The gains of kinematic controller are tuned online to minimize the velocity error and improve the tracking performance. An adaptive neural network control for unknown cart-pendulum system was proposed in (Hsu, 2014), providing tracking control of the pendulum without considering the cart's position. A NN-based control system with output

feedback was designed in (Ping, 2013) to address the tracking problem for a spherical inverted pendulum. A combined PID and neural network compensation approach was proposed in (Jung and Kim, 2008) to control a wheel-driven mobile inverted pendulum system, and the results were experimentally analysed. The literature above demonstrates that only a few works have addressed the problem of trajectory tracking control of underactuated systems. Furthermore, it is noted that very few reported studies on this subject have presented rigorous analysis of the closed-loop system trajectories. Therefore, the problem of trajectory tracking control of underactuated systems with uncertainties remains an open problem and requires in-depth investigations.

Through the utilization of the unique physical properties of the UMSs, the overall underactuated system breaks down into two subsystems, where the first one is fully actuated and the other one is unactuated (passive). Radial basis neural network (RBFNN) has simple structure, fast convergence rate and it overcomes the local minimum problem, therefore it is utilized as a nonlinear function approximator of uncertain dynamics of the unactuated (passive) subsystem of the UMSs. The NN control has the ability of universal approximation, and it has been extensively studied in both discrete-time system (Liu et al., 2012; Y.-J. Liu et al., 2011; Xu et al., 2011; H. Zhang et al., 2014) and continuous-time systems (Wang et al., 2016; H. Zhang et al., 2013, 2014; Zou et al., 2011).

As stated, the existing and prevailing adaptive control schemes, which are mainly developed for fully actuated systems, are not directly applicable for UMSs. This research extends and enriches the existing control models to UMSs to stabilize the collocated and non-collocated state space. The main idea is to design an auxiliary state variable whose dynamics is considered to map the non-collocated subset and to define the sliding variable as the differences between the velocities of the system. RBFNN is adopted to approximate the system nonlinearities, the adaptive control algorithm is constructed to estimate the neural networks approximation error and the bounded unmatched disturbance. The combination of NN approximation, variable structure control and adaptive approach makes the

constructed new controller more robust, and as such, errors resulting from trajectory tracking, parameter uncertainties, unmatched external disturbances as well as NN approximation are sufficiently counteracted. Theoretical background of these methods is presented with rigorous analysis and developed in detail for two examples including a manipulation system and a locomotion system, which are two major research domains of control and robotics communities. The schemes promote the utilization of linear filters in the control input to improve the system robustness. Stability and convergence of time-varying reference trajectories for the system dynamics are shown by means of Lyapunov synthesis. In addition, adaptation laws for the weights of the proposed control systems are derived from this procedure. The main contributions of this chapter are listed as follows:

1. For fully actuated mechanical systems, adaptive stabilization of time-varying reference trajectories can be achieved based on existing control schemes. However, the applications of these control models to the underactuated case is not straightforward. This chapter extends and enriches the existing adaptive control schemes to stabilize the state space of underactuated systems by designing auxiliary control variables that contain NN approximator and robust compensator.
2. The existing control models for UMSs are mainly developed for uncertainties and matched disturbances which is associated with the collocated subset. The unmatched disturbances have been neglected in most of existing methods for the tracking control of underactuated systems. In this research, the parametric uncertainties, both matched and unmatched external disturbances are considered in the control scheme design, which feature a generic control model for underactuated systems.
3. Employing the adaptive control approach, in cooperation with variable structure and NNs, all exact values of the parameters of the underactuated systems are not required to be known *a priori*.
4. Designing robust compensators to counteract matched and unmatched disturbances, and function approximation error of NNs and nonlinear

frictions. The tracking error can be reduced as small as desired in finite time by selecting appropriate controller parameters.

The rest of this chapter is organized as follows. In Section 6.2, notations, assumptions, the system dynamic model for UMSs, and preliminary knowledge of NN approximation are presented. Section 6.3 presents the main theoretical results concerning the adaptive NN-based control systems design for a class of UMSs. Validations of the effectiveness of the proposed approach are presented in Section 6.4 through simulation studies on an underactuated manipulator and an underactuated VDC system. Finally, concluding remarks and perspectives are given in Section 6.5.

## 6.2 Theoretical Preliminaries

Let  $\|\cdot\|$  denotes any suitable vector Euclidean norm. Specifically,  $\|\cdot\|_p$  represents the  $p$ -norm of given vector. The Frobenius norm of the given matrix  $H = [h_{ij}] \in \mathcal{R}^{n \times m}$  is defined as  $\|H\|_F^2 = \text{Tr}(H^T H) = \text{Tr}(H H^T) = \sum_{i,j} h_{ij}^2$  with  $\text{Tr}(\cdot)$  denoting the trace operator. The Frobenius norm is associated with the 2-norm in a manner that  $\|Hx\|_2 \leq \|H\|_F \|x\|_2$  with  $H \in \mathcal{R}^{n \times m}$  and  $x \in \mathcal{R}^m$ . The trace operator has the property of  $A^T B = \text{Tr}(A B^T)$  with  $\forall A, B \in \mathcal{R}^n$ .  $\lambda_{\min}(\cdot)$  and  $\lambda_{\max}(\cdot)$  are the minimum and maximum eigenvalue of the given matrix, respectively.  $I_n$  represents the identity matrix of dimension  $n \times n$ .

### 6.2.1 Dynamic Model and Properties

The dynamics of a  $n$ -DOF underactuated mechanical system can be expressed in the generalized coordinates via the Euler-Lagrangian approach, given by

$$D(q, \alpha)\ddot{q} + C(q, \dot{q}, \alpha)\dot{q} + G(q, \alpha) + F_v(\alpha)\dot{q} + F_c(q, \dot{q}, \alpha) + \tau_d = B(q)\tau \quad (6.1)$$

with  $q = [q_1, \dots, q_n]^T \in \mathcal{R}^n$  describes the vector of generalized configurations,  $\alpha \in \mathcal{R}^p$  is the vector of the unknown parameters of the system mainly including the base initial parameters and possible loading parameters ( $p$  indicates the number of uncertain parameters),  $D(q, \alpha) \in \mathcal{R}^{n \times n}$  is a symmetric, positive definite inertial

matrix,  $C(q, \dot{q}, \alpha) \in \mathcal{R}^{n \times n}$  is the vector of centripetal and Coriolis matrix,  $G(q, \alpha) \in \mathcal{R}^n$  is the gravitational torque/force,  $F_v(\alpha) \in \mathcal{R}^{n \times n}$  denotes the viscous friction coefficients which is a positive definite matrix,  $F_c(q, \dot{q}, \alpha) \in \mathcal{R}^n$  models the nonlinear friction torques,  $\tau_d$  denotes bounded unknown disturbances and unmodeled dynamics,  $B(q) \in \mathcal{R}^{n \times (n-m)}$  is the input transformation matrix and  $\tau \in \mathcal{R}^{n-m}$  represents the vector of control inputs to be constructed to obtain specific control objectives.

The Lagrangian dynamic model of the underactuated mechanical system described by (6.1) have the following beneficial properties (Fang et al., 2012; Pucci et al., 2015; Yang et al., 2013) that are employed in the subsequent control laws design and analysis:

**Property 6.1.** The inertia matrix  $D(q, \alpha)$  is symmetric and positive-definite, i.e.,  $D(q, \alpha) = D^T(q, \alpha)$ ; it is uniformly positive definite, and has upper and lower boundaries, which implies

$$0 < \lambda_{min}(\alpha)\|x\|^2 \leq x^T D(q, \alpha)x \leq \lambda_{max}(\alpha)\|x\|^2 < +\infty, \forall x \in \mathcal{R}^{n-m} \quad (6.2)$$

**Property 6.2.** The centripetal and Coriolis term  $C(q, \dot{q}, \alpha)\dot{q}$  is quadratic in the generalized velocity  $\dot{q}$  and satisfies

$$\|C(q, \dot{q}, \alpha)\dot{q}\| \leq \lambda_3(\alpha)\|\dot{q}\| \quad (6.3)$$

for some bounded scalar constant  $\lambda_3(\alpha)$ .

**Property 6.3.** The above matrixes  $D(q, \alpha)$  and  $C(q, \dot{q}, \alpha)$  have the following particular skew-symmetric interconnection

$$x^T [\dot{D}(q, \alpha) - 2C(q, \dot{q}, \alpha)]x = 0, \quad \forall x \in \mathcal{R}^{n-m} \quad (6.4)$$

under an appropriate definition of  $C(q, \dot{q}, \alpha)$ . This property is a matrix version of energy conservation.

**Property 6.4.** The gravitational torque/force  $G(q, \alpha)$  is bounded and satisfies

$$\|G(q, \alpha)\| \leq \lambda_4(\alpha) \quad (6.5)$$

where  $\lambda_4(\alpha)$  is a bounded scalar constant.

**Property 6.5.** The dynamic model (1) can be rewritten in a linear form with respect to an appropriate selection of the system's base initial parameters and load parameters  $\alpha$ . Furthermore, there exists a regressor matrix  $Y(q, \dot{q}, \ddot{q})$  and a vector  $Y_0(q, \dot{q}, \ddot{q})$  which contain known functions, gives

$$D(q, \alpha)\ddot{q} + C(q, \dot{q}, \alpha)\dot{q} + G(q, \alpha) + F_v(\alpha)\dot{q} + F_n(q, \dot{q}, \alpha) = Y(q, \dot{q}, \ddot{q})\alpha + Y_0(q, \dot{q}, \ddot{q}) \quad (6.6)$$

where  $Y(\cdot) \in \mathcal{R}^{(n-m) \times p}$  is the regressor matrix containing known functions.

**Remark 6.1.** Based on Property 6.5, we introduce  $\hat{\alpha}$  be the time-varying estimation of  $\alpha$ , and define  $\hat{D}$ ,  $\hat{C}$ ,  $\hat{G}$ ,  $\hat{F}_v$  and  $\hat{F}_n$  be the corresponding affine matrices respectively estimated from  $D$ ,  $C$ ,  $G$ ,  $F_v$  and  $F_n$  through substitution  $\hat{\alpha}$  for the real  $\alpha$ . Then the linear parameterization is given by

$$\begin{aligned} \tilde{D}(q, \alpha)\ddot{q} + \tilde{C}(q, \dot{q}, \alpha)\dot{q} + \tilde{G}(q, \alpha) + \tilde{F}_v(\alpha)\dot{q} + \tilde{F}_n(q, \dot{q}, \alpha) \\ = Y(q, \dot{q}, \ddot{q})\tilde{\alpha} + Y_0(q, \dot{q}, \ddot{q}) \end{aligned} \quad (6.7)$$

where  $\tilde{\alpha}(t) = \hat{\alpha}(t) - \alpha$  is the parameter estimation error, and  $\varrho \in \mathcal{R}^n$  is an arbitrary vector.

**Remark 6.2.** Concretely, the unmodeled friction torque/force  $F$  in (6.1) can be partitioned into two aspects as

$$F = F_v(\alpha)\dot{q} + F_c(q, \dot{q}, \alpha) \quad (6.9)$$

where  $F_v(\alpha)\dot{q} = [F_{v1}(\alpha)\dot{q}_1, F_{v2}(\alpha)\dot{q}_2, \dots, F_{vn}(\alpha)\dot{q}_n]^T$  is the viscous friction torque describing the linear part,  $F_c(q, \dot{q}, \alpha) = [F_{c1}(q_1, \dot{q}_1, \alpha), F_{c2}(q_2, \dot{q}_2, \alpha), \dots, F_{cn}(q_n, \dot{q}_n, \alpha)]^T$  denotes the nonlinear friction torques.

**Assumption 6.1.** The matched and unmatched external disturbances are assumed to be bounded.

**Assumption 6.2.** It is assumed that each subsystem is equipped with encoder and tachometer for the position and velocity measurement.

### 6.2.2 Radial Basis Function NN

It has been well-established that the radial basis function neural network (RBFNN) is capable of universally approximation of any continuous function  $\chi(z): \mathcal{R}^n \rightarrow \mathcal{R}$  over a compact set  $\Omega_z$ , the approximation capability of RBFNN can be expressed as

$$\chi(z) = W^{*T} \phi(z) + \varepsilon(z) \quad \forall z \in \Omega_z \subset \mathcal{R}^n, \|\varepsilon(z)\| \leq \varepsilon_N \quad (6.10)$$

where  $z \in \Omega_z \subset \mathcal{R}^n$  denotes the input vector of dimension  $n$ ,  $\chi(z)$  is the unknown function to be approximated,  $W^* = [W_1^*, W_2^*, \dots, W_k^*]^T \in \mathcal{R}^k$  is the bounded ideal synaptic weight vector with dimension (or the NN node number)  $k > 1$  (i.e.,  $\forall$  positive constant  $W_N$  such that  $\|W_k^*\| \leq W_N$  and  $tr\{W_k^{*T} W_k^*\} \leq W_N$ ),  $\varepsilon(z) \in \mathcal{R}$  is a bounded approximation error over the compact set,  $\varepsilon_N$  is an upper bound (positive constant) of the approximation error which satisfies  $\varepsilon_N = \sup \|\hat{\chi}(z, W^*) - \chi(z)\|$ ,  $\phi(z) = [\phi_1(z), \phi_2(z), \dots, \phi_k(z)]^T$  is the NN basis function which is conventionally chosen as Gaussian functions as

$$\phi_i(z) = \exp\left(-\frac{\|z - C_i\|^2}{2b_i^2}\right), \quad i = 1, 2, \dots, k \quad (6.11)$$

where vector  $C_i$  and  $b_i$  represent the centre and the width of the  $i$ -th receptive field.

The Gaussian function is chosen as NN basis function, and it is well known that given sufficient number of neural networks nodes and properly adopted centres and the widths of the node, RBFNN can approximate any unknown nonlinearities to arbitrarily close to a compact set with any desired accuracy. Note that the approximation error  $\varepsilon(z)$  decreases along with the increase of the number of NN node  $k$ .

It is noted that the bounded ideal weight matrix  $W^*$  is merely a quantity utilized for analysis purposes, whilst in real control applications, its estimate  $\hat{W}$  is utilized for practical approximation of unknown function  $\chi(z)$ . Therefore, the estimation of  $\chi(z)$  is denoted by

$$\hat{\chi}(z) = \hat{W}^{*T} \phi(z) \quad (6.12)$$

Based on the neural network defined by (6.12), the function approximation error can be described as

$$\chi(z) - \hat{\chi}(z) = \tilde{W}^T \phi(z) + \varepsilon(z) \quad (6.13)$$

where  $\tilde{W} = W^* - \hat{W}$ .

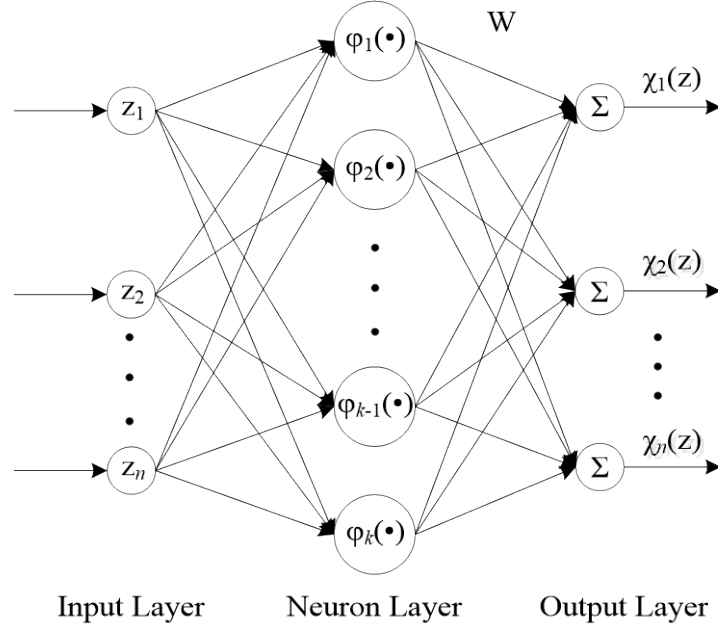


Figure 6.1 Structure of the RBF neural network

**Assumption 6.3.**  $\hat{\chi}(z, W^*)$  is the output of the NNs and continuous, there exists a sufficient small positive constant such that

$$\max \|\hat{\chi}(z, W^*) - \chi(z)\| \leq \varepsilon_0 \quad (6.14)$$

where the ideal weight vector  $W^*$  is usually defined as the optimal value of  $W$  such that the approximation error  $\varepsilon(z)$  could be minimized for all  $z \in \Omega_z$  as

$$W^* := \arg \min_{W \in \mathcal{R}^k} \{ \sup_{z \in \Omega_z} \|\chi(z) - W^{*T} \phi(z)\| \} \quad (6.15)$$

### 6.3 Controller Design and Stability Analysis

Assuming that for system (6.1), there are only  $m$  control inputs are equipped with actuators, then the generalized coordinate vector  $q$  can be partitioned into collocated and non-collocated vectors as

$$q := [q_c \ q_n]^T \quad (6.16)$$

where  $q_c \in \mathcal{R}^m$  and  $q_n \in \mathcal{R}^{n-m}$  denote the actuated and unactuated coordinate vector, respectively.

Without loss of generality, system (6.1) can be rewritten into the following partitioned form

$$\begin{cases} D_{cc}(q, \alpha)\ddot{q}_c + D_{cn}(q, \alpha)\ddot{q}_n + C_{cc}(q, \dot{q}, \alpha)\dot{q}_c + C_{cn}(q, \dot{q}, \alpha)\dot{q}_n \\ \quad + G_c(q, \alpha) + F_{vc}(\alpha)\dot{q}_c + F_{cc}(q, \dot{q}, \alpha) + \tau_{dc} = \tau \\ D_{nc}(q, \alpha)\ddot{q}_c + D_{nn}(q, \alpha)\ddot{q}_n + C_{nc}(q, \dot{q}, \alpha)\dot{q}_c + C_{nn}(q, \dot{q}, \alpha)\dot{q}_n \\ \quad + G_n(q, \alpha) + F_{vn}(\alpha)\dot{q}_n + F_{cn}(q, \dot{q}, \alpha) + \tau_{dn} = 0 \end{cases} \quad (6.17)$$

where  $\tau_{dc}$  and  $\tau_{dn}$  denote the bounded unknown disturbances including unmodeled dynamics to the collocated and non-collocated subsystems, respectively.

Let the reference trajectories for the collocated and non-collocated subsystems be described by the vector-valued functions  $\|q_{cd}\|_\infty \leq \vartheta_1$  and  $\|q_{nd}\|_\infty \leq \vartheta_2$ , respectively, and assume that these functions are bounded in norm and uniformly continuous on  $\mathcal{R}^+$ , and homogeneously on the same set, its first and second order derivatives are well-defined, bounded and uniformly continuous. Introducing the trajectory tracking error as

$$\tilde{q}_c = q_c - q_{cd}, \quad \tilde{q}_n = q_n - q_{nd} \quad (6.18)$$

which is to be stabilized to zero without the knowledge of the system parameters  $\alpha$ .  $\vartheta_1$  and  $\vartheta_2$  are positive upper bounds of the desired reference trajectories. Noted that the design of  $\vartheta_1$  and  $\vartheta_2$  has to satisfy the zero dynamics as

$$\begin{aligned} D_{nc}(q, \alpha)\ddot{\vartheta}_1 + D_{nn}(q, \alpha)\ddot{\vartheta}_2 + C_{nc}(q, \dot{q}, \alpha)\dot{\vartheta}_1 + C_{nn}(q, \dot{q}, \alpha)\dot{\vartheta}_2 + G_n(q, \alpha) \\ + F_{vn}(\alpha)\dot{\vartheta}_2 + F_{cn}(q, \dot{q}, \alpha) + \tau_{dn} = 0 \end{aligned} \quad (6.19)$$

In the following, auxiliary kinematic vector variables  $\varrho = [\varrho_c \varrho_n]^T$  and  $\delta = [\delta_c \delta_n]^T$  are defined as

$$\varrho_c = \dot{q}_{cd} - \Lambda_c \tilde{q}_c, \quad \varrho_n = \dot{q}_{nd} - \Lambda_n \tilde{q}_n \quad (6.20a)$$

$$\delta_c = \dot{q}_c - \varrho_c = \dot{\tilde{q}}_c + \Lambda_c \tilde{q}_c, \quad \delta_n = \dot{q}_n - \varrho_n = \dot{\tilde{q}}_n + \Lambda_n \tilde{q}_n \quad (6.20b)$$

where  $\varrho_c, \delta_c \in \mathcal{R}^m$  and  $\varrho_n, \delta_n \in \mathcal{R}^{n-m}$ .  $\delta$  denotes the filtered error signal and describes the measure of tracking accuracy,  $\varrho$  is referred to as vector of the reference trajectory,  $\Lambda = \text{diag}[\Lambda_c I_{m \times m}, \Lambda_n I_{(n-m) \times (n-m)}]$  with  $\Lambda_c$  and  $\Lambda_n$  be positive constants selected by designers.  $I_{i \times i}$  denotes  $i \times i$  identity matrix. The choice of  $\Lambda > 0$  guarantees that (6.20b) is an exponentially stable system for  $q$ . Indeed, the trajectory  $q$  converges to an adjacent of  $q_d$  exponentially fast as long as the controller drives  $\delta$  to an adjacent of zero.

Applying the defined variables in the system dynamics (6.17), we have

$$\begin{cases} D_{cc}(q, \alpha)(\dot{\delta}_c + \dot{\varrho}_c) + D_{cn}(q, \alpha)(\dot{\delta}_n + \dot{\varrho}_n) + C_{cc}(q, \dot{q}, \alpha)(\delta_c + \varrho_c) \\ + C_{cn}(q, \dot{q}, \alpha)(\delta_n + \varrho_n) + G_c(q, \alpha) + F_{vc}(\alpha)\dot{q}_c + F_{cc}(q, \dot{q}, \alpha) + \tau_{dc} = \tau \\ D_{nc}(q, \alpha)(\dot{\delta}_c + \dot{\varrho}_c) + D_{nn}(q, \alpha)(\dot{\delta}_n + \dot{\varrho}_n) + C_{nc}(q, \dot{q}, \alpha)(\delta_c + \varrho_c) \\ + C_{nn}(q, \dot{q}, \alpha)(\delta_n + \varrho_n) + G_n(q, \alpha) + F_{vn}(\alpha)\dot{q}_n + F_{cn}(q, \dot{q}, \alpha) + \tau_{dn} = 0 \end{cases} \quad (6.21)$$

The corresponding lumped error equation can be obtained as

$$\begin{cases} D_{cc}(q, \alpha)\dot{\delta}_c + D_{cn}(q, \alpha)\dot{\delta}_n + C_{cc}(q, \dot{q}, \alpha)\delta_c \\ + C_{cn}(q, \dot{q}, \alpha)\delta_n + \tau_{dc} = \tau - Y_c(q, \dot{q}, \dot{\varrho}_c, \dot{\varrho}_n, \varrho_c, \varrho_n)\alpha_c \\ D_{nc}(q, \alpha)\dot{\delta}_c + D_{nn}(q, \alpha)\dot{\delta}_n + C_{nc}(q, \dot{q}, \alpha)\delta_c \\ + C_{nn}(q, \dot{q}, \alpha)\delta_n + \tau_{dn} = -\chi(z) \end{cases} \quad (6.22)$$

where  $Y_c(q, \dot{q}, \dot{\varrho}_c, \dot{\varrho}_n, \varrho_c, \varrho_n)\alpha_c = D_{cc}(q, \alpha)\dot{\varrho}_c + D_{cn}(q, \alpha)\dot{\varrho}_n + C_{cc}(q, \dot{q}, \alpha)\varrho_c + C_{cn}(q, \dot{q}, \alpha)\varrho_n + G_c(q, \alpha) + F_{vc}(\alpha)\dot{q}_c + F_{cc}(q, \dot{q}, \alpha)$ ,  $\chi(z) = D_{nc}(q, \alpha)\dot{\varrho}_c + D_{nn}(q, \alpha)\dot{\varrho}_n + C_{nc}(q, \dot{q}, \alpha)\varrho_c + C_{nn}(q, \dot{q}, \alpha)\varrho_n + G_n(q, \alpha) + F_{vn}(\alpha)\dot{q}_n + F_{cn}(q, \dot{q}, \alpha)$ , and  $\alpha_c = \hat{\alpha}_c - \tilde{\alpha}_c$ ,  $\alpha_n = \hat{\alpha}_n - \tilde{\alpha}_n$ . The input  $\chi(z)$  is adopted as  $z = [\tilde{q}^T, \dot{\tilde{q}}^T, q_d^T, \dot{q}_d^T, \ddot{q}_d^T]$ .

The estimation of nonlinear function  $\chi(z) = -Y_n(q, \dot{q}, \dot{\varrho}_c, \dot{\varrho}_n, \varrho_c, \varrho_n)\alpha_n$  is expressed as

$$\hat{\chi}(z) = \hat{W}^T \phi(z) \quad (6.23)$$

where  $\hat{W}$  is the NN adaptation law,  $\phi(z)$  is the basis function.

Accordingly, (6.22) evolves to the following form

$$\begin{cases} D_{cc}(q, \alpha) \dot{\delta}_c + D_{cn}(q, \alpha) \dot{\delta}_n + C_{cc}(q, \dot{q}, \alpha) \delta_c \\ + C_{cn}(q, \dot{q}, \alpha) \delta_n + \tau_{dc} = \tau - Y_c(q, \dot{q}, \dot{q}_c, \dot{q}_n, q_c, q_n) \alpha_c \\ D_{nc}(q, \alpha) \dot{\delta}_c + D_{nn}(q, \alpha) \dot{\delta}_n + C_{nc}(q, \dot{q}, \alpha) \delta_c \\ + C_{nn}(q, \dot{q}, \alpha) \delta_n + \tau_{dn} = \hat{W}^T \phi + \tilde{W}^T \phi + \varepsilon \end{cases} \quad (6.24)$$

where  $\tilde{W} = W^* - \hat{W}$ .

Concretely, with these derivations, the adaptive control problem for underactuated mechanical systems can be formulated as follows: given the reference trajectories  $q_d \in \mathcal{R}^n$ , find a nonlinear control law for  $\tau$  such that for any  $q(0) \in \mathcal{R}^n$  and in the presence of parameter variation and other uncertainties, the tracking error  $\tilde{q}$  and its derivative tend to zero in finite time as  $t \rightarrow \infty$ .

The following theorem presents NNs-based control laws that ensure the asymptotic convergence of the closed loop signals.

**Theorem 6.1.** Consider the aforementioned properties, assumptions and definitions and apply the following control laws to the uncertain underactuated system (6.24)

$$\tau = \tau_c + \tau_n \quad (6.25a)$$

$$\tau_c = Y_c \hat{\alpha}_c - K_1 \delta_c - \xi, \quad \tau_n = -sgn(\delta_c) \|\delta_n\| |\eta| - K_2 sgn(\delta_c) \|\delta_n\| \quad (6.25b)$$

where the *Adaptation Algorithm 6.1* for the collocated subsystem is designed as

$$\dot{\hat{\alpha}}_c = -\Gamma Y_c \delta_c \quad (6.25c)$$

and the auxiliary input  $\eta$  in (6.25b) is constructed as

$$\dot{\eta} = \eta^{\frac{1}{2n+1}} (-K_3 \|\delta_n\|^2 - \|\delta_n\| \hat{W}^T \phi + \delta_n^T \zeta) \quad (6.25d)$$

with robust compensator  $\zeta$  for the non-collocated subsystem designed as

$$\zeta = -\frac{\delta_n}{\|\delta_n\| + \mu} \kappa \quad (6.25e)$$

and its adaptation law

$$\dot{\kappa} = \frac{\|\delta_n\|^2}{\|\delta_n\| + \mu} \quad (6.25f)$$

where  $K_1 \in \mathcal{R}^{m \times m}$ ,  $K_2, K_3 \in \mathcal{R}^{(n-m) \times (n-m)}$  are diagonal, constant positive definite matrixes and  $\Gamma \in \mathcal{R}^{p \times p}$  are positive definite matrixes.  $\xi$  and  $\zeta$  are auxiliary robust compensator designed later for convenience of stability analysis of the closed-loop system, and they are designed to compensate for matched and unmatched disturbances, and function approximation error of NNs and nonlinear frictions.  $\mu > 0$  is selected in a manner that  $\int_0^\infty \mu dt < \infty$ . Then the following conclusions hold:

- (1)  $tr\{\widehat{W}^T \widehat{W}\} \leq W_N$  holds.
- (2) The control objective of asymptotically stabilization can be achieved;
- (3) All signals within the closed-loop system are bounded and the trajectory tracking errors  $\tilde{q}$  and  $\dot{\tilde{q}}$  will converge to zero asymptotically.

**Proof.** Consider the following candidate Lyapunov function

$$V = \frac{1}{2} \delta^T D \delta + \frac{1}{2} \tilde{\alpha}_c^T \Gamma^{-1} \tilde{\alpha}_c + \frac{1}{2} tr\{\tilde{W}^T \Upsilon^{-1} \tilde{W}\} + \frac{2n+1}{2n} \eta^{\frac{2n}{2n+1}} + \frac{1}{2} (\kappa - \varepsilon_T)^2 \quad (6.26)$$

where  $\varepsilon_T \geq \|\varepsilon - \tau_{dn}\|$  is the upper bound of the unmatched disturbance and approximation error.

Differentiating both sides of (6.26) and applying the control laws (6.25), yields

$$\begin{aligned} \dot{V} &= \delta^T \left( \begin{bmatrix} \tau - Y_c \alpha_c \\ W^T \phi + \varepsilon \end{bmatrix} - \tau_d \right) + \dot{\tilde{\alpha}}_c^T \Gamma^{-1} \tilde{\alpha}_c + tr\{\tilde{W}^T \Upsilon^{-1} \dot{\tilde{W}}\} + \eta^{\frac{-1}{2n+1}} \dot{\eta} + (\kappa - \varepsilon_T) \dot{\kappa} \\ &= [\delta_c^T \ \delta_n^T] \begin{bmatrix} -K_1 \delta_c - Y_c \tilde{\alpha}_c - sgn(\delta_c) \|\delta_n\| |\eta| - K_2 sgn(\delta_c) \|\delta_n\| - \xi \\ W^T \phi + \varepsilon \end{bmatrix} - \delta^T \tau_d \\ &\quad + \dot{\tilde{\alpha}}_c^T \Gamma^{-1} \tilde{\alpha}_c + tr\{\tilde{W}^T \Upsilon^{-1} \dot{\tilde{W}}\} + \eta^{\frac{-1}{2n+1}} \dot{\eta} + (\kappa - \varepsilon_T) \dot{\kappa} \\ &= -\delta_c^T K_1 \delta_c - \delta_c^T sgn(\delta_c) \|\delta_n\| |\eta| - \delta_c^T K_2 sgn(\delta_c) \|\delta_n\| - \delta_c^T \xi + \delta_n^T (W^T \phi + \varepsilon) \\ &\quad - \delta^T \tau_d + tr\{\tilde{W}^T \Upsilon^{-1} \dot{\tilde{W}}\} + \eta^{\frac{-1}{2n+1}} \dot{\eta} + (\kappa - \varepsilon_T) \dot{\kappa} \end{aligned}$$

$$\begin{aligned}
 &= -\delta_c^T K_1 \delta_c - \|\delta_c\| \|\delta_n\| |\eta| - K_2 \|\delta_c\| \|\delta_n\| - \delta_c^T \xi - \delta^T \tau_d + \delta_n^T \varepsilon + \delta_n^T W^T \phi \\
 &\quad + \text{tr} \left\{ \tilde{W}^T \Upsilon^{-1} \dot{\tilde{W}} \right\} + \eta^{\frac{-1}{2n+1}} \dot{\eta} + (\kappa - \varepsilon_T) \dot{\kappa} \\
 &= -\delta_c^T K_1 \delta_c - \|\delta_c\| \|\delta_n\| |\eta| - K_2 \|\delta_c\| \|\delta_n\| - \delta_c^T \xi - \delta^T \tau_d + \delta_n^T \varepsilon + \delta_n^T W^T \phi \\
 &\quad + \text{tr} \left\{ \tilde{W}^T \Upsilon^{-1} \dot{\tilde{W}} \right\} - K_3 \|\delta_n\|^2 - \|\delta_n\| \widehat{W}^T \phi - \delta_n^T \zeta + (\kappa - \varepsilon_T) \dot{\kappa} \\
 &= -\delta_c^T K_1 \delta_c - \|\delta_c\| \|\delta_n\| |\eta| - K_2 \|\delta_c\| \|\delta_n\| - \delta_c^T \xi - \delta_c^T \tau_{dc} + \delta_n^T (\varepsilon - \tau_{dn}) \\
 &\quad - \frac{\|\delta_n\|^2}{\|\delta_n\| + \mu} \kappa - K_3 \|\delta_n\|^2 + \text{tr} \left\{ \tilde{W}^T \Upsilon^{-1} (\dot{\tilde{W}} + \Upsilon \delta_n^T \phi) \right\} + (\kappa - \varepsilon_T) \dot{\kappa} \\
 &\leq -\delta_c^T K_1 \delta_c - \|\delta_c\| \|\delta_n\| |\eta| - K_2 \|\delta_c\| \|\delta_n\| - \delta_c^T \xi - \delta_c^T \tau_{dc} + \|\delta_n\| \varepsilon_T - \frac{\|\delta_n\|^2}{\|\delta_n\| + \mu} \kappa \\
 &\quad - K_3 \|\delta_n\|^2 + \text{tr} \left\{ \tilde{W}^T \Upsilon^{-1} (\dot{\tilde{W}} + \Upsilon \delta_n^T \phi) \right\} + (\kappa - \varepsilon_T) \dot{\kappa}
 \end{aligned} \tag{6.27}$$

Towards the parameter drifting problem, the neural weight adaptation law for  $\widehat{W}$  is constructed based on the projection algorithm, given by

$$\dot{\widehat{W}} = -\dot{\tilde{W}} = \begin{cases} \Upsilon \phi \delta_n^T - \frac{\delta_n^T \widehat{W}^T \Upsilon \phi \widehat{W}}{W_N}, & \text{if } \text{tr}\{\widehat{W}^T \widehat{W}\} = W_N \text{ and } \delta_n^T \widehat{W}^T \phi \leq 0; \\ \Upsilon \phi \delta_n^T, & \text{if } \text{tr}\{\widehat{W}^T \widehat{W}\} < W_N \text{ or if } \text{tr}\{\widehat{W}^T \widehat{W}\} = W_N \text{ and } \delta_n^T \widehat{W}^T \phi > 0. \end{cases} \tag{6.28}$$

**Corollary 6.1.** Let  $V_{tr1} \triangleq \text{tr}\{\widehat{W}^T \widehat{W}\}$  and  $V_{tr2} \triangleq \text{tr}\{\tilde{W}^T \Upsilon^{-1} (\dot{\tilde{W}} + \Upsilon \delta_n^T \phi)\}$  and apply weight adaptation law (6.28), then the following results hold for the boundedness of  $\widehat{W}$

$$1) V_{tr1} \leq W_N \tag{6.29}$$

$$2) V_{tr2} \leq 0 \tag{6.30}$$

**Proof. (1)** Recalling (6.28), it is evident that

(a) If  $V_{tr1} = W_N$  and  $\delta_n^T \widehat{W}^T \phi > 0$ ,

$$\dot{V}_{tr1} = 2 \text{tr} \left\{ \widehat{W}^T \dot{\widehat{W}} \right\} = 2 \text{tr} \left\{ \widehat{W}^T \Upsilon \phi \delta_n^T \right\} - 2 \delta_n^T \widehat{W}^T \Upsilon \phi = 0.$$

(b) If  $V_{tr1} = W_N$  and  $\delta_n^T \hat{W}^T \phi \leq 0$ ,

$$\dot{V}_{tr1} = 2tr\{\hat{W}^T \Upsilon \phi \delta_n^T\} < 0.$$

(c) If  $V_{tr1} < W_N$ , the result 1) holds by itself.

(2) Adopting  $\hat{W}$  in (6.28), it is apparent that

(a) If  $V_{tr1} = W_N$  and  $\delta_n^T \hat{W}^T \Upsilon \phi > 0$ ,

$$V_{tr2} = \frac{\delta_n^T \hat{W}^T \Upsilon \phi}{W_N} tr\{\hat{W}^T \hat{W}\} \leq \frac{\delta_n^T \hat{W}^T \Upsilon \phi}{W_N} \left( \frac{1}{2} tr\{W^{*T} W^*\} - \frac{1}{2} W_N \right) \leq 0$$

(b) If  $\dot{\hat{W}} = \Upsilon \phi \delta_n^T$ , we have  $V_{tr2} = 0$ . ■

Substituting (6.30) into (6.27), the time derivative of Lyapunov candidate function becomes

$$\begin{aligned} \dot{V} &\leq -\delta_c^T K_1 \delta_c - \|\delta_c\| \|\delta_n\| |\eta| - K_2 \|\delta_c\| \|\delta_n\| - \delta_c^T \xi - \delta_c^T \tau_{dc} + \|\delta_n\| \varepsilon_T \\ &\quad - \frac{\|\delta_n\|^2}{\|\delta_n\| + \mu} \kappa - K_3 \|\delta_n\|^2 + (\kappa - \varepsilon_T) \dot{\kappa} \\ &= -\delta_c^T K_1 \delta_c - \|\delta_c\| \|\delta_n\| |\eta| - K_2 \|\delta_c\| \|\delta_n\| - \delta_c^T \xi - K_3 \|\delta_n\|^2 - \delta_c^T \tau_{dc} + \|\delta_n\| \varepsilon_T \\ &\quad + (\kappa - \varepsilon_T) \left( \dot{\kappa} - \frac{\|\delta_n\|^2}{\|\delta_n\| + \mu} \right) - \frac{\|\delta_n\|^2}{\|\delta_n\| + \mu} \varepsilon_T \\ &\leq -\delta_c^T K_1 \delta_c - \|\delta_c\| \|\delta_n\| |\eta| - K_2 \|\delta_c\| \|\delta_n\| - \delta_c^T \xi - K_3 \|\delta_n\|^2 - \delta_c^T \tau_{dc} + \|\delta_n\| \varepsilon_T \\ &\quad - \frac{\|\delta_n\|^2}{\|\delta_n\| + \mu} \varepsilon_T \\ &= -\delta_c^T K_1 \delta_c - \|\delta_c\| \|\delta_n\| |\eta| - K_2 \|\delta_c\| \|\delta_n\| - \delta_c^T \xi - K_3 \|\delta_n\|^2 - \delta_c^T \tau_{dc} + \frac{\|\delta_n\| \mu \varepsilon_T}{\|\delta_n\| + \mu} \\ &\leq -\delta_c^T K_1 \delta_c - \|\delta_c\| \|\delta_n\| |\eta| - K_2 \|\delta_c\| \|\delta_n\| - \delta_c^T \xi - K_3 \|\delta_n\|^2 - \delta_c^T \tau_{dc} + \mu \varepsilon_T \\ &\leq K_1 \|\delta_c\|^2 - K_3 \|\delta_n\|^2 - \delta_c^T \xi - \delta_c^T \tau_{dc} + \mu \varepsilon_T \\ &= -\|\delta\|^T K \|\delta\| - \delta_c^T \xi - \delta_c^T \tau_{dc} + \mu \varepsilon_T \end{aligned} \tag{6.31}$$

where  $K = \begin{bmatrix} K_1 & 0 \\ 0 & K_3 \end{bmatrix}$ .

When no disturbance exerts on the collocated subsystem ( $\tau_{dc} = 0$ ), i.e., the system is only subject to unmatched disturbances, we design the collocated robust compensator as  $\xi = 0$  and integrate both sides of (6.31) from  $t = 0$  to  $t = T$  as

$$V(T) - V(0) \leq - \int_0^T \|\delta\|^T K \|\delta\| dt + \varepsilon_T \int_0^T \mu dt \quad (6.32)$$

Considering that  $V(T) \geq 0$  and  $\int_0^\infty \mu dt < \infty$ , we have

$$\lim_{T \rightarrow \infty} \sup \frac{1}{T} \int_0^T \|\delta\|^2 dt \leq \frac{1}{K} \left( V(0) + \varepsilon_T \int_0^T \mu dt \right) \lim_{T \rightarrow \infty} \frac{1}{T} = 0 \quad (6.33)$$

From the definition of Lyapunov function  $V$  in (6.26) and  $\dot{V}$  derived from (6.31)-(6.33), the global uniform boundedness of the filtered tracking error  $\delta_c$  for collocated subsystem and  $\delta_n$  for non-collocated subsystem, the parameter estimation error  $\tilde{W}$  are guaranteed. From the definition and assumption 1 of filtered tracking error  $\delta$ , it is evident that  $\delta$  is bounded. The boundedness of control input is obvious from (6.25). It can be concluded that since  $\delta = [\delta_c \ \delta_n]^T \in L_2^n \cap L_\infty^n$ ,  $\delta_c$  and  $\delta_n$  are continuous and  $\delta_c \rightarrow 0, \delta_n \rightarrow 0$  as  $t \rightarrow \infty$ , and  $\eta \in L_\infty$ . From (6.25c), it can be shown that  $\tilde{\alpha}_c \in L_\infty^p$ . This in turn implies, based on property 6.1 and (6.22), that  $\dot{\delta} \in L_\infty^n$ ,  $\ddot{q} = [\ddot{q}_c \ \ddot{q}_n]^T \in L_\infty^n$  and  $\tilde{q} = [\tilde{q}_c \ \tilde{q}_n]^T \in L_\infty^{2n}$ . Therefore,  $\tilde{q}_c$  and  $\tilde{q}_n$  are uniformly continuous and  $\tilde{q} = [\tilde{q}_c \ \tilde{q}_n]^T \in L_\infty^{2n}$ , it is evident that  $\tilde{q} \rightarrow 0$  as  $t \rightarrow \infty$ .

**Remark 6.3.** One of the novelties of this chapter is the design and introduction of auxiliary control variable  $\eta$  with the governing function in (6.25d) to map the non-collocated subset and enhance the robustness. It is noted that in the literature of control of UMSs, attentions have been extensively paid to find implicit control trajectory/action to indirectly control the passive dynamics, such as (Fang et al., 2012; M. Huang et al., 2010; Yang et al., 2013; X. Zhang et al., 2014). However, this work designs  $\eta$  to overcome the underactuated properties.

**Remark 6.4.** The NNs is adopted to approximate the unmatched system uncertainties, the adaptive control algorithm is constructed to estimate the NN approximation error and the bounded unmatched disturbance. The combination of variable structure control, NN approximation and adaptive approach makes the constructed new

controller more robust, and such errors resulting from trajectory tracking, parameter uncertainties, unmatched external disturbances as well as NN approximation are compensated.

For the case  $\tau_{dc} \neq 0$  and  $\|\tau_{dc}\| < \beta_m$ , i.e. the system is subject to both matched and unmatched disturbances, one can only conclude that  $\delta$  is bounded from (6.26) and (6.31), but  $\tilde{\alpha}_c$  and  $\tilde{W}$  may tend to be unbounded since (6.31) only contains a negative definite component of  $\|\delta\|^2$  and no negative terms of  $\tilde{\alpha}_c$  and  $\tilde{W}$  are apparently included. Hence, the system may become unstable. To improve the robustness of Theorem 1, the following adaptation algorithm is therefore proposed.

**Adaptation Algorithm 6.2.** Consider the following algorithm for the adaptation law  $\hat{\alpha}_c$

$$\dot{\hat{\alpha}}_c = -\Gamma' \tilde{\alpha}_c - \Gamma Y_c \delta_c \quad (6.34)$$

**Corollary 6.2.** For the error equation (6.22) with sliding surface designed in (6.20) under the adaptive NNs-based control law in (6.25), the following proposition holds: If adaptation algorithm 6.2 is adopted, the system error signals  $\tilde{q}$ ,  $\dot{\tilde{q}}$  and  $\tilde{\alpha}$  converge to zero asymptotically. If  $\tau_{dc} \neq 0$  and  $\|\tau_{dc}\| < \beta_m$ , the system becomes globally uniformly ultimately stable and the boundedness depends on  $\tau_{dc}$ .

**Proof.** Adopting *Adaptation Algorithm 6.2* in the derivative of Lyapunov candidate function (6.27), we have

$$\begin{aligned} \dot{V} &= [\delta_c^T \ \delta_n^T] \left[ \begin{array}{c} -K_1 \delta_c - Y_c \tilde{\alpha}_c - \text{sgn}(\delta_c) \|\delta_n\| |\eta| - K_2 \text{sgn}(\delta_c) \|\delta_n\| - \xi \\ W^T \phi + \varepsilon \end{array} \right] - \delta^T \tau_d \\ &\quad + \dot{\hat{\alpha}}_c^T \Gamma^{-1} \tilde{\alpha}_c + \text{tr} \left\{ \tilde{W}^T \Upsilon^{-1} \dot{\tilde{W}} \right\} + \eta^{\frac{-1}{2n+1}} \dot{\eta} + (\kappa - \varepsilon_T) \dot{\kappa} \\ &= -\delta_c^T K_1 \delta_c - \|\delta_c\| \|\delta_n\| |\eta| - K_2 \|\delta_c\| \|\delta_n\| - \delta_c^T \xi - \delta_c^T \tau_{dc} + \delta_n^T (\varepsilon - \tau_{dn}) \\ &\quad - \frac{\|\delta_n\|^2}{\|\delta_n\| + \mu} \kappa - K_3 \|\delta_n\|^2 + \text{tr} \left\{ \tilde{W}^T \Upsilon^{-1} (\dot{\tilde{W}} + \Upsilon \delta_n^T \phi) \right\} + (\kappa - \varepsilon_T) \dot{\kappa} \\ &\quad - \tilde{\alpha}_c^T \Gamma' \Gamma^{-1} \tilde{\alpha}_c \end{aligned}$$

$$\begin{aligned}
 &\leq -\delta_c^T K_1 \delta_c - \|\delta_c\| \|\delta_n\| |\eta| - K_2 \|\delta_c\| \|\delta_n\| - \delta_c^T \xi - \delta_c^T \tau_{dc} + \|\delta_n\| \varepsilon_T - \frac{\|\delta_n\|^2}{\|\delta_n\| + \mu} \kappa \\
 &\quad - K_3 \|\delta_n\|^2 + \text{tr} \left\{ \tilde{W}^T \Upsilon^{-1} (\dot{\tilde{W}} + \Upsilon \delta_n^T \phi) \right\} + (\kappa - \varepsilon_T) \dot{\kappa} - \tilde{\alpha}_c^T \Gamma' \Gamma^{-1} \tilde{\alpha}_c \\
 &\leq -\delta_c^T K_1 \delta_c - \|\delta_c\| \|\delta_n\| |\eta| - K_2 \|\delta_c\| \|\delta_n\| - \delta_c^T \xi - K_3 \|\delta_n\|^2 - \delta_c^T \tau_{dc} + \mu \varepsilon_T \\
 &\quad - \tilde{\alpha}_c^T \Gamma' \Gamma^{-1} \tilde{\alpha}_c
 \end{aligned} \tag{6.35}$$

$$\begin{aligned}
 \dot{V} &\leq -K_1 \|\delta_c\|^2 - K_3 \|\delta_n\|^2 - \Gamma' \Gamma^{-1} \|\tilde{\alpha}_c\|^2 - \delta_c^T \xi - \delta_c^T \tau_{dc} + \mu \varepsilon_T \\
 &= -\|\delta'\|^T K' \|\delta'\| - \delta_c^T \xi - \delta_c^T \tau_{dc} + \mu \varepsilon_T
 \end{aligned} \tag{6.36}$$

where  $K' = \text{diag}[K_1, K_3, \Gamma' \Gamma^{-1}]$  and  $\delta' = [\delta_c, \delta_n, \tilde{\alpha}_c]^T$ .

It is evident that  $\Gamma' \Gamma^{-1}$  is a positive definite diagonal matrix since  $\Gamma'$  and  $\Gamma^{-1}$  are positive definite diagonal matrix.

**Case 6.1.** For the case when  $\tau_{dc} = 0$ , design the collocated robust compensator as  $\xi = 0$  and integrate both sides of (6.36) from  $t = 0$  to  $t = T$  as

$$V(T) - V(0) \leq -\int_0^T \|\delta'\|^T K' \|\delta'\| dt + \varepsilon_T \int_0^T \mu dt \tag{6.37}$$

Considering that  $V(T) \geq 0$  and  $\int_0^\infty \mu dt < \infty$ , we have

$$\lim_{T \rightarrow \infty} \sup \frac{1}{T} \int_0^T \|\delta'\|^2 dt \leq \frac{1}{K'} \left( V(0) + \varepsilon_T \int_0^T \mu dt \right) \lim_{T \rightarrow \infty} \frac{1}{T} = 0 \tag{6.38}$$

**Case 6.2.** For the case when  $\tau_{dc} \neq 0$  and  $\|\tau_{dc}\| < \beta_m$ , the collocated robust compensator  $\xi$  is designed to satisfy the following conditions

$$\begin{cases} \delta_c^T \xi \geq 0 \\ \beta_m \|\delta_c\| - \delta_c^T \xi \leq \rho \end{cases} \tag{6.39}$$

where  $\beta_m$  is the upper bound of  $\tau_{dc}$  and  $\rho$  is a positive design scalar.

**Theorem 6.2.** Consider following control laws to the uncertain underactuated system

$$\tau = \tau_c + \tau_n \tag{6.40a}$$

$$\tau_c = Y_c \hat{\alpha}_c - K_1 \delta_c - \xi, \quad \tau_n = -\text{sgn}(\delta_c) \|\delta_n\| |\eta| - K_2 \text{sgn}(\delta_c) \|\delta_n\| \tag{6.40b}$$

with the *Adaptation Algorithm 6.2* designed in (6.34), and the collocated robust compensator  $\xi$  designed using hyperbolic tangent function as

$$\xi = \beta_m \tanh\left(\frac{\eta_r \beta_m \delta_c}{\rho}\right) \quad (6.40c)$$

with  $\eta_r$  is a gain constant chosen as  $\eta_r = 0.2785$  here, and the auxiliary input  $\eta$  in (6.40b) is constructed as

$$\dot{\eta} = \eta^{\frac{1}{2n+1}} (-K_3 \|\delta_n\|^2 - \|\delta_n\| \widehat{W}^T \phi) \quad (6.40d)$$

with the adaptation law for  $\widehat{W}$  based on the projection algorithm, given by

$$\begin{aligned} \dot{\widehat{W}} &= -\dot{\widehat{W}} \\ &= \begin{cases} Y\phi\delta_n^T - \beta Y\|\delta_n\|\widehat{W} - \frac{\delta_n^T \widehat{W}^T Y\phi\widehat{W}}{W_N}, & \text{if } \text{tr}\{\widehat{W}^T \widehat{W}\} = W_N \text{ and } \delta_n^T \widehat{W}^T \phi \leq 0; \\ Y\phi\delta_n^T - \beta Y\|\delta_n\|\widehat{W}, & \text{if } \text{tr}\{\widehat{W}^T \widehat{W}\} < W_N \text{ or if } \text{tr}\{\widehat{W}^T \widehat{W}\} = W_N \text{ and } \delta_n^T \widehat{W}^T \phi > 0. \end{cases} \end{aligned} \quad (6.40e)$$

Then it follows:

- (1)  $\text{tr}\{\widehat{W}^T \widehat{W}\} \leq W_N$  holds.
- (2) All signals in the collocated and non-collocated systems are UUB.

**Proof.** Consider the following candidate Lyapunov function

$$V = \frac{1}{2} \delta^T D \delta + \frac{1}{2} \tilde{\alpha}_c^T \Gamma^{-1} \tilde{\alpha}_c + \frac{1}{2} \text{tr}\{\tilde{W}^T \Upsilon^{-1} \tilde{W}\} + \frac{2n+1}{2n} \eta^{\frac{2n}{2n+1}} \quad (6.41)$$

The derivative of Lyapunov candidate function is given by

$$\begin{aligned} \dot{V} &= [\delta_c^T \ \delta_n^T] \begin{bmatrix} -K_1 \delta_c - Y_c \tilde{\alpha}_c - \text{sgn}(\delta_c) \|\delta_n\| |\eta| - K_2 \text{sgn}(\delta_c) \|\delta_n\| - \xi \\ W^T \phi + \varepsilon \end{bmatrix} - \delta^T \tau_d \\ &\quad + \dot{\tilde{\alpha}}_c^T \Gamma^{-1} \tilde{\alpha}_c + \text{tr}\{\tilde{W}^T \Upsilon^{-1} \dot{\tilde{W}}\} + \eta^{\frac{-1}{2n+1}} \dot{\eta} \\ &= -\delta_c^T K_1 \delta_c - \|\delta_c\| \|\delta_n\| |\eta| - K_2 \|\delta_c\| \|\delta_n\| - \delta_c^T \xi - \delta_c^T \tau_{dc} + \delta_n^T (\varepsilon - \tau_{dn}) \\ &\quad - K_3 \|\delta_n\|^2 + \text{tr}\{\tilde{W}^T \Upsilon^{-1} (\dot{\tilde{W}} + Y \delta_n^T \phi)\} - \tilde{\alpha}_c^T \Gamma^{-1} \tilde{\alpha}_c \end{aligned}$$

$$\begin{aligned}
 &\leq -\delta_c^T K_1 \delta_c - \|\delta_c\| \|\delta_n\| |\eta| - K_2 \|\delta_c\| \|\delta_n\| - \delta_c^T \xi - \delta_c^T \tau_{dc} + \|\delta_n\| \varepsilon_T - K_3 \|\delta_n\|^2 \\
 &\quad + \text{tr}\{\tilde{W}^T \Upsilon^{-1} (-\Upsilon \phi \delta_n^T + \beta \Upsilon \|\delta_n\| \hat{W} + \Upsilon \delta_n^T \phi)\} - \tilde{\alpha}_c^T \Gamma' \Gamma^{-1} \tilde{\alpha}_c \\
 \dot{V} &\leq -\delta_c^T K_1 \delta_c - K_3 \|\delta_n\|^2 - \Gamma' \Gamma^{-1} \|\tilde{\alpha}_c\|^2 + \beta \|\delta_n\| \text{tr}\{\tilde{W}^T (W - \tilde{W})\} - \delta_c^T \xi - \delta_c^T \tau_{dc} \\
 &\quad + \delta_n^T \varepsilon_T
 \end{aligned} \tag{6.42}$$

Let us decompose (6.42) into the following functions

$$\dot{V}_1 = -K_3 \|\delta_n\|^2 + \beta \|\delta_n\| \text{tr}\{\tilde{W}^T (W - \tilde{W})\} + \delta_n^T \varepsilon_T \tag{6.43a}$$

$$\dot{V}_2 = -\Gamma' \Gamma^{-1} \|\tilde{\alpha}_c\|^2 - \delta_c^T K_1 \delta_c - \delta_c^T \tau_{dc} - \delta_c^T \xi \tag{6.43b}$$

We have

(1) For  $\dot{V}_1$ , considering that

$$\text{tr}\{\tilde{W}^T (W - \tilde{W})\} = (\tilde{W}, W)_F - \|\tilde{W}\|_F^2 \leq \|\tilde{W}\|_F \|W\|_F - \|\tilde{W}\|_F^2 \tag{6.44}$$

Substituting (6.44) into (6.43a), we have

$$\begin{aligned}
 \dot{V}_1 &\leq -\lambda_{\min}(K_3) \|\delta_n\|^2 + \beta \|\delta_n\| \|\tilde{W}\|_F (W_{\max} - \|\tilde{W}\|_F) + \varepsilon_T \|\delta_n\| \\
 &= -\|\delta_n\| (\lambda_{\min}(K_3) \|\delta_n\| + \beta \|\tilde{W}\|_F (\|\tilde{W}\|_F - W_{\max})) - \varepsilon_T
 \end{aligned}$$

Since

$$\begin{aligned}
 &\lambda_{\min}(K_3) \|\delta_n\| + \beta \|\tilde{W}\|_F (\|\tilde{W}\|_F - W_{\max}) - \varepsilon_T \\
 &= \beta \left( \|\tilde{W}\|_F - \frac{W_{\max}}{2} \right)^2 - \beta \frac{W_{\max}^2}{4} + \lambda_{\min}(K_3) \|\delta_n\| - \varepsilon_T
 \end{aligned} \tag{6.45}$$

To guarantee  $\dot{V}_1 \leq 0$ , the following inequality needs to be satisfied

$$\|\delta_n\| > \frac{\beta W_{\max}^2 + 4\varepsilon_T}{4\lambda_{\min}(K_3)} \quad \text{or} \quad \|\tilde{W}\|_F > \frac{W_{\max}}{2} + \sqrt{\frac{W_{\max}^2}{4} + \frac{\varepsilon_T}{\beta}} \tag{6.46}$$

Therefore,  $\dot{V}_1$  is negative outside a compact set. Based on the standard Lyapunov theorem extension, the UUB of both  $\delta_n$  and  $\|\tilde{W}\|_F$  are demonstrated.

Through (6.43b), the time derivative of  $V_2$  can be given by

$$\dot{V}_2 \leq -\Gamma'\Gamma^{-1}\|\tilde{\alpha}_c\|^2 - \delta_c^T K_1 \delta_c + \beta_m \|\delta_c\| - \delta_c^T \xi \quad (6.47)$$

Based on the above knowledge of the design requirement (6.39), the definition of  $V$  and  $\dot{V}_2$ , as well as the assumption of boundedness of neural network weight, we substitute the collocated robust compensator (6.40c) into (6.43b), yields

$$\begin{aligned} \dot{V}_2 &\leq -\Gamma'\Gamma^{-1}\|\tilde{\alpha}_c\|^2 - \delta_c^T K_1 \delta_c + \rho \\ &= -\vartheta^T K_4 \vartheta + \rho \\ &\leq -\lambda_{\min}(K_4)\|\vartheta\|^2 + \rho \end{aligned} \quad (6.48)$$

where  $K_4 = \text{diag}\{\Gamma'\Gamma^{-1}, K_1\}$  and  $\lambda_{\min}(K_4)$  is the minimum eigenvalue of matrix  $K_4$ . Therefore  $\dot{V}_2$  is strictly negative outside the following compact set  $\Sigma_\vartheta$ :

$$\Sigma_\vartheta = \left\{ \vartheta(t) \mid 0 \leq \|\vartheta\| \leq \sqrt{\frac{\rho}{\lambda_{\min}(K_4)}} \right\} \quad (6.49)$$

Therefore, it is concluded that filtered tracking error  $\delta_c$  for collocated subsystem and  $\delta_n$  for non-collocated subsystem, the parameter estimation error  $\tilde{W}$  are the uniformly ultimately bounded. The tracking error of collocated subsystem decreases whenever  $\vartheta$  is outside the compact set  $\Sigma_\vartheta$ , and thus  $\|\vartheta\|$  is UUB. Considering that all the signals involved in the controller (6.40) are UUB, it is therefore concluded that the control input (6.40) is uniformly ultimately bounded.

## 6.4 Simulation Studies

### 6.4.1 2-DOF Underactuated Manipulator

To verify the effectiveness of the proposed control algorithms, simulation is firstly conducted from the case study of an underactuated manipulator as shown in Figure 6.2. The two-link planar manipulator has its first link actuated and the second link

unactuated. Link 1 and link 2 are connected by two revolute joints, and link 1 is able to rotate 360 degrees in the horizontal plane.

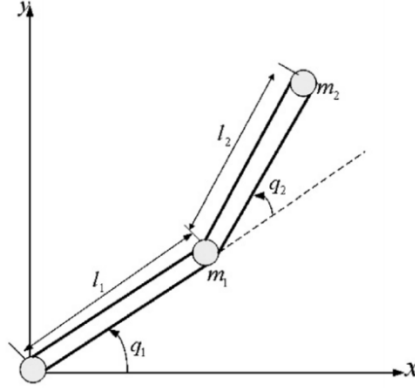


Figure 6.2 The planar underactuated manipulator with two revolute joints

For the link  $i, i = 1, 2$ ,  $q_i$  denotes the joint angle and serves as the generalized coordinate,  $m_i$  and  $l_i$  are the mass and length, respectively.  $l_{ci}$  represents the distance from the previous joint to the COM of link  $i$ ,  $I_i$  is the moment of inertia about the axis coming out of the page and coming through the COM of link  $i$ .

The equation of motion can be derived using Lagrange's approach, gives

$$D(q)\ddot{q} + C(q, \dot{q})\dot{q} + G(q) + F_v\dot{q} + F_c(q, \dot{q}) + \tau_d = \tau \quad (6.50)$$

where

$$D(q) = \begin{bmatrix} m_1 l_{c1}^2 + m_2 (l_1^2 + l_{c2}^2 + 2l_1 l_{c2} \cos q_2) + I_1 + I_2 & m_2 (l_{c2}^2 + l_1 l_{c2} \cos q_2) + I_2 \\ m_2 (l_{c2}^2 + l_1 l_{c2} \cos q_2) + I_2 & m_2 l_{c2}^2 + I_2 \end{bmatrix},$$

$$C(q, \dot{q}) = \begin{bmatrix} -m_2 l_1 l_{c2} \sin q_2 \dot{q}_2 & -m_2 l_1 l_{c2} \sin q_2 (\dot{q}_1 + \dot{q}_2) \\ m_2 l_1 l_{c2} \sin q_2 \dot{q}_1 & 0 \end{bmatrix},$$

$$G(q) = \begin{bmatrix} (m_1 l_{c1} + m_2 l_1) g \cos q_1 + m_2 l_{c2} g \cos(q_1 + q_2) \\ m_2 l_{c2} g \cos(q_1 + q_2) \end{bmatrix},$$

$$F_v \dot{q} + F_c(q, \dot{q}) = \begin{bmatrix} f_{v1} \dot{q}_1 + c_1 \operatorname{sgn}(\dot{q}_1) \\ f_{v2} \dot{q}_2 + c_2 \operatorname{sgn}(\dot{q}_2) \end{bmatrix}, \quad \tau_d = \begin{bmatrix} a_1 \sin(t) \\ a_2 \sin(t) \end{bmatrix}, \quad \tau = \begin{bmatrix} \tau_1 \\ 0 \end{bmatrix}.$$

It is assumed that the moments of inertia are calculated in the form of  $I_i = \frac{m_i l_i^2}{12}$ .

The unknown parameters are chosen as  $\alpha_1 = m_1 l_{c1}^2 + m_2 (l_1^2 + l_{c2}^2) + I_1 + I_2$ ,  $\alpha_2 = m_2 l_1 l_{c2}$ ,  $\alpha_3 = m_2 l_{c2}^2 + I_2$ ,  $\alpha_4 = m_1 l_{c1} + m_2 l_1$ ,  $\alpha_5 = m_2 l_{c2}$ , then the uncertain parameter is  $\alpha = [\alpha_1 \alpha_2 \alpha_3 \alpha_4 \alpha_5]^T \in R^5$ . Based on the auxiliary kinematic vector variables defined in (6.20), the collocated regressor  $Y_c$  is therefore obtained as  $Y_c = [-\dot{q}_1 Y_{c2} - \dot{q}_2 - g \cos q_1 - g \cos(q_1 + q_2)]$  with  $Y_{c2} = -(2 \cos q_2 \dot{q}_1 + \cos q_2 \dot{q}_2 - \dot{q}_2 \varrho_1 \sin q_2 - \sin q_2 (\dot{q}_1 + \dot{q}_2) \varrho_2)$ .

Generically, the adaptive NN-based tracking control scheme in (6.40) is evaluated in the presence of matched and unmatched uncertainties. The rationality of selection of the system parameter values of the manipulator in the simulation are configured from studies in literature as reported in (Pucci et al., 2015) as follows:  $m_1 = m_2 = 2Kg$ ,  $I_1 = I_2 = 0.2528Kgm^2$ ,  $l_{c1} = l_{c2} = 0.75m$ ,  $l_1 = l_2 = 1.5m$ . The initial conditions are set as  $q(0) = [q_1(0) q_2(0)]^T = [0.09 - 0.09]^T$ ,  $\dot{q}(0) = [\dot{q}_1(0) \dot{q}_2(0)]^T = [0 0]^T$ , and the reference trajectory is given as  $q_{1d}(t) = 0.5\pi(1 + \sin(0.1t))$  (Pucci et al., 2015).

The parameter values of friction and disturbance are chosen as  $c_1 = c_2 = 0.02$ ,  $a_1 = a_2 = 0.2$ . The bandwidth of the first-order filter is set as  $\Lambda = [\Lambda_1 \Lambda_2]^T = [12 30]^T$ . In the simulation, the controller parameters are chosen to be  $K_1 = 2I$ ,  $K_2 = 5I$  and  $K_3 = 20I$ . The adaptation gains are chosen as  $\Gamma' = 8I$  and  $\Gamma = 4I$ . Parameter values for the collocated robust compensator are set as  $\beta_m = 20$ ,  $\rho = 0.5$ . In addition, the weight tuning parameter of the proposed control system are selected as  $\Upsilon = 0.005$  and  $\beta = 0.1$ . The selection of the parameters is based on iterative simulations.

The simulation results of trajectory tracking performance of the adaptive NN-based control system (6.40) are shown in Figures 6.3 to 6.8 with time-varying matched and unmatched disturbances. The reference trajectory (red solid line), the tracking trajectory performance of joint 1 (blue dashed line) in Figure 6.3, the trajectory of joint 2 in Figure 6.4, the trajectory tracking error in Figure 6.5, the control torque in Figure 6.6, the NN approximation performance in Figures 6.7 and 6.8 are portrayed. We can see that the proposed approach demonstrates good

performance under the effects of the model uncertainties, frictions and time-varying external disturbances. It can be observed that the system tracks the reference trajectory accurately and the tracking error converges to a quite small and bounded compact set near zero in finite time from Figure 6.5 and the NNs approximate the nonlinear uncertainties  $\chi(z)$  effectively from Figure 6.7. From the simulation studies, we can draw a conclusion that the proposed control scheme has the ability to adapt model uncertainties and is robust against matched and unmatched external disturbances.

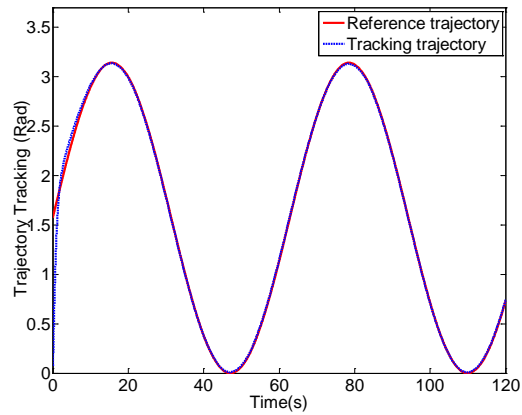


Figure 6.3 Trajectory tracking performance of joint 1

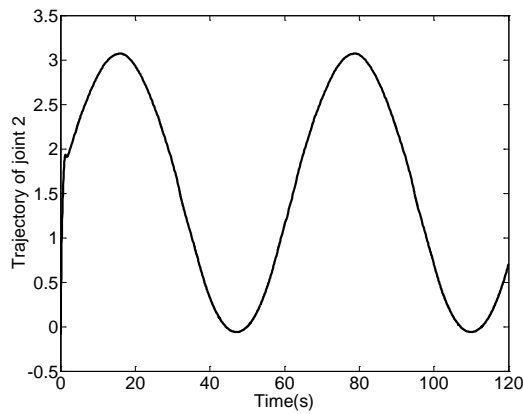


Figure 6.4 Trajectory tracking performance of joint 2

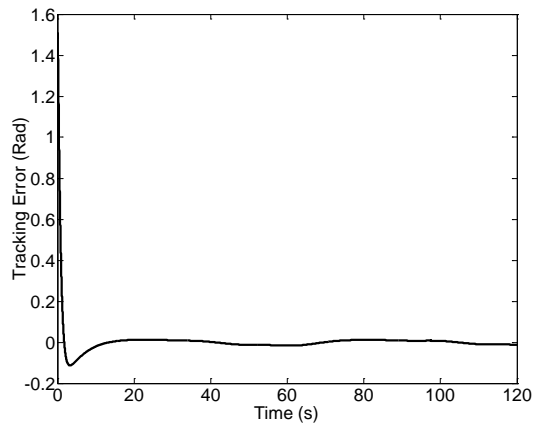


Figure 6.5 Trajectory tracking error of joint 1

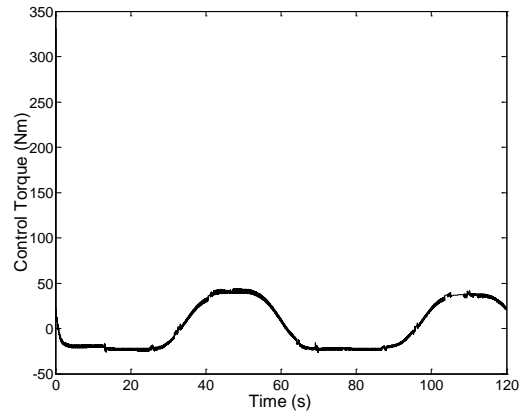


Figure 6.6 Control torque

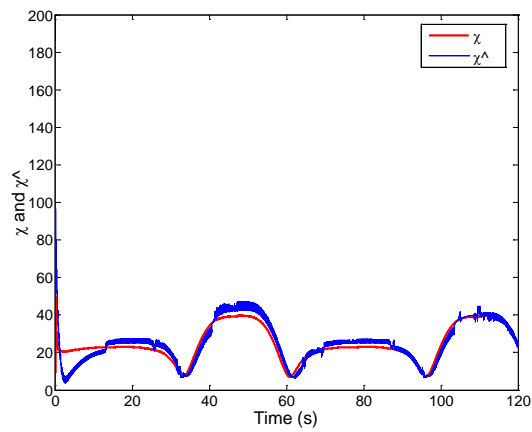


Figure 6.7  $\chi(z)$  and  $\hat{\chi}(z)$

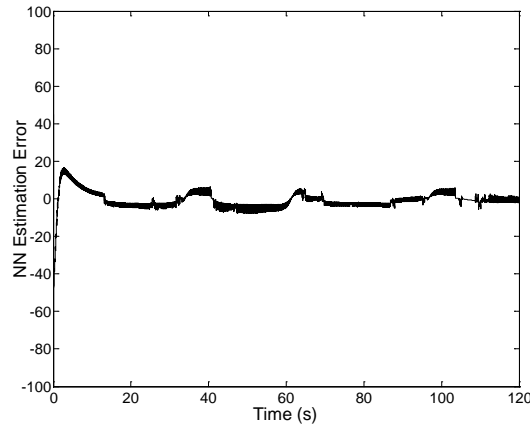


Figure 6.8 NN approximation error

### 6.4.2 2-DOF Underactuated VDC System

The case study in Subsection 6.4.1 considers an underactuated manipulator with its base mounted on the working surface under uncertain dynamics and environmental disturbances. The underactuated dynamics of the second link and the actuated dynamics of the first link are coupled in such a way that the unmodeled motions of the second link contribute additional time-varying inertia and nonlinearity to the description of the manipulator dynamics. In this subsection, we consider the context of a mobile robotic model proposed in the thesis—the underactuated VDC system as shown in Figure 4.2 for which the actuated and unactuated dynamics are strongly coupled.

In the presence of matched and unmatched external disturbances, the underactuated dynamics of the VDC model are given based on the derivations discussed in Chapter 4, we have

$$D(q)\ddot{q} + C(q, \dot{q})\dot{q} + K(q)q + G(q) + F + \tau_d = Bu \quad (6.51)$$

where  $D(q) = \begin{bmatrix} ml^2 & -mlc_\theta \\ -mlc_\theta & (M+m) \end{bmatrix}$  is the inertia matrix,  $C(q, \dot{q}) = \begin{bmatrix} 0 & 0 \\ mls_\theta\dot{\theta} & 0 \end{bmatrix}$  denotes the Centripetal-Coriolis matrix,  $K(q) = \begin{bmatrix} k & 0 \\ 0 & 0 \end{bmatrix}$  is the generalized stiffness matrix,  $G(q) = [-mgl s_\theta \ 0]^T$  represents the gravitational torques,  $F = [c\dot{\theta} \ f]^T$  is

the friction forces,  $\tau_d = [\tau_{dc} \ \tau_{dn}]^T = \begin{bmatrix} a_1 \sin(t) \\ a_2 \sin(t) \end{bmatrix}$  denotes the external matched and unmatched disturbances,  $B = [1 \ 0]^T$  is the input force matrix,  $u \in \mathcal{R}^1$  denotes the control input applied to the system.

In the simulation, the rationality of the parameter values selection in this section is specified as follows: the system parameter values are configured from the studies in literature as reported in (Li et al., 2006; Y. Liu et al., 2008, 2011) as  $M = 0.5 \text{ kg}$ ,  $m = 0.138 \text{ kg}$ ,  $l = 0.3 \text{ m}$ ,  $g = 9.81 \text{ m/s}^2$ ,  $\mu = 0.01 \text{ N/ms}$ . The initial conditions are set as  $\theta(0) = \theta_0 = \pi/3$ ,  $\dot{\theta}(0) = 0$ ,  $x(0) = 0$  and  $\dot{x}(0) = 0$ . The simulation is conducted in 6.6s which is one full motion cycle. The parameter values for the matched and unmatched external disturbances from the environments on the system are chosen as  $a_1 = a_2 = 0.2$ . The bandwidth of the first-order filter is set as  $\Lambda = [\Lambda_1 \ \Lambda_2]^T = [15 \ 20]^T$ . In the simulation, the controller parameters are chosen to be  $K_1 = 10I$ ,  $K_2 = 20I$  and  $K_3 = 50I$ . The adaptation gains are chosen as  $\Gamma' = 10I$  and  $\Gamma = 6I$ . Parameter values for the collocated robust compensator are set as  $\beta_m = 20$ ,  $\rho = 0.5$ . In addition, the weight tuning parameter of the proposed control system are selected as  $\Upsilon = 0.005$  and  $\beta = 0.1$ . The rationality of these selections is configured using iterative simulations. The reference trajectory for the actuated subsystem is chosen as the planned trajectory in (4.14) of Chapter 4.

The tracking performance of the actuated subsystem is shown in Figure 6.9, from which we see that, although the response of the proposed controller is slightly slower, the controlled pendulum trajectory tracks the desired trajectory. The response is due to the learning process of the adaptive controller to make the estimated parameters adapt to appropriate values. The tracking error is shown in Figure 6.10, from which the tracking error converges to a quite small and bounded compact set near zero in finite time. The trajectory of the VDC system is presented in Figure 6.11 that shows the cart travels at the speed about 7cm within 6.6s. The control torque is shown in Figure 6.12 that demonstrates the boundedness of the torque input. As clearly shown by the simulation results, in the presence of unknown system parameters and external disturbances, the proposed NN adaptive control scheme can guarantee exact tracking of the pendulum subsystem, while the cart subsystem is able to maintain a forward

velocity at some desired level. Therefore, the proposed control scheme is efficient in the presence of unknown nonlinear dynamic systems and environmental disturbances.

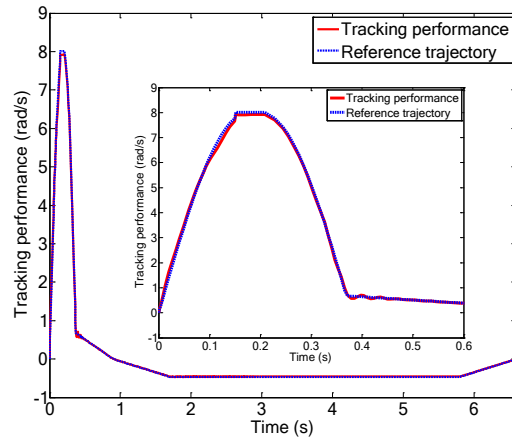


Figure 6.9 Trajectory tracking performance

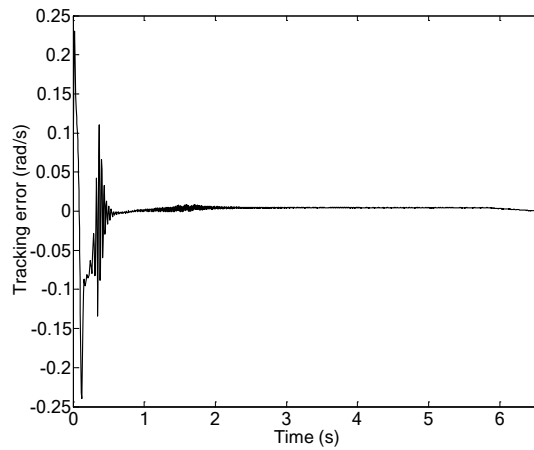


Figure 6.10 Trajectory tracking error

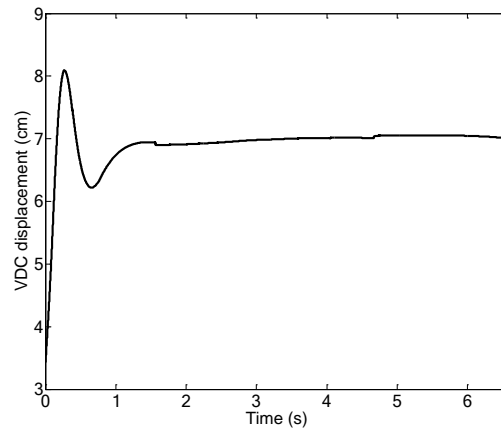


Figure 6.11 Performance of the VDC system

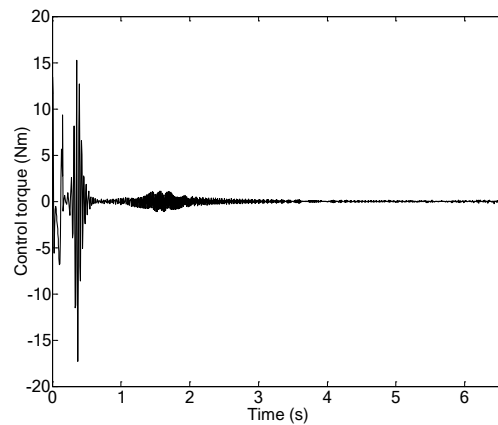


Figure 6.12 Control torque

## 6.5 Conclusions

This chapter proposed a systematic adaptive control scheme for a class of UMSs with matched and unmatched disturbances. Coping with the internal uncertain dynamics and external disturbances, adaptive neural network control schemes have been developed with an auxiliary control variable to enhance the robustness. RBF neural networks have been employed to approximate the nonlinearities in the non-collocated subset, the adaptive control algorithm has been constructed to estimate the neural networks approximation error and the bounded unmatched disturbance. The combination of variable structure control, NN approximation and adaptive approach makes the constructed new controller more robust, and such

errors resulting from trajectory tracking, parameter uncertainties, unmatched external disturbances as well as NN approximation are compensated. The simulation studies on an underactuated manipulator and an underactuated VDC system have shown the effectiveness of the proposed adaptive control systems.

# Chapter 7

## Conclusions and Future Works

### 7.1 Conclusions

This research has performed the investigations into underactuated mobile robotic systems towards trajectory planning, tracking control and analysis of dynamic interactions. The microrobotic systems proposed in this thesis have extensive fields of application working in restricted space and vulnerable media, such as minimally invasive sensing, diagnosis and intervention, medical endoscopy, engineering diagnosis, pipeline inspection, seabed exploration and disaster rescues.

Key techniques and three main principles related to energy efficacy, dynamic compliance interactions and adaptability have been investigated. Towards this end, this research has presented four elaborate studies: (1) design of a novel bio-inspired self-propelled robotic model with viscoelastic property; (2) control systems design of 2-DOF UMSs with underactuation one; (2) geometric analysis-based trajectory planning and control; (3) analysis and characterization of dynamic frictional interactions; and (4) adaptive neural network-based robust control systems. (1) was based on the coordinate transformation of the UMSs with PFL and PFL-free approach. The control problems of trajectory planning and tracking control of UMSs have been formulated. The control properties of partial integrability and complete integrability

of 2-DOF Class I, II UMSs have been investigated with some propositions. Subsequently, a trajectory planning scheme has been proposed for a class of UMSs with bio-inspired viscoelastic property based on the integrability. The planned motion trajectory is based on a rest-to-rest motion, wherein the unactuated subsystem is controlled by the planned trajectory of the actuated subsystem. Trajectory tracking control schemes have been proposed for UMSs with and without parametric uncertainties, respectively.

A benchmark model for underactuated microrobotic systems has been proposed in this thesis, together with a novel geometric analysis-based trajectory planning algorithm with considerations of bio-inspired viscoelastic property. The main idea is to reduce the complexity and to characterize the coupling by imposing a harmonic drive and then to compute the dynamics projection onto a hyper-manifold, such that the issue of trajectory planning is converted into geometric analysis and trajectory optimization. An analytical two-stage velocity trajectory has been developed based on the control indexes and dynamic constraints. A locomotion-performance index has been proposed and evaluated to identify the optimal viscoelastic parameters. The trajectory was optimally parameterized through rigorous analytical analysis. Nonlinear tracking controllers have been designed using collocated partial feedback linearization and variable structure control with an auxiliary control variable, respectively. For the sake of efficiency in progression and energy, the proposed method provides a novel approach in characterizing and planning motion trajectory for underactuated VDC systems such that the optimal locomotion can be achieved.

Towards underactuated vibro-driven capsule systems with bio-inspired viscoelastic property, this thesis proposed a novel method to analysis and characterise the dynamic frictional interactions. Up to now, most investigations in frictional interactions towards capsule systems were confined into static or quasi-dynamic circumstance, where it is difficult to facilitate online utilization and control. In this thesis, it is the first time the dynamic frictional characteristics (non-reversible drooping and hysteretic) have been studied towards the capsule systems. Primary attention was devoted to the modelling and characterization of frictional interaction

dynamics using a combined physics-based and analytical-based approach, in a manner that non-reversible characteristic for static friction, presliding as well as pure sliding regimes were revealed, and the frictional limit boundaries were identified. Subsequently, the studies were mainly focused on numerical analysis and comparison of friction-induced vibrational responses and qualitative changes triggered by the control parameters in capsule dynamics. It was found that the models predict periodic responses for the parameters considered and the average capsule velocity can be controlled through proper tuning of the control parameter around identified control points.

This thesis also proposed advanced control schemes for a class of UMSs with matched and unmatched disturbances. Coping with the internal uncertain dynamics and external disturbances, adaptive neural network control schemes have been developed with an auxiliary control variable to close the unactuated feedback loops. RBF neural networks was adopted to approximate the unmatched system uncertainties, the adaptive control algorithm has been constructed to estimate the neural networks approximation error and the bounded unmatched disturbance. The combination of variable structure control, NN approximation and adaptive approach makes the constructed new controller more robust, and such errors resulting from trajectory tracking, parameter uncertainties, unmatched external disturbances as well as NN approximation are compensated.

This thesis has demonstrated novel solutions in bio-inspired control for underactuated robotic systems in terms of energy efficacy, dynamic compliant interactions with the environment and adaptability. The rigorous theoretical analysis, analytical and numerical studies have validated the proposed schemes.

## **7.2 Aims and Objectives Revisited**

This research aimed to study the principles for energy efficacy, compliant dynamic interaction and adaptability of underactuated robotic systems from the perspectives of bio-inspired viscoelastic property and bio-inspired control approaches. This research has successfully proposed benchmark vibro-driven models for microrobotic

systems with bio-inspired viscoelastic property. The research has developed the trajectory planning algorithm and tracking control systems. It has performed elaborate analytical and simulation studies towards the formulated problems.

The objectives of the research are revisited individually as follows.

1. To investigate the state-of-art in the UMSs and bio-inspired approaches and identify the theoretical challenges and common difficulties: the state-of-art and challenges has been presented from Section 2.2 to Section 2.4 of Chapter 2, including the researches on modelling, bio-inspired design principles and bio-inspired motor/behaviour control approaches, periodic trajectory planning, and nonlinear control systems; The challenges have been identified in Section 2.5, which has focused on the optimal design with bio-inspired viscoelastic property, energy efficient underactuated operation/locomotion, dynamic coupling characterization with system performance, establishment of global controllability, planning of optimal motion trajectories, analysis and prediction of frictional interaction dynamics and dealing with uncertainties; The future trends and research directions have been summarized and presented.
2. To study control systems for UMSs with underactuation degree one using coordinate transformation and decoupling: The control system design has been studied in Sections 3.5 and 3.6 of Chapter 3. The control problems of UMSs have been formulated. The control properties of partial integrability and complete integrability of 2-DOF Class I, II UMSs have been investigated with some propositions.
3. To study the structural control properties of partial integrability and complete integrability of UMSs with underactuation degree one: the structural control properties of partial integrability and complete integrability have been studied in Section 3.4 for the ease of control systems construction.
4. To propose a novel self-propelled robotic model that draws inspirations from the biological systems: A bio-inspired robotic model has been proposed

inspired by undulatory locomotion of the nematode worm in Section 4.2.1 of Chapter 4.

5. To propose a novel and systematic algorithm for trajectory planning and control for a class of UMSs with bio-inspired viscoelastic property: The trajectory planning algorithm has been proposed in Section 4.4 of Chapter 4. The non-collocated dynamic constraints have been considered into the control indexes, wherein it was found that characterization of viscoelastic interaction plays vital role in the optimal control of stick-slip propulsion and the energy efficacy. The qualitative variation laws of the control parameters have been studied and identified through geometric and dynamic analysis. The dynamic coupling has been characterized through rigorous analysis on the Poincaré maps. The two-stage analytical motion trajectory has been constructed based on the control indexes and dynamic constraints, which have been evaluated analytically, and the trajectory has been optimized and parameterized via rigorous analysis. two trajectory tracking control schemes have been constructed in Section 4.5 of Chapter 4. A closed-loop feedback controller has been designed for the system with accurate model. An adaptive controller has been proposed for the system with unknown base parameters, wherein an auxiliary control variable is designed to closure the non-collocated feedback loop. Asymptotic stability and convergence of time-varying reference trajectories for the system dynamics have been shown by means of Lyapunov synthesis.
6. To design 3D models and develop the prototype of the proposed vibro-driven model, and to conduct preliminary experimental studies to verify the robotic model and motion principle: the 3D design of the vibro-driven system has been presented in Subsection 4.7.1, the experimental setup and preliminary experimental results have been given in Subsections 4.7.2 to 4.7.4, respectively. Some basic experiments have been conducted to demonstrate the locomotion of the system and validate the motion principles.
7. To perform combined physics-based and analytical analysis for the vibro-driven capsule system and develop mathematical model of the

frictional interaction dynamics: the dynamic frictional interactions have been studied using a combined physics-based and analytical-based approach in Subsection 5.2.3 of Chapter 5. Thereafter, the frictional limits for the static friction, presliding regime as well as pure sliding regime are identified. The mathematical model of the frictional interaction dynamics has been developed through the combined physics-based and analytical analysis and characterization of the interaction dynamics in Section 5.2 of Chapter 5.

8. To conduct analytical and numerical studies on the frictional interaction dynamic of the vibro-driven capsule system: The non-reversible characteristics of friction force (drooping and hysteresis) have been studied in Section 5.3 of Chapter 5. Dynamic analysis of the friction-driven vibrational responses is then conducted and the qualitative variations laws induced by the control parameter are identified. The analytical and numerical results have good agreements with the seminal findings in the literature. The proposed work is an advisable benchmark to exploit the challenges in friction compensation and control of underactuated micro-robotic systems.
9. To extends and encompasses the adaptive control schemes to stabilize the state space of a class of underactuated systems: The adaptive control systems have been designed using an auxiliary control variable and neural network-based approximation in Section 6.3. Asymptotic stability and convergence of time-varying reference trajectories for the system dynamics are shown by means of Lyapunov synthesis. Section 6.4 of Chapter 6 has presented the simulation studies on the trajectory tracking and NN estimation performance towards an underactuated manipulator case. The proposed approach has demonstrated good performance under the effects of the model uncertainties, frictions and time-varying external disturbances. It has been observed that the system tracks the reference trajectory accurately and the tracking error converges to zero in finite time.
10. To counteract matched and mismatched disturbances, and function approximation error of a class of underactuated systems: Robust compensators are designed in Section 6.3 to counteract matched and

mismatched disturbances, and function approximation error of NNs and nonlinear frictions. The tracking error can be reduced as small as desired in finite time by selecting appropriate controller parameters.

### 7.3 Future Works

Future works along the direction of this research are described as follows.

**Further studies towards trajectory planning and tracking control** In this research, geometric-analysis based trajectory planning algorithm and tracking control systems have been developed. The following future works can be conducted to improve the ‘intelligence’ of the trajectory generator and tracking performance of the controllers

1. Optimally on-line selection and tuning of the trajectory parameters. The proposed algorithm is off-line planning and tuning, therefore development of online selection and tuning algorithm can reduce the computation time and improve the tracking performance.
2. To improve the robustness of the control algorithm and the efficiency of underactuated locomotion, the investigation of the vibro-impact dynamics of the actuator and the system can be conducted through studying the parameter dependence and exploring new motion/propulsion mechanism.
3. To further investigate the bio-inspired morphological design strategies, analytical and experimental studies on bio-inspired viscoelastic property can be conducted, including optimization and identification.
4. Optimal selection and determination of parameter values of the adaptive controllers. There is no systematic approach for the optimal selection and determination of controller parameter values. Conventionally, they are chosen using iterative simulations, and thus a trade-off between system response and control torques should be made.

**Further experimentations and applications** Experimental implementation of the vibro-driven robotic models proposed in this research is an essential part of the

development and evaluation of the proposed system. It is also clearly necessary to identify the practical values and test the robustness capability of the proposed control algorithms in physical system. The effectiveness of the proposed algorithms is demonstrated using analytical studies and numerical simulations. Preliminary experimental works have been conducted in this study. Hence, it is important to verify the theory through further practical experiments, which is the motivation for this research. It is also of great significance to apply the design ideas and main findings to real environment applications, such as embedded the bio-inspired model into a capsule shell and conduct field tests in different environment. The future experimental works can be conducted in the following aspects:

1. Identification of the bio-inspired viscoelastic parameters and comparison with the theoretical studies in this research, including the coefficients of the elasticity and viscosity.
2. Trajectory tracking and real-time position feedback control of the robots on the surfaces with different friction coefficients, identification of the friction parameters. This will take into consideration of both the collocated subsystem (pendulum angle) and the non-collocated subsystem (cart displacement). To realise real-time implementation, an online optimal trajectory generator will be developed based on improvement of the proposed off-line trajectory control model. An evaluation of computational complexity of the proposed algorithm will be conducted through real-time implementation.
3. Trajectory tracking of the robots in the tubular environments such as the gas and water pipes to test the performance of the adaptive control systems.

# Appendix A

## A.1 Underactuated Mechanical Systems

### A.1.1 Lagrangian Mechanical Systems

The Euler-Lagrangian equation is a formalism providing fundamental laws to classical mechanical systems to describe how they move under the action of external forces, particularly towards the systematic representation of robotic dynamics (Arnold, 1989; Craig, 2005; Papastavridis, 2014; Spong et al., 2006). In terms of a classical mechanical system, the Lagrangian is expressed by the difference between kinetic energy and potential energy (Dutton et al., 1997),

$$L(q, \dot{q}) = T(q, \dot{q}) - V(q) = \frac{1}{2} \dot{q}^T D(q) \dot{q} - V(q) \quad (\text{A.1})$$

where  $q = [q_1, \dots, q_n]^T$  represent the generalized configuration vectors that belong to an  $n$ -dimensional configuration manifold  $Q$ ,  $\dot{q} = [\dot{q}_1, \dots, \dot{q}_n]^T$  are generalized velocities,  $D(q)$  is a symmetric and positive-definite matrix of inertias.  $T(q, \dot{q}) = \frac{1}{2} \dot{q}^T D(q) \dot{q}$  and  $V(q)$  denote the kinetic energy and potential energy of the mechanical system, respectively.

For an object system with  $n$ -DOF ( $n > 1$ ), the governing equation is given by

$$\frac{d}{dt} \frac{\partial L(q_i, \dot{q}_i)}{\partial \dot{q}_i} - \frac{\partial L(q_i, \dot{q}_i)}{\partial q_i} = (B(q)u)_i, \quad i = \{1, 2 \dots n\} \quad (\text{A.2})$$

where  $u = [u_1, \dots, u_k]^T$  denote the vector of  $k$  external forces applied on the systems.  $B(q)$  is the input force matrix and assumed to be of full column rank, together with  $B(q)u$  describing the generalized forces resulting from the control inputs  $u$ .

(Aneke, 2003; Olfati-Saber, 2000) rewrote (A.2) in an alternative way as

$$\sum_j d_{kj}(q)\ddot{q}_j + \sum_{ij} \Gamma_{ij}^k(q)\dot{q}_i \dot{q}_j + g_k(q) = p_k^T B(q)u \quad (\text{A.3})$$

where  $k = 1, 2, \dots, n$ ,  $p_k$  is the  $k$ th standard basis in  $\mathcal{R}^n$ ,  $d_{kj}$  is the element of inertia matrix,  $g_k(q) = \frac{\partial V(q)}{\partial q_k}$ , and  $\Gamma_{ij}^k(q)$  are so-called Christoffel symbols and is defined as

$$\Gamma_{ij}^k(q) = \frac{1}{2} \left( \frac{\partial d_{kj}(q)}{\partial q_i} + \frac{\partial d_{ki}(q)}{\partial q_j} - \frac{\partial d_{ij}(q)}{\partial q_k} \right) \quad (\text{A.4})$$

The vector form of (A.4) can be obtained as

$$D(q)\ddot{q} + C(q, \dot{q})\dot{q} + G(q) = B(q)u \quad (\text{A.5})$$

where  $c_{ij} = \sum_{k=1}^n \Gamma_{ij}^k(q)\dot{q}_k$  is the element of  $C(q, \dot{q})$ . Two types of terms are involved in  $C(q, \dot{q})\dot{q} \in \mathcal{R}^n$  which are called Centrifugal terms (when  $i = j$ ) and Coriolis terms (when  $i \neq j$ ),  $G(q)$  represents the gravitational terms.

A series of fundamental properties (Siciliano and Khatib, 2008; Slotine and Weiping, 1988; Yu, 1998; Yu and Lloyd, 1997) of Lagrangian mechanical systems, which advance the analysis and nonlinear control, are achieved from (A.5) as

**Property A.1.** The initial matrix  $D(q)$  is symmetric and positive-definite matrix of inertias with upper and lower boundaries, gives

$$0 < \varepsilon_{min}(q)I_n \leq D(q) \leq \varepsilon_{max}(q)I_n \leq \infty \quad (\text{A.6})$$

**Property A.2.** The initial matrix  $D(q)$  and the matrix  $C(q, \dot{q})$  are not independent. The matrix  $C(q, \dot{q})\dot{q}$  containing Centrifugal terms and Coriolis terms is uniquely defined, but it is not true for the matrix  $C(q, \dot{q})$ . Therefore, a proper definition is employed for  $C(q, \dot{q})$ , thus  $\dot{D}(q) - 2C(q, \dot{q})$  is skew-symmetric such that

$$X^T [\dot{D}(q) - 2C(q, \dot{q})]X = 0 \quad (\text{A.7})$$

where  $X^T$  is the transposed matrix of  $X \in \mathcal{R}^n$ , which is an arbitrary vector.

**Property A.3.** For conservative systems, introducing the total energy  $H(q, \dot{q})$  as

$$H(q, \dot{q}) = T(q, \dot{q}) + V(q) = \frac{1}{2} \dot{q}^T D(q) \dot{q} - V(q) \quad (\text{A.8})$$

Then the change rate of total energy can be obtained as follows

$$\dot{H}(q, \dot{q}) = \dot{q}^T [B(q)u - \frac{\partial p(\dot{q})}{\partial \dot{q}}] \quad (\text{A.9})$$

### A.1.2 Underactuated Mechanical Systems

A control system described by equation (A.2) is referred as an underactuated system if  $m = \text{rank}(B(q)) < n$ , which means it has fewer independent control inputs  $m$  than the degree of freedom  $n$ , and as such  $k = n - m$  DOF cannot be directly actuated. Following the aforementioned principles of Lagrangian mechanical systems, the equations of motion for an UMS can be directly derived below

$$D(q)\ddot{q} + C(q, \dot{q})\dot{q} + G(q) = B(q)u \quad (\text{A.10})$$

Assuming that  $B(q) = [0, I_m]^T$ , without loss of generality, (A.10) can be rewritten in a generic form and further partitioned as  $q = [q_p, q_a]^T \in \mathcal{R}^{n-m} \times \mathcal{R}^m$ , where  $q_p$  and  $q_a$  respectively represent the unactuated (passive) and actuated configuration vectors, we have

$$\begin{bmatrix} D_{pp}(q) & D_{pa}(q) \\ D_{ap}(q) & D_{aa}(q) \end{bmatrix} \begin{bmatrix} \ddot{q}_p \\ \ddot{q}_a \end{bmatrix} + \begin{bmatrix} C_p(q, \dot{q}) \\ C_a(q, \dot{q}) \end{bmatrix} \begin{bmatrix} \dot{q}_p \\ \dot{q}_a \end{bmatrix} + \begin{bmatrix} G_p(q) \\ G_a(q) \end{bmatrix} = \begin{bmatrix} 0 \\ u \end{bmatrix} \quad (\text{A.11})$$

where the inertia matrix  $D(q) = \begin{bmatrix} D_{pp}(q) & D_{pa}(q) \\ D_{ap}(q) & D_{aa}(q) \end{bmatrix}$  is symmetric positive-definite, the matrix  $C(q, \dot{q}) = \begin{bmatrix} C_p(q, \dot{q}) \\ C_a(q, \dot{q}) \end{bmatrix} \in \begin{bmatrix} \mathcal{R}^{n-m} \\ \mathcal{R}^m \end{bmatrix}$  contains the Centrifugal and Coriolis forces,  $G(q) = \begin{bmatrix} G_p(q) \\ G_a(q) \end{bmatrix}$  represents gravitational forces applied respectively on the passive and actuated configurations.

## References

- Ackerman, J., Seipel, J., 2013. Energy Efficiency of Legged Robot Locomotion With Elastically Suspended Loads. *IEEE Trans. Robot.* 29, 321–330. doi:10.1109/TRO.2012.2235698
- Acosta, J.A., Ortega, R., Astolfi, A., Mahindrakar, A.D., 2005. Interconnection and damping assignment passivity-based control of mechanical systems with underactuation degree one. *IEEE Trans. Autom. Control* 50, 1936–1955. doi:10.1109/TAC.2005.860292
- Adhikary, N., Mahanta, C., 2013. Integral backstepping sliding mode control for underactuated systems: Swing-up and stabilization of the Cart–Pendulum System. *ISA Trans.* 52, 870–880. doi:10.1016/j.isatra.2013.07.012
- Al-Bender, F., Swevers, J., 2008. Characterization of friction force dynamics. *IEEE Control Syst.* 28, 64–81.
- Albu-Schäffer, A., Petit, C.O.F., 2012. Energy Shaping Control for a Class of Underactuated Euler-Lagrange Systems. *IFAC Proc. Vol., 10th IFAC Symposium on Robot Control* 45, 567–575. doi:10.3182/20120905-3-HR-2030.00132
- Alexander, R., Dimery, N.J., Ker, R.F., 1985. Elastic structures in the back and their role in galloping in some mammals. *J. Zool.* 207, 467–482.
- Aneke, N.P., 2003. Control of underactuated mechanical systems.
- Antoine, G.O., Batra, R.C., 2015. Optimization of Transparent Laminates for Specific Energy Dissipation under Low Velocity Impact using Genetic Algorithm. *Compos. Struct.*
- Anvar, S.M.M., Hassanzadeh, I., Alizadeh, G., 2010. Design and implementation of sliding mode-state feedback control for stabilization of Rotary Inverted

- Pendulum, in: Control Automation and Systems (ICCAS), 2010 International Conference on. IEEE, pp. 1952–1957.
- Argall, B.D., Billard, A.G., 2010. A survey of tactile human–robot interactions. *Robot. Auton. Syst.* 58, 1159–1176.
- Armstrong-Helouvry, B., 2012. Control of machines with friction. Springer Science & Business Media.
- Armstrong-Hélouvry, B., Dupont, P., De Wit, C.C., 1994. A survey of models, analysis tools and compensation methods for the control of machines with friction. *Automatica* 30, 1083–1138. doi:10.1016/0005-1098(94)90209-7
- Arnold, V.I., 1989. *Mathematical Methods of Classical Mechanics*, Graduate Texts in Mathematics. Springer New York, New York, NY.
- Ashrafiuon, H., Muske, K.R., McNinch, L.C., 2010. Review of nonlinear tracking and setpoint control approaches for autonomous underactuated marine vehicles, in: Proceedings of the 2010 American Control Conference. Presented at the Proceedings of the 2010 American Control Conference, pp. 5203–5211. doi:10.1109/ACC.2010.5530450
- Astrom, K.J., Canudas-De-Wit, C., 2008. Revisiting the LuGre friction model. *Control Syst. IEEE* 28, 101–114.
- Becker, T.C., Mahin, S.A., 2013. Effect of support rotation on triple friction pendulum bearing behavior. *Earthq. Eng. Struct. Dyn.* 42, 1731–1748.
- Biorobotics Lab, n.d. URL <http://biorobotics.ri.cmu.edu/index.php>.
- Biswas, S., Chatterjee, A., 2014. A reduced-order model from high-dimensional frictional hysteresis, in: Proceedings of the Royal Society of London A: Mathematical, Physical and Engineering Sciences. The Royal Society, p. 20130817.
- Blajer, W., Dziewiecki, K., Kołodziejczyk, K., Mazur, Z., 2011. Inverse dynamics of underactuated mechanical systems: a simple case study and experimental verification. *Commun. Nonlinear Sci. Numer. Simul.* 16, 2265–2272.
- Bolotnik, N.N., Figurina, T.Y., 2008. Optimal control of the rectilinear motion of a rigid body on a rough plane by means of the motion of two internal masses. *J. Appl. Math. Mech.* 72, 126–135.
- Bongard, J., Zykov, V., Lipson, H., 2006. Resilient Machines Through Continuous Self-Modeling. *Science* 314, 1118–1121. doi:10.1126/science.1133687
- Boyle, J.H., Johnson, S., Dehghani-Saniij, A.A., 2013. Adaptive undulatory locomotion of a *C. elegans* inspired robot. *IEEEASME Trans. Mechatron.* 18, 439–448.

- Carpi, F., Kastelein, N., Talcott, M., Pappone, C., 2011. Magnetically controllable gastrointestinal steering of video capsules. *IEEE Trans. Biomed. Eng.* 58, 231–234.
- Casini, P., Giannini, O., Vestroni, F., 2012. Persistent and ghost nonlinear normal modes in the forced response of non-smooth systems. *Phys. Nonlinear Phenom.* 241, 2058–2067.
- Celani, F., 2011. Output regulation for the TORA benchmark via rotational position feedback. *Automatica* 47, 584–590. doi:10.1016/j.automatica.2011.01.008
- Chang, D.E., 2010. Stabilizability of controlled Lagrangian systems of two degrees of freedom and one degree of under-actuation by the energy-shaping method. *Autom. Control IEEE Trans. On* 55, 1888–1893.
- Chang, Y.-H., Chan, W.-S., Chang, C.-W., 2013. TS fuzzy model-based adaptive dynamic surface control for ball and beam system. *IEEE Trans. Ind. Electron.* 60, 2251–2263.
- Chanthasopeephan, T., Jarakorn, A., Polchankajorn, P., Maneewarn, T., 2014. Impact reduction mobile robot and the design of the compliant legs. *Robot. Auton. Syst.* 62, 38–45.
- Chatterjee, S., 2007. Non-linear control of friction-induced self-excited vibration. *Int. J. Non-Linear Mech.* 42, 459–469. doi:10.1016/j.ijnonlinmec.2007.01.015
- Chen, I.-M., Yeo, S.H., 2003. Locomotion of a Two-Dimensional Walking-Climbing Robot Using A Closed-Loop Mechanism: From Gait Generation to Navigation. *Int. J. Robot. Res.* 22, 21–40. doi:10.1177/0278364903022001003
- Chen, Y.-F., Huang, A.-C., 2012. Controller design for a class of underactuated mechanical systems. *IET Control Theory Appl.* 6, 103–110.
- Cheng, L., Hou, Z.G., Tan, M., Zhang, W.J., 2012. Tracking Control of a Closed-Chain Five-Bar Robot With Two Degrees of Freedom by Integration of an Approximation-Based Approach and Mechanical Design. *IEEE Trans. Syst. Man Cybern. Part B Cybern.* 42, 1470–1479. doi:10.1109/TSMCB.2012.2192270
- Chernous'ko, F.L., 2005. On the motion of a body containing a movable internal mass, in: *Doklady Physics*. Springer, pp. 593–597.
- Chernous'ko, F.L., 2002. The optimum rectilinear motion of a two-mass system. *J. Appl. Math. Mech.* 66, 1–7.
- Chernous'ko, F.L., 2011. Analysis and optimization of the rectilinear motion of a two-body system. *J. Appl. Math. Mech.* 75, 493–500.

- Chevallereau, C., Bessonnet, G., Abba, G., Aoustin, Y., 2013. *Bipedal Robots: Modeling, Design and Walking Synthesis*. John Wiley & Sons.
- Chowdhury, M.A., Helali, M., 2008. The effect of amplitude of vibration on the coefficient of friction for different materials. *Tribol. Int.* 41, 307–314. doi:10.1016/j.triboint.2007.08.005
- Chwa, D., 2011. Global tracking control of underactuated ships with input and velocity constraints using dynamic surface control method. *IEEE Trans. Control Syst. Technol.* 19, 1357–1370.
- Ciuti, G., Valdastri, P., Menciassi, A., Dario, P., 2010. Robotic magnetic steering and locomotion of capsule endoscope for diagnostic and surgical endoluminal procedures. *Robotica* 28, 199–207. doi:10.1017/S0263574709990361
- Collins, S., Ruina, A., Tedrake, R., Wisse, M., 2005. Efficient bipedal robots based on passive-dynamic walkers. *Science* 307, 1082–1085.
- Collins, S.H., Wiggin, M.B., Sawicki, G.S., 2015. Reducing the energy cost of human walking using an unpowered exoskeleton. *Nature* 522, 212–215.
- Cong, S., Liang, Y., 2009. PID-like neural network nonlinear adaptive control for uncertain multivariable motion control systems. *IEEE Trans. Ind. Electron.* 56, 3872–3879.
- Cornejo, C., Alvarez-Icaza, L., 2011. Passivity based control of under-actuated mechanical systems with nonlinear dynamic friction. *J. Vib. Control* 1077546311408469.
- Craig, J.J., 2005. *Introduction to Robotics: Mechanics and Control*. Pearson/Prentice Hall.
- Cristofaro, A., Salaris, P., Pallottino, L., Giannoni, F., Bicchi, A., 2014. On time-optimal trajectories for differential drive vehicles with field-of-view constraints, in: 2014 IEEE 53rd Annual Conference on Decision and Control (CDC). Presented at the 2014 IEEE 53rd Annual Conference on Decision and Control (CDC), pp. 2191–2197. doi:10.1109/CDC.2014.7039723
- Cui, R., Ge, S.S., How, B.V.E., Choo, Y.S., 2010. Leader–follower formation control of underactuated autonomous underwater vehicles. *Ocean Eng.* 37, 1491–1502.
- Damadi, S.S., Tolue, H.R., Talebi, H.A., 2011. Bang-bang control of a flexible-link manipulator with actuator saturation using neural network, in: Control and Decision Conference (CCDC), 2011 Chinese. IEEE, pp. 1458–1464.
- Davey, J., Kwok, N., Yim, M., 2012. Emulating self-reconfigurable robots - design of the SMORES system, in: 2012 IEEE/RSJ International Conference on Intelligent Robots and Systems. Presented at the 2012 IEEE/RSJ

- International Conference on Intelligent Robots and Systems, pp. 4464–4469. doi:10.1109/IROS.2012.6385845
- De Wit, C.C., Olsson, H., Astrom, K.J., Lischinsky, P., 1995. A new model for control of systems with friction. *Autom. Control IEEE Trans. On* 40, 419–425.
- Dimery, N.J., Alexander, R., Ker, R.F., 1986. Elastic extension of leg tendons in the locomotion of horses (*Equus caballus*). *J. Zool.* 210, 415–425.
- Do, K.D., 2015. Coordination control of quadrotor VTOL aircraft in three-dimensional space. *Int. J. Control* 88, 543–558.
- Dutton, K., Thompson, S., Barraclough, B., 1997. *The Art of Control Engineering*. Addison Wesley.
- Dydek, Z.T., Annaswamy, A.M., Lavretsky, E., 2013. Adaptive control of quadrotor UAVs: A design trade study with flight evaluations. *IEEE Trans. Control Syst. Technol.* 21, 1400–1406.
- Eckenstein, N., Yim, M., 2014. Area of acceptance for 3D self-aligning robotic connectors: Concepts, metrics, and designs, in: *Robotics and Automation (ICRA), 2014 IEEE International Conference on*. IEEE, pp. 1227–1233.
- Eckenstein, N., Yim, M., 2012. The x-face: An improved planar passive mechanical connector for modular self-reconfigurable robots, in: *Intelligent Robots and Systems (IROS), 2012 IEEE/RSJ International Conference on*. IEEE, pp. 3073–3078.
- Erez, T., Todorov, E., 2012. Trajectory optimization for domains with contacts using inverse dynamics, in: *Intelligent Robots and Systems (IROS), 2012 IEEE/RSJ International Conference on*. IEEE, pp. 4914–4919.
- Fallaha, C.J., Saad, M., Kanaan, H.Y., Al-Haddad, K., 2011. Sliding-mode robot control with exponential reaching law. *IEEE Trans. Ind. Electron.* 58, 600–610.
- Fang, H., Xu, J., 2013. Stick-Slip Effect in a Vibration-Driven System With Dry Friction: Sliding Bifurcations and Optimization. *J. Appl. Mech.* 81, 051001–051001. doi:10.1115/1.4025747
- Fang, H., Xu, J., 2011. Dynamics of a mobile system with an internal acceleration-controlled mass in a resistive medium. *J. Sound Vib.* 330, 4002–4018. doi:10.1016/j.jsv.2011.03.010
- Fang, H.-B., Xu, J., 2012. Controlled motion of a two-module vibration-driven system induced by internal acceleration-controlled masses. *Arch. Appl. Mech.* 82, 461–477.

- Fang, Y., Ma, B., Wang, P., Zhang, X., 2012. A motion planning-based adaptive control method for an underactuated crane system. *Control Syst. Technol. IEEE Trans.* On 20, 241–248.
- Fateh, M.M., 2012. Robust control of flexible-joint robots using voltage control strategy. *Nonlinear Dyn.* 67, 1525–1537.
- Felton, S.M., Tolley, M.T., Onal, C.D., Rus, D., Wood, R.J., 2013. Robot self-assembly by folding: A printed inchworm robot, in: *Robotics and Automation (ICRA), 2013 IEEE International Conference on.* IEEE, pp. 277–282.
- Flacco, F., De Luca, A., Sardellitti, I., Tsagarakis, N.G., 2012. On-line estimation of variable stiffness in flexible robot joints. *Int. J. Robot. Res.* 31, 1556–1577. doi:10.1177/0278364912461813
- Freidovich, L., Robertsson, A., Shiriaev, A., Johansson, R., 2010. LuGre-Model-Based Friction Compensation. *IEEE Trans. Control Syst. Technol.* 18, 194–200. doi:10.1109/TCST.2008.2010501
- Freidovich, L., Shiriaev, A., Gordillo, F., Gomez-Esternt, F., Aracil, J., 2007. Partial-energy-shaping control for orbital stabilization of high frequency oscillations of the Furuta pendulum, in: *Decision and Control, 2007 46th IEEE Conference on.* IEEE, pp. 4637–4642.
- Freidovich, L.B., Mettin, U., Shiriaev, A.S., Spong, M.W., 2009. A passive 2-DOF walker: hunting for gaits using virtual holonomic constraints. *Robot. IEEE Trans.* On 25, 1202–1208.
- Ge, S.S., Li, Z., Yang, H., 2012. Data driven adaptive predictive control for holonomic constrained under-actuated biped robots. *IEEE Trans. Control Syst. Technol.* 20, 787–795.
- Ghommam, J., Mnif, F., Derbel, N., 2010. Global stabilisation and tracking control of underactuated surface vessels. *IET Control Theory Appl.* 4, 71–88.
- Ghommam, J., Saad, M., 2014. Backstepping-based cooperative and adaptive tracking control design for a group of underactuated AUVs in horizontal plan. *Int. J. Control* 87, 1076–1093.
- Giannini, O., Casini, P., Vestroni, F., 2011. Experimental evidence of bifurcating nonlinear normal modes in piecewise linear systems. *Nonlinear Dyn.* 63, 655–666.
- Globe Motors, n.d. URL <http://www.globe-motors.com/home.html>.
- Grebenstein, M., Albu-Schäffer, A., Bahls, T., Chalon, M., Eiberger, O., Friedl, W., Gruber, R., Haddadin, S., Hagn, U., Haslinger, R., Hoppner, H., Jorg, S., Nickl, M., Nothhelfer, A., Petit, F., Reill, J., Seitz, N., Wimbock, T., Wolf, S.,

- Wusthoff, T., Hirzinger, G., 2011. The DLR hand arm system, in: 2011 IEEE International Conference on Robotics and Automation (ICRA). Presented at the 2011 IEEE International Conference on Robotics and Automation (ICRA), pp. 3175–3182. doi:10.1109/ICRA.2011.5980371
- Gregg, R.D., Bretl, T., Spong, M.W., 2010. Asymptotically stable gait primitives for planning dynamic bipedal locomotion in three dimensions, in: Robotics and Automation (ICRA), 2010 IEEE International Conference on. IEEE, pp. 1695–1702.
- Gribovskaya, E., Kheddar, A., Billard, A., 2011. Motion learning and adaptive impedance for robot control during physical interaction with humans, in: Robotics and Automation (ICRA), 2011 IEEE International Conference on. IEEE, pp. 4326–4332.
- Grimmer, M., Holgate, M., Holgate, R., Boehler, A., Ward, J., Hollander, K., Sugar, T., Seyfarth, A., 2016. A powered prosthetic ankle joint for walking and running. *Biomed. Eng. OnLine* 15, 286. doi:10.1186/s12938-016-0286-7
- Grizzle, J.W., Abba, G., Plestan, F., 2001. Asymptotically stable walking for biped robots: Analysis via systems with impulse effects. *Autom. Control IEEE Trans. On* 46, 51–64.
- H. B. Fang, J.X., 2010. Dynamic Analysis and Optimization of a Three-phase Control Mode of a Mobile System with an Internal Mass. *J. Vib. Control - J VIB CONTROL* 16. doi:10.1177/1077546309345631
- Habib, M.K., 2007. *Bioinspiration and Robotics: Walking and Climbing Robots*. I-Tech Education and Publishing.
- Haldane, D.W., Peterson, K.C., Bermudez, F.L.G., Fearing, R.S., 2013. Animal-inspired design and aerodynamic stabilization of a hexapedal millirobot, in: Robotics and Automation (ICRA), 2013 IEEE International Conference on. IEEE, pp. 3279–3286.
- Harne, R.L., 2013. Development and testing of a dynamic absorber with corrugated piezoelectric spring for vibration control and energy harvesting applications. *Mech. Syst. Signal Process.* 36, 604–617.
- Hassani, V., Tjahjowidodo, T., Do, T.N., 2014. A survey on hysteresis modeling, identification and control. *Mech. Syst. Signal Process.* 49, 209–233. doi:10.1016/j.ymssp.2014.04.012
- He, W., Chen, Y., Yin, Z., 2016a. Adaptive neural network control of an uncertain robot with full-state constraints. *IEEE Trans. Cybern.* 46, 620–629.

- He, W., Dong, Y., Sun, C., 2016b. Adaptive neural impedance control of a robotic manipulator with input saturation. *IEEE Trans. Syst. Man Cybern. Syst.* 46, 334–344.
- Hetzler, H., Schwarzer, D., Seemann, W., 2007. Analytical investigation of steady-state stability and Hopf-bifurcations occurring in sliding friction oscillators with application to low-frequency disc brake noise. *Commun. Nonlinear Sci. Numer. Simul.* 12, 83–99.
- Hinrichs, N., Oestreich, M., Popp, K., 1998. ON THE MODELLING OF FRICTION OSCILLATORS. *J. Sound Vib.* 216, 435–459. doi:10.1006/jsvi.1998.1736
- Home - STMicroelectronics, n.d. URL [http://www.st.com/content/st\\_com/en.html](http://www.st.com/content/st_com/en.html).
- Hsu, C.-F., 2014. Adaptive backstepping Elman-based neural control for unknown nonlinear systems. *Neurocomputing* 136, 170–179.
- Hu, Q., Xu, L., Zhang, A., 2012. Adaptive backstepping trajectory tracking control of robot manipulator. *J. Frankl. Inst.* 349, 1087–1105. doi:10.1016/j.jfranklin.2012.01.001
- Hu, Y., Yan, G., Lin, Z., 2011. Feedback control of planar biped robot with regulable step length and walking speed. *IEEE Trans. Robot.* 27, 162–169.
- Hua, M.D., Hamel, T., Morin, P., Samson, C., 2013. Introduction to feedback control of underactuated VTOL vehicles: A review of basic control design ideas and principles. *IEEE Control Syst.* 33, 61–75. doi:10.1109/MCS.2012.2225931
- Huang, C.-J., Lin, J.-S., Chen, C.-C., 2010. Road-adaptive algorithm design of half-car active suspension system. *Expert Syst. Appl.* 37, 4392–4402.
- Huang, H.J., Kram, R., Ahmed, A.A., 2012. Reduction of Metabolic Cost during Motor Learning of Arm Reaching Dynamics. *J. Neurosci.* 32, 2182–2190. doi:10.1523/JNEUROSCI.4003-11.2012
- Huang, J., Ding, F., Fukuda, T., Matsuno, T., 2013. Modeling and Velocity Control for a Novel Narrow Vehicle Based on Mobile Wheeled Inverted Pendulum. *IEEE Trans. Control Syst. Technol.* 21, 1607–1617. doi:10.1109/TCST.2012.2214439
- Huang, J., Guan, Z.-H., Matsuno, T., Fukuda, T., Sekiyama, K., 2010. Sliding-mode velocity control of mobile-wheeled inverted-pendulum systems. *Robot. IEEE Trans.* On 26, 750–758.
- Huang, J., Liang, Z., Zang, Q., 2015. Dynamics and swing control of double-pendulum bridge cranes with distributed-mass beams. *Mech. Syst. Signal Process.* 54, 357–366.

- Huang, M., Xian, B., Diao, C., Yang, K., Feng, Y., 2010. Adaptive tracking control of underactuated quadrotor unmanned aerial vehicles via backstepping, in: American Control Conference (ACC), 2010. IEEE, pp. 2076–2081.
- Huang, Y., Chen, B., Wang, Q., Wang, L., 2010. Adding segmented feet to passive dynamic walkers, in: 2010 IEEE/ASME International Conference on Advanced Intelligent Mechatronics. IEEE, pp. 652–657.
- Huda, M.N., Yu, H., 2015. Trajectory tracking control of an underactuated capsbot. *Auton. Robots* 39, 183–198. doi:10.1007/s10514-015-9434-3
- Huda, M.N., Yu, H., Cang, S., 2014. Behaviour-based control approach for the trajectory tracking of an underactuated planar capsule robot. *IET Control Theory Appl.* 9, 163–175.
- Hung, L.-C., Chung, H.-Y., 2007. Decoupled control using neural network-based sliding-mode controller for nonlinear systems. *Expert Syst. Appl.* 32, 1168–1182.
- Hussain, S., Xie, S.Q., Jamwal, P.K., 2013. Adaptive Impedance Control of a Robotic Orthosis for Gait Rehabilitation. *IEEE Trans. Cybern.* 43, 1025–1034. doi:10.1109/TSMCB.2012.2222374
- Hwang, C.-L., Chiang, C.-C., Yeh, Y.-W., 2014. Adaptive fuzzy hierarchical sliding-mode control for the trajectory tracking of uncertain underactuated nonlinear dynamic systems. *IEEE Trans. Fuzzy Syst.* 22, 286–299.
- Hwang, C.-L., Wu, H.-M., 2013. Trajectory tracking of a mobile robot with frictions and uncertainties using hierarchical sliding-mode under-actuated control. *IET Control Theory Appl.* 7, 952–965.
- Ibanez, C.A., Suarez-Castanon, M.S., Gutierrez-Frias, O.O., 2013. A switching controller for the stabilization of the damping inverted pendulum cart system. *Int. J. Innov. Comput. Inf. Control* 9, 3585–3597.
- Iida, F., 2009. Biologically Inspired Motor Control for Underactuated Robots – Trends and Challenges, in: Kozłowski, K.R. (Ed.), *Robot Motion and Control 2009, Lecture Notes in Control and Information Sciences*. Springer London, pp. 145–154. doi:10.1007/978-1-84882-985-5\_14
- Inspurger, T., Milton, J., Stépán, G., 2013. Acceleration feedback improves balancing against reflex delay. *J. R. Soc. Interface* 10, 20120763.
- Islam, S., Liu, X.P., 2011. Robust sliding mode control for robot manipulators. *IEEE Trans. Ind. Electron.* 58, 2444–2453.
- Iyer, R.V., Tan, X., Krishnaprasad, P.S., 2005. Approximate inversion of the Preisach hysteresis operator with application to control of smart actuators. *Autom. Control IEEE Trans. On* 50, 798–810.

- Jiang, Y., Jiang, Z.-P., 2012. Computational adaptive optimal control for continuous-time linear systems with completely unknown dynamics. *Automatica* 48, 2699–2704.
- Jiang, Z.-P., 2010. Controlling Underactuated Mechanical Systems: A Review and Open Problems, in: Lévine, J., Müllhaupt, P. (Eds.), *Advances in the Theory of Control, Signals and Systems with Physical Modeling, Lecture Notes in Control and Information Sciences*. Springer Berlin Heidelberg, pp. 77–88. doi:10.1007/978-3-642-16135-3\_7
- Jung, S., Kim, S.S., 2008. Control Experiment of a Wheel-Driven Mobile Inverted Pendulum Using Neural Network. *IEEE Trans. Control Syst. Technol.* 16, 297–303. doi:10.1109/TCST.2007.903396
- Kanamiya, Y., Ota, S., Sato, D., 2010. Ankle and hip balance control strategies with transitions, in: *Robotics and Automation (ICRA), 2010 IEEE International Conference on*. IEEE, pp. 3446–3451.
- Karssen, J.D., Wisse, M., 2011. Running with improved disturbance rejection by using non-linear leg springs. *Int. J. Robot. Res.* 30, 1585–1595.
- Khansari-Zadeh, S.M., Billard, A., 2011. Learning Stable Nonlinear Dynamical Systems With Gaussian Mixture Models. *IEEE Trans. Robot.* 27, 943–957. doi:10.1109/TRO.2011.2159412
- Kim, D., Turner, J.D., 2014. Near-minimum-time control of asymmetric rigid spacecraft using two controls. *Automatica* 50, 2084–2089.
- Kim, H.M., Yang, S., Kim, J., Park, S., Cho, J.H., Park, J.Y., Kim, T.S., Yoon, E.-S., Song, S.Y., Bang, S., 2010. Active locomotion of a paddling-based capsule endoscope in an in vitro and in vivo experiment (with videos). *Gastrointest. Endosc.* 72, 381–387. doi:10.1016/j.gie.2009.12.058
- Kim, J.-S., Sung, I.-H., Kim, Y.-T., Kim, D.-E., Jang, Y.-H., 2007. Analytical model development for the prediction of the frictional resistance of a capsule endoscope inside an intestine. *Proc. Inst. Mech. Eng. [H]* 221, 837–845. doi:10.1243/09544119JEIM173
- Kober, J., Wilhelm, A., Oztop, E., Peters, J., 2012. Reinforcement learning to adjust parametrized motor primitives to new situations. *Auton. Robots* 33, 361–379. doi:10.1007/s10514-012-9290-3
- Koh, J.-S., Cho, K.-J., 2013. Omega-shaped inchworm-inspired crawling robot with large-index-and-pitch (LIP) SMA spring actuators. *IEEEASME Trans. Mechatron.* 18, 419–429.

- Kolhe, J.P., Shaheed, M., Chandar, T.S., Talole, S.E., 2013. Robust control of robot manipulators based on uncertainty and disturbance estimation. *Int. J. Robust Nonlinear Control* 23, 104–122.
- Korayem, M.H., Rahimi, H.N., Nikoobin, A., 2012. Mathematical modeling and trajectory planning of mobile manipulators with flexible links and joints. *Appl. Math. Model.* 36, 3229–3244.
- Krupinski, S., Allibert, G., Hua, M.-D., Hamel, T., 2012. Pipeline tracking for fully-actuated autonomous underwater vehicle using visual servo control, in: *American Control Conference (ACC), 2012. IEEE*, pp. 6196–6202.
- Lai, T.T., Chen, Y.T., Huang, P., Chu, H., 2010. PipeProbe: a mobile sensor droplet for mapping hidden pipeline, in: *Proceedings of the 8th ACM Conference on Embedded Networked Sensor Systems. ACM*, pp. 113–126.
- Lam, T.L., Xu, Y., 2011. A flexible tree climbing robot: Treebot-design and implementation, in: *Robotics and Automation (ICRA), 2011 IEEE International Conference on. IEEE*, pp. 5849–5854.
- Le, T.A., Kim, G.-H., Kim, M.Y., Lee, S.-G., 2012. Partial feedback linearization control of overhead cranes with varying cable lengths. *Int. J. Precis. Eng. Manuf.* 13, 501–507.
- Le, T.A., Lee, S.-G., Moon, S.-C., 2014. Partial feedback linearization and sliding mode techniques for 2D crane control. *Trans. Inst. Meas. Control* 36, 78–87. doi:10.1177/0142331213492369
- Lee, N., Kamamichi, N., Li, H., Furuta, K., 2008. Control system design and experimental verification of Capsubot, in: *IEEE/RSJ International Conference on Intelligent Robots and Systems, 2008. IROS 2008. Presented at the IEEE/RSJ International Conference on Intelligent Robots and Systems, 2008. IROS 2008*, pp. 1927–1932. doi:10.1109/IROS.2008.4650933
- Lee, S., Kim, W., 2010. Active suspension control with direct-drive tubular linear brushless permanent-magnet motor. *IEEE Trans. Control Syst. Technol.* 18, 859–870.
- Lee, S.-G., Dang, V.-H., Moon, S., Kim, B., others, 2013. Partial feedback linearization control of a three-dimensional overhead crane. *Int. J. Control Autom. Syst.* 11, 718–727.
- Lee, T.H., Tan, K.K., Huang, S., 2011. Adaptive Friction Compensation With a Dynamical Friction Model. *IEEEASME Trans. Mechatron.* 16, 133–140. doi:10.1109/TMECH.2009.2036994

- Li, H., Furuta, K., Chernousko, F.L., 2006. Motion generation of the capsbot using internal force and static friction, in: Decision and Control, 2006 45th IEEE Conference on. pp. 6575–6580.
- Li, J., Guo, X., Li, Z., Chen, W., 2014. Stochastic adaptive optimal control of under-actuated robots using neural networks. *Neurocomputing, SI Computational Intelligence Techniques for New Product Development* 142, 190–200. doi:10.1016/j.neucom.2014.04.049
- Li, Y., Xu, Q., 2010. Adaptive sliding mode control with perturbation estimation and PID sliding surface for motion tracking of a piezo-driven micromanipulator. *IEEE Trans. Control Syst. Technol.* 18, 798–810.
- Li, Z., Canny, J.F., 2012. *Nonholonomic motion planning*. Springer Science & Business Media.
- Li, Z., Yang, C., Su, C.-Y., Ye, W., 2014. Adaptive fuzzy-based motion generation and control of mobile under-actuated manipulators. *Eng. Appl. Artif. Intell.* 30, 86–95.
- Li, Z., Yang, Y., Li, J., 2010. Adaptive motion/force control of mobile under-actuated manipulators with dynamics uncertainties by dynamic coupling and output feedback. *Control Syst. Technol. IEEE Trans. On* 18, 1068–1079.
- Li, Z., Zuo, L., Luhrs, G., Lin, L., Qin, Y., 2013. Electromagnetic energy-harvesting shock absorbers: design, modeling, and road tests. *IEEE Trans. Veh. Technol.* 62, 1065–1074.
- Liljebäck, P. al, Stavadahl, Ø., Pettersen, K.Y., 2005. *Modular Pneumatic Snakerobot: 3D Modelling, Implementation and Control*.
- Liljebäck, P., Pettersen, K.Y., Stavadahl, Ø., Gravadahl, J.T., 2012. A review on modelling, implementation, and control of snake robots. *Robot. Auton. Syst.* 60, 29–40. doi:10.1016/j.robot.2011.08.010
- Liljebäck, P., Stavadahl, O., Beitnes, A., 2006. SnakeFighter - Development of a Water Hydraulic Fire Fighting Snake Robot, in: 9th International Conference on Control, Automation, Robotics and Vision, 2006. ICARCV '06. Presented at the 9th International Conference on Control, Automation, Robotics and Vision, 2006. ICARCV '06, pp. 1–6. doi:10.1109/ICARCV.2006.345311
- Liu, C.Y., Liao, W.-H., 2004. A snake robot using shape memory alloys, in: *Robotics and Biomimetics, 2004. ROBIO 2004. IEEE International Conference on*. IEEE, pp. 601–605.
- Liu, D., Wang, D., Zhao, D., Wei, Q., Jin, N., 2012. Neural-network-based optimal control for a class of unknown discrete-time nonlinear systems using

- globalized dual heuristic programming. *IEEE Trans. Autom. Sci. Eng.* 9, 628–634.
- Liu, P., Yu, H., Cang, S., 2016. Modelling and dynamic analysis of underactuated capsule systems with friction-induced hysteresis, in: *Intelligent Robots and Systems (IROS), 2016 IEEE/RSJ International Conference on.* IEEE, pp. 549–554.
- Liu, P., Yu, H., Cang, S., 2014. Modelling and control of an elastically joint-actuated cart-pole underactuated system, in: *Automation and Computing (ICAC), 2014 20th International Conference on.* IEEE, pp. 26–31.
- Liu, Y., Pavlovskaja, E., Hendry, D., Wiercigroch, M., 2013a. Vibro-impact responses of capsule system with various friction models. *Int. J. Mech. Sci.* 72, 39–54.
- Liu, Y., Pavlovskaja, E., Wiercigroch, M., Peng, Z., 2015. Forward and backward motion control of a vibro-impact capsule system. *Int. J. Non-Linear Mech., Nonlinear Dynamics in Engineering: Modelling, Analysis and Applications* 70, 30–46. doi:10.1016/j.ijnonlinmec.2014.10.009
- Liu, Y., Wiercigroch, M., Pavlovskaja, E., Yu, H., 2013b. Modelling of a vibro-impact capsule system. *Int. J. Mech. Sci.* 66, 2–11. doi:10.1016/j.ijmecsci.2012.09.012
- Liu, Y., Yu, H., 2013. A survey of underactuated mechanical systems. *IET Control Theory Appl.* 7, 921–935. doi:10.1049/iet-cta.2012.0505
- Liu, Y., Yu, H., Vladareanu, L., Cang, S., Gao, F., 2011. Trajectory planning of a Pendulum-Driven Underactuated Cart. *Romanian J. Tech. Sci. Appl. Mech.* 56.
- Liu, Y., Yu, H., Yang, T.C., 2008. Analysis and Control of a Capsubot. *city* 10, 2.
- Liu, Y.-J., Chen, C.P., Wen, G.-X., Tong, S., 2011. Adaptive neural output feedback tracking control for a class of uncertain discrete-time nonlinear systems. *IEEE Trans. Neural Netw.* 22, 1162–1167.
- Man, W.-S., Lin, J.-S., 2010. Nonlinear Control Design for a Class of underactuated systems., in: *CCA.* pp. 1439–1444.
- Manchester, I.R., Mettin, U., Iida, F., Tedrake, R., 2011. Stable dynamic walking over uneven terrain. *Int. J. Robot. Res.* 0278364910395339.
- Martínez, R., Álvarez, J., 2012. Control of mechanical systems with dry friction. *Comput. Syst.* 16, 5–13.
- Martinez, R., Alvarez, J., Orlov, Y., 2008. Hybrid sliding-mode-based control of underactuated systems with dry friction. *Ind. Electron. IEEE Trans. On* 55, 3998–4003.

- Mathis, F.B., Jafari, R., Mukherjee, R., 2014. Impulsive Actuation in Robot Manipulators: Experimental Verification of Pendubot Swing-Up. *Mechatron. IEEEASME Trans.* On 19, 1469–1474.
- Matos, A., Silva, E., Cruz, N., Alves, J.C., Almeida, D., Pinto, M., Martins, A., Almeida, J., Machado, D., 2013. Development of an Unmanned Capsule for large-scale maritime search and rescue, in: *MTS/IEEE OCEANS*.
- McMahon, T.A., 1985. The role of compliance in mammalian running gaits. *J. Exp. Biol.* 115, 263–282.
- McMillan, A.J., 1997. A NON-LINEAR FRICTION MODEL FOR SELF-EXCITED VIBRATIONS. *J. Sound Vib.* 205, 323–335. doi:10.1006/jsvi.1997.1053
- Memon, A.B., Verriest, E.I., Hyun, N.-S.P., 2014. Graceful gait transitions for biomimetic locomotion - the worm, in: *2014 IEEE 53rd Annual Conference on Decision and Control (CDC)*. Presented at the 2014 IEEE 53rd Annual Conference on Decision and Control (CDC), pp. 2958–2963. doi:10.1109/CDC.2014.7039844
- Meza-Sánchez, I.M., Aguilar, L.T., Shiriaev, A., Freidovich, L., Orlov, Y., 2011. Periodic motion planning and nonlinear  $\mathcal{H}_\infty$  tracking control of a 3-DOF underactuated helicopter. *Int. J. Syst. Sci.* 42, 829–838. doi:10.1080/00207721.2010.517874
- Mills, A., Wills, A., Ninness, B., 2009. Nonlinear model predictive control of an inverted pendulum, in: *American Control Conference, 2009. ACC'09. IEEE*, pp. 2335–2340.
- Mistry, M., Buchli, J., Schaal, S., 2010. Inverse dynamics control of floating base systems using orthogonal decomposition, in: *Robotics and Automation (ICRA), 2010 IEEE International Conference on. IEEE*, pp. 3406–3412.
- Miyata, C., Chisholm, K., Baba, J., Ahmadi, M., 2016. A Limb Compliant Sensing Strategy for Robot Collision Reaction. *IEEEASME Trans. Mechatron.* 21, 674–682.
- Mohammadi, A., Rezapour, E., Maggiore, M., Pettersen, K.Y., 2014. Direction following control of planar snake robots using virtual holonomic constraints, in: *2014 IEEE 53rd Annual Conference on Decision and Control (CDC)*. Presented at the 2014 IEEE 53rd Annual Conference on Decision and Control (CDC), pp. 3801–3808. doi:10.1109/CDC.2014.7039981
- Mohanty, A., Yao, B., 2011. Indirect Adaptive Robust Control of Hydraulic Manipulators With Accurate Parameter Estimates. *IEEE Trans. Control Syst. Technol.* 19, 567–575. doi:10.1109/TCST.2010.2048569

- Mohareri, O., Dhaouadi, R., Rad, A.B., 2012. Indirect adaptive tracking control of a nonholonomic mobile robot via neural networks. *Neurocomputing, Intelligent and Autonomous Systems* 88, 54–66. doi:10.1016/j.neucom.2011.06.035
- Moreira, P., Zemiti, N., Liu, C., Poignet, P., 2014. Viscoelastic model based force control for soft tissue interaction and its application in physiological motion compensation. *Comput. Methods Programs Biomed.* 116, 52–67.
- Na, J., Chen, Q., Ren, X., Guo, Y., 2014. Adaptive prescribed performance motion control of servo mechanisms with friction compensation. *IEEE Trans. Ind. Electron.* 61, 486–494.
- Nayfeh, A.H., Balachandran, B., 2008. *Applied Nonlinear Dynamics: Analytical, Computational and Experimental Methods*. John Wiley & Sons.
- Neis, P.D., De Baets, P., Ost, W., Delgado, Y.P., Loccufer, M., Al-Bender, F., Ferreira, N.F., Lorini, F.J., 2011. Investigation of the dynamic response in a dry friction process using a rotating stick–slip tester. *Wear* 271, 2640–2650.
- Nematode, 2017. . Wikipedia.
- Ngo, Q.H., Hong, K.S., 2012. Sliding-Mode Antisway Control of an Offshore Container Crane. *IEEEASME Trans. Mechatron.* 17, 201–209. doi:10.1109/TMECH.2010.2093907
- Nguyen, C.H., Alici, G., Mutlu, R., 2014. Modeling a soft robotic mechanism articulated with dielectric elastomer actuators, in: *Advanced Intelligent Mechatronics (AIM), 2014 IEEE/ASME International Conference on*. IEEE, pp. 599–604.
- Oh, S.-R., Sun, J., 2010. Path following of underactuated marine surface vessels using line-of-sight based model predictive control. *Ocean Eng.* 37, 289–295.
- Olfati-Saber, R., 2002. Normal forms for underactuated mechanical systems with symmetry. *IEEE Trans. Autom. Control* 47, 305–308.
- Olfati-Saber, R., 2000. *Nonlinear control of underactuated mechanical systems with application to robotics and aerospace vehicles*. Massachusetts Institute of Technology.
- Olsson, H., Åström, K.J., Canudas de Wit, C., Gäfvert, M., Lischinsky, P., 1998. Friction Models and Friction Compensation. *Eur. J. Control* 4, 176–195. doi:10.1016/S0947-3580(98)70113-X
- Ordaz, P., Espinoza, E.S., Muñoz, F., 2014. Research on Swing up Control Based on Energy for the Pendubot System. *J. Dyn. Syst. Meas. Control* 136, 041018–041018. doi:10.1115/1.4026658

- Oriolo, G., Nakamura, Y., 1991. Control of mechanical systems with second-order nonholonomic constraints: Underactuated manipulators, in: *Decision and Control, 1991.*, Proceedings of the 30th IEEE Conference on. IEEE, pp. 2398–2403.
- Outirba, B., Hendrick, P., 2014. Experimental Testing of Carbon Brush Seals for Aero Engines Bearing Chambers, in: *ASME Turbo Expo 2014: Turbine Technical Conference and Exposition*. American Society of Mechanical Engineers, p. V05CT16A017–V05CT16A017.
- Papastavridis, J.G., 2014. *Analytical Mechanics: A Comprehensive Treatise on the Dynamics of Constrained Systems*, Reprint. ed. WORLD SCIENTIFIC.
- Park, B.S., Yoo, S.J., Park, J.B., Choi, Y.H., 2010. A simple adaptive control approach for trajectory tracking of electrically driven nonholonomic mobile robots. *IEEE Trans. Control Syst. Technol.* 18, 1199–1206.
- Park, M.-S., Chwa, D., 2009. Swing-up and stabilization control of inverted-pendulum systems via coupled sliding-mode control method. *Ind. Electron. IEEE Trans. On* 56, 3541–3555.
- Pavlovskaia, E., Hendry, D.C., Wiercigroch, M., 2015. Modelling of high frequency vibro-impact drilling. *Int. J. Mech. Sci., Mechanics of Solids & Structures* 91, 110–119. doi:10.1016/j.ijmecsci.2013.08.009
- Pavlovskaia, E., Wiercigroch, M., 2003. Periodic solution finder for an impact oscillator with a drift. *J. Sound Vib.* 267, 893–911.
- Peng, Z., Wang, D., Chen, Z., Hu, X., Lan, W., 2013. Adaptive Dynamic Surface Control for Formations of Autonomous Surface Vehicles With Uncertain Dynamics. *IEEE Trans. Control Syst. Technol.* 21, 513–520. doi:10.1109/TCST.2011.2181513
- Pereira, P., Cunha, R., Cabecinhas, D., Silvestre, C., Oliveira, P., 2014. Trailer-like leader following trajectory planning, in: *2014 IEEE 53rd Annual Conference on Decision and Control (CDC)*. Presented at the 2014 IEEE 53rd Annual Conference on Decision and Control (CDC), pp. 3725–3730. doi:10.1109/CDC.2014.7039969
- Perelman, L., Ostfeld, A., 2013. Operation of remote mobile sensors for security of drinking water distribution systems. *Water Res.* 47, 4217–4226.
- Peters, S.C., Bobrow, J.E., Iagnemma, K., 2010. Stabilizing a vehicle near rollover: An analogy to cart-pole stabilization, in: *2010 IEEE International Conference on Robotics and Automation*. Presented at the 2010 IEEE International Conference on Robotics and Automation, pp. 5194–5200. doi:10.1109/ROBOT.2010.5509367

- Petković, D., Issa, M., Pavlović, N.D., Zentner, L., 2013a. Intelligent rotational direction control of passive robotic joint with embedded sensors. *Expert Syst. Appl.* 40, 1265–1273.
- Petković, D., Pavlović, N.D., Čojbašić, Ž., Pavlović, N.T., 2013b. Adaptive neuro fuzzy estimation of underactuated robotic gripper contact forces. *Expert Syst. Appl.* 40, 281–286.
- Pfeifer, R., Lungarella, M., Iida, F., 2012. The challenges ahead for bio-inspired 'soft' robotics. *Commun. ACM* 55, 76–87.
- Ping, Z., 2013. Tracking problems of a spherical inverted pendulum via neural network enhanced design. *Neurocomputing* 106, 137–147.
- Plestan, F., Grizzle, J.W., Westervelt, E.R., Abba, G., 2003. Stable walking of a 7-DOF biped robot. *Robot. Autom. IEEE Trans. On* 19, 653–668.
- Pucci, D., Romano, F., Nori, F., 2015. Collocated adaptive control of underactuated mechanical systems. *IEEE Trans. Robot.* 31, 1527–1536.
- Qiao, J., Shang, J., Goldenberg, A., 2013. Development of inchworm in-pipe robot based on self-locking mechanism. *Mechatron. IEEEASME Trans. On* 18, 799–806.
- Raffaella, A.D.L.S.I., Oriolo, M.G., n.d. *Underactuated Manipulators: Control Properties and Techniques*.
- Raffo, G.V., Ortega, M.G., Rubio, F.R., 2011. Path tracking of a UAV via an underactuated control strategy. *Eur. J. Control* 17, 194–213.
- Ramirez-Neria, M., Sira-Ramirez, H., Garrido-Moctezuma, R., Luviano-Juarez, A., 2014. Linear active disturbance rejection control of underactuated systems: The case of the Furuta pendulum. *ISA Trans.* 53, 920–928.
- Ravichandran, M.T., Mahindrakar, A.D., 2011. Robust stabilization of a class of underactuated mechanical systems using time scaling and Lyapunov redesign. *IEEE Trans. Ind. Electron.* 58, 4299–4313.
- RMDS, n.d. . RMDS. URL <https://rmdservice.com/>.
- Ruderman, M., 2012. *Modeling of elastic robot joints with nonlinear damping and hysteresis*. INTECH Open Access Publisher.
- Ryu, J.-C., Agrawal, S.K., 2010. Planning and control of under-actuated mobile manipulators using differential flatness. *Auton. Robots* 29, 35–52. doi:10.1007/s10514-010-9185-0
- Saha, A., Wahi, P., Wiercigroch, M., Stefański, A., 2015. A modified LuGre friction model for an accurate prediction of friction force in the pure sliding regime. *Int. J. Non-Linear Mech.*

- Sazonov, E.S., Klinkhachorn, P., Klein, R.L., 2003. Hybrid LQG-Neural controller for inverted pendulum system, in: *System Theory, 2003. Proceedings of the 35th Southeastern Symposium on. IEEE*, pp. 206–210.
- Seipel, J., 2011. Emphasizing Mechanical Feedback in Bio-Inspired Design and Education 859–860. doi:10.1115/IMECE2011-65587
- Shang, J., Noonan, D.P., Payne, C., Clark, J., Sodergren, M.H., Darzi, A., Yang, G.-Z., 2011. An articulated universal joint based flexible access robot for minimally invasive surgery, in: *Robotics and Automation (ICRA), 2011 IEEE International Conference on. IEEE*, pp. 1147–1152.
- Shenzhen Zvepower Technology Co., Ltd., n.d. URL <https://zvepower.m.en.alibaba.com/>.
- Shi, C., Parker, R.G., 2012. Modal properties and stability of centrifugal pendulum vibration absorber systems with equally spaced, identical absorbers. *J. Sound Vib.* 331, 4807–4824.
- Shiriaev, A.S., Freidovich, L.B., Spong, M.W., 2014. Controlled invariants and trajectory planning for underactuated mechanical systems. *IEEE Trans. Autom. Control* 59, 2555–2561.
- Shkolnik, A., Levashov, M., Manchester, I.R., Tedrake, R., 2010. Bounding on rough terrain with the LittleDog robot. *Int. J. Robot. Res.* 0278364910388315.
- Siciliano, B., Khatib, O. (Eds.), 2008. *Springer Handbook of Robotics*. Springer Berlin Heidelberg, Berlin, Heidelberg.
- Slotine, J.-J.E., Weiping, L., 1988. Adaptive manipulator control: A case study. *IEEE Trans. Autom. Control* 33, 995–1003. doi:10.1109/9.14411
- Soltanpour, M.R., Khooban, M.H., Soltani, M., 2014. Robust fuzzy sliding mode control for tracking the robot manipulator in joint space and in presence of uncertainties. *Robotica* 32, 433–446.
- Spong, M.W., 1998. Underactuated mechanical systems, in: *Control Problems in Robotics and Automation*. Springer, pp. 135–150.
- Spong, M.W., Hutchinson, S., Vidyasagar, M., 2006. *Robot modeling and control*. Wiley New York.
- Sprangers, O., Babuška, R., Nagesh Rao, S.P., Lopes, G.A., 2015. Reinforcement learning for port-Hamiltonian systems. *IEEE Trans. Cybern.* 45, 1017–1027.
- Stefański, A., Wojewoda, J., Wiercigroch, M., Kapitaniak, T., 2006. Regular and chaotic oscillations of friction force. *Proc. Inst. Mech. Eng. Part C J. Mech. Eng. Sci.* 220, 273–284.

- Su, G., Zhang, C., Tan, R., Li, H., 2009. A linear driving mechanism applied to capsule robots, in: 2009 International Conference on Networking, Sensing and Control. pp. 206–209.
- Sun, N., Fang, Y., Zhang, X., 2013. Energy coupling output feedback control of 4-DOF underactuated cranes with saturated inputs. *Automatica* 49, 1318–1325.
- Sun, N., Fang, Y., Zhang, X., Yuan, Y., 2012. Transportation task-oriented trajectory planning for underactuated overhead cranes using geometric analysis. *IET Control Theory Appl.* 6, 1410–1423.
- Sun, Ning, Fang, Y., Zhang, Y., Ma, B., 2012. A novel kinematic coupling-based trajectory planning method for overhead cranes. *Mechatron. IEEEASME Trans. On* 17, 166–173.
- Sun, T., Pei, H., Pan, Y., Zhou, H., Zhang, C., 2011. Neural network-based sliding mode adaptive control for robot manipulators. *Neurocomputing* 74, 2377–2384.
- Sun, Tianjia, Xie, X., Li, G., Gu, Y., Deng, Y., Wang, Z., 2012. A two-hop wireless power transfer system with an efficiency-enhanced power receiver for motion-free capsule endoscopy inspection. *IEEE Trans. Biomed. Eng.* 59, 3247–3254.
- Taheri, B., Case, D., Richer, E., 2014. Force and Stiffness Backstepping-Sliding Mode Controller for Pneumatic Cylinders. *IEEEASME Trans. Mechatron.* 19, 1799–1809. doi:10.1109/TMECH.2013.2294970
- Tan, X., Baras, J.S., 2004. Modeling and control of hysteresis in magnetostrictive actuators. *Automatica* 40, 1469–1480.
- Tao, C.W., Taur, J., Chang, J.H., Su, S.-F., 2010. Adaptive fuzzy switched swing-up and sliding control for the double-pendulum-and-cart system. *IEEE Trans. Syst. Man Cybern. Part B Cybern.* 40, 241–252.
- Tedrake, R., Manchester, I.R., Tobenkin, M., Roberts, J.W., 2010. LQR-trees: Feedback Motion Planning via Sums-of-Squares Verification. *Int. J. Robot. Res.* doi:10.1177/0278364910369189
- Terry, P., Byl, K., 2014. A higher order partial feedback linearization based method for controlling an underactuated hopping robot with a compliant leg, in: Decision and Control (CDC), 2014 IEEE 53rd Annual Conference on. IEEE, pp. 2971–2978.
- Theodorou, E., Buchli, J., Schaal, S., 2010. Reinforcement learning of motor skills in high dimensions: A path integral approach, in: 2010 IEEE International Conference on Robotics and Automation. Presented at the 2010 IEEE

- International Conference on Robotics and Automation, pp. 2397–2403. doi:10.1109/ROBOT.2010.5509336
- Tlalolini, D., Chevallereau, C., Aoustin, Y., 2011. Human-like walking: Optimal motion of a bipedal robot with toe-rotation motion. *IEEEASME Trans. Mechatron.* 16, 310–320.
- Tong, S.C., Li, Y.M., Zhang, H.G., 2011. Adaptive Neural Network Decentralized Backstepping Output-Feedback Control for Nonlinear Large-Scale Systems With Time Delays. *IEEE Trans. Neural Netw.* 22, 1073–1086. doi:10.1109/TNN.2011.2146274
- Transth, A.A., Leine, R.I., Glocker, C., Pettersen, K.Y., LiljeÄck, P., 2008. Snake Robot Obstacle-Aided Locomotion: Modeling, Simulations, and Experiments. *IEEE Trans. Robot.* 24, 88–104. doi:10.1109/TRO.2007.914849
- Transth, A.A., Pettersen, K.Y., LiljeÄck, P., 2009. A survey on snake robot modeling and locomotion. *Robotica* 27, 999–1015. doi:10.1017/S0263574709005414
- Ulmen, J., Cutkosky, M.R., 2010. A robust, low-cost and low-noise artificial skin for human-friendly robots., in: *ICRA*. pp. 4836–4841.
- Vakil, M., Fotouhi, R., Nikiforuk, P.N., 2011. Energy-based approach for friction identification of robotic joints. *Mechatronics* 21, 614–624.
- Valentinis, F., Donaire, A., Perez, T., 2015. Energy-based motion control of a slender hull unmanned underwater vehicle. *Ocean Eng.* 104, 604–616.
- Vanderborght, B., Albu-Schäffer, A., Bicchi, A., Burdet, E., Caldwell, D.G., Carloni, R., Catalano, M., Eiberger, O., Friedl, W., Ganesh, G., others, 2013. Variable impedance actuators: A review. *Robot. Auton. Syst.* 61, 1601–1614.
- Venkatesh, C., Mehra, R., Kazi, F., Singh, N.M., 2013. Passivity based controller for underactuated PVTOL system, in: *Electronics, Computing and Communication Technologies (CONECCT), 2013 IEEE International Conference on.* IEEE, pp. 1–5.
- Wai, R.-J., Kuo, M.-A., Lee, J.-D., 2008. Design of Cascade Adaptive Fuzzy Sliding-Mode Control for Nonlinear Two-Axis Inverted-Pendulum Servomechanism. *IEEE Trans. Fuzzy Syst.* 16, 1232–1244. doi:10.1109/TFUZZ.2008.924277
- Wai, R.J., Muthusamy, R., 2014. Design of Fuzzy-Neural-Network-Inherited Backstepping Control for Robot Manipulator Including Actuator Dynamics. *IEEE Trans. Fuzzy Syst.* 22, 709–722. doi:10.1109/TFUZZ.2013.2270010

- Wang, H., 2016. Adaptive control of robot manipulators with uncertain kinematics and dynamics. *IEEE Trans. Autom. Control*.
- Wang, H., Kosuge, K., 2012. Control of a robot dancer for enhancing haptic human-robot interaction in waltz. *IEEE Trans. Haptics* 5, 264–273.
- Wang, K., Yan, G., Ma, G., Ye, D., 2008. An Earthworm-Like Robotic Endoscope System for Human Intestine: Design, Analysis, and Experiment. *Ann. Biomed. Eng.* 37, 210–221. doi:10.1007/s10439-008-9597-6
- Wang, Q., Huang, Y., Wang, L., 2010. Passive dynamic walking with flat feet and ankle compliance. *Robotica* 28, 413–425.
- Wang, Q., Su, C.-Y., 2006. Robust adaptive control of a class of nonlinear systems including actuator hysteresis with Prandtl–Ishlinskii presentations. *Automatica* 42, 859–867.
- Wang, T., Gao, H., Qiu, J., 2016. A combined adaptive neural network and nonlinear model predictive control for multirate networked industrial process control. *IEEE Trans. Neural Netw. Learn. Syst.* 27, 416–425.
- Wang, W., Lee, J.-Y., Rodrigue, H., Song, S.-H., Chu, W.-S., Ahn, S.-H., 2014. Locomotion of inchworm-inspired robot made of smart soft composite (SSC). *Bioinspir. Biomim.* 9, 046006.
- Wang, Z., Sun, Z., Phee, S.J., 2013. Haptic feedback and control of a flexible surgical endoscopic robot. *Comput. Methods Programs Biomed.* 112, 260–271.
- Weber, F., 2014. Semi-active vibration absorber based on real-time controlled MR damper. *Mech. Syst. Signal Process.* 46, 272–288.
- Westervelt, E.R., Grizzle, J.W., Chevallereau, C., Choi, J.H., Morris, B., 2007. Feedback control of dynamic bipedal robot locomotion. CRC press.
- Wojewoda, J., Stefański, A., Wiercigroch, M., Kapitaniak, T., 2008. Hysteretic effects of dry friction: modelling and experimental studies. *Philos. Trans. R. Soc. Lond. Math. Phys. Eng. Sci.* 366, 747–765.
- Wolf, S., Bahls, T., Chalon, M., Friedl, W., Grebenstein, M., Höppner, H., Kühne, M., Lakatos, D., Mansfeld, N., Özparpucu, M.C., others, 2015. Soft robotics with variable stiffness actuators: Tough robots for soft human robot interaction, in: *Soft Robotics*. Springer, pp. 231–254.
- Wright, C., Buchan, A., Brown, B., Geist, J., Schwerin, M., Rollinson, D., Tesch, M., Choset, H., 2012. Design and architecture of the unified modular snake robot, in: *Robotics and Automation (ICRA), 2012 IEEE International Conference on*. IEEE, pp. 4347–4354.

- Wu, X., He, X., 2016. Partial feedback linearization control for 3-D underactuated overhead crane systems. *ISA Trans.* 65, 361–370. doi:10.1016/j.isatra.2016.06.015
- Xia, D., Wang, L., Chai, T., 2014. Neural-network-friction compensation-based energy swing-up control of pendubot. *IEEE Trans. Ind. Electron.* 61, 1411–1423.
- Xin, X., Liu, Y., 2014. *Control Design and Analysis for Underactuated Robotic Systems*. Springer Science & Business Media.
- Xin, X., Tanaka, S., She, J., Yamasaki, T., 2013. New analytical results of energy-based swing-up control for the Pendubot. *Int. J. Non-Linear Mech.* 52, 110–118. doi:10.1016/j.ijnonlinmec.2013.02.003
- Xin, X., Yamasaki, T., 2012. Energy-based swing-up control for a remotely driven Acrobot: Theoretical and experimental results. *Control Syst. Technol. IEEE Trans. On* 20, 1048–1056.
- Xu, B., Sun, F., Yang, C., Gao, D., Ren, J., 2011. Adaptive discrete-time controller design with neural network for hypersonic flight vehicle via back-stepping. *Int. J. Control* 84, 1543–1552.
- Xu, J.-X., Guo, Z.-Q., Lee, T.H., 2014. Design and implementation of integral sliding-mode control on an underactuated two-wheeled mobile robot. *IEEE Trans. Ind. Electron.* 61, 3671–3681.
- Xu, J.X., Guo, Z.Q., Lee, T.H., 2013. Design and Implementation of a Takagi #x2013;Sugeno-Type Fuzzy Logic Controller on a Two-Wheeled Mobile Robot. *IEEE Trans. Ind. Electron.* 60, 5717–5728. doi:10.1109/TIE.2012.2230600
- Xu, R., Özgüner, Ü., 2008. Sliding mode control of a class of underactuated systems. *Automatica* 44, 233–241. doi:10.1016/j.automatica.2007.05.014
- Yamagata, Y., Higuchi, T., 1995. A micropositioning device for precision automatic assembly using impact force of piezoelectric elements, in: , 1995 IEEE International Conference on Robotics and Automation, 1995. Proceedings. Presented at the , 1995 IEEE International Conference on Robotics and Automation, 1995. Proceedings, pp. 666–671 vol.1. doi:10.1109/ROBOT.1995.525360
- Yan, Z., Wang, J., 2012. Model predictive control for tracking of underactuated vessels based on recurrent neural networks. *IEEE J. Ocean. Eng.* 37, 717–726.
- Yang, C., Ganesh, G., Haddadin, S., Parusel, S., Albu-Schaeffer, A., Burdet, E., 2011. Human-Like Adaptation of Force and Impedance in Stable and Unstable

- Interactions. IEEE Trans. Robot. 27, 918–930. doi:10.1109/TRO.2011.2158251
- Yang, C., Li, Z., Cui, R., Xu, B., 2014. Neural Network-Based Motion Control of an Underactuated Wheeled Inverted Pendulum Model. IEEE Trans. Neural Netw. Learn. Syst. 25, 2004–2016. doi:10.1109/TNNLS.2014.2302475
- Yang, C., Li, Z., Li, J., 2013. Trajectory planning and optimized adaptive control for a class of wheeled inverted pendulum vehicle models. Cybern. IEEE Trans. On 43, 24–36.
- Yih, C.-C., 2013. Sliding Mode Control for Swing-Up and Stabilization of the Cart-Pole Underactuated System. Asian J. Control 15, 1201–1214. doi:10.1002/asjc.577
- Yim, S., Gultepe, E., Gracias, D.H., Sitti, M., 2014. Biopsy using a Magnetic Capsule Endoscope Carrying, Releasing, and Retrieving Untethered Microgrippers. IEEE Trans. Biomed. Eng. 61, 513–521. doi:10.1109/TBME.2013.2283369
- Yu, H., 1998. Robust combined adaptive and variable structure adaptive control of robot manipulators. Robotica 16, 623–650.
- Yu, H., Huda, M.N., Wane, S.O., 2011. A novel acceleration profile for the motion control of capsubots, in: 2011 IEEE International Conference on Robotics and Automation (ICRA). Presented at the 2011 IEEE International Conference on Robotics and Automation (ICRA), pp. 2437–2442. doi:10.1109/ICRA.2011.5980344
- Yu, H., Liu, Y., Yang, T., 2008. Closed-loop tracking control of a pendulum-driven cart-pole underactuated system. Proc. Inst. Mech. Eng. Part J. Syst. Control Eng. 222, 109–125.
- Yu, H., Lloyd, S., 1997. Variable structure adaptive control of robot manipulators. Control Theory Appl. IEE Proc. - 144, 167–176. doi:10.1049/ip-cta:19970803
- Yu, R., Zhu, Q., Xia, G., Liu, Z., 2012. Sliding mode tracking control of an underactuated surface vessel. IET Control Theory Appl. 6, 461–466. doi:10.1049/iet-cta.2011.0176
- Yu, X., Kaynak, O., 2009. Sliding-Mode Control With Soft Computing: A Survey. IEEE Trans. Ind. Electron. 56, 3275–3285. doi:10.1109/TIE.2009.2027531
- yue, m., Hu, P., Sun, W., 2010. Path following of a class of non-holonomic mobile robot with underactuated vehicle body. IET Control Theory Appl. 4, 1898–1904. doi:10.1049/iet-cta.2009.0617

- Yue, M., An, C., Du, Y., Sun, J., 2016. Indirect adaptive fuzzy control for a nonholonomic/underactuated wheeled inverted pendulum vehicle based on a data-driven trajectory planner. *Fuzzy Sets Syst., Theme: Control Engineering and Applications* 290, 158–177. doi:10.1016/j.fss.2015.08.013
- Yuk, H., Kim, D., Lee, H., Jo, S., Shin, J.H., 2011. Shape memory alloy-based small crawling robots inspired by *C. elegans*. *Bioinspir. Biomim.* 6, 046002.
- Yusupov, A., Liu, Y., 2016. Development of a self-propelled capsule robot for pipeline inspection, in: *Automation and Computing (ICAC), 2016 22nd International Conference on*. IEEE, pp. 84–88.
- Zeinali, M., Notash, L., 2010. Adaptive sliding mode control with uncertainty estimator for robot manipulators. *Mech. Mach. Theory* 45, 80–90. doi:10.1016/j.mechmachtheory.2009.08.003
- Zhan, X., Xu, J., 2015. Locomotion analysis of a vibration-driven system with three acceleration-controlled internal masses. *Adv. Mech. Eng.* 7, 1687814015573766.
- Zhang, A., She, J., Lai, X., Wu, M., 2013. Motion planning and tracking control for an acrobot based on a rewinding approach. *Automatica* 49, 278–284.
- Zhang, C., Liu, H., Li, H., 2014a. Experimental investigation of intestinal frictional resistance in the starting process of the capsule robot. *Tribol. Int.* 70, 11–17. doi:10.1016/j.triboint.2013.09.019
- Zhang, C., Liu, H., Li, H., 2014b. Modeling of Frictional Resistance of a Capsule Robot Moving in the Intestine at a Constant Velocity. *Tribol. Lett.* 53, 71–78. doi:10.1007/s11249-013-0244-5
- Zhang, C., Liu, H., Tan, R., Li, H., 2012. Modeling of Velocity-dependent Frictional Resistance of a Capsule Robot Inside an Intestine. *Tribol. Lett.* 47, 295–301. doi:10.1007/s11249-012-9980-1
- Zhang, H., Cui, L., Luo, Y., 2013. Near-optimal control for nonzero-sum differential games of continuous-time nonlinear systems using single-network ADP. *IEEE Trans. Cybern.* 43, 206–216.
- Zhang, H., Qin, C., Luo, Y., 2014. Neural-network-based constrained optimal control scheme for discrete-time switched nonlinear system using dual heuristic programming. *IEEE Trans. Autom. Sci. Eng.* 11, 839–849.
- Zhang, H., Wang, Z., Liu, D., 2014. A comprehensive review of stability analysis of continuous-time recurrent neural networks. *IEEE Trans. Neural Netw. Learn. Syst.* 25, 1229–1262.

- Zhang, Q., Xiao, X., Guo, Z., 2016. Power Efficiency-Based Stiffness Optimization of a Compliant Actuator for Underactuated Bipedal Robot, in: International Conference on Intelligent Robotics and Applications. Springer, pp. 186–197.
- Zhang, S., An, R., Shao, S., 2011. A new type of adaptive neural network fuzzy controller in the double inverted pendulum system, in: Artificial Intelligence and Computational Intelligence. Springer, pp. 149–157.
- Zhang, X., Fang, Y., Sun, N., 2014. Minimum-Time Trajectory Planning for Underactuated Overhead Crane Systems With State and Control Constraints. *IEEE Trans. Ind. Electron.* 61, 6915–6925. doi:10.1109/TIE.2014.2320231
- Zhao, B., Li, M., Yu, H., Hu, H., Sun, L., 2010. Dynamics and motion control of a two pendulums driven spherical robot, in: 2010 IEEE/RSJ International Conference on Intelligent Robots and Systems. Presented at the 2010 IEEE/RSJ International Conference on Intelligent Robots and Systems, pp. 147–153. doi:10.1109/IROS.2010.5651154
- Zoso, N., Gosselin, C., 2012. Point-to-point motion planning of a parallel 3-dof underactuated cable-suspended robot, in: 2012 IEEE International Conference on Robotics and Automation. Presented at the 2012 IEEE International Conference on Robotics and Automation, pp. 2325–2330. doi:10.1109/ICRA.2012.6224598
- Zou, A.-M., Kumar, K.D., Hou, Z.-G., Liu, X., 2011. Finite-time attitude tracking control for spacecraft using terminal sliding mode and Chebyshev neural network. *IEEE Trans. Syst. Man Cybern. Part B Cybern.* 41, 950–963.